Studies Towards Synthesis and Efficacy of New Heterocyclic Scaffolds and Zwitter Ionic Molecules

A Thesis
Submitted for the
Degree of Doctor of Philosophy
in the Faculty of Science
Jadavpur University
2024

By

Debabrata Sarkar

CSIR-Indian Institute of Chemical Biology 4, Raja S. C. Mullick Road, Jadavpur Kolkata-700032, India

INDIAN INSTITUTE OF CHEMICAL BIOLOGY
CSIR-IICB, 4, RAJA S.C.MULLICK ROAD, JADAVPUR,KOLKTA 700032, INDIA
PHONE:+91-33-24730492/3491/3493/6793, FAX: 033-2473 5197/ 2472 3967

Dr. Biswadip Banerji, Senior Principal Scientist
Ph.D (IIT - Kanpur), M.Sc.(Calcutta University)
2009 – Onwards: CSIR-IICB, Kolkata, India
2008: Team Lead, Chembiotek-Kolkata
2006 – 2008: Postdoctoral Research Fellow, (Prof. K.C. Nicolaou); CSL@ICES-A*-STAR
2003 – 2006: Postdoctoral Research Fellow, (Prof. C.J. Schofield); Oxford Centre for Molecular Science (OCMS) & Chemistry-Research Laboratory (CRL), Oxford University, UK.

Office address:
Room No. 17 & 12 (Ground Floor)
Phone No. +91-33-24735709
Hand Phone No. 09903752881
Email: biswadip@iicb.res.in
biswadip.banerji@gmail.com

CERTIFICATE FROM THE SUPERVISOR(S)

This is to certify that the thesis entitled **"Studies Towards Synthesis and Efficacy of New Heterocyclic Scaffolds and Zwitter Ionic Molecules"** Submitted by Sri **DEBABRATA SARKAR** who got his name registered on **08.08.2019** for the award of Ph.D. (Science) Degree of Jadavpur University, is absolutely based upon his own work under the supervision of **PROF. BISWADIP BANERJI**. and that neither this thesis nor any part of it has been submitted for either any degree / diploma or any other academic award anywhere before.

.....

Biswadip Banerji .. 23/12/2024

.....

(Signature of the Supervisor(s) date with official seal)

डॉ. बिश्वदीप बनर्जी / Dr. Biswadip Banerji
PhD (IIT-Kanpur), M. Sc (Cal)
प्रधान वैज्ञानिक / Chief Scientist
आर्गेनिक एवं औषधीय रसायन प्रभाग
Organic & Medicinal Chemistry Division
सीएसआईआर-भारतीय रासायनिक जीवविज्ञान संस्थान
CSIR-Indian Institute of Chemical Biology
(भारत सरकार / Govt. of India)
कोलकाता - 700 032 / Kolkata - 700 032

DECLARATION

I, **Debabrata Sarkar** hereby declare that the work focused in this thesis entitled **"Studies Towards Synthesis and Efficacy of New Heterocyclic Scaffolds and Zwitter Ionic Molecules"** is my own work which has been carried out under the supervision of **Dr. Biswadip Banerji**, Chief Scientist, Organic and Medicinal Chemistry Division, CSIR-Indian Institute of Chemical Biology, Kolkata, India. To the best of my knowledge, this work is original and has not been submitted in part or full towards the award of a degree/diploma in this University or any others.

Debabrata Sarkar

(**Debabrata Sarkar**)
23/12/2024
Organic & Medicinal Chemistry Division
CSIR-Indian Institute of Chemical Biology
Jadavpur, Kolkata- 700032, India

DEDICATED TO

MY

PARENTS

Acknowledgement

"Do not depend on something until you are sure it will happen."

During my school days I heard this line for the first time from my teacher, sir Anjan Kumar Ghosh, and it serves as a gentle reminder to keep pushing forward and striving for greatness in every aspect of life.

This PhD thesis could not have been written without the assistance and encouragement of the kind individuals in my life, just a few of whom can be specifically mentioned here.

First and foremost, I express my heartfelt gratitude to my research supervisor Prof Biswadip Banerji for his invaluable guidance, constant encouragement, unflinching support and profound understanding towards the completion of my research work. His continuous support towards research had given me enough freedom to think, plan and execute my ideas towards my work, which has provided a good basis for the present thesis. I am also indebted to Prof. Biswadip Banerji for instilling in me a craving for perfection. I believe, it will always be a part of my life moving forward.

Besides my supervisor, I would like to thank my Doctoral Advisory Committee (DAC) members Dr. Nakul Chandra Maity, Head of Department of Chemistry Division of Jadavpur University for their valuable suggestions and comments during all assessments in the entire period of my doctoral studies.

Several of my research's findings wouldn't have been achieved without adequate collaboration with other labs. I would like to extend my sincere gratitude to Prof. Krishnananda Chattapadhaya & Dr. Ramaligam Natarajan and his student Dr. Sumangal Roychowdhury for giving me such wonderful memories of working with them. My deepest gratitude to Dr. Chinmay Chowdhury, Dr. Parasuraman Jaisankar, Dr. Ranjan Jana, Dr. Ramalingam Natarajan, Dr. Sanjay Dutta, Dr. Arindam Talukdar, and Dr. Indrajit Das for allowing me to use the instruments and chemical in their lab. During my doctoral studies, I would like to thank Dr. Titash Kumar Mukhopadhaya (NIT Jamshedpur) providing me with such lovely memories of working with them.

I want to express my admiration to the current and former directors of the CSIR-Indian Institute of Chemical Biology (CSIR-IICB), Dr. Arun Bandyopadhyay and Dr. Samit Chattopadhyay and also to our head of the division (organic and medicinal chemistry division, IICB) Dr. Parasuraman Jaisankar, for giving me the chance to accomplish my PhD at such a prestigious institute.I thank to DST-INSPIRE for my fellowship and Jadavpur University in fulfillment of the requirements for the award of the degree of Doctor of Philosophy (Ph.D.).

A special acknowledgement goes to Dr. Tapas Sarkar, Gautam Karmakar and Dr. E. Padmanaban for 300, 400 and 600 MHz NMR facility, Sri Diptendu Bhattacharya, Soumik Laha and Sri Sandip Chowdhury for ESI/EI mass facility. Dr. Ramdhan Maji for HPLC facility and Sri Sandip Kundu for XRD facility and all member of IICB who help me in during my PhD tenure. I would like to thank Debasree Das for their assistance in making the official process go smoothly.

It's my fortune to gratefully rejuvenate the support of my lab mates. Words fail me to express my pleasure to Subhankar da, Satadru Da, Sunil da, Chandu da, Moumita Di, SaswatiDi,LeenaDi,ShrinathAnna,KrishnenduDa, Saswati, Abhudaya, Vijay, Subhankar, Arindam, Kousik, Arpan and Asikul for their support & selfless Co-Oparation

and the homely feeling in the lab. You all have provided me stimulating and fun filled environment that helped me to pass hard times and filled the end of my journey with happiness.

I don't know how to express my gratitude to Krishnendu da, Saswati & Vijay for their excellent paper writing and representation skills and knowledge, which have enhanced me greatly. I believe, it will always remain with me in my life.

I would like to express my heartfelt gratitude to several seniors: Subhankar da, Satadru Da, Sunil da, Chandu da, Moumita Di, Saswati Di, Leena Di for their unwavering support and encouragement in every aspect. I also want to express my sincere appreciation to the other members of Sudip, Subhendu, Sukanya, Debasmita, Sarat, Subhajit and Suman who always supported me in both my professional and personal endeavors. I want to thank all room mates including Arnab, Sandip da who helped me duringmy PhD.

It gives me an immense pleasure to express my thanks to Ph.D. batch mates, research scholars in the organic and medicinal chemistry division, M.Sc. friends (Bhim, Debomita, Arup and others) for their support and joyful moments shared with them.

My special thanks also go to my parents for constant support and encouragement in all respects. I am indebted to my family, whose value to me only grows with age. Without their love and support, none of this would have been possible.

Debabrata Sarkar
Organic and Medicinal Chemistry Division,
CSIR-Indian Institute of Chemical Biology (CSIR-IICB)
Jadavpur, Kolkata-700032, India
Email: sarkar.debu691@gmail.com
Mobile no: 6291678372

LIST OF ABBREVIATIONS

CDC: Cross Dehydrogenative Coupling
ESIPT: Excited StateInternal ProtonTransfer
OLEDs: Organic Light Emitting Diodes
DMF: Dimethylformamide
DMSO: Dimethyl sulphoxide
HOAc: Acetic acid
PivOH: Pivalic acid

^{o}C: Temperature in degree Celsius

hr.: Hour
min: Minute

BQ: Benzoquinone

UV: Ultraviolet

µM: Micromolarg: Gram
eq.: Equivalents
mg: Milligram
mL: Milliliter
DCB: Dichlorobenzene
m.p: Melting point
NMR: Nuclear magnetic resonance
MHz: Mega hertz
ppm: Parts permillion
EI: Electronionization
HRMS: High resolution mass spectrometry
Da: Dalton
FTIR: Fourier-transforminfraredspectroscopy
TLC: Thin layer chromatography
XRD: X-rayDiffraction

DMEM: Dulbecco‘s Modified Eagles Media

FBS: Fetal bovine serum
PBS: Phosphate buffer salin
IC_{50}: Concentration of a compound that exhibits 50% cell-viability

THF: Tetrahydrofuran
TEA:Triethylamine
SET:Single electron transfer
mM: Millimolar
nM:Nano molar

ESI: Electro spray ionization

IHB:Intramolecular hydrogen bonding

Vis: Visible
DAPI:4′,6-diamidino-2-phenylindole

EDC.HCl:1-Ethyl-3-(3-dimethylaminopropyl)carbodiimidehydrochloride

HOBt: Hydroxybenzotriazole
^{n}Bu: n-butyl
(M): Molar

ROESY: Rotating-frame Overhauser Spectroscopy
NOESY: Nuclear Overhauser effect spectroscopy
MeOD: Deuterated methanol
CT-DNA: Calf ThymusDNA
r.t.: Room temperature
CD: Circulardichroism
ng: Nano gram
μg: Micro gram
Ms: Millisecond
EDTA:Ethylene diamine tetra aceticacid PET:
Photo induced electron transfer
PD: Parkinson's disease
DEM:Diethyl malonate
NaP:Sodium phosphate EtOH:
Ethanol
WT: Wild type
α-Syn: Alpha synuclein
BSA: Bovine serum albumin
LOD: Limit of detection
NAC:Non-Abetacomponent
pM: Pico molar
ThT:ThioflavinT
TCEP: tris(2-carboxyethyl) phosphine
PSN:Penicillin-Streptomycin-neomycin
DCM: Dichloromethane

Contents

GENERAL INFORMATION

- Unless otherwise mentioned, all the chemicals were bought from Sigma Aldrich, TCI chemicals and Acros Organics India. All the solvents were bought fromThermoFisher Scientific India.
- Melting points were recorded on a SPAC-NSERVICE (India) open capillary melting point apparatus and are uncorrected.
- ^{1}HNMR and ^{13}CNMR were measure done BrukerDPX300MHz and Bruker Avance 600 MHz NMR instrument. $CDCl_3$, and DMSO-d_6 were generally used for sample preparation. Chemical shifts (δ) were reported in parts per million (ppm) and tetramethylsilane (δ = 0.00) was used as an internal standard. The standard abbreviations s, d, t, q, m, dd, bs, *J* refers to singlet, doublet, triplet, quartet, multiplet, doublet of doublet, broad singlet and the coupling constant respectively.
- Infrared spectra were recorded on a Bruker TENSOR27. Spectra were calibrated against the polystyrene absorption at 1601 cm^{-1}. Samples were scanned in neat or KBr discs.
- EI-MS mass spectra were recorded on a JEOLThe Mstation JMS-700 instrument and ESI-MS were measured on Micro mass Q-TOF Micro™ spectrometer. All the mass spectral data associated with EI-MS and ESI-MS and are given in m/z unit. MALDI TOF analysis was perfor medinan Applied Biosystems Q104800MALDITOF/TOF™ analyser.
- Analytical thin layer chromatography (TLC) was obtained via standard Merck TLC silica gel 60 F254 aluminium sheets. Visualization of the spots on TLC plate was achieved through exposure of UVlight, iodine vapour etc. Progress of the reactions was monitored via TLC checking. Moisture sensitive reactions were carried out using standard syringe septum techniques. Column chromatography was carried out with silica gel of 60-120 and 100-200 mesh and neutral alumina.
- Unless otherwise mentioned, petroleum ether referst of raction boiling in the range 60- 80^{0}C. All reagents and solvents were purified and dried by conventional protocol.
- The evaporation of solvents was carried out under reduced pressure in Heidolph Rotary Evaporator of Cat. No: P/N Hei-VAP Value/G3: 560-01300-001.
- The compounds have been crystallized from pet ether-ethyl acetate and dichloromethane-methanol solvent mixture.
- CD spectra (230-360 nm) were recorded at 200 nm/min scan speed, with 1 nm band width on a JASCO J815 spectrometer using a 10 mm quartz cell.
- Fluorescence spectra were measured with the Cary Eclipse (Agilent Technology) & PTI Quanta Master™ 400 spectrofluorometer.
- In X-raycrystallography, the crystals were mounted on glassfibre, aligned on a Bruker Kappa Apex II diffractometer. Intensity data were collected with silicon 111monochromatized synchrotron radiation (ı = 0.71073 Å) at 273.15 and

- 296.15 K using the ω-rotation scan techniques with narrow frames. Absorption corrections based on multi scan were done by the SADABS software3. The structure was solved by direct methods and least square refinement anisotropic displacement parameters, hydrogen atoms in the riding model. Data reduction swere performed with Bruker SAINT and

  —Bruker SAINTV7.23 all software package sand crystallographic diagrams were drawn using —Bruker SHELXTLll at 50% probability level as well as using DIAMOND program

PRELUDE

The research work emboded in the thesis entitled, **"Studies Towards Synthesis and Efficacy of New Heterocyclic Scaffolds and Zwitter Ionic Molecules"** contains total four chapters; a general introduction, followed by tree other chapters containing the present research work. In the second chapter the research work is focused on the Influence of ester functionality on the rotational behaviour of complex molecules. It was observed that a simple tertiary- benzamides where the aromatic ring contains ortho substituted halogen atoms then it shows complex NMR spectra with multiple peaks. In the present research the rotational behaviour of simple ortho-halo substituted tertiary amides were first studied. Then this study was elaborated with the example of anti-cancer drug Azatoxin analogues synthesis. In this complex molecular framework, it was observed that an appended ester moiety highly influences this rotational behaviour of the tertiary amide present within the molecule. The third chapter deals with Palladium catalyzed C(sp^3)-H arylation followed by de-esterification reactions. In this study ortho-halo benzamide derivatives having different esters were synthesised and these molecules were cyclised to the corresponding indolinone or isoindolinone derivatives via palladium catalysed intramolecular arylation followed by de-esterification reactions. In the next and final chapter, a small series of zwitterionic molecules were synthesised and their biological efficacies towards inhibiting liquid-liquid phase separation and thereby modulating alpha-synuclein protein aggregation phenomenon were studied.

OBJECTIVES OF THE THESIS

The objectives of the present research work embodied in the thesis entitiled “Studies Towards Synthesis and Efficacy of New Heterocyclic Scaffolds and Zwitter Ionic Molecules” are as follows:

(i) Herein the main objective of the thesis is to address a basic and fundamental problem of rotational isomers observed in case of tertiary amides. During the synthesis of an anti-cancer molecule, Azatoxin analogues in an ongoing project in our laboratory it was observed that ortho-halo substituted benzamide analogues of simple amino acid esters showed complex ^{1}H and ^{13}C NMR spectra with multiple peaks for single proton. These results encouraged to investigate further the rotational behaviour of this kind of molecules elaborately. Thus the first objective of the thesis is to synthesise few ortho-halo substituted benzamide derivatives and study their rotational behaviour and also the influence of an ester functionality on the rotational behaviour of the amide bond in a complex molecular framework.

(ii) In the third chapter the objective is to study a palladium catalyzed C(sp^3)-H arylation followed by de-esterification reactions. A number of isoindolinone and indolinone derivatives will be synthesised by the said protocol. This protocol will be further elaborated by synthesising Azatoxin analogues.

(iii) In the fourth and final chapter the objectives of the research work is to disrupted the liquid-liquid phase separation (LLPS), which is responsible for fibrillation/aggregation phenomenon by some charged molecules. The pathophiology of Parkinson’s disease (PD) is controlled by an intrinsically disordered protein called alpha-Synuclein (α-Syn). The major objective of this part is to synthesize a small series of pyridine derived zwitter ionic molecules and study their effacies towards modulating α-Syn aggregation phenomenon via inhibition of LLPS.

Therefore, the overall objectives of this thesis is to synthesize some heterocyclic and zwitter ionic molecules and their efficacy studies.

CHAPTER-1

General Introduction

In this chapter a general introduction relevant to the research work carried out in this thesis has been given. The different heterocyclic molecules partaining to the thesis, the rotational isomerization problem in tertiary amides, palladium catalysed arylation reactions are some of the areas covered under this chapter. Also cause of Parkinson's disease due to the aggragation of α-Syn protein, inhibition of LLPS by small molecules and their implications in Parkinson's disease pathophysiology are also discussed.

1.0 INTRODUCTION:

1.1 Naturally Occurring Indoloquinoline Alkaloids: Cryptolepine and Isocryptolepine.

Heterocycles, organic compounds characterized by the presence of at least one heteroatom (such as nitrogen, oxygen, or sulfur) as a ring member in place of carbon within a carbocyclic structure, play a pivotal role in diverse scientific fields.[1] Their exceptional versatility and wide-ranging applications, particularly in biomedicine and materials science, have consistently driven research efforts toward the discovery and development of novel synthetic methodologies for constructing these essential molecular frameworks.[2],[3]This ongoing pursuit reflects the significant impact of heterocycles on advancing scientific knowledge and technological innovation[4]. While nitrogen, oxygen, and sulfur heterocycles are extensively documented in both natural sources and scientific literature, heterocycles incorporating other heteroatoms such as phosphorus, boron, and selenium are also prevalent, albeit less frequently. The properties of these heterocyclic systems are often significantly influenced by the incorporated heteroatom. Heterocycles are ubiquitous in nature, serving as essential components in a wide range of biomolecules. [6] Examples include chlorophyll, hemoglobin, myoglobin, vitamins, adenosine triphosphate (ATP) [7], deoxyribonucleic acid (DNA), ribonucleic acid (RNA)[8], and neurotransmitters such as serotonin[9]. These compounds play crucial roles in fundamental biological processes, including nerve impulse transmission, oxygen transport, and metabolism. Furthermore, numerous naturally occurring medicinal compounds, such as codeine, theobromine, quinine, emetine, theophylline, papaverine, atropine, procaine, reserpine, and morphine, incorporate heterocyclic structures. Similarly, many synthetic pharmaceuticals, including diazepam, isoniazid, chlorpromazine, barbiturates, metronidazole, azidothymidine, antipyrine, captopril, and methotrexate, rely on heterocycles as key structural elements for their therapeutic activity. [10] Analysis of the 2024 FDA-approved drug list reveals that a significant proportion of these pharmaceuticals incorporate at least one heterocyclic moiety as a core structural element (Table 1)

Table 1.

Name of Drugs	Active Ingredient	FDA approval date	Structure	Uses
BIZENGRI	zenocutuzumab-zbco	**12/4/2024**	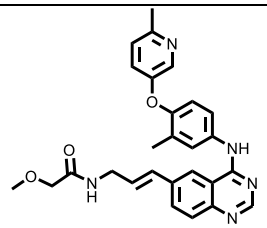	To treat non-small cell lung cancer and pancreatic adenocarcinoma
Iomervu	iomeprol	**11/27/2024**	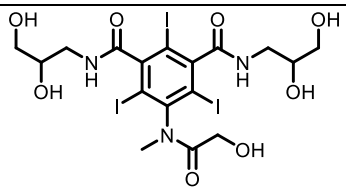	For use as a radiographic contrast agent
Attruby	acoramidis	**11/22/2024**	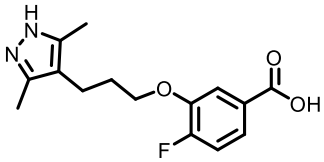	To treat cardiomyopathy of wild-type or variant transthyretin-mediated amyloidosis
Revuforj	revumenib	**11/15/2024**	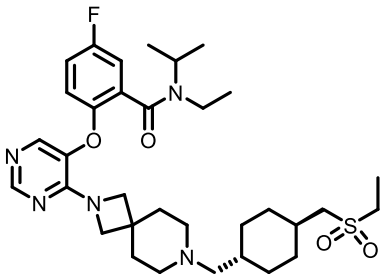	To treat relapsed or refractory acute leukemia
Itovebi	inavolisib	**10/10/2024**	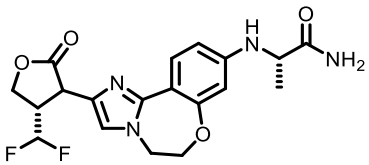	To treat locally advanced or metastatic breast cancer

Over recent decades, tetracyclic indoloquinoline alkaloids have become a subject of considerable scientific interest within the biological and chemical disciplines due to their pronounced biological activities, notably antimalarial efficacy and DNA-binding affinity [8]. These alkaloids are characterized by a distinct molecular architecture consisting of fused quinoline and indole ring systems. [11]

In 1996, two independent research groups, led by Schiff and Pieter, reported the discovery of new indoloquinoline-based alkaloids: cryptotackieine and neocryptolepine, respectively [13, 14]. Neocryptolepine is a linearly fused indoloquinoline alkaloid featuring an indolo[2,3-b] quinoline core. [15]

Cryptolepis sanguinolenta, a plant indigenous to West Africa, has been identified as the principal natural source of these compounds, specifically within its root system. This species has a history of use in traditional West African medicine, with root extracts employed in the treatment of diverse pathologies, including malaria, amoebiasis, hypertension, hepatitis, jaundice, pyrexia, inflammation, and other infectious diseases.[16] The broad spectrum of therapeutic applications highlights the pharmacological significance of tetracyclic indoloquinoline alkaloids and suggests their potential as lead structures in the development of novel therapeutic agents.[17],[18]

Structurally, tetracyclic indoloquinolines are defined by a unique fused ring system comprising both quinoline and indole moieties, forming a complex molecular architecture (Figure 1)[19]. This distinctive structural motif is hypothesized to be crucial for their diverse biological activities.Carbolines, a class of indole alkaloids[20],[21], are characterized by a pyridine ring fused to an indole moiety. Based on the position of the nitrogen atom within the pyridine ring, carbolines are classified into four distinct groups. Further classification based on the saturation of the β-carboline core yields three subtypes[22].

1.1 Positional β-carboline

Among these carbolines, beta carbolines are having much importance in medicinal purpose and many researches are going on it, when compared to α-, γ- and δ-carbolines [23].

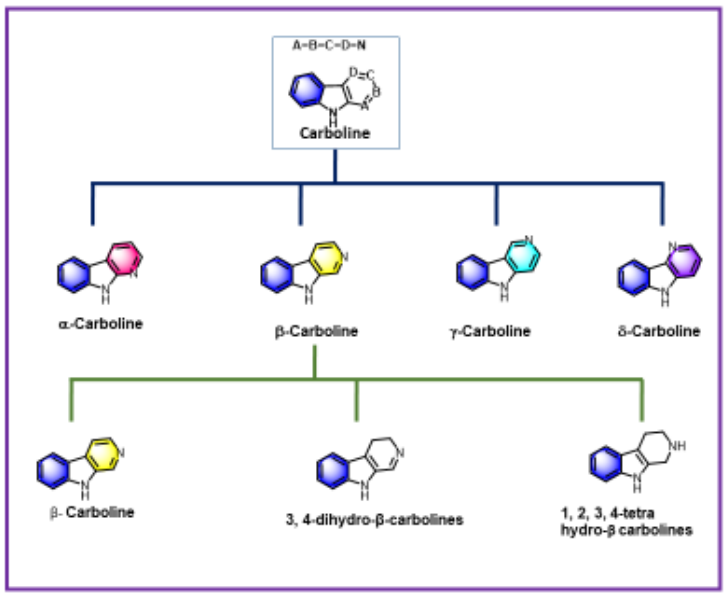

Figure 1: A variety of Carbolins having varied position of nitrogen atom.

1.2 Medicinal Applications of β-Carboline-Based Compounds. [24]:

β-Carboline-derived compounds have been of prime interest in pharmacology because they show various therapeutic properties. The medicinal applications of this class of compounds are controlled mainly by the presence or position of substituents in their core structure as this decides their biological activity or how they interact with various molecular targets. Some essential medicinal applications of β-carboline derivatives are found in the following:

- **Neuroprotection and Neurodevelopment:**

Certain β-carbolines, such as harmine, are selective inhibitors of DYRK1A protein kinase, an enzyme essential for neurodevelopment. Such activity makes them promising candidates for the treatment of neurodevelopmental disorders, including Down syndrome and neurodegenerative conditions like Alzheimer's disease.

- **Antidepressant Activity:**

β-Carbolines have displayed many antidepressant-like pharmacology. Harmine, a compound, acts on a serotonin receptor 2A (5-HT2A). However, it increases the quantity of BDNF molecules in the hippocampus where the levels of BDNF are low in major depressive disorder. Therefore, antidepressives can be considered as novel drugs.

- **Monoamine oxidase inhibition:**

β-Carbolines, including harmine and harmaline, are monoamine oxidase A (MAO-A) inhibitors. This is an enzyme that breaks down neurotransmitters like serotonin and noradrenaline. Its inhibition by these compounds would increase the availability of neurotransmitters, which is useful in the treatment of depression and anxiety disorders.

- **Anticancer Activity:**

Some β-carbolines have shown antitumor activity due to their ability to induce apoptosis in cancerous cells and inhibit cellular proliferation. This is attributed to their ability to interact with DNA, topoisomerases, and other crucial pathways of signaling that contribute to cancerous growth.

- **Cognitive Enhancement:**

β-carbolines have been found to be nootropics that enhance learning and memory. Their interaction with neuroprotective pathways, enhancement of synaptic plasticity, and so on, add to their potential as cognitive enhancers.

- **Antimicrobial and Antiparasitic Effects:**

Some β-carboline derivatives have been found to possess antibacterial, antifungal, and antiparasitic activities. These are due to their interference with microbial metabolism and the disruption of critical cellular functions.

- **Treatment of Addiction:**

Some β-carbolines are under investigation for their potential in the treatment of substance use disorders. They may act by modulating dopaminergic and serotonergic systems implicated in addiction pathways.

- **Antioxidant and Anti-inflammatory Activities:**

β-Carbolines exhibit antioxidant activity, which contributes to scavenging free radicals and reducing oxidative stress. These properties together with their anti-inflammatory activity make them suitable for treating chronic inflammatory and oxidative stress-related disorders.

- **Anticonvulsant and Sedative Activity:**

Certain β-carbolines activate GABA-A receptors resulting in sedative and anticonvulsant activity. Hence, they are considered promising for the treatment of epilepsy and anxiety disorders.

The diverse pharmacological activities of β-carboline-based molecules illustrate their therapeutic potential for many neurological, psychiatric, and systemic disorders. Ongoing research work is aimed at optimizing these molecules for efficacy and safety in clinical applications**.**

5H-pyrido [3, 2-b] indoles, commonly called as δ- carbolines. They are very rare in nature when compared to other carbolines. **Cryptolepine** was isolated from the roots of Cryptolepis sanguinolenta having antimalarial activity [15], anti-inflammatory properties [16], and antibacterial activity [17]. It posses cytotoxicity against B16 melanoma and M109 Madison lung cancer cells and also interact with Topoisomerase II inhibiting DNA synthesis **[18]. Quindoline** had the ability to stabilize the G-quadruplexes in C-MYC and also induced the G-rich telomeric repeated DNA sequence to fold into quadruplex [19]

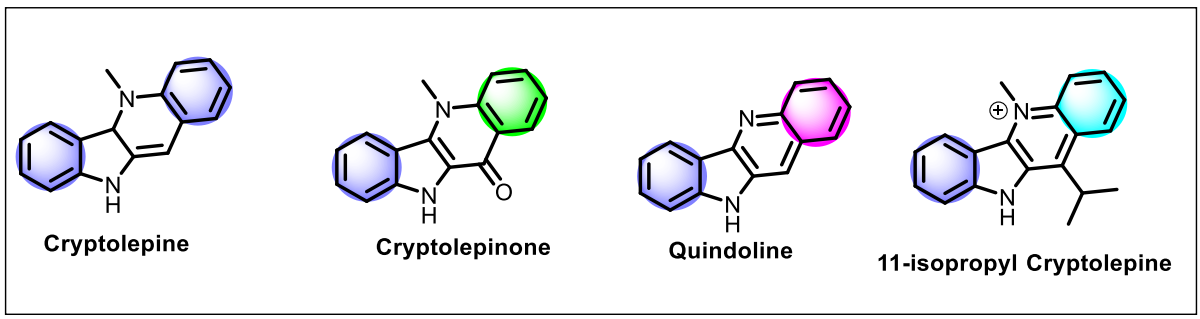

Figure 2: Different ezample of δ- carbolines darivatives

The extensive therapeutic applications of tetracyclic indoloquinoline alkaloids highlight their immense pharmacological value. They represent a promising avenue for the development of new and effective drugs, particularly in regions where the diseases they target are endemic. Ongoing research into their mechanisms of action and potential modifications to their chemical structure could unlock even greater possibilities for their use in modern medicine [24]. As such,

these compounds continue to stand at the crossroads of natural product chemistry and drug discovery, offering hope for addressing some of the most pressing global health challenges.

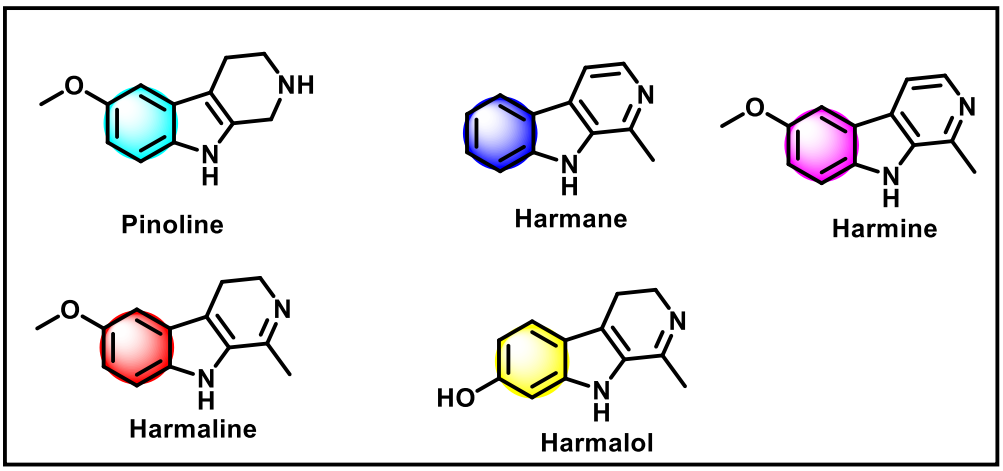

Figure 3: Different example of β-carbolines derivatives.

The pharmacological effects of specific β-carbolines are closely influenced by the nature and position of their chemical substituents, which dictate their binding affinities and biological activities. For example, harmine is a naturally occurring β-carboline with characteristic substituents at positions 7 and 1 of its molecular structure. These structural features make it possible for harmine to be a selective inhibitor of the DYRK1A protein kinase, an enzyme which plays a significant role in neurodevelopment by regulating processes like neuronal differentiation, cell cycle progression, and brain function [25]. Such selective inhibition positions harmine as a potential therapeutic agent for neurological and developmental disorders associated with DYRK1A dysfunction. Harmine also shows antidepressant-like effects in preclinical models, including rats, which are mediated by interactions with serotonin receptor 2A (5-HT2A). This receptor has been implicated in mood and cognition regulation; thus, harmine is thought to modulate serotonergic neurotransmission to treat depression [26]. Additionally, it has been demonstrated that harmine increases the expression of BDNF in the hippocampus of rats. BDNF is a neurotrophin of importance for neuronal survival, synaptic plasticity, and overall brain health [27]. As the decreased level of BDNF has been associated closely with major depressive disorder in human patients, upregulation of BDNF by harmine might contribute greatly to its anti-depressive action.

Harmine's antidepressant action also is attributed to its activity as a monoamine oxidase A inhibitor. Through inhibition of this enzyme, harmine diminishes the breakdown of essential neurotransmitters such as serotonin and noradrenaline, both of which play important roles in stabilizing mood and emotional responses [28]. The convergence of these mechanisms of action-DYRK1A inhibition, serotonin receptor modulation, BDNF enhancement, and MAO-A inhibition-show the complex pharmacological profile of

harmine and its promise as a therapeutic agent in the treatment of neuropsychiatric disorders. [29]

1.3 Fluxional behaviour observed in amides and esters:

This characteristic of amide and ester bonds, namely their planarity, is directly linked to the resonance stabilization within the groups. In this work, we report a detailed investigation in which structural analysis is coupled with computational modeling to understand the effect of ortho-substitution on the resonance and rotational barriers of tertiary aromatic amides, also containing ester groups. These results provide useful insight into the interplay of steric and electronic factors that influence the chemical behavior and properties of such compounds.

In particular, we show that the introduction of ortho-substitution into a selected class of benzamides—compounds of significant importance in both synthetic reactivity and medicinal chemistry—substantially increases the barriers to rotation along both the N−C(O) (amide bond) and C−C(O) (ester bond) axes. The presence of ortho-substituents leads to steric hindrance, forcing the molecule to take up non-planar conformations that alter resonance stabilization and rotational dynamics. These factors go on to significantly affect electronic properties and structural rigidity of amide and ester groups that enhance their resonance effects.

To elucidate these effects, we systematically investigate how the presence of ortho-substituents affects some of the key parameters under the influence of steric hindrance.

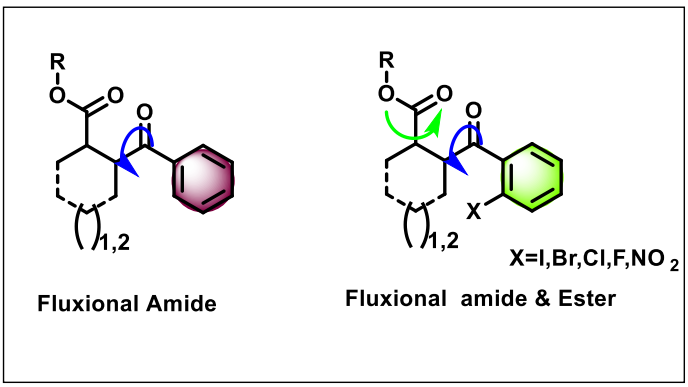

Figure 4: Rotational isomers in presence amide and ester group

The results of this work decisively support the strategic use of ortho-substitution in benzamides as a way to enhance their resonance stabilization, structural rigidity, and electronic properties. Thus, there is strong potential for these to act as better biological agents because these

structures show enhanced resonance while lowering conformational flexibility; both these factors lead towards improvements in the biological and pharmacokinetic activities. of even higher potential, these insights provide ways into synthetic strategies that depend upon ortho-substitution as a method of further refinement of the reactivity of benzamides, similar compounds.

1.4 Aromatic Amino Acids Carboline -based multifarious Arylation & alkylation

A strategy for expanding the repertoire of topoisomerase II-targeted anticancer agents involves the design of novel compounds through the combination of structural motifs from drugs known to induce enzyme-mediated DNA cleavage. Azatoxin, a hybrid molecule incorporating structural elements from etoposide and ellipticine, represents the first example of this rational drug design approach. Given the distinct structural and mechanistic characteristics of etoposide and ellipticine, azatoxin could potentially retain the functional properties of one parent compound, exhibit hybrid characteristics, or function as a novel pharmacophore. Consequently, the properties of azatoxin were investigated to elucidate the relationship between its mechanism of action and those of its parent compounds.

Azatoxin, like etoposide, binds to DNA through a non-intercalative mechanism. However, similar to ellipticine, it does not affect enzyme-mediated DNA religation and appears to stimulate scission primarily by enhancing cleavage complex formation. The cleavage potency of azatoxin varies depending on the topoisomerase II species examined, resembling that of either etoposide or ellipticine. Analysis of 43 DNA cleavage sites revealed that approximately 90% of those induced by azatoxin are also induced by either etoposide, ellipticine, or both. Furthermore, competition studies indicate that azatoxin interacts with topoisomerase II within the enzyme domain utilized by both etoposide and ellipticine. Pallladium Catalyzed, a series of azatoxin analogue molecules were synthesized with new methodologies to find out DNA non-intercalative mechanism for better result of biological purposes.

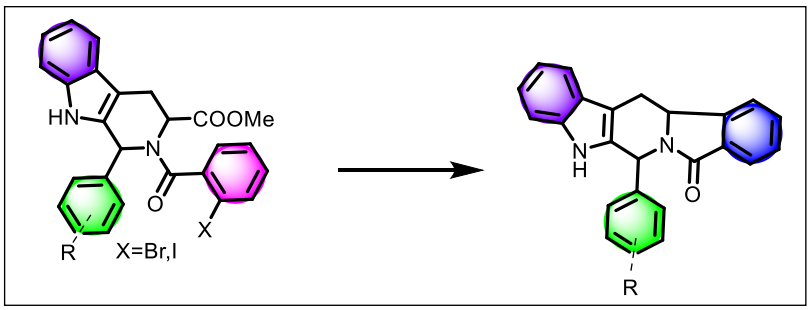

Figure 5: C-C bond formation followed by de-estrification

1.5 Liquid-liquid phase separation, fibrillation/aggregation of α-Syn protein, Parkinson's disease:

The phenomenon of liquid–liquid phase separation (LLPS) with biological polymers, such as proteins and nucleic acids, has been of great interest because it is involved in the formation of membraneless organelles. Examples of such organelles include nucleoli, Cajal bodies, and PML bodies within the nucleus, as well as stress granules in the cytoplasm. These liquid condensates concentrate biomolecules (proteins and nucleic acids) at specific cellular locations, facilitating various intracellular functions. These condensates can exchange material with their environment rapidly, since they do not have a surrounding membrane. Most of them can merge into larger droplets by Ostwald ripening and resume their original spherical shape. The proteins participating in LLPS usually have intrinsically disordered regions (IDRs) or sequence architectures that resemble prion-like low-complexity domains (PrLDs) and low-complexity regions (LCRs). These IDRs promote LLPS through weak, multivalent interactions among protein molecules, enabling homotypic and heterotypic interactions with other biomolecules. For instance, α-synuclein, a protein implicated in Parkinson's disease (PD), forms liquid droplets in vitro and in vivo under crowded conditions or intracellular stress. It is well-established that α-synuclein aggregation nucleates via LLPS, highlighting the importance of understanding the molecular mechanisms behind phase separation for elucidating aggregation pathways.

Notably, along with wild-type α-synuclein, C-terminal truncated variants are found within Lewy bodies in the human brain. Environmental factors such as temperature, pressure, and pH are already known to affect protein phase separation. Moreover, nucleic acids (DNA and RNA) and small molecules also affect phase separation through heterotypic interactions. On the other hand, negatively charged nucleic acids interact with positively charged peptide chains in a process called complex coacervation, where positively charged small molecules bind to negatively charged proteins.

For α-synuclein, crowding agents can be replaced by salt concentration and pH as significant external factors influencing the phase separation. Acidic pH (~5.4) can induce phase separation even at lower protein concentrations (10 μM). High salt concentrations favor the phase separation process, whereas low salt delays it. Multivalent cations

associated with PD further change the material properties of α-synuclein condensates. Beyond phase transition, small molecules have important roles modulating condensates by shifting phase boundaries, perturbing equilibria for multiphasic condensates or even preventing phase separation. For example, ANS (8-Anilino-1-naphthalenesulfonic acid) and bis-ANS modulate the phase behavior of tau protein whereas curcumin and its derivatives are inhibiting the phase separation of α-synuclein and tau respectively. These interactions possess disease-preventing potential to be developed by modulating the phase behavior.

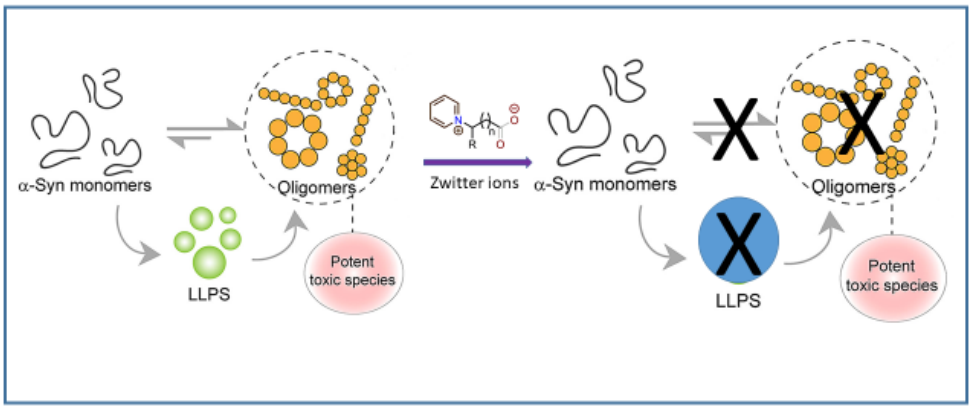

Figure 6: The aggregation landscape of α-Syn protein.

This chapter discusses charge-based ligands to explain the role of electrostatic interactions in α-synuclein phase separation. Proteins are complex macromolecules that have positively and negatively charged surface regions, thus creating electrostatic forces. Proteins with oppositely charged regions experience attractive interactions that drive aggregation into distinct liquid phases. These interactions are modulated by environmental factors such as ionic strength and pH, which influence the strength and dynamics of phase separation. Understanding the interplay between electrostatic forces and LLPS is important for the discovery of mechanisms underlying cellular compartmentalization and regulation of protein function.

Our work shows that the n-terminal domain plays a role in charge-driven phase separation. Charged ligands according to their hydrophobicity induced stronger phase separation and the effect was enhanced when the acidic C-terminal domain of α-synuclein was truncated. The molecular mechanisms of α-synuclein condensate formation under charged co-solutes are investigated with this work on the basis of charge-based ligand screening. In its potential, the charge-based complex coacervation model offers insights into biochemical processes occurring at the interface of condensates and therefore is the basis for studying phase separation in biological systems.

CHAPTER-2

Influence of Ester Functionality on The Rotational Behaviour of Amides in Complex Molecular Framework

2.1 INTRODUCTION:

For nearly 80 years, the study of deviations from amide bond planarity has captivated researchers, given its implications for molecular design, enzymatic mechanisms, and material science. Initial studies highlighted the remarkable rigidity of the amide bond, but recent advances have enabled systematic manipulation of this rigidity [31]. In conventional acyclic amides, substituting nitrogen with electron-withdrawing or electron-donating groups has emerged as a method to modulate resonance effects and induce predictable amide bond twisting. These studies have provided invaluable insights into the electronic factors controlling amide resonance and their impact on bond dynamics [32].

The planarity of amide and ester bonds arises primarily from the resonance stabilization between the lone pair of electrons on the nitrogen or oxygen atoms and the adjacent carbonyl group [33]. This resonance creates partial double-bond character in the amide or ester linkages, restricting free rotation and enforcing a planar configuration around the bond. This property is crucial for the structural and functional stability of these groups in various chemical and biological systems [31].

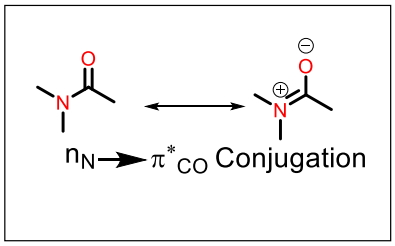

Figure 1: Canonical forms of acetamide.

In this study, we develop deeper into how ortho-substitution affects these properties in tertiary aromatic amides with ester groups. By employing structural analysis and computational techniques, we have identified that the introduction of bulky or electronically active substituents in the ortho position of benzamide derivatives significantly disrupts the resonance interactions between aromatic ring and C=O. This disruption increases the steric and electronic constraints around the molecule, resulting

- ❖ Increases the Rotational energy barriers:
- ❖ Restrict the possibility of resonance between C=O and phenyl ring

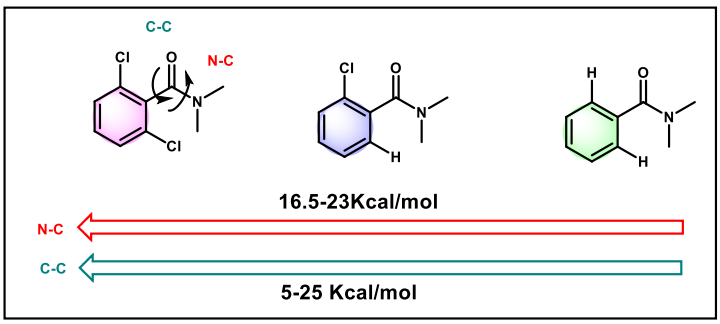

Figure 2: Effect of ortho substitution on rotational energy barrier.

These findings are particularly relevant for medicinal chemistry, where the structural rigidity imparted by such substitutions can influence binding affinities and biological activity of compounds [30]. Moreover, the increased rotational barriers may also affect the reactivity of these molecules, as restricted rotation can impact how functional groups approach or react with substrates. This study underscores the intricate interplay between steric and electronic factors in modulating the properties of aromatic amides and esters, with broad implications for their design and application in chemistry and pharmacology [32]. This investigation shows the vital role of steric hindrance introduced by ortho-substitution in modulating the structural and electronic properties of benzamide derivatives [30],[52]. Introduction of bulky groups in ortho positions adjacent to the amide and ester functionalities creating a spatial and electronic constraints that influence several key molecular characteristics such as

- **Molecular Structures**: Ortho-substitution affects the overall geometry of the molecule. Bulky substituents cause deviations from ideal bond angles and distances, potentially leading to distortions that influence the planarity of the amide and ester bonds. These structural modifications often enforce conformations that enhance the overlap between π orbitals, amplifying resonance effects.
- **Resonance Energies**: The resonance stabilization of both the amide and ester functional groups is sensitive to steric and electronic influences. Ortho-substitution can augment resonance energies by aligning substituent electronic effects with the π-system of the benzamide framework, thereby enhancing delocalization. Electron-donating groups can strengthen resonance stabilization, while electron-withdrawing groups may either enhance or compete with resonance effects, depending on their nature.
- **Rotational Barriers**: Increased steric hindrance in ortho-substituted benzamides raises the energy barriers for rotation around key bonds, particularly the N−C(O) amide bond and the C−C(O) ester bond. This occurs due to the steric clash between the substituents and neighboring atoms, as well as alterations in conjugation that make the transition state for rotation less favorable.
- The findings of this study strongly advocate for the strategic use of ortho-substitution in designing benzamides with enhanced resonance characteristics [30]. By carefully selecting substituents that align with the desired electronic and steric effects, chemists can tailor the resonance and rigidity of these molecules to meet specific functional or pharmacological requirements which also improve the molecular stability [32],[52]. Optimize binding interactions in drug design and influence reactivity in synthetic applications making this approach a valuable tool in advanced chemical and medicinal chemistry strategies. [55]

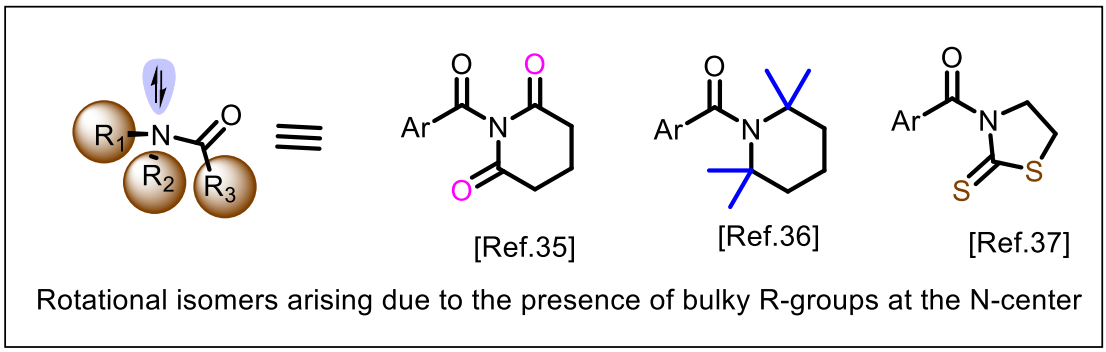

Figure 3: Substitution on amide N affecting rotational energy barrier.

The rotational barrier around the C−N single bond in amides is a defining feature of their structural chemistry, arising from the resonance interaction between the nitrogen's lone pair and the carbonyl π-system [38]. This resonance imparts partial double-bond character to the C−N bond, significantly restricting its free rotation and enforcing planarity. This property is fundamental to the stability and conformational behavior of amides, which play critical roles in peptides, proteins, and a wide range of functional molecules. [39]

2.2 Significance of this study:

From the literature precedence the fluxionality due to the rotation of an amide bond is well known. However, fluxionality of a molecule at room temperature is very rare. This study emphasizes the fluxionality behaviour of an organic compound at room temperature via incorporation of an ester moiety at a specific position, which also further supported by extensive proton (^{1}H) NMR study at variable temperature (VT) and detailed theoretical calculation using DFTstudy. [40]

2.3 Rotational behaviour observed in o-halo arylamides in reported molecules:

The presence of ortho-substitution in tertiary aromatic amides introduces steric and electronic effects that influence molecular conformation and reactivity. [41] These features are exploited in

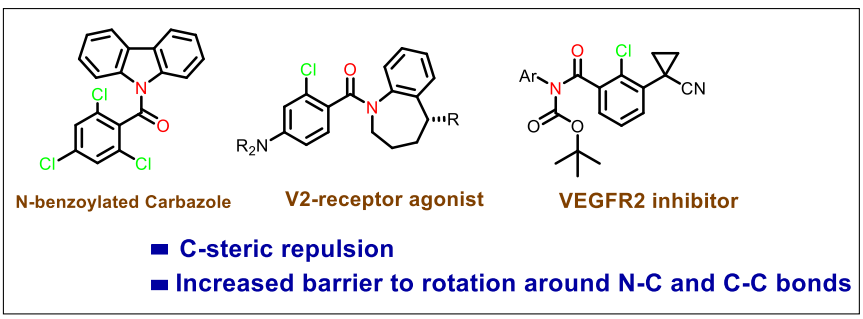

Figure 4: Examples of some biologically active ortho substituted benzamide derivatives

Ortho-substituted amides often exhibit enhanced binding affinity and specificity in biological systems due to their rigidified structures, which can better align with target sites. Examples include inhibitors, receptor agonists, and enzyme modulators. [48]

Rotational behaviour in tertiary amides: Present study

In synthetic chemistry, the geometry of the amide bond, influenced by ortho-substitution, plays a crucial role in determining the success and selectivity of cross-coupling reactions. Ortho-substituents modulate the steric environment and electronic properties of the amide, enabling selective activation and functionalization. [54]

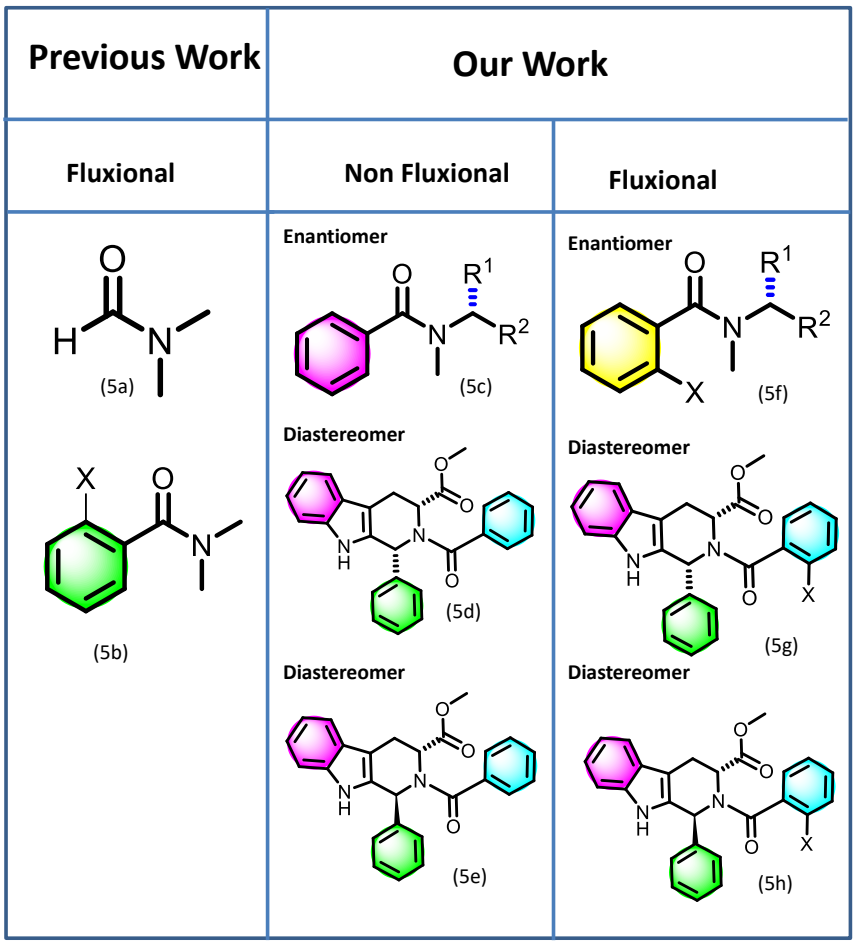

Figure 5: schematic representation of previous and the present study.

Introduction of ester groups into the aromatic ring can further modulate resonance by introducing additional electronic effects. These effects may either enhance or disrupt the delocalization in the amide and ester functional groups, influencing both structural stability and chemical reactivity. Ortho-substitution can amplify steric hindrance, forcing deviations from ideal bond angles and planarity. This disruption may alter the resonance

energies of both amide and ester bonds, impacting properties such as rotational barriers, hydrogen bonding potential, and proton affinities.

As a part of our continued research into amide and ester bonds, this study offers a detailed examination of the influence of ortho-substitution on resonance and rotational barriers in tertiary aromatic amides. We combine structural analysis with computational insights to quantify how ortho-substitution affects the structure, amidic resonance, rotational barriers, and proton affinities. The findings strongly support the strategic use of ortho-substitution in common benzamides to enhance amidic resonance. Remarkably, no previous studies have evaluated the energetic properties of ortho-substituted benzamides in contexts relevant to medicinal chemistry and organic synthesis. Similarly, the influence of steric ortho-substitution on the aromatic ring in benzamide derivatives regarding amide bond structure and energetics remains unexplored.

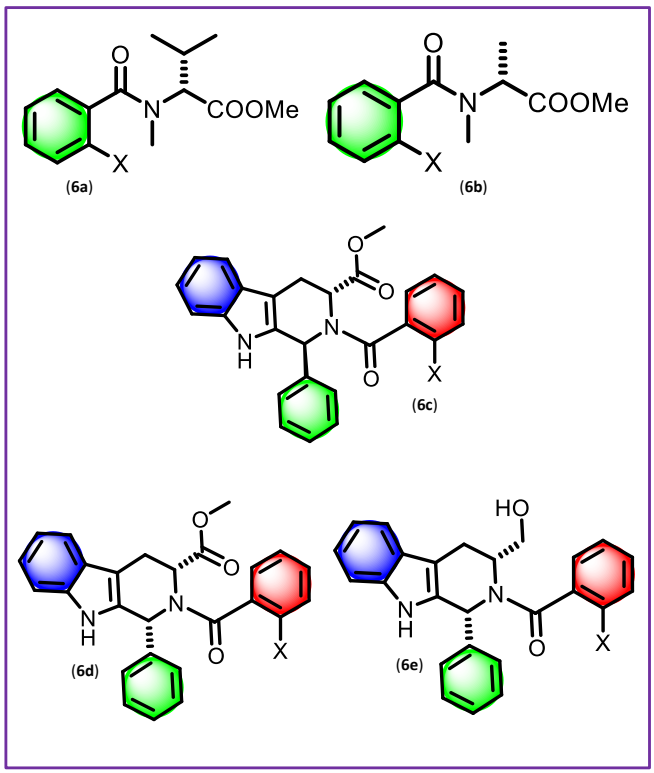

Figure 6: Rotational problem in o-halo benzamide derived tertiary amides in complex molecular framework: case study with molecules **6a**,**6b**,**6c**, and **6d** showing four rotational isomers at room temperature whereas **6e** shows two rotational isomers in absence of ester bonds.

2.4 RESULTS AND DISCUSSION:

Tertiary amides are capable of generating rotational isomers due to the rotation around the N–C(O) bonds. The dynamic structures mentioned throughout this paper adopt conformations which can be sorted adequately by comparing the relative orientation of the consecutive amide carbonyls, and methyl ester as seen the dynamic structures are observed perpendicular also parallel to the aromatic rings and this fluxional orientation bonds with ester carbonyls on one hand, and with amide carbonyls on the other hand, as a result of rotamers at room temperature. From the Temperature variant ^{1}H NMR study support that the number of rotamers were characterized. At low temperature actually exist as four rotational isomers.

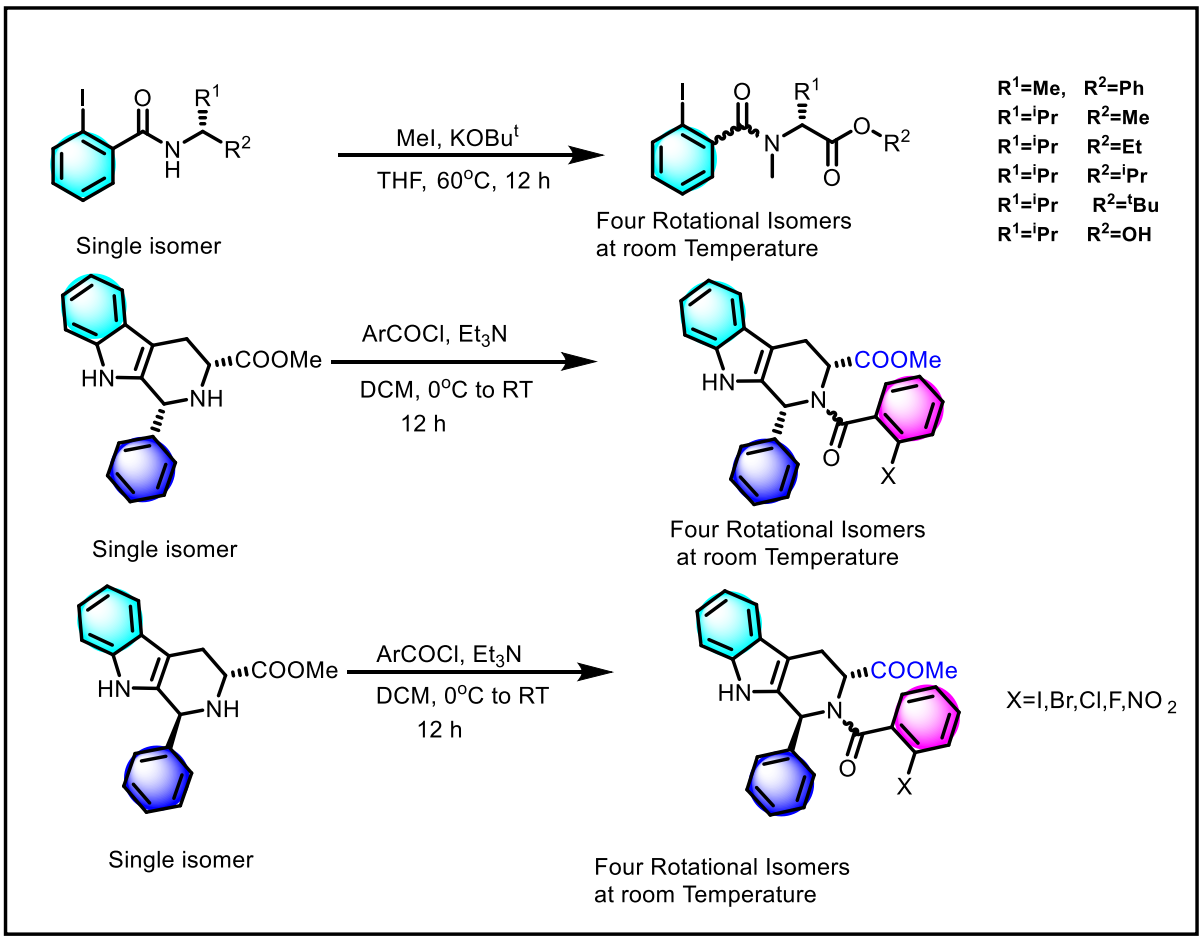

Figure 7: Synthesis of Various ortho substituted benzamide analouges under consideration.

Variable temperature ^{1}H NMR study:

Recording the proton NMR of the various synthesized molecules at room temperature provides very complicated spectra indicating the presence of several rotamers in solution at room temperature. In order to obtain information on the various structural conformers Variable temperature (VT) NMR experiments were performed and provides the following informations.

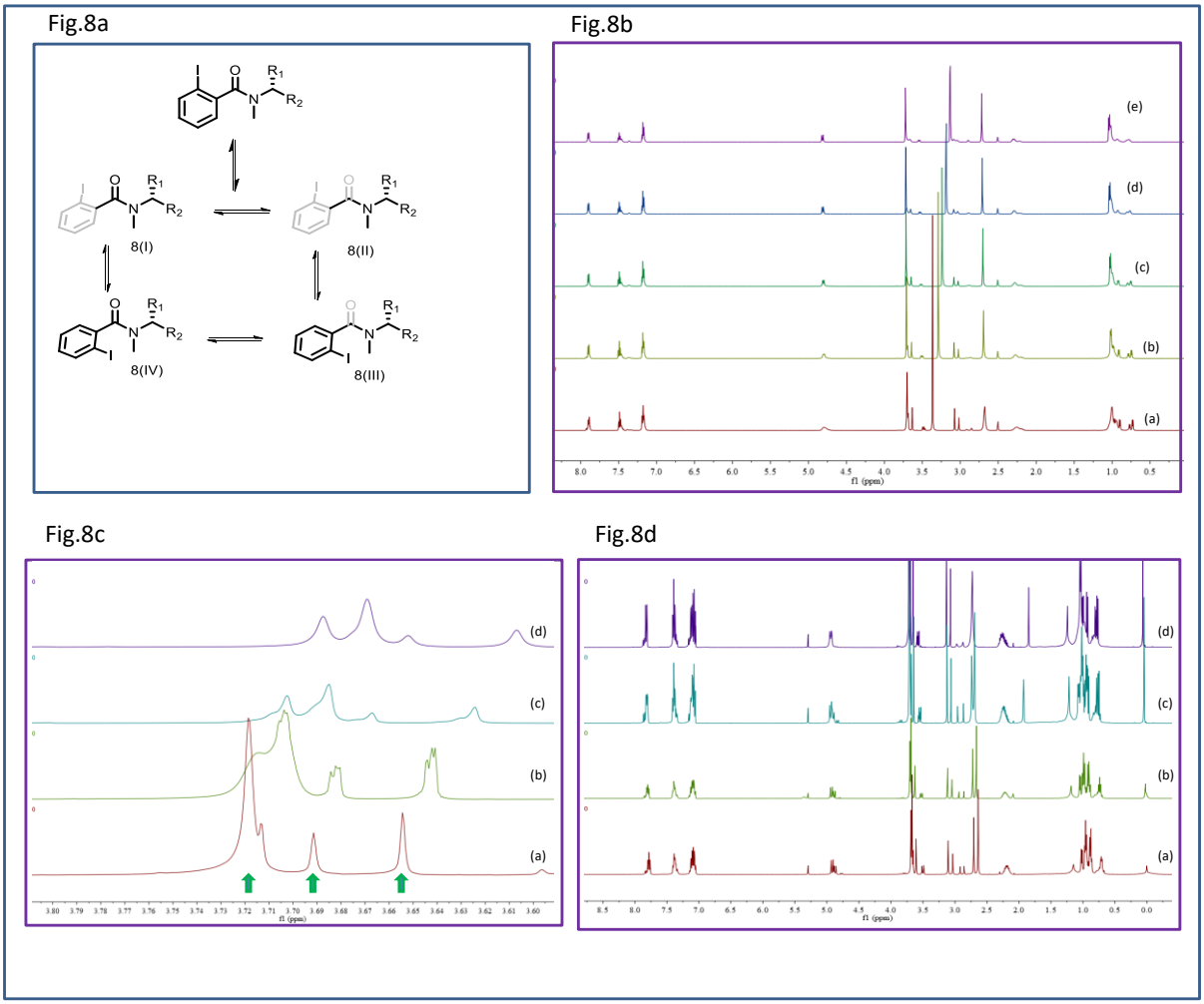

Figure 8: Variable temperature (VT) ^{1}H-NMR study of methyl N-(2-iodobenzoyl)-N-methyl -L-valinate **(8)**.

Observations:

- In CD_2Cl_2, the N-methyl signals of the amide group showed significant sensitivity to temperature increases. The signals broadened at 298 K, indicating the onset of dynamic exchange.
- In DMSO-d_6, these signals coalesced into a single lower-field signal at δ 3.10 ppm at 343 K, confirming dynamic averaging due to faster rotate at higher temperatures.

- The ester methyl signals remained in a rotate higher at 343 K in CD_2Cl_2, showing little temperature sensitivity compared to the amide group.
- In DMSO-d_6, at 343 K, the ester methyl signals merged into a single higher-field signal at δ 3.75 ppm, indicating unpredictable range in magnetic field.

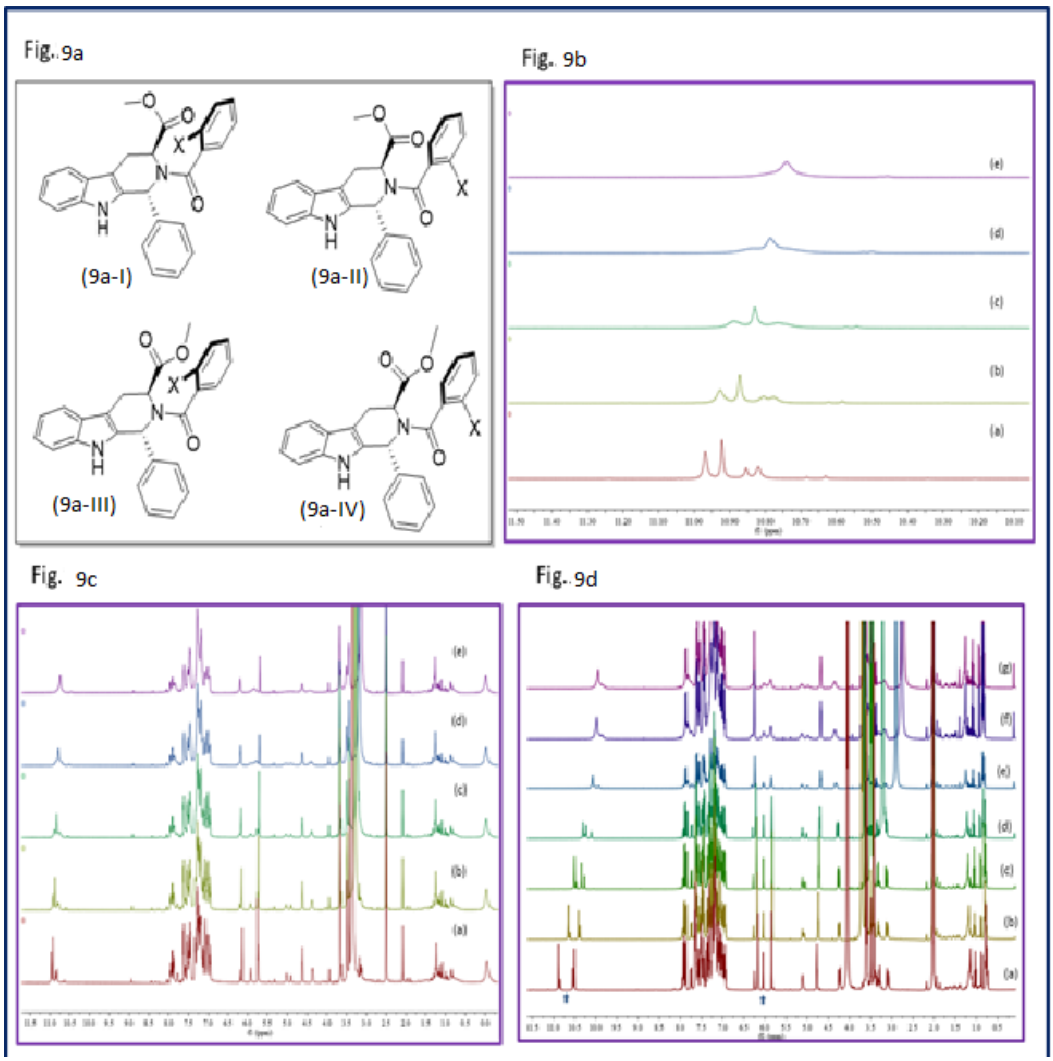

Figure 9: VT experiment on single diastereomer of **9a** molecule (where X=I, separated by column chromatography) to confirm the presence of rotamers.

In Fig. 9, VT-^{1}H-NMR spectroscopy was carried out in all the substituted amides to verify existence of various rotamers with geometrically perpendicular and parallel orientation of both amide and ester bonds one single diastereomer containing four rotamers. In conformation **9a(I)** C=O bond of both ester and amide are antiparallel to each other in addition to that the amide C=O and the phenyl are also antiparallel to each other. Whereas, in conformation 9a-II the C=O groups of both the mentioned functional groups are anti parallel but the phenyl ring and ester are parallel. In the next possible rotamer

(9a-III) both the C=O groups are parallel and the aryl ring is anti parallel to the amide C=O. Furthermore, in rotamer 9a-IV parallel orientation of both the ester amide C=O is observed and the aryl ring orients itself anti to the ester group. In Fig.9b enlarge overlap NH group peaks of Variable-temperature ^{1}H-NMR spectra of methyl (1R,3S)-2-(2-iodobenzoyl)-1-phenyl-2,3,4,9-tetrahydro-1H-pyrido[3,4-b]indole-3-carboxylate in DMSO-d_6 where (a) 303K, (b) 313K, (c) 323 K(d),333K.(e),343K. Fig.9c four rotational isomers at different temperature where (a),303K. (b),313K. (c),323K. (d),333K. (e),343K.. Fig.1d. Variable -temperature ^{1}H-NMR spectra of methyl (1R,3S)-2-(2-iodobenzoyl)-1-phenyl-2,3,4,9-tetrahydro-^{1}H-pyrido[3,4-b] indole-3-carboxylate in Acetone d_6 (a) 298K, (b)273K (c) 263K, (d)253K, (e)233K, (f) 213K, (g) 193K. Marking arrow represents how benzylic C-H proton and NH proton affects with temperature.

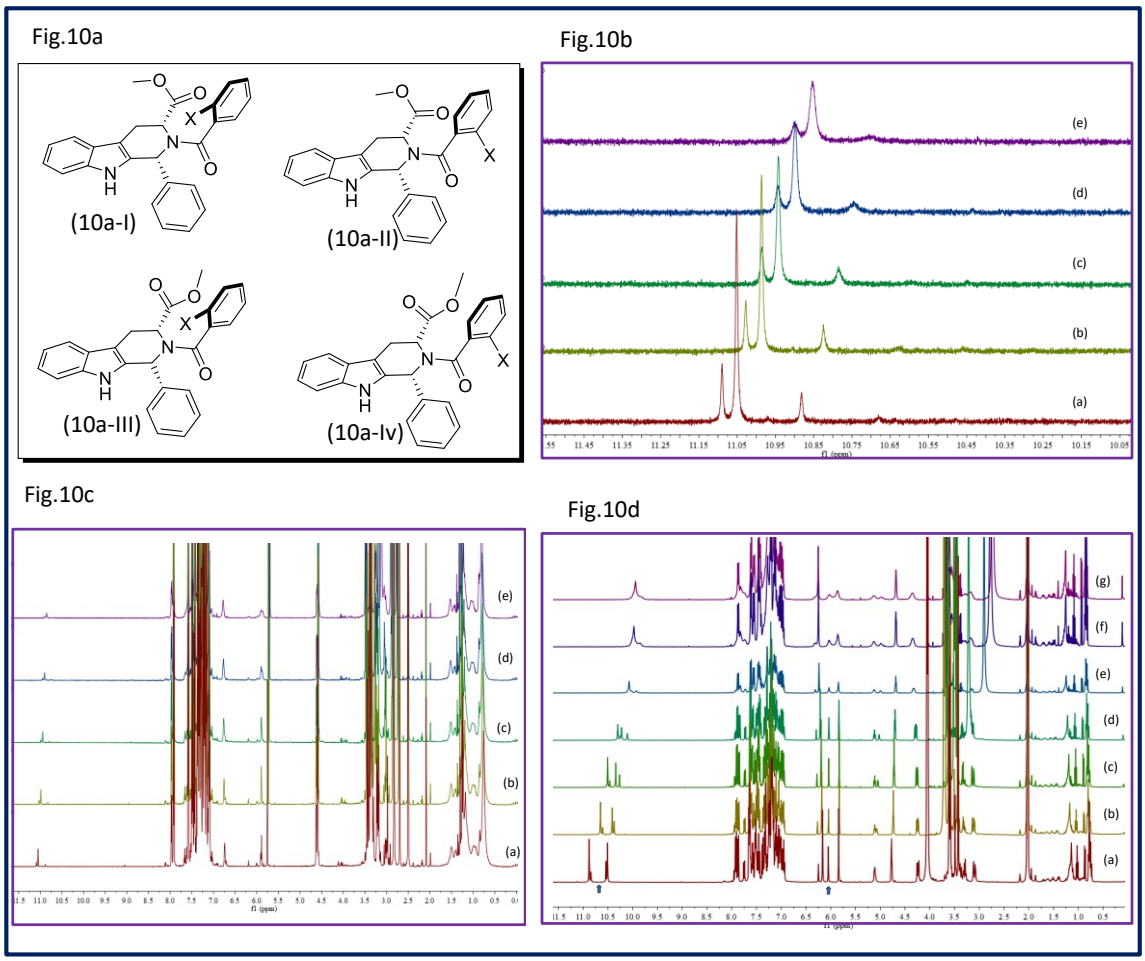

Figure 10: VT experiment with the other diastereomer of **9a** (separated by column chromatography).

The similar VT-^{1}H-NMR experiment was carried out with the corresponding diastereomer of **9a**, methyl-(1R,3R)-2-(2-iodobenzoyl)-1-phenyl-2,3,4,9-tetrahydro-1H-pyrido[3,4-b]indole-3-carboxylate in DMSO-d_6 at (a) 303 K, (b) 313 K, (c) 323 K, (d) 333 K, and (e) 343 K Similar observations of these diastereomers are observed as depicted earlier.

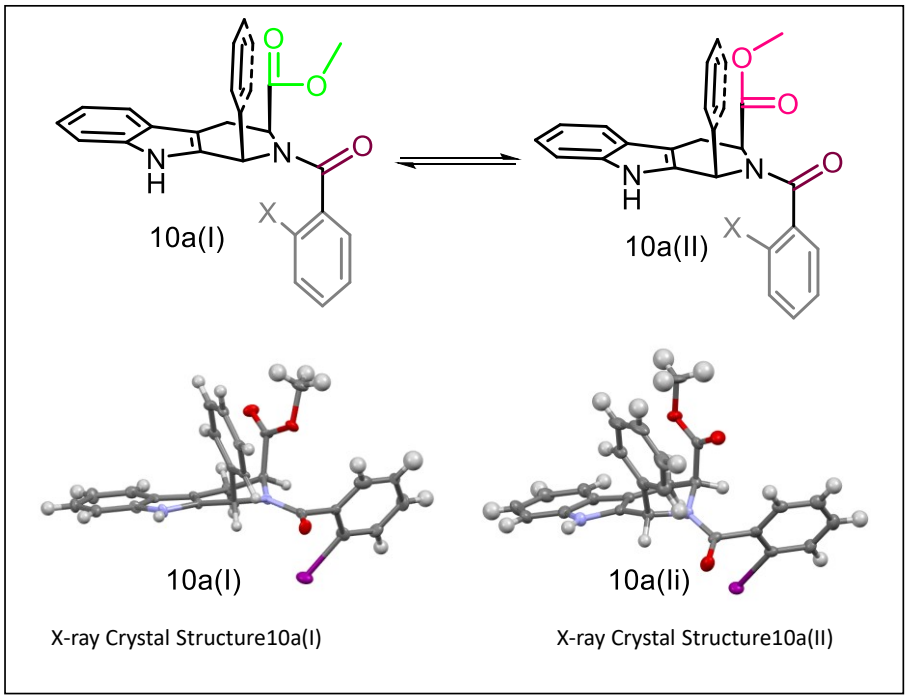

Figure 11: Crystal structure of isomers **10a** (X=I)

2.5 NMR solvent effect on rotational behaviour of two diastereomers:

Variable-temperature ^{1}H-NMR spectroscopy was employed to investigate the presence and dynamic behavior of rotamers in substituted amides, focusing on methyl (1R,3S)-2-(2-iodobenzoyl)-1-phenyl-2,3,4,9-tetrahydro-1H-pyrido[3,4-b]indole-3-carboxylate and methyl (1S,3S)-2-(2-iodobenzoyl)-1-phenyl-2,3,4,9-tetrahydro-1H-pyrido[3,4-b]indole-3-carboxylate. The study was conducted in different solvents, **DMSO-d_6** (at 600 MHz) and **acetone-d_6** (at 400 MHz), over a range of temperatures, as illustrated in **Fig. 9 and 10**.

DMSO-d_6:

- ✓ At 298 K, multiple overlapping signals were observed in the 1H-NMR spectra, indicating the existence of multiple rotamers due to restricted rotation about the amide and ester bonds.
- ✓ Upon heating to 343 K, the multiplicity of the methyl and aromatic proton signals resolved into distinct peaks. This change suggests faster exchange between rotameric states at elevated temperatures, leading to spectral simplification.
- ✓ Integration ratios of the resolved peaks matched the expected proportions, confirming the coexistence of rotamers.

- ✓ At both 298 K and 343 K, four distinct signals corresponding to indole-NH groups were consistently observed. This result suggests that the indole-NH groups maintain their proton environments and

do not participate in dynamic exchange processes under the experimental conditions.

Acetone-d_6:

- ✓ Similar spectral trends were observed in acetone-d_6 at 400 MHz, with signal multiplicity resolving upon heating. This consistency across solvents highlights that the rotational barriers are intrinsic to the molecular structure and not significantly influenced by solvent interactions.

2.6 Characterization of the rotamers:

Rotational Dynamics:

- ✓ The observed multiplicity at lower temperatures arises from restricted rotation around the ester bond, creating two distinct rotameric states.
- ✓ Upon heating, increased thermal energy allows these states to interconvert rapidly, resulting in averaged signals at higher temperatures.

Single-Crystal X-Ray Diffraction:

- ✓ Structural analysis confirmed the presence of two distinct rotameric structures, both characterized by the orientation of the ester group relative to the amide backbone.
- ✓ Interestingly, these two rotamers were isolated and crystallized under a single set of conditions, providing direct evidence of their equilibrium coexistence.

3.0 Computational details:

All quantum chemistry calculations were performed using the Gaussian 16 package. The molecules were optimized using different levels of theory. For X= F, Cl, and NO_2, quantum chemistry calculations involved the B3LYP functional and the 6-31+G(d,p) basis set. On the other hand, for X= Br, and I, the B3LYP/6-31+G(d,p) level of theory was employed for the lighter elements, while the B3LYP functional and both of the Karlsruhe valence triple-zeta polarization (def2-TZVP), and the augmented correlation-consistent polarized valence-only triple zeta (aug-cc-pVTZ-PP) basis sets were used separately in order to confirm the results.

2.7 Results and discussion:

We obtained four different rotamers for each of the different substituents originating from the rotation around the O=C-N-C, and the C-C-C(ester)-O dihedrals. Each of these rotamers had different extents of stability. The magnitudes of the mentioned dihedral angles associated with the different rotamers are summarized in Table 1. The most stable rotamer (II), was found to be associated with a O=C-N-C dihedral of nearly 0 degrees, and a C-C-C(ester)-O dihedral of -13 to -17 degrees for all of the variants except for X=NO_2, where the C-C-C(ester)-O dihedral was found to be around – 46 degrees. The next stable rotamer (I) was less stable with respect to the rotamer II, having a O=C-N-C dihedral of around -3 to -4 degrees and C-C-C(ester)-O dihedral of 174 to 175 degrees. Rotamer III was found to be slightly less stable compared to rotamer II, and consisted of a O=C-N-C dihedral of -172 to -178 degrees, and C-C-C(ester)-O dihedral of -53 to -58 degrees for all variants except for X=NO_2, where the C-C-C(ester)-O dihedral was found to be around – 46 degrees. The least stable rotamer (IV) was 3-3.5 kcal/mol less stable as compared to rotamer I, having a O=C-N-C dihedral of -171 to -179 degrees, and C-C-C(ester)-O dihedral of -147 to -159 degrees. The different rotational relationships which produce the rotamers have been shown in Figure 12.

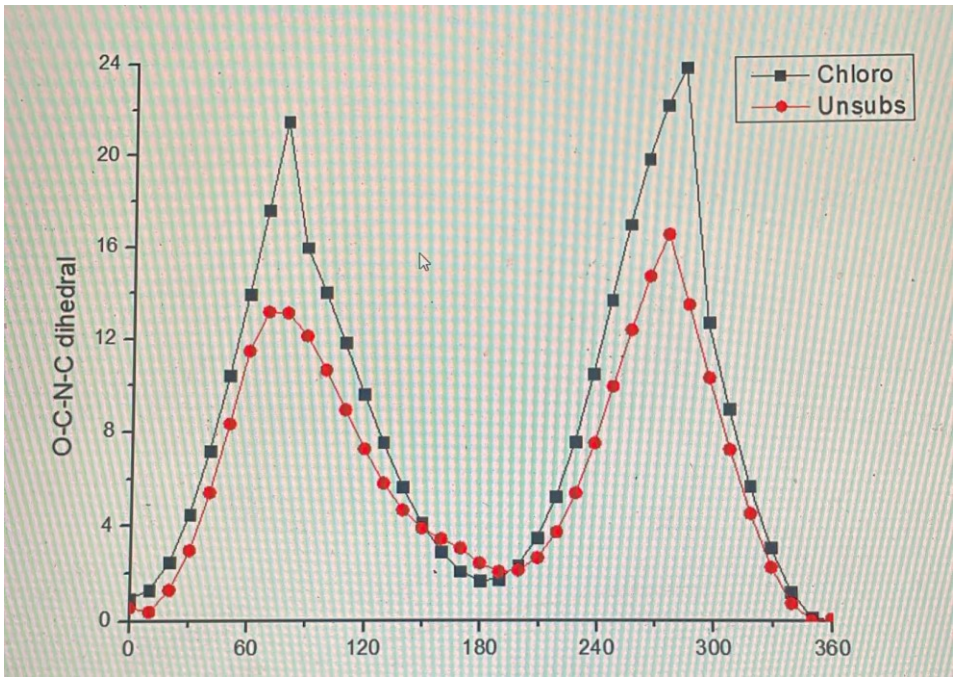

Figure 12: Different rotational relationships of rotamers

Different rotamers of the molecule for various substituents along with the O=C-N-C, and the C-C-C(ester)-O dihedral angles associated with them, and their relative energies, as obtained from quantum chemical calculations.

Substituent (level of theory of optimization)	Rotamer	O=C-N-C dihedral 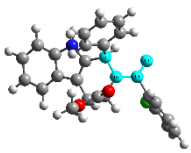	C-C-C(ester)-O dihedral 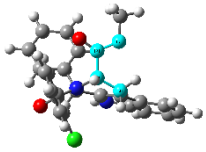	Relative energy (kcal/mol)
X=F B3LYP/6-31+G(d,p)	I	0.24	-13.29	1.26
	II	-4.37	175.50	0
	III	-171.97	-58.32	1.44
	IV	-176.07	147.05	3.39
X= Cl B3LYP/6-31+G(d,p)	I	-0.27	-15.12	0.94
	II	-3.72	174.86	0
	III	-176.55	-53.86	1.63
	IV	-179.98	153.11	3.51
X= NO_2 B3LYP/6-31+G(d,p)	I	-0.01	-46.37	0.13
	II	-3.54	174.22	0
	III	-172.12	-46.71	1.32
	IV	-171.15	158.98	3.26
X= Br (B3LYP/def2-TZVP for Br)	I	-0.23	-14.60	0.94
	II	-3.52	174.53	0
	III	-177.38	-53.55	1.69
	IV	-179.16	154.28	3.51
X= Br (B3LYP/aug-cc-pVTZ-PP for Br)	I	-0.28	-14.22	0.94
	II	-3.54	174.68	0
	III	-177.61	-53.46	1.69
	IV	-178.97	154.33	3.51
X=I (B3LYP/def2-TZVP for I)	I	0.16	-17.40	0.88
	II	-3.39	174.04	0
	III	-178.14	-52.83	1.88

	IV	-178.32	155.54	3.64
(B3LYP/aug-cc-pVTZ-PP for I)	I	0.14	-17.33	0.88
	II	-3.40	174.05	0
	III	-178.15	-52.75	1.88
	IV	-178.30	155.54	3.64

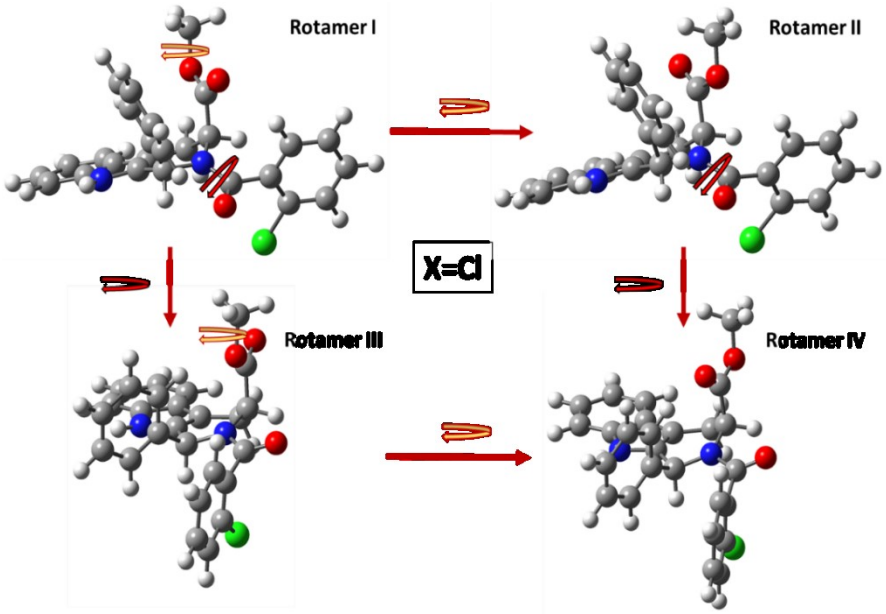

Figure 13: Structures of the four rotamers obtained from the quantum chemical optimization of the molecule for X=Cl at the B3LYP/6-31+G(d,p) level, and rotational relationship between them. Rotamer II and IV can be obtained through the rotation along the C-C-C(ester)-O dihedral to produce rotamers I and III respectively, while rotamer III and IV can be produced from rotamers I and II through the rotation along the O=C-N-C dihedral.

3.2 Conclusion:

In conclusion, our study delves into the computational exploration of the impact of ortho-substitution on resonance and barriers to rotation in tertiary aromatic amides. Notably, ortho-substituted amidesand ester, prominently featured in biologically relevant compounds and pivotal for reactivity, exhibit heightened barriers to rotation along both the N−C(O) and C−C(O) axes. This effect aligns with steric repulsion between the ortho-substituent and the amide and ester oxygen atom. The rotational profiles depict a substantial increase in rotational barriers around the C−C(O) bond (up to 3.64 kcal/mol) and a notable increase in barriers to rotation along the N−C(O) bond (up to 1.88 kcal/mol). Additionally, we have explored proton affinities and variations in proton affinities in ortho-substituted amides. Our findings highlight the potential to manipulate amidic resonance, ranging from virtually nonexistent to >3.0 kcal/mol, through a thoughtful selection of amide bond substitution. Ongoing efforts in our research focus on

further investigating the structural and energetic properties of amides. We anticipate that these endeavors will ultimately contribute to the establishment of a well-defined resonance scale for the amide bond and ester bond. The VT-^{1}H-NMR and single-crystal X-ray diffraction studies reveal critical details about the rotational dynamics and structural flexibility of substituted amides. The coexistence of two rotameric states, observable across different solvents and confirmed by crystallographic analysis, provides a comprehensive picture of how molecular structure dictates dynamic behavior. These findings have significant implications for the design and application of substituted amides in fields such as medicinal chemistry and materials science, where rotational flexibility can influence function and reactivity. Addressing the impact of ortho- and ester-substitution on the resonance and conformational behavior of benzamides could unlock new possibilities in:

- **Drug Design**: Enhanced understanding of these interactions can lead to the design of more potent and selective biologically active compounds.
- **Synthetic Applications**: Tailored resonance effects and restricted conformations can enable the development of more efficient and selective catalytic systems, as well as novel synthetic strategies.
- **Material Science**: Rigid, resonance-stabilized structures have potential applications in advanced materials with tunable properties.

This study underscores the need for a comprehensive exploration of these effects using a combination of computational modeling and experimental validation. Such investigations will not only fill a critical knowledge gap but also pave the way for innovative applications in both chemical and biological sciences.

Supporting Information

2.8 General Information

All the reagents and solvents used in the present study were purchased from Sigma-Aldrich, TCI and Thermo Fischer Scientific, respectively. All reactions were carried out in an oven-dried reaction tube under an air atmosphere. Silica gel TLC plate were used to perform TLC analysis.All the ^{1}H and ^{13}C NMR spectra were recorded in a 400 MHz and 600 MHz spectrometer. ESI mass spectral analysis was done using the LCQ-ORBITRAP-XL instrument. Bruker Kappa Apex II X-ray crystallography machine was used to solve the crystal structure. Singlet (s), doublet (d), triplet (t), and multiplet (m) were designated as ^{1}H NMR multiplicity patterns. Silica gel (100−200 mesh) and

(230−400 mesh) were used for column chromatographic separations. Single crystals of products were obtained through slow evaporation (at room temperature) of a solution in chloroform.

4.1 General Synthetic Procedure.

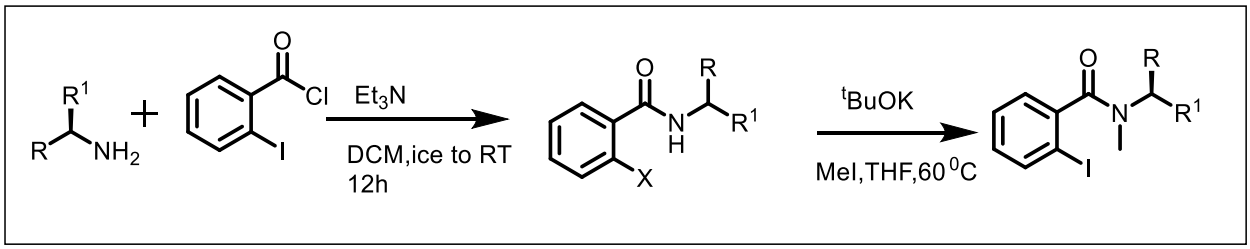

4.1.1 General Procedure A: Synthesis of Amide from Acid Chloride

To a dried round bottom flask equipped with a magnetic stir bar was added a solution of the respective aryl carboxylic acid chloride (2.0mmol, 1 equiv) in DCM (20 Eqv), corresponding amine (2.4 mmol,1.2 equiv.), 0 °C under N_2 atmosphere. The reaction was allowed to stir for 12 h. After completion, the reaction mixture was diluted with DCM (50 mL). The organic layer was washed with aq. $NaHCO_3$ (15 mL), brine (25 mL). Combined organic layer was dried over anhydrousNa_2SO_4, evaporated under *vaccuo*. Resulting crude mixture was purified by column chromatography using EtOAc:Hexane to afford the desired Amide compound.

4.1.2 General ProcedureB : Synthesis of N-methyl amide from their corresponding amide.

To a dried round bottom flask equipped with a magnetic stir bar was added a solution of the respective Amide (1.0mmol, 1 equiv) in Dry THF (20 Eqv), Potassium tertbutoxide (1.5 mmol,1.5 equiv.), 0 °C under N_2 atmosphere, Then methyl iodide (3 mmol,3Eqv). Was added. The reaction was allowed to stir for 12 hours at 60^0C . After completion, the reaction mixture was Evaporate to Dryness & diluted with Ehyl acetate(50 mL). The organic layer was washed with saturated $NaHCO_3$ (15 mL), brine (25 mL). Combined organic layer was dried over anhydrous Na_2SO_4, evaporated under *vaccuo*. Resulting crude mixture was purified by column chromatography using EtOAc:Hexane to afford the desired n-methyl Amide(3yy).

4.1.3 Procedure C.Synthesis of different alkyl ester from their corresponding methyl ester.

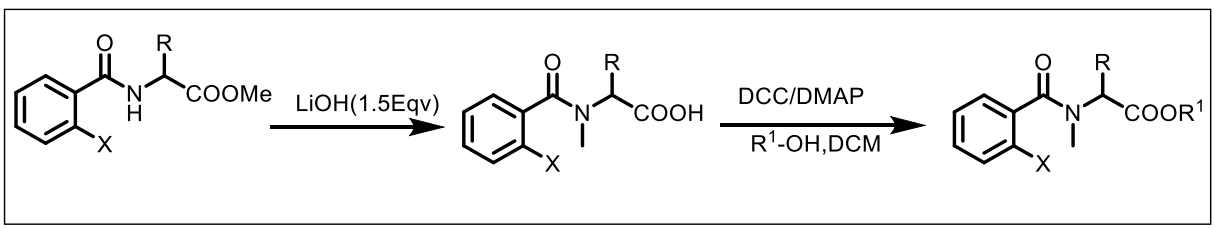

4.1.3.1 Procedure C(A) .To a dried round bottom flask equipped with a magnetic stir bar was added a solution of the respective methyl Ester(3yy) (1.0mmol, 1 equiv) in THF:MeOH:Water (1:1:1), Lithium Hydroxide (1.5 mmol,1.5 equiv.), 0 °C under N_2 atmosphere. The reaction was allowed to stir for 12 hours at Room Temperature. After completion, the reaction mixture was Evaporate to Dryness & diluted with Ehyl acetate(50 mL). The organic layer was washed with saturated aq. Citric Acid (15 mL), brine (25 mL) Combined organic layer was dried over anhydrous Na_2SO_4, evaporated under *vaccuo*. Resulting crude mixture was purified by column chromatography using EtOAc:Hexane to afford the desired Acid compound .

4.1.3.2 Procedure C(B). This Acid was added in a dried round bottom flask equipped with a magnetic stir bar, Dichloromethane was added at 0^0C. Then alcohol (5Eqv),DCC(1.3Eqv), DMAP(0.1Eqv) was added. The reaction was allowed to stir for 12 hours at Room Temperature.The Reaction mixture was passed through the celite pad, evaporated under *vaccuo*. Resulting crude mixture was purified by column chromatography using EtOAc:Hexane to afford the desired Acid compound (5ww).

4.2 Synthesis Of methyl N-(2-iodobenzoyl)-N-methyl-L-valinate.

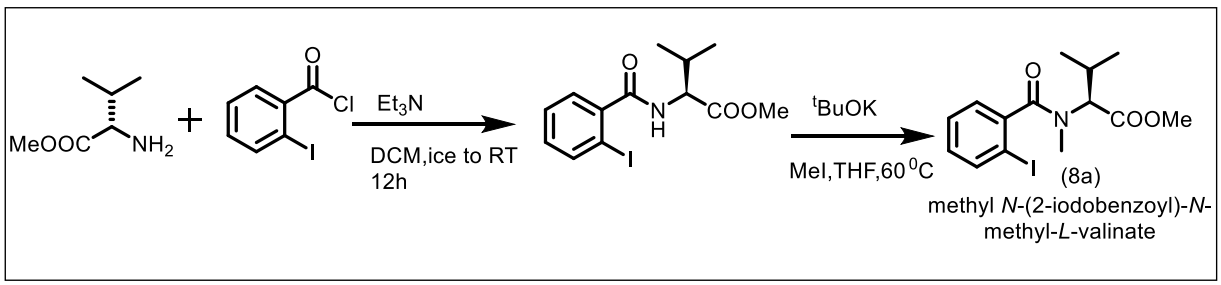

The same general procedure A&B was followed with 2-Iodobenzoyl Chloride 0.25g (2.0mmol, 1.0 equiv.),l-Valine methyl ester Hydrochloride(2.4mmol, 1.2 equiv.), potassium tertbutoxide (3.0mmol, 1.5 equiv.), Methyl Iodide(6.0mmol, 3.0 equiv.),Column chromatography (SiO_2, eluting with 20% ethyl acetate/pet ether) afforded the desired product 3a as liquid

^{1}H NMR (400 MHz, Chloroform-*d*) δ 7.86 – 7.72 (m, 1H), 7.42 – 7.18 (m, 7H), 7.09 – 6.98 (m, 1H), 6.27 (s, 1H), 5.26 (q, *J* = 7.2 Hz, 1H), 1.59 (d, 3H).
^{13}C NMR (101 MHz, CHLOROFORM-*D*) δ 168.50, 142.71, 142.22, 139.86, 131.11, 128.77, 128.40, 128.21, 127.59, 126.57, 92.56, 49.56, 21.60.

^{1}H NMR Of methyl (2-iodobenzoyl)-L-valinate(8a)

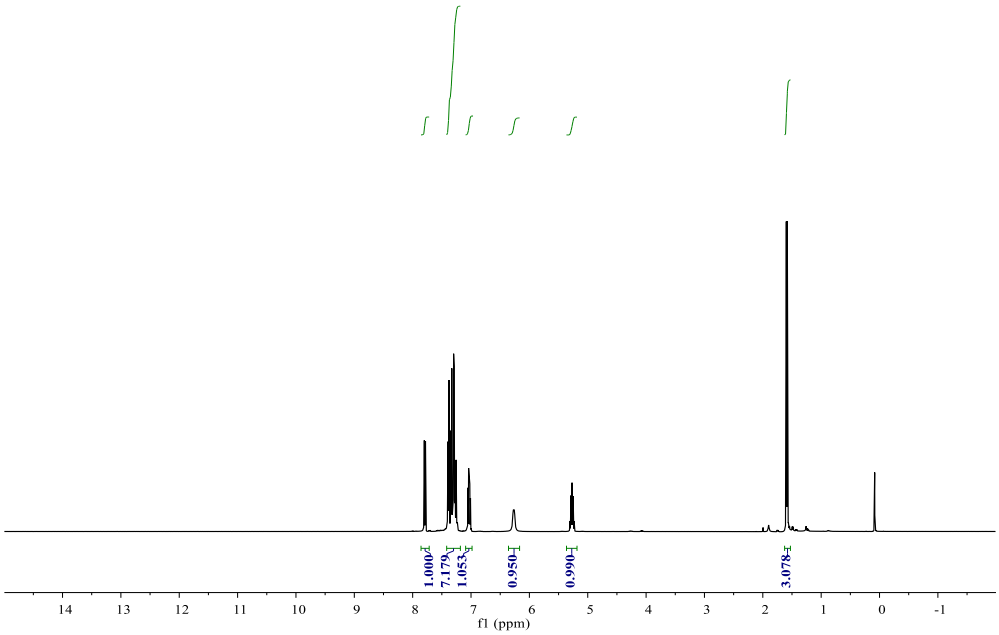

^{13}C NMR Of methyl (2-iodobenzoyl)-L-valinate(8a)

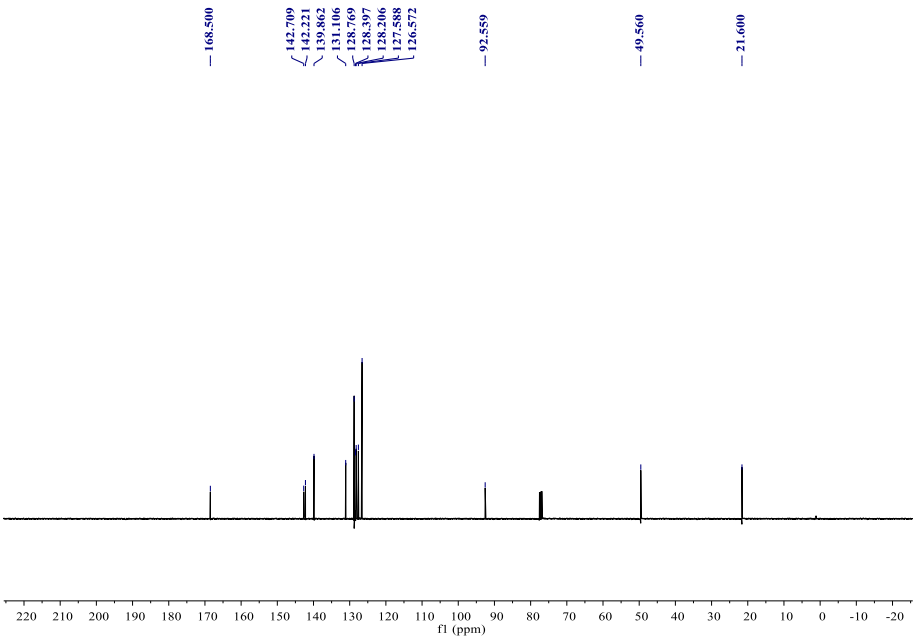

^{1}H NMR Of methyl N-(2-iodobenzoyl)-N-methyl-L-valinate(8a)

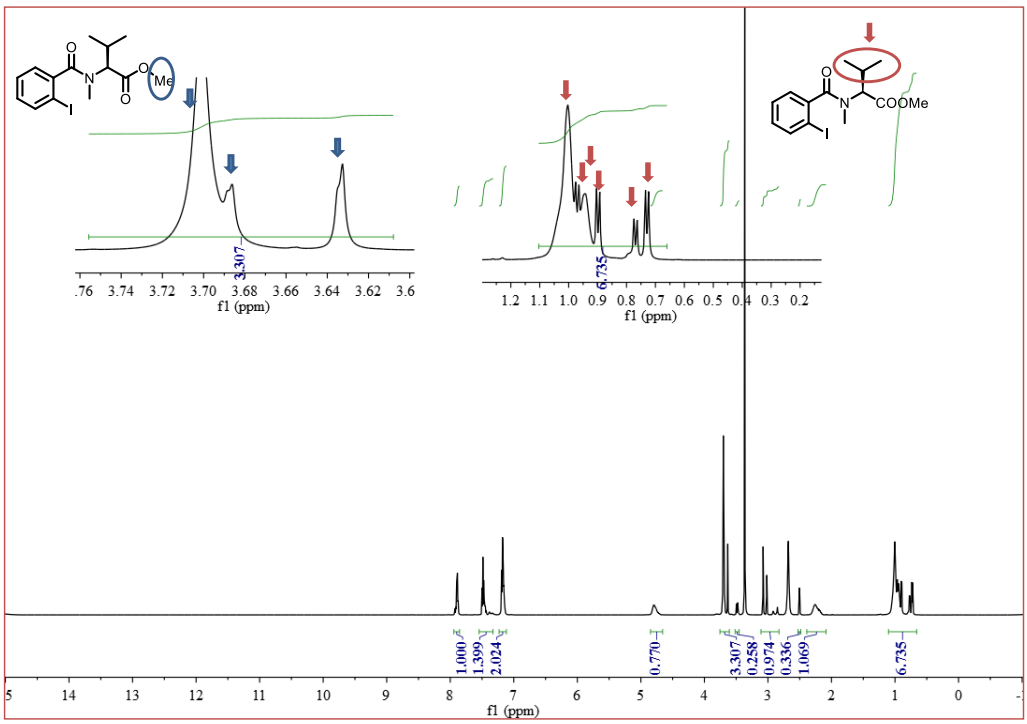

^{13}C NMR of methyl N-(2-iodobenzoyl)-N-methyl-L-valinate(8a) at room temperature

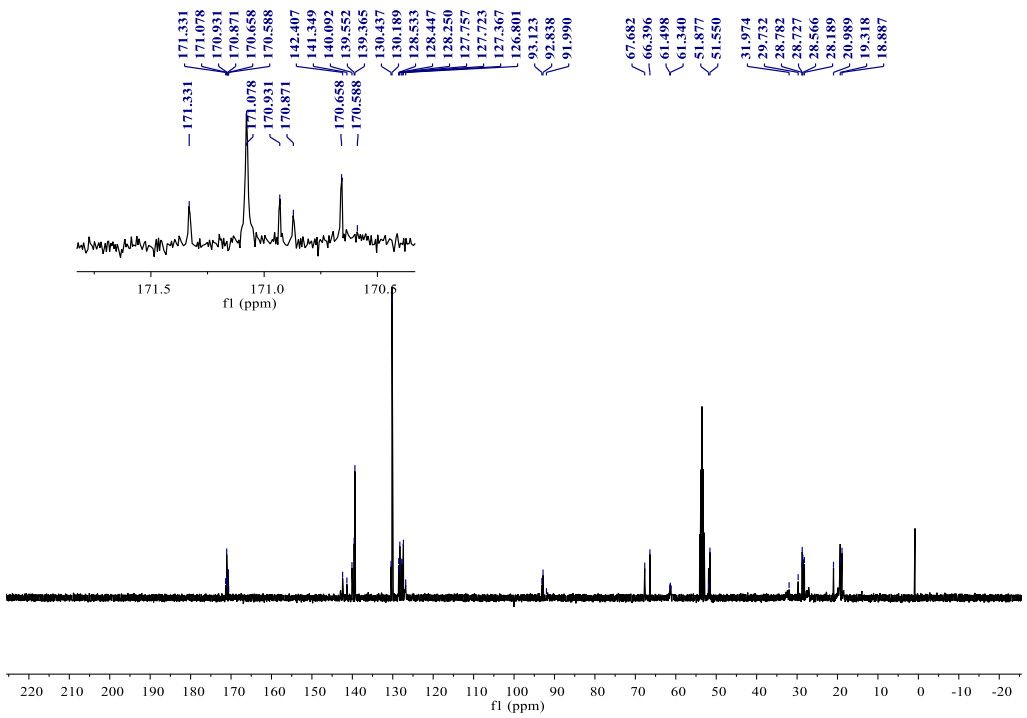

^{1}H NMR Of methyl N-(2-iodobenzoyl)-N-methyl-L-valinate(8a) in Different temperature in DMSO-D6

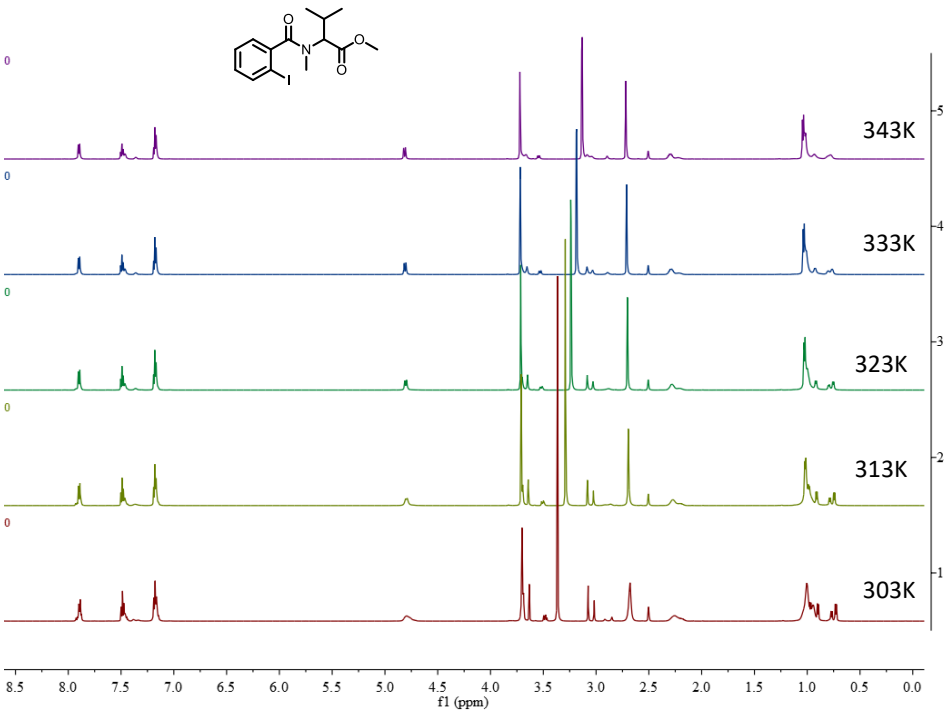

^{1}H NMR Of methyl N-(2-iodobenzoyl)-N-methyl-L-valinate(8a) in Different temperature in DMSO-D6

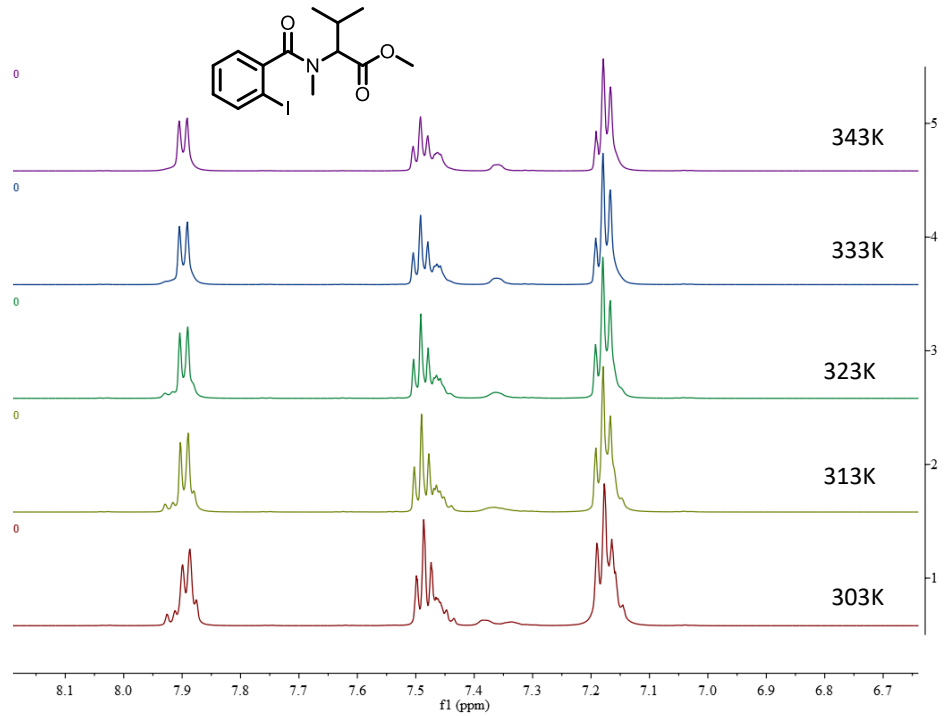

[1]H NMR Of methyl N-(2-iodobenzoyl)-N-methyl-L-valinate(8a) at 343K temperature in DMSO-D6

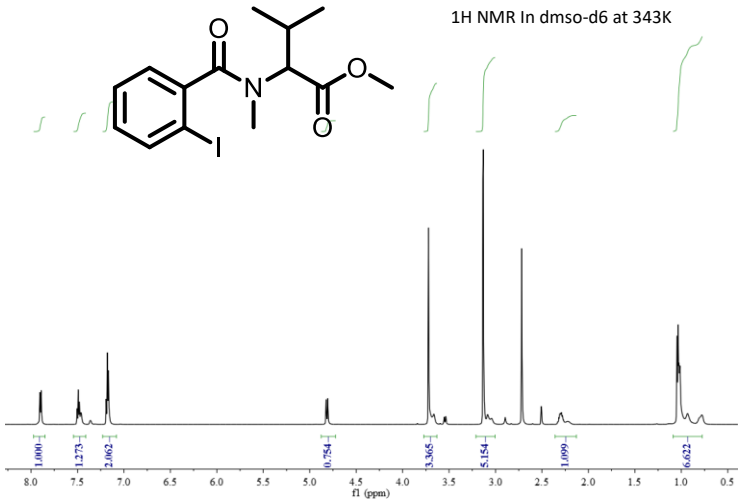

[13]C NMR of methyl N-(2-iodobenzoyl)-N-methyl-L-valinate(8a) at 343K temperature in DMSO-D6

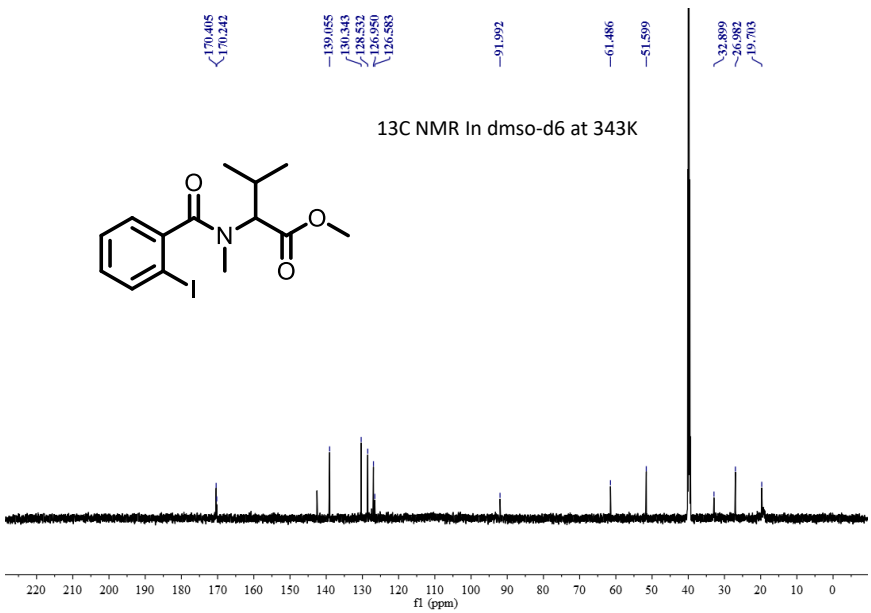

3.3 Synthesis of methyl N-(2-iodobenzoyl)-N-methyl-L-alaninate.

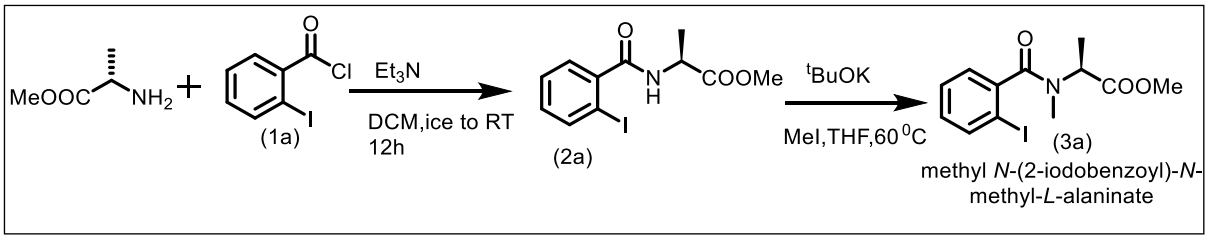

The same general procedure A&B was followed with 2-Iodobenzoyl Chloride 0.25g (2.0mmol, 1.0 equiv.),l-alanine methyl ester Hydrochloride(2.4mmol, 1.2 equiv.), potassium tertbutoxide(3.0mmol, 1.5 equiv.), Methyl Iodide(6.0mmol, 3.0 equiv.),Column chromatography (SiO_2, eluting with 20% ethyl acetate/pet ether) afforded the desired product 3a as liquid

1H NMR in $CDCl_3$ methyl N-(2-iodobenzoyl)-N-methyl-L-alaninate.

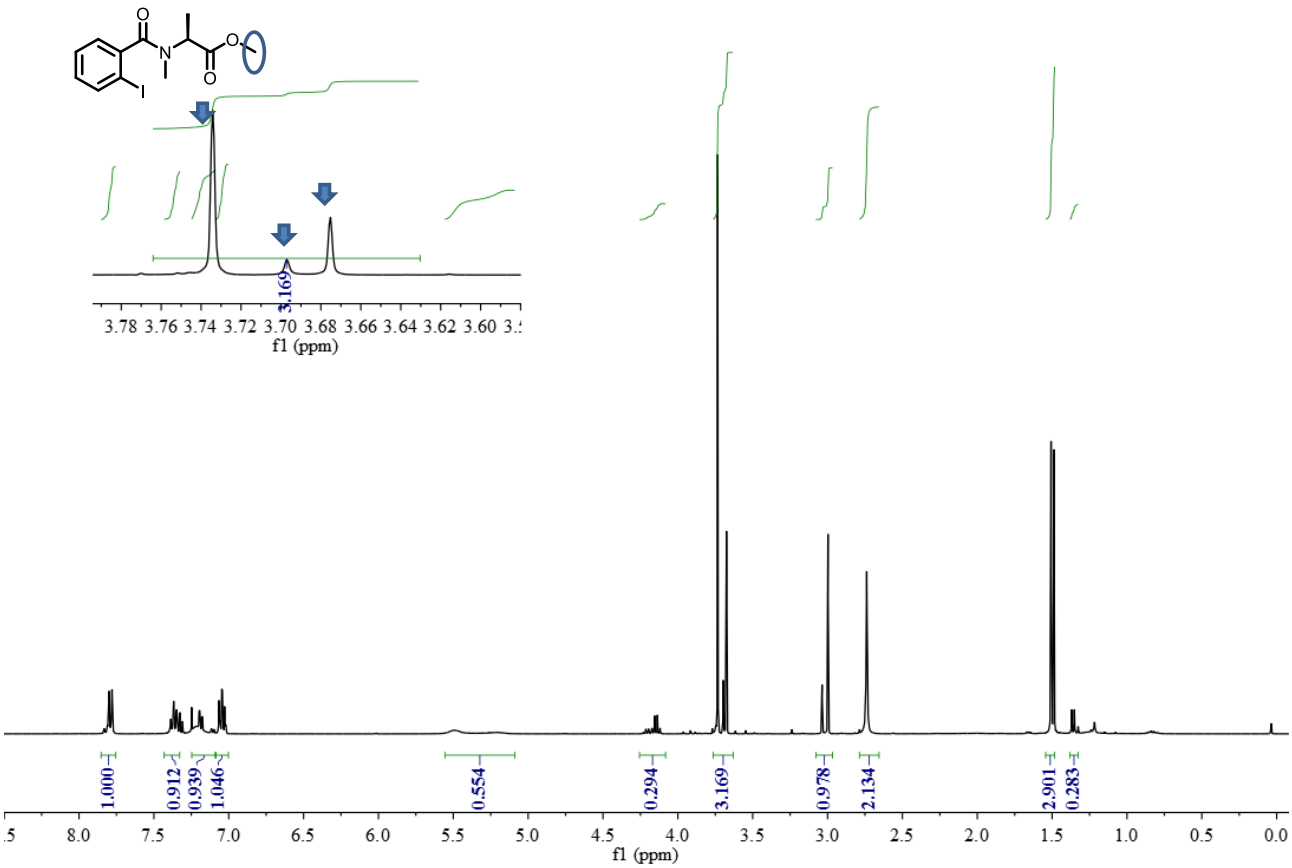

^{13}C NMR in $CDCl_3$ methyl N-(2-iodobenzoyl)-N-methyl-L-alaninate.

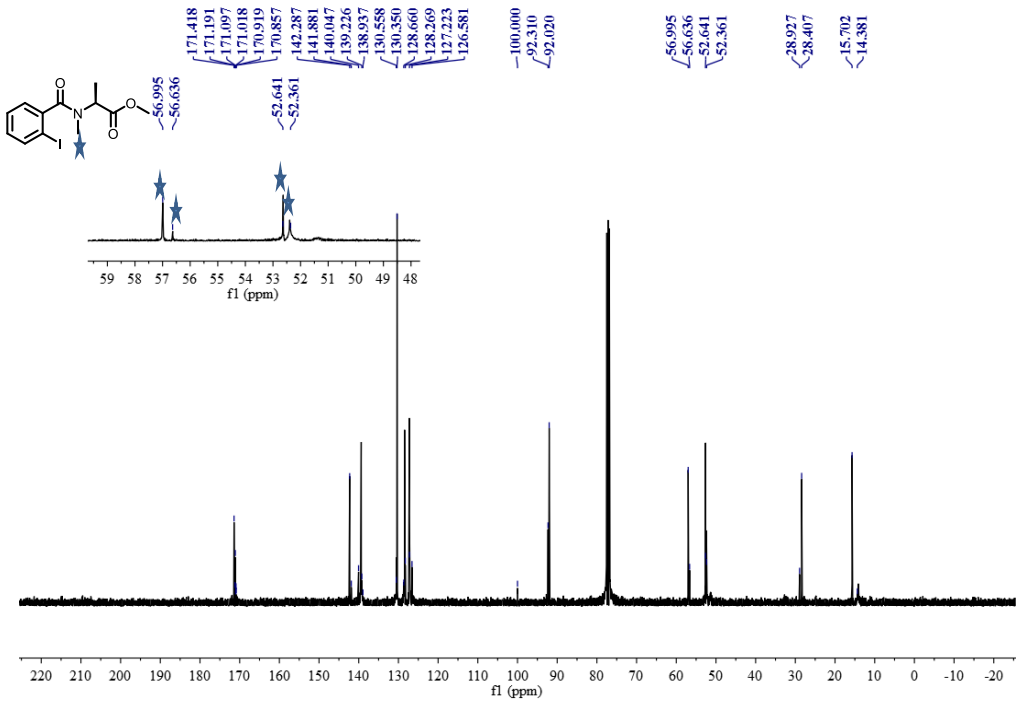

3.4 Synthesis Of N-(2-iodobenzoyl)-N-methyl-L-valine.

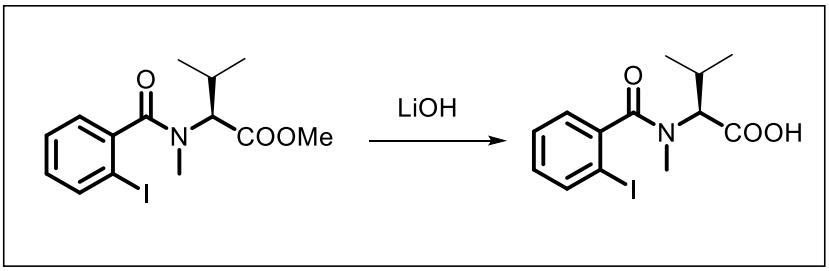

The same general procedure C(A) was followed with methyl N-(2-iodobenzoyl)-N-methyl-L-valinate.(3a) (2.0mmol, 1.0 equiv.), Lithium Hydroxide (3mmol, 1.5 equiv.), THF:MeOH:Water=1:1:1,Column chromatography (SiO_2, eluting with 60% ethyl acetate/pet ether) afforded the desired product 4a as White Solid (, 80 %yield)

^{1}H NMR in $CDCl_3$ of Of N-(2-iodobenzoyl)-N-methyl-L-valine.

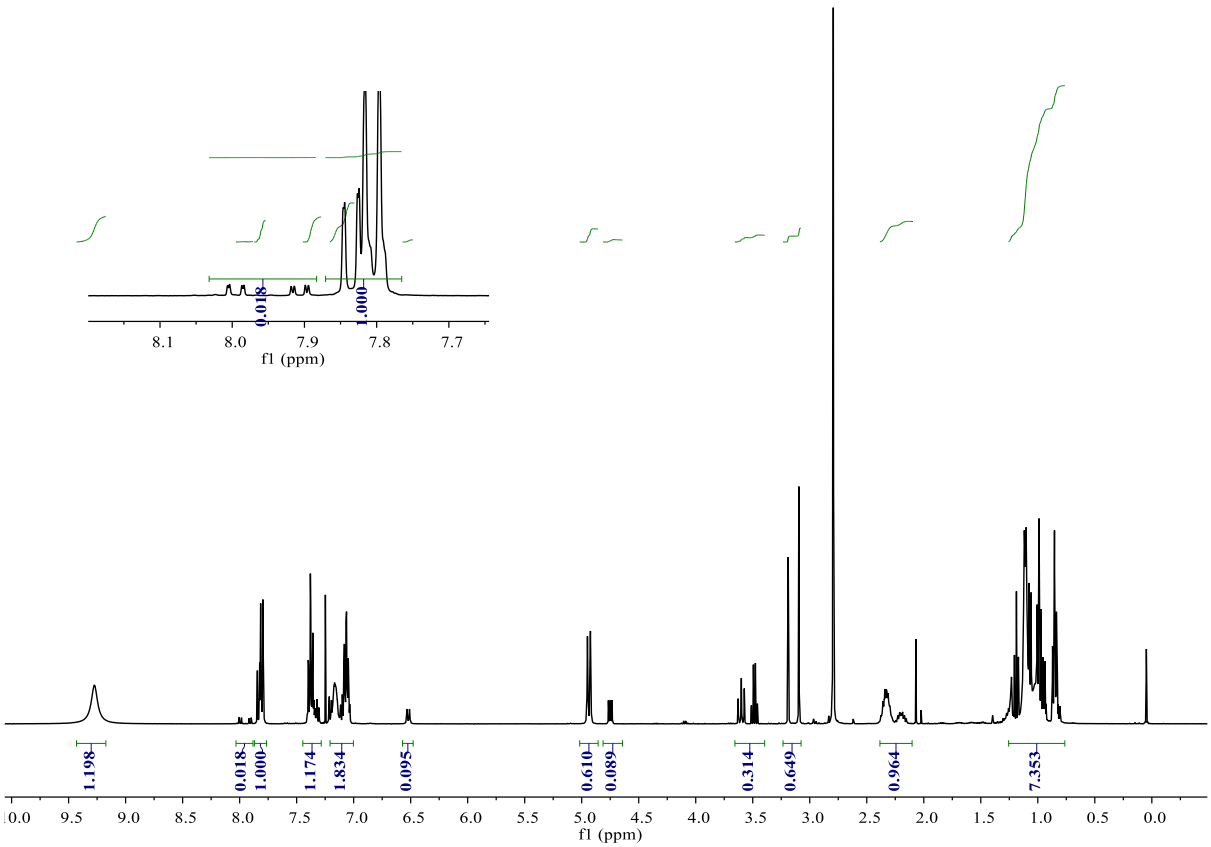

^{13}C NMR in $CDCl_3$ Of N-(2-iodobenzoyl)-N-methyl-L-valine.

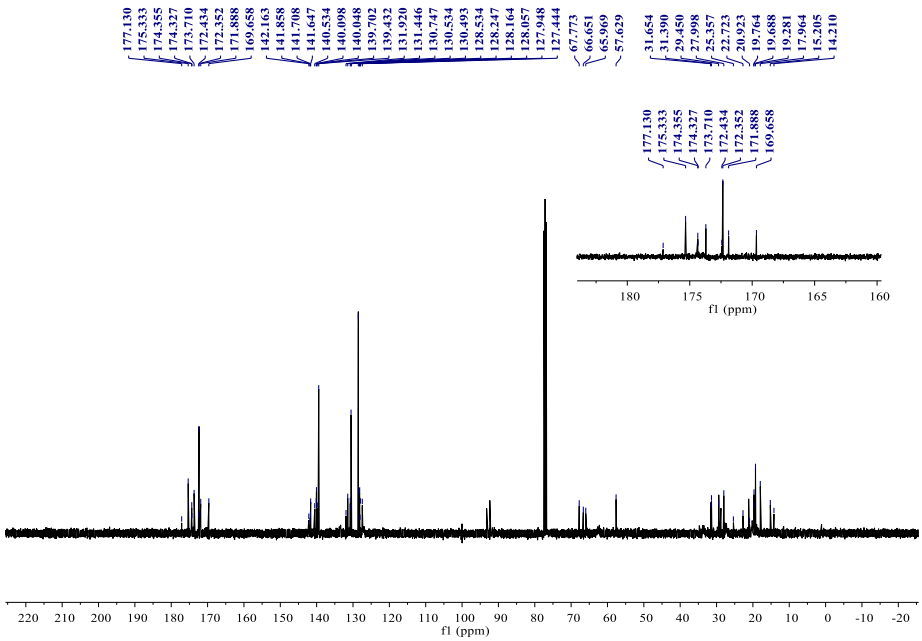

3.6 Synthesis Of ethyl N-(2-iodobenzoyl)-N-methyl-L-valinate.

Fig.20

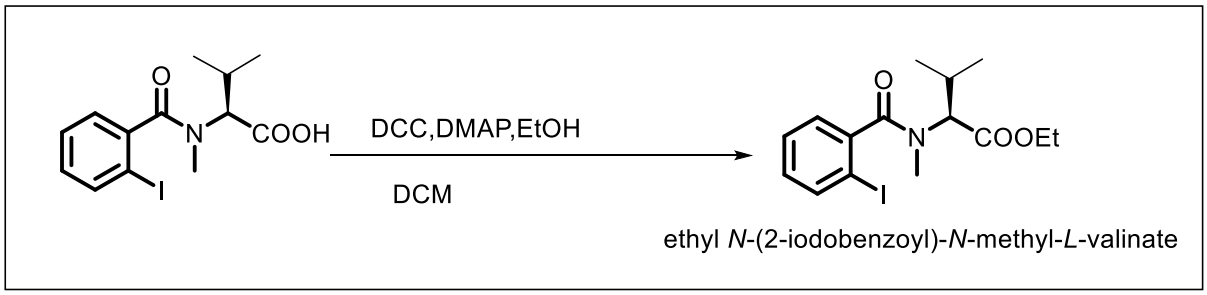

The same general procedure C(B) was followed with N-(2-iodobenzoyl)-N-methyl-L-valine (3a) (2.0mmol, 1.0 equiv.), DCC (2.6mmol, 1.3 equiv.), DMAP (0.1mmol, 0.1 equiv.), EtOH (3mmol, 1.5 equiv.), ,Column chromatography (SiO_2, eluting with 20% ethyl acetate/pet ether) afforded the desired product 5a as White Solid (, 80 %yield).

^{1}H NMR in $CDCl_3$ of ethyl N-(2-iodobenzoyl)-N-methyl-L-valinate.

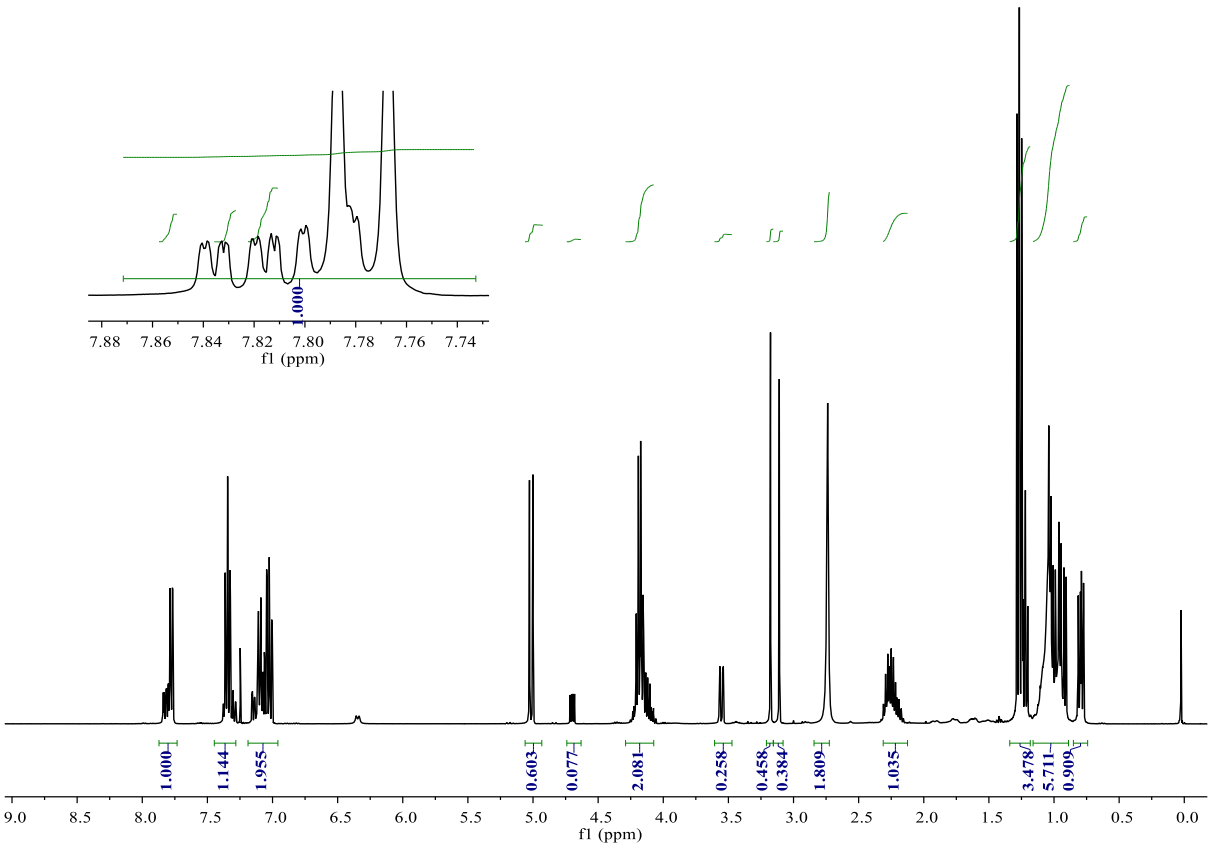

^{13}C NMR in $CDCl_3$,ethyl N-(2-iodobenzoyl)-N-methyl-L-valinate.

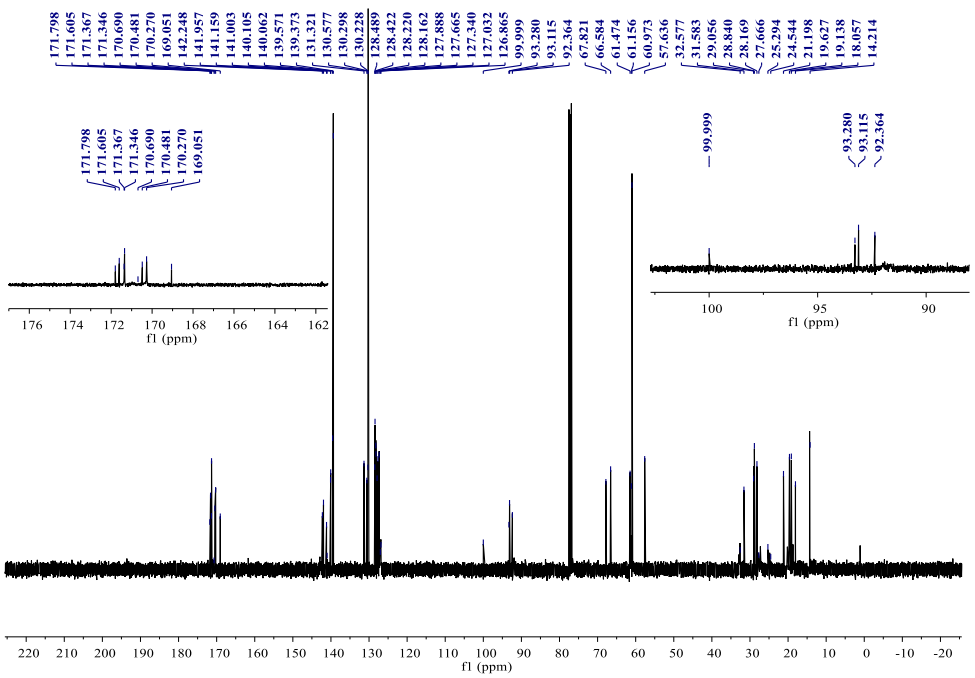

3.7 Synthesis of isopropyl N-(2-iodobenzoyl)-N-methyl-L-valinate.

Fig.21

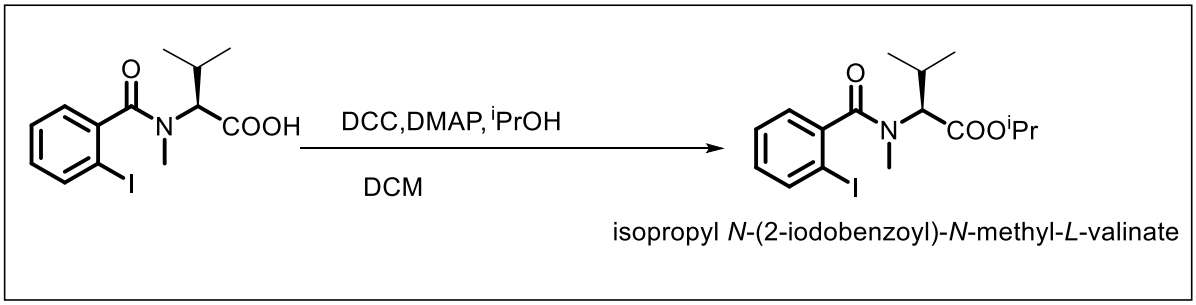

isopropyl *N*-(2-iodobenzoyl)-*N*-methyl-*L*-valinate

The same general procedure C(B) was followed with N-(2-iodobenzoyl)-N-methyl-L-valine (3a) (2.0mmol, 1.0 equiv.), DCC (2.6mmol, 1.3 equiv.), DMAP (0.1mmol, 0.1 equiv.), ^{i}PrOH (3mmol, 1.5 equiv.) ,Column chromatography (SiO_2, eluting with 20% ethyl acetate/pet ether) afforded the desired product 5a as White Solid (, 80 %yield).

^{1}H NMR in $CDCl_3$ of isopropyl N-(2-iodobenzoyl)-N-methyl-L-valinate.

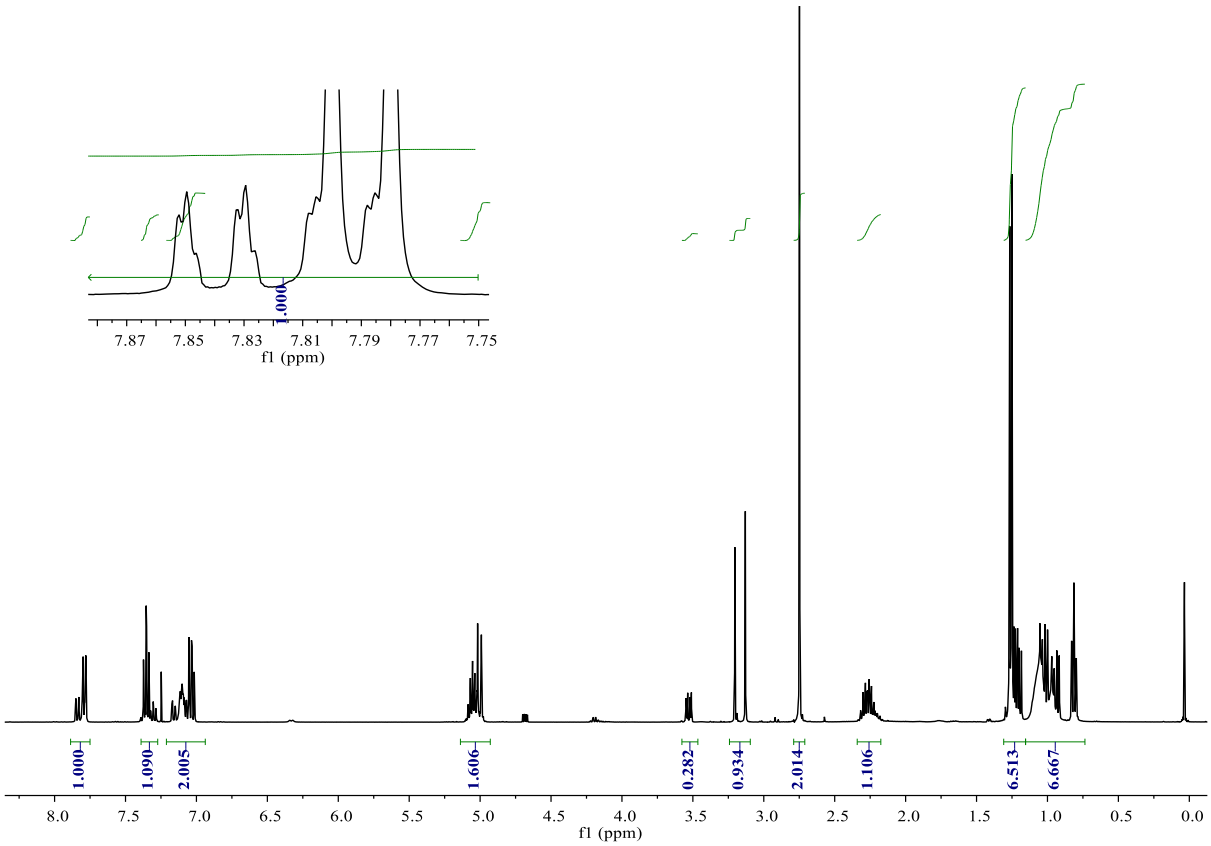

^{13}C NMR in $CDCl_3$ isopropyl N-(2-iodobenzoyl)-N-methyl-L-valinate.

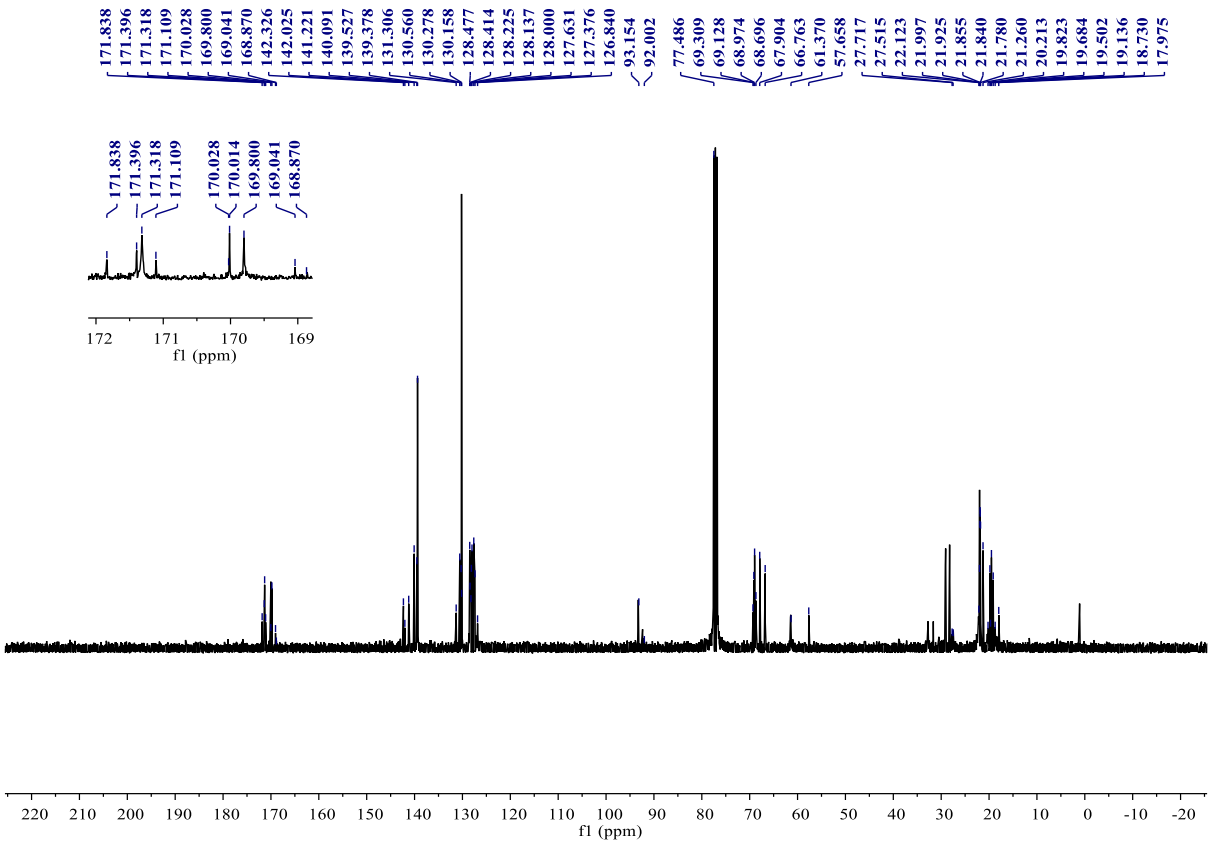

3.8 Synthesis Of terbutyl N-(2-iodobenzoyl)-N-methyl-L-valinate.

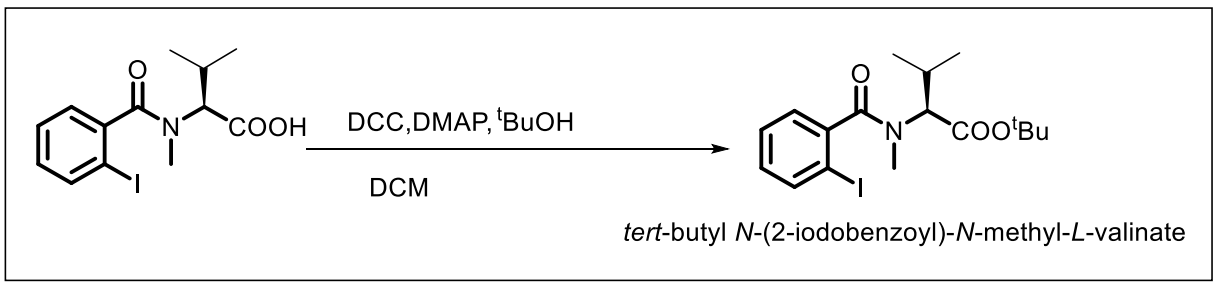

The same general procedure C(B) was followed with N-(2-iodobenzoyl)-N-methyl-L-valine (3a) (2.0mmol, 1.0 equiv.), DCC (2.6mmol, 1.3 equiv.), DMAP (0.1mmol, 0.1 equiv.), ^{t}BuOH (3mmol, 1.5 equiv.), ,Column chromatography (SiO_2, eluting with 20% ethyl acetate/pet ether) afforded the desired product 5a as White Solid (, 80 %yield).

^{1}H NMR in $CDCl_3$ of tertbutyl N-(2-iodobenzoyl)-N-methyl-L-valinate.

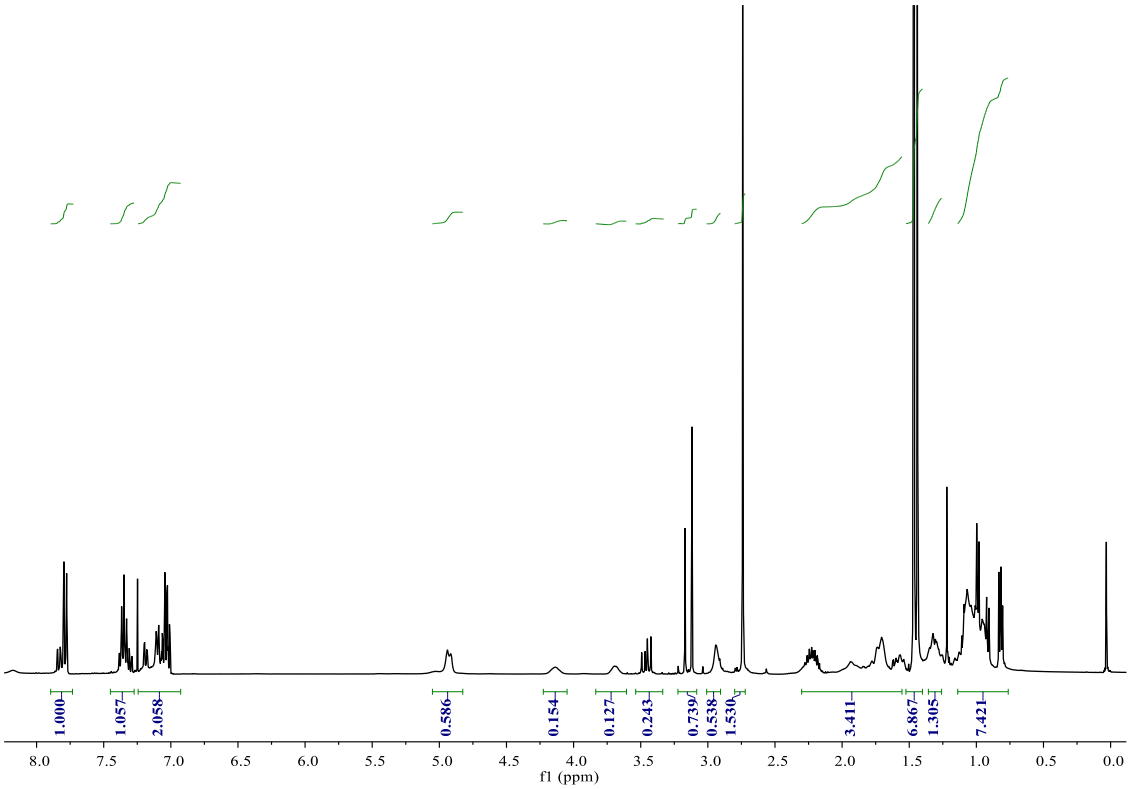

^{13}C NMR in $CDCl_3$ of tert butyl N-(2-iodobenzoyl)-N-methyl-L-valinate.

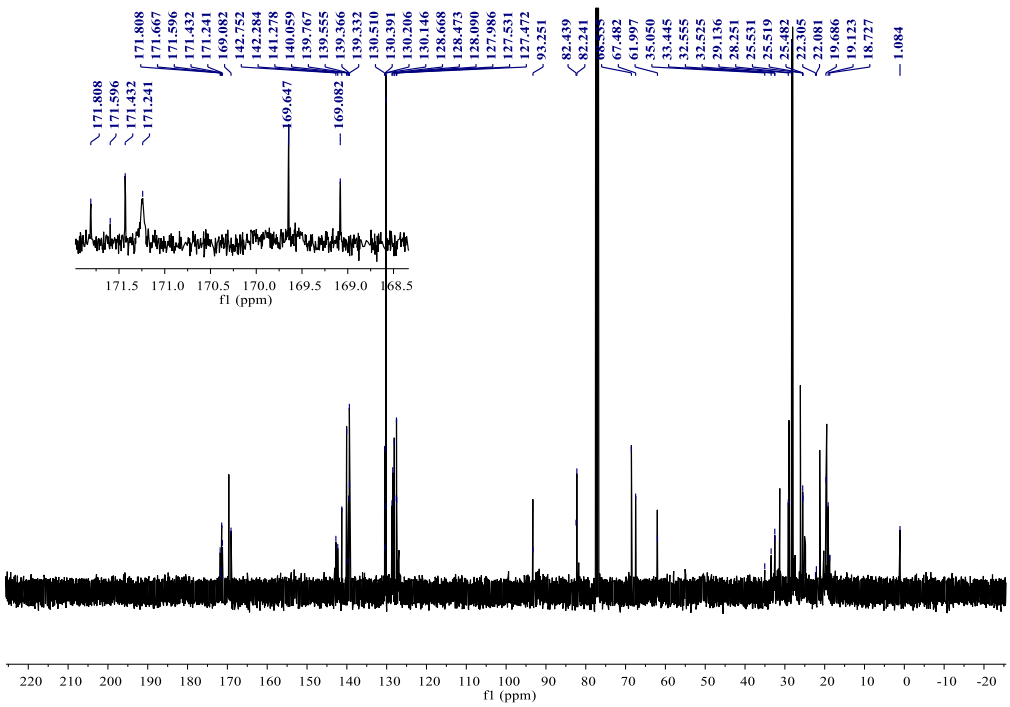

3.10 Synthesis Of methyl (1S,3R)-2-benzoyl-1-phenyl-2,3,4,9-tetrahydro-1H-pyrido[3,4-b]indole-3-carboxylate

The same general procedure A methyl (1S,3R)-1-phenyl-2,3,4,9-tetrahydro-1H-pyrido[3,4-b]indole-3-carboxylate was followed with 2-Iodobenzoyl Chloride.(3a) (2.0mmol, 1.0 equiv.), Trethylamine (3mmol, 1.5 equiv.), DCM 30ml,Column chromatography (SiO_2, eluting with 18% ethyl acetate/pet ether) afforded the desired product 4a as White Solid (, 80 %yield). Fig.24

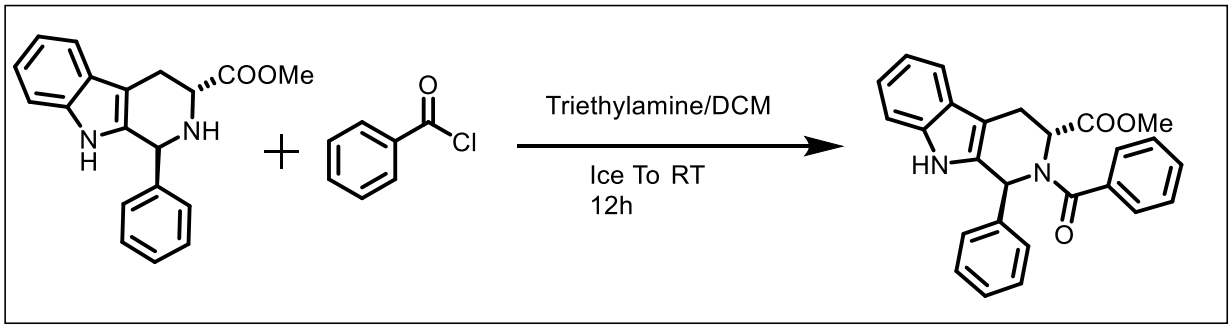

^{1}H NMR (400 MHz, DMSO-d_6) δ 10.86 (s, 1H), 7.66 – 6.87 (m, 14H), 6.26 – 5.86 (m, 1H), 4.84 (d, *J* = 152.8 Hz, 1H), 3.62 – 3.33 (m, 4H), 1.10 – 1.01 (m, 0H).
^{13}C NMR (101 MHz, DMSO-D_6) δ 171.40, 130.81, 129.34, 128.86, 128.83, 126.48, 123.92, 121.93, 119.42, 118.61, 111.84, 65.45, 55.45, 52.89, 15.70.

^{1}H NMR in DMSO-D_6 of methyl (1S,3R)-2-benzoyl-1-phenyl-2,3,4,9-tetrahydro-1H-pyrido[3,4-b]indole-3-carboxylate

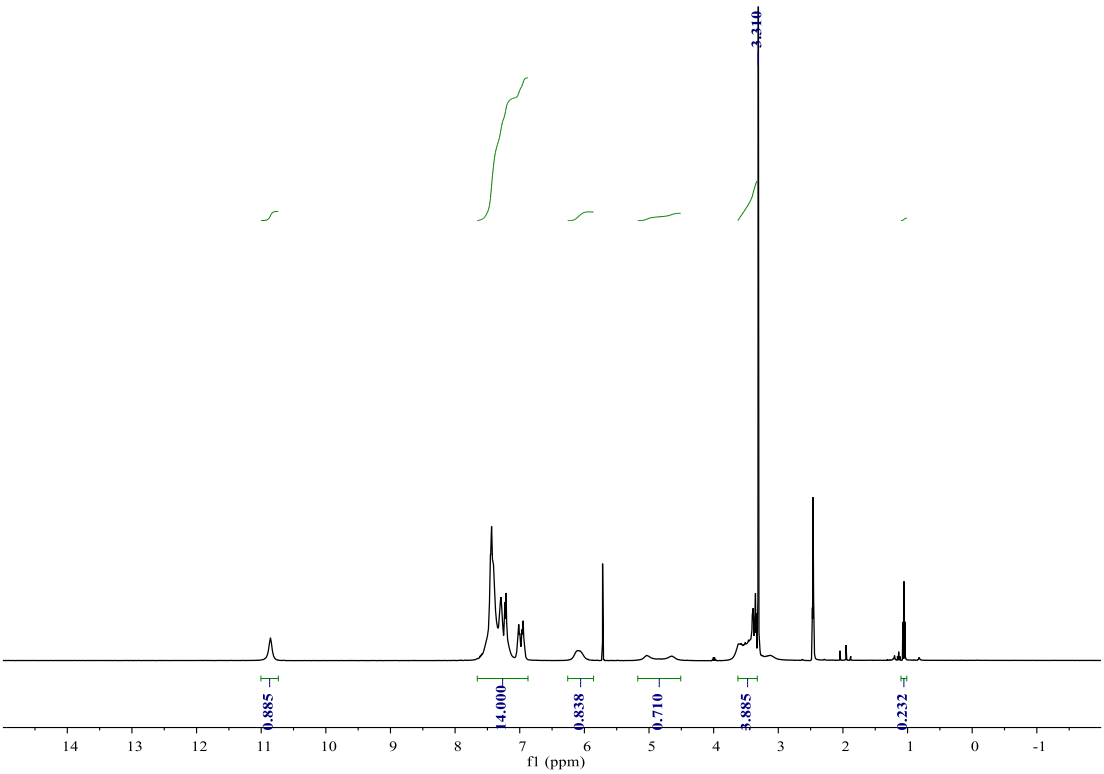

^{13}C NMR in DMSO-D6 of methyl (1S,3R)-2-benzoyl-1-phenyl-2,3,4,9-tetrahydro-1H-pyrido[3,4-b]indole-3-carboxylate

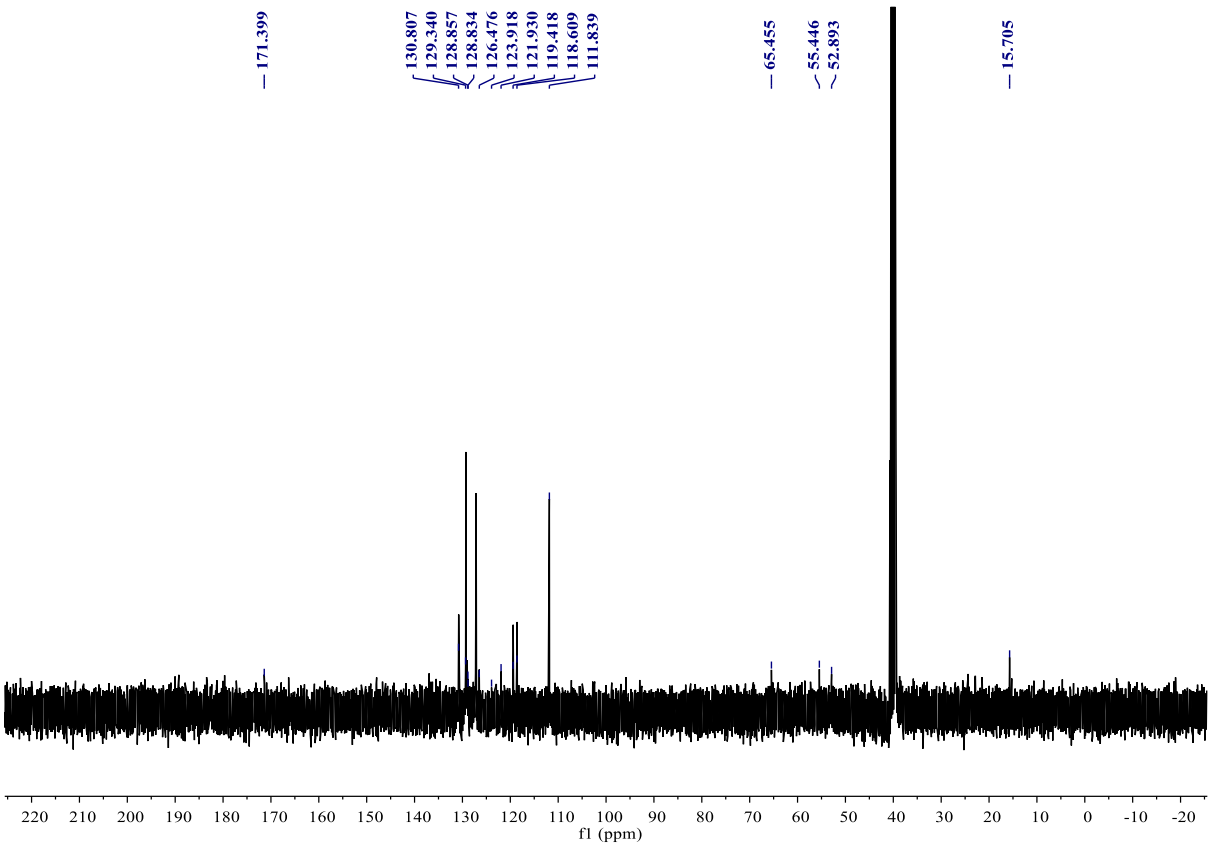

3.11 Synthesis Of methyl (1R,3R)-2-benzoyl-1-phenyl-2,3,4,9 tetrahydro - 1H-pyrido [3,4-b]indole-3-carboxylate

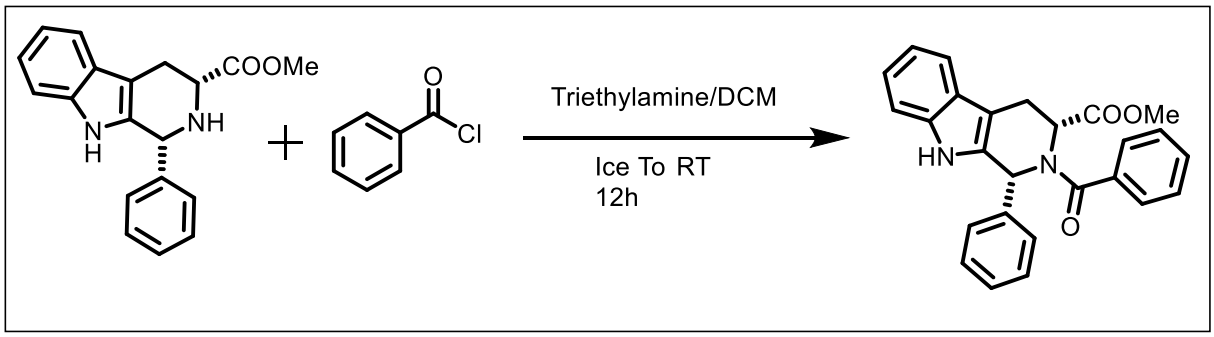

The same general procedure A methyl (1R,3R)-1-phenyl-2,3,4,9-tetrahydro-1H-pyrido[3,4-b]indole-3-carboxylate was followed with benzoyl Chloride.(3a) (2.0mmol, 1.0 equiv.), Trethylamine (3mmol, 1.5 equiv.), DCM 30ml,Column chromatography (SiO_2, eluting with 18% ethyl acetate/pet ether) afforded the desired product 4a as White Solid (, 80 %yield).

^{1}H NMR (400 MHz, DMSO-d_6) δ 10.99 (s, 1H), 7.51 – 7.43 (m, 7H), 7.36 – 7.21 (m, 5H), 7.20 – 7.16 (m, 1H), 7.11 – 6.98 (m, 3H), 4.79 (s, 1H), 2.98 – 2.71 (m, 4H), 1.15 – 0.89 (m, 1H).

^{13}C NMR (101 MHz, DMSO-D_6) δ 171.74, 140.22, 136.91, 136.56, 130.17, 129.28, 128.57, 128.21, 126.81, 126.63, 122.06, 119.22, 118.58, 111.80, 107.16, 65.46, 52.00, 22.01, 15.71.

^{1}H NMR in DMSO-D6 of methyl (1R,3R)-2-benzoyl-1-phenyl-2,3,4,9 tetrahydro - 1H-pyrido [3,4-b]indole-3-carboxylate

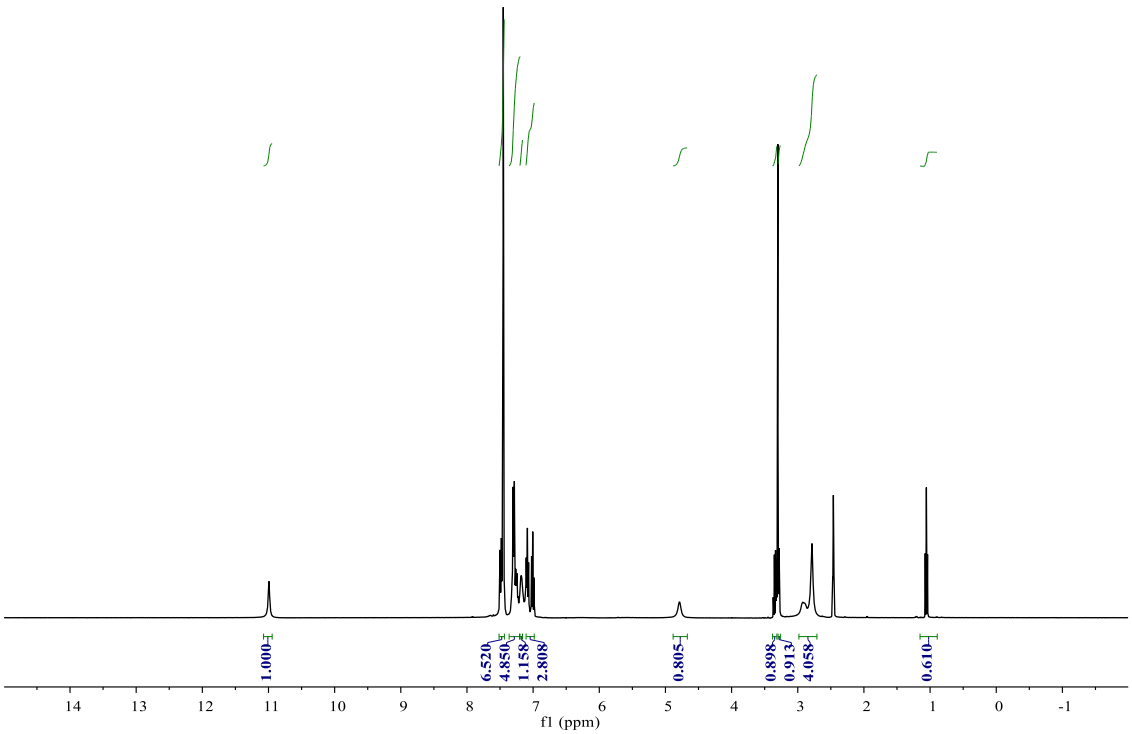

^{13}C NMR in DMSO-D6 of methyl (1R,3R)-2-benzoyl-1-phenyl-2,3,4,9 tetrahydro - 1H-pyrido [3,4-b]indole-3-carboxylate

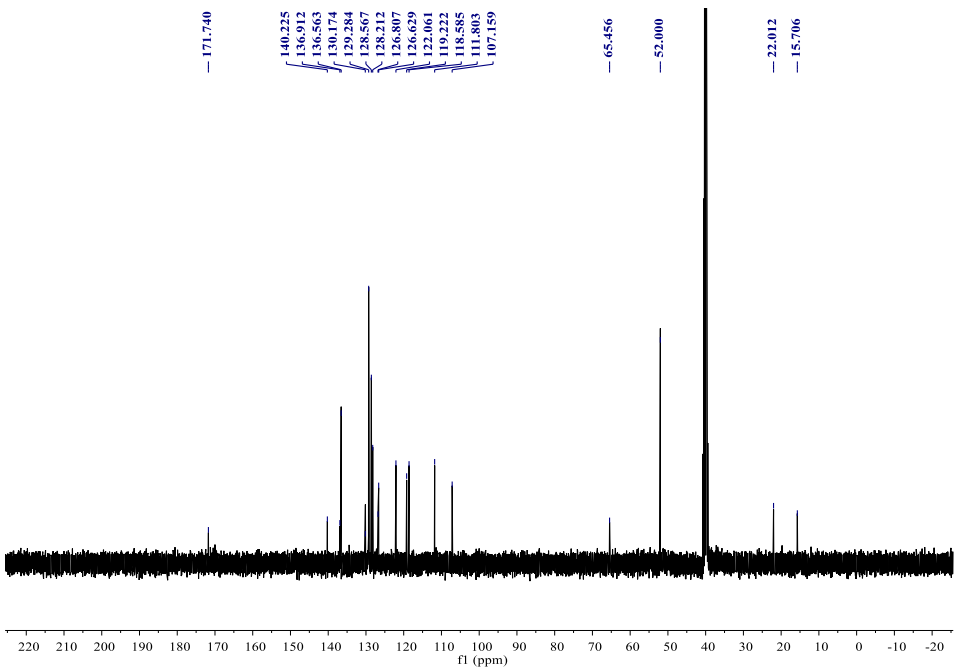

3.12 Synthesis Of methyl (1S,3R)-2-(2-iodobenzoyl)-1-phenyl-2,3,4,9-tetrahydro-1H-pyrido[3,4-b]indole-3-carboxylate

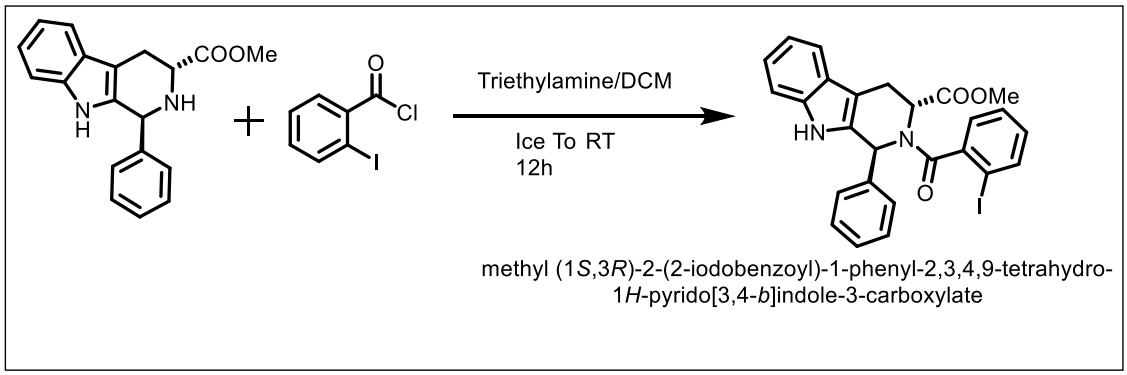

methyl (1*S*,3*R*)-2-(2-iodobenzoyl)-1-phenyl-2,3,4,9-tetrahydro-1*H*-pyrido[3,4-*b*]indole-3-carboxylate

The same general procedure A methyl (1S,3R)-1-phenyl-2,3,4,9-tetrahydro-1H-pyrido[3,4-b]indole-3-carboxylate was followed with 2-Iodobenzoyl Chloride.(3a) (2.0mmol, 1.0 equiv.), Trethylamine (3mmol, 1.5 equiv.), DCM 30ml,Column chromatography (SiO_2, eluting with 18% ethyl acetate/pet ether) afforded the desired product 4a as White Solid (, 80 %yield).

1H NMR Of methyl (1S,3R)-2-(2-iodobenzoyl)-1-phenyl-2,3,4,9-tetrahydro-1H-pyrido[3,4-b]indole-3-carboxylate at 343K temperature

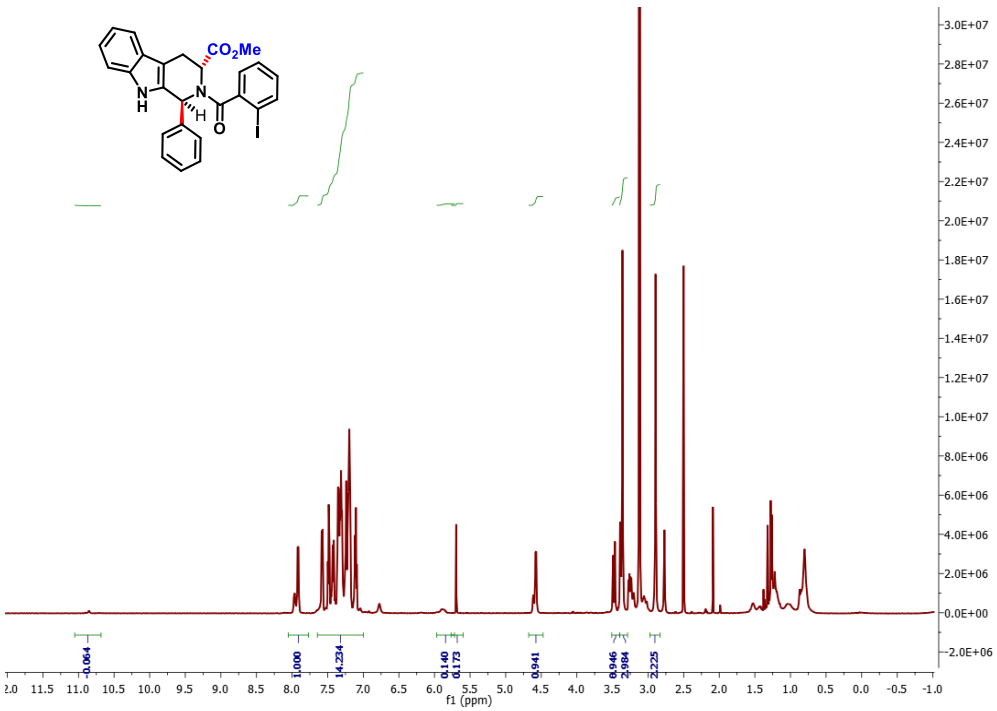

13C NMR Of methyl (1S,3R)-2-(2-iodobenzoyl)-1-phenyl-2,3,4,9-tetrahydro-1H-pyrido[3,4-b]indole-3-carboxylate at Room temperature

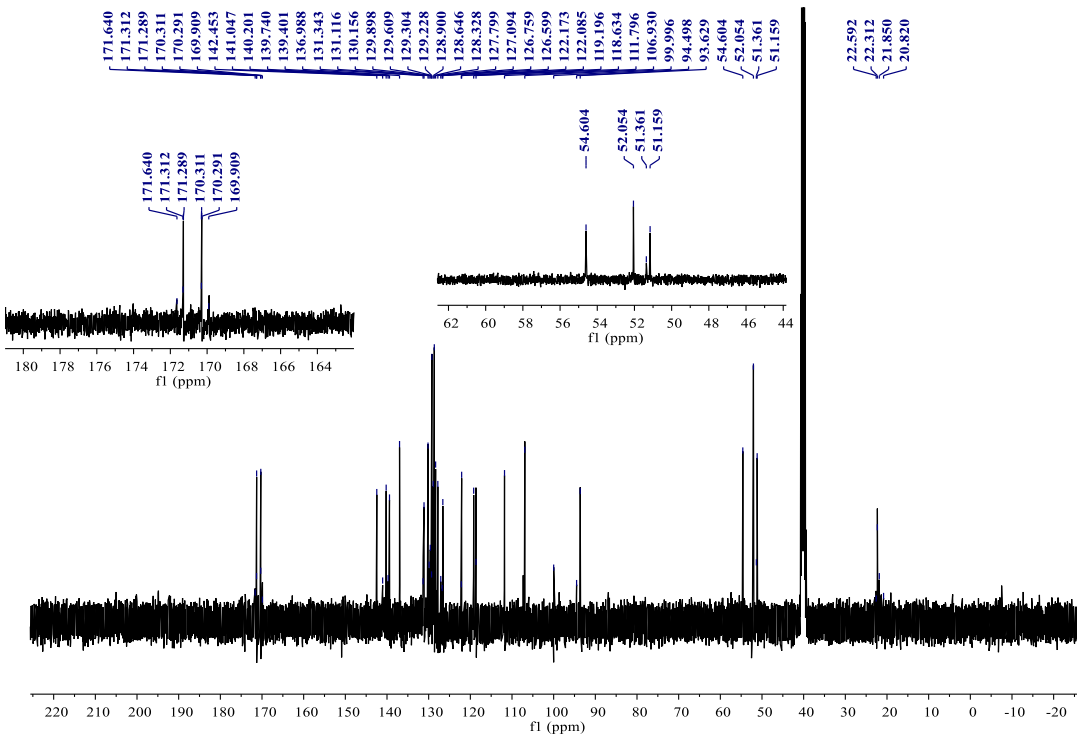

^{1}H NMR of methyl (1S,3R)-2-(2-iodobenzoyl)-1-phenyl-2,3,4,9-tetrahydro-1H-pyrido[3,4-b]indole-3-carboxylate at Different temperature.

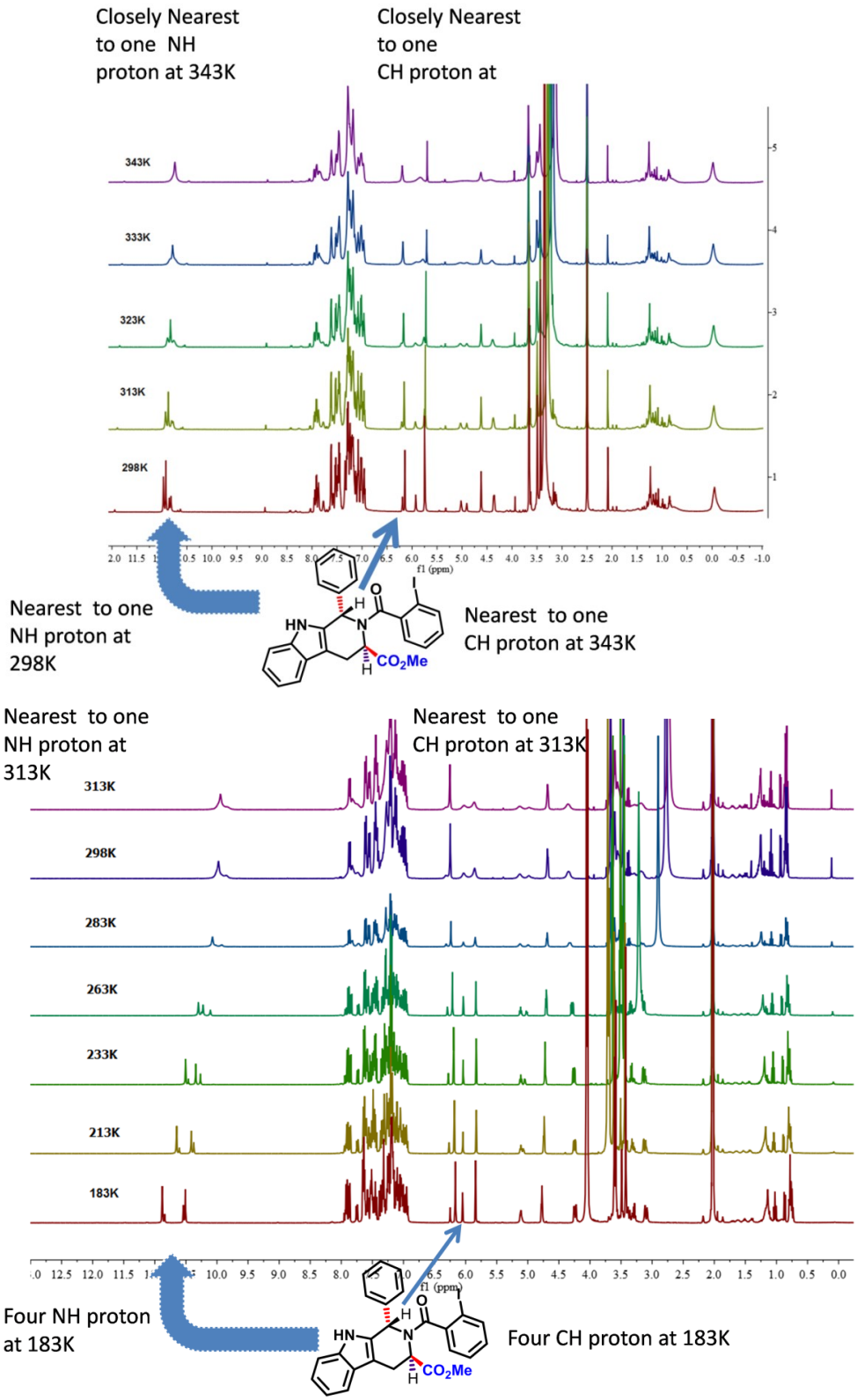

3.13 Synthesis Of methyl (1R,3R)-2-(2-iodobenzoyl)-1-phenyl-2,3,4,9-tetrahydro-1H-pyrido[3,4-b]indole-3-carboxylate.

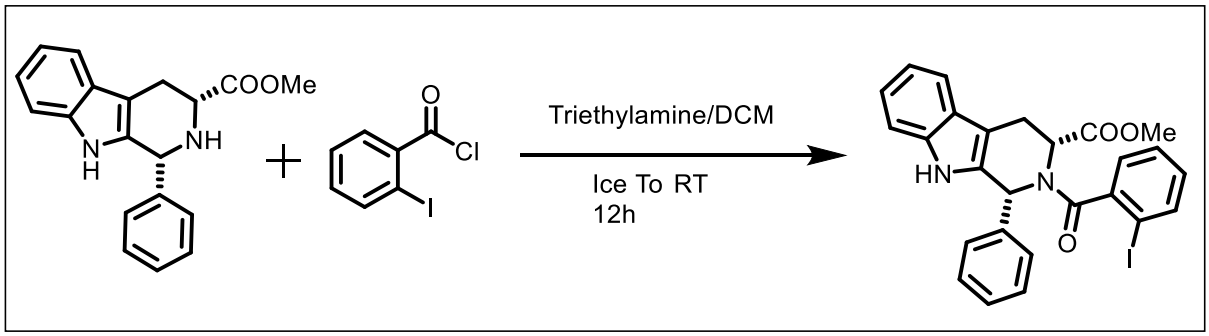

The same general procedure A methyl (1R,3R)-1-phenyl-2,3,4,9-tetrahydro-1H-pyrido[3,4-b]indole-3-carboxylatewas followed with 2-Iodobenzoyl Chloride.(3a) (2.0mmol, 1.0 equiv.), Trethylamine (3mmol, 1.5 equiv.), DCM 30ml,Column chromatography (SiO_2, eluting with 18% ethyl acetate/pet ether) afforded the desired product 4a as White Solid (, 80 %yield).

^{1}H NMR Of methyl (1R,3R)-2-(2-iodobenzoyl)-1-phenyl-2,3,4,9-tetrahydro-1H-pyrido[3,4-b]indole-3-carboxylate at 343K temperature.

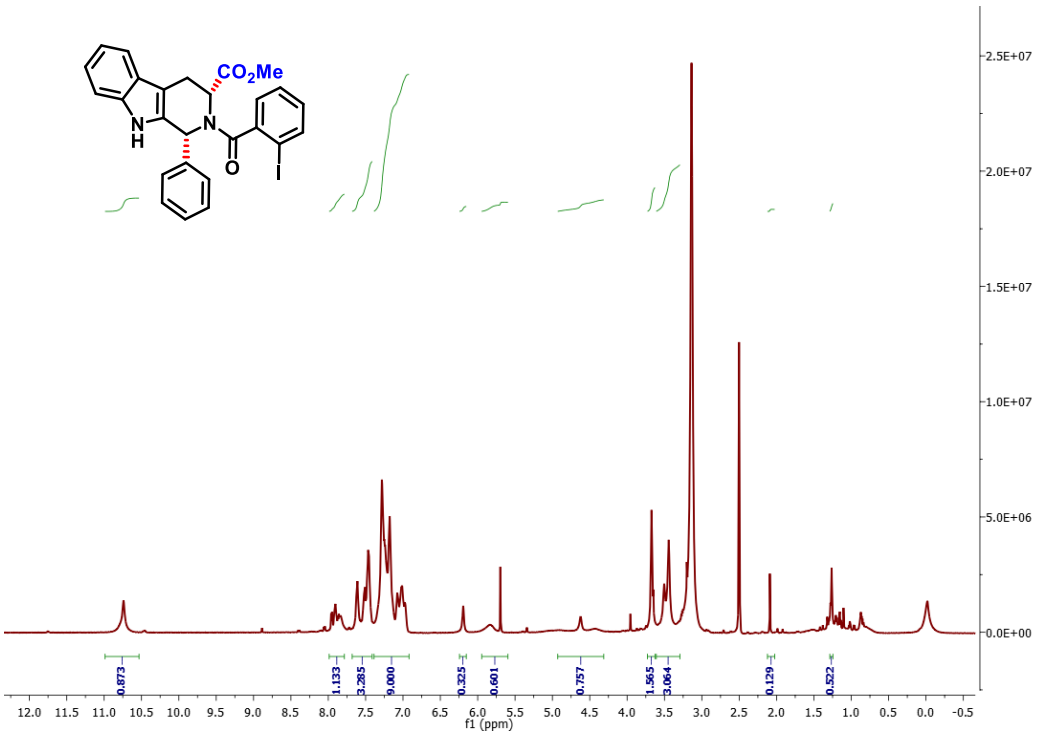

1H NMR Of methyl (1R,3R)-2-(2-iodobenzoyl)-1-phenyl-2,3,4,9-tetrahydro-1H-pyrido[3,4-b]indole-3-carboxylate at Different temperature.

Nearest to one NH proton at 313K

Nearest to one CH proton at 313K

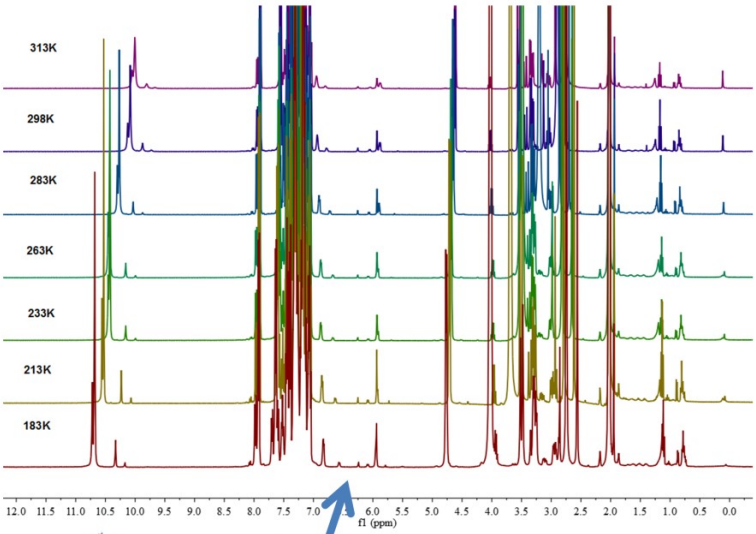

Four NH proton at 183K

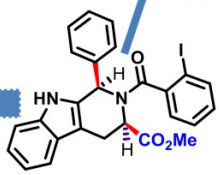

Four CH proton at 183K

Closely Nearest to one NH proton at 343K

Closely Nearest to one CH proton at 343K

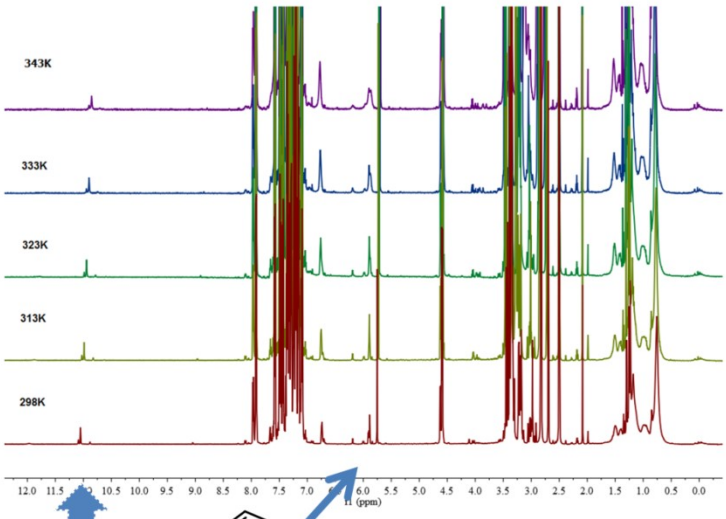

Nearest to one NH proton at 298K

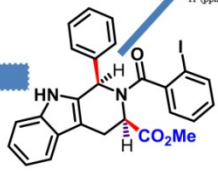

Nearest to one CH proton at 343K

3.14 Synthesis Of methyl (1S,3R)-2-(2-Bromobenzoyl)-1-phenyl-2,3,4,9-tetrahydro-1H-pyrido[3,4-b]indole-3-carboxylate

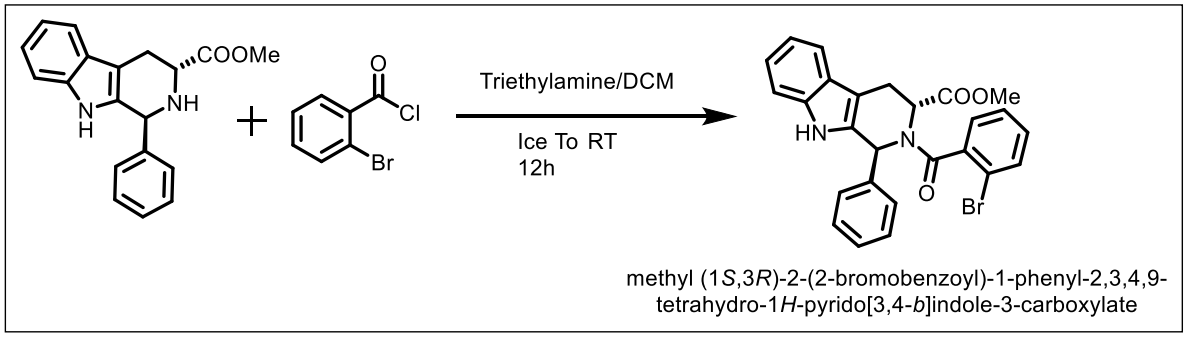

methyl (1*S*,3*R*)-2-(2-bromobenzoyl)-1-phenyl-2,3,4,9-tetrahydro-1*H*-pyrido[3,4-*b*]indole-3-carboxylate

The same general procedure A methyl (1S,3R)-1-phenyl-2,3,4,9-tetrahydro-1H-pyrido[3,4-b]indole-3-carboxylate was followed with 2-Bromobenzoyl Chloride.(3a) (2.0mmol, 1.0 equiv.), Trethylamine (3mmol, 1.5 equiv.), DCM 30ml,Column chromatography (SiO_2, eluting with 18% ethyl acetate/pet ether) afforded the desired product 4a as White Solid (, 80 %yield).

^{1}H NMR Of methyl (1S,3R)-2-(2-Bromobenzoyl)-1-phenyl-2,3,4,9-tetrahydro-1H-pyrido[3,4-b]indole-3-carboxylate.

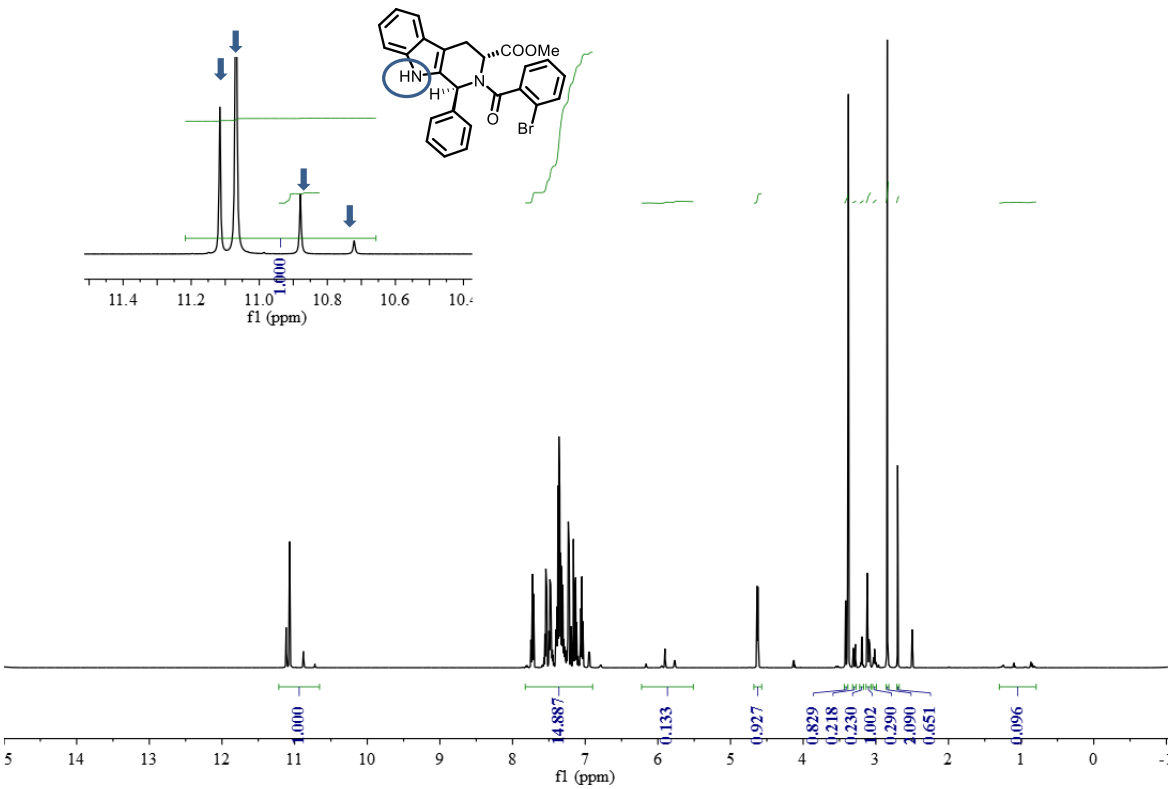

^{13}C NMR Of methyl (1S,3R)-2-(2-Bromobenzoyl)-1-phenyl-2,3,4,9-tetrahydro-1H-pyrido[3,4-b]indole-3-carboxylate.

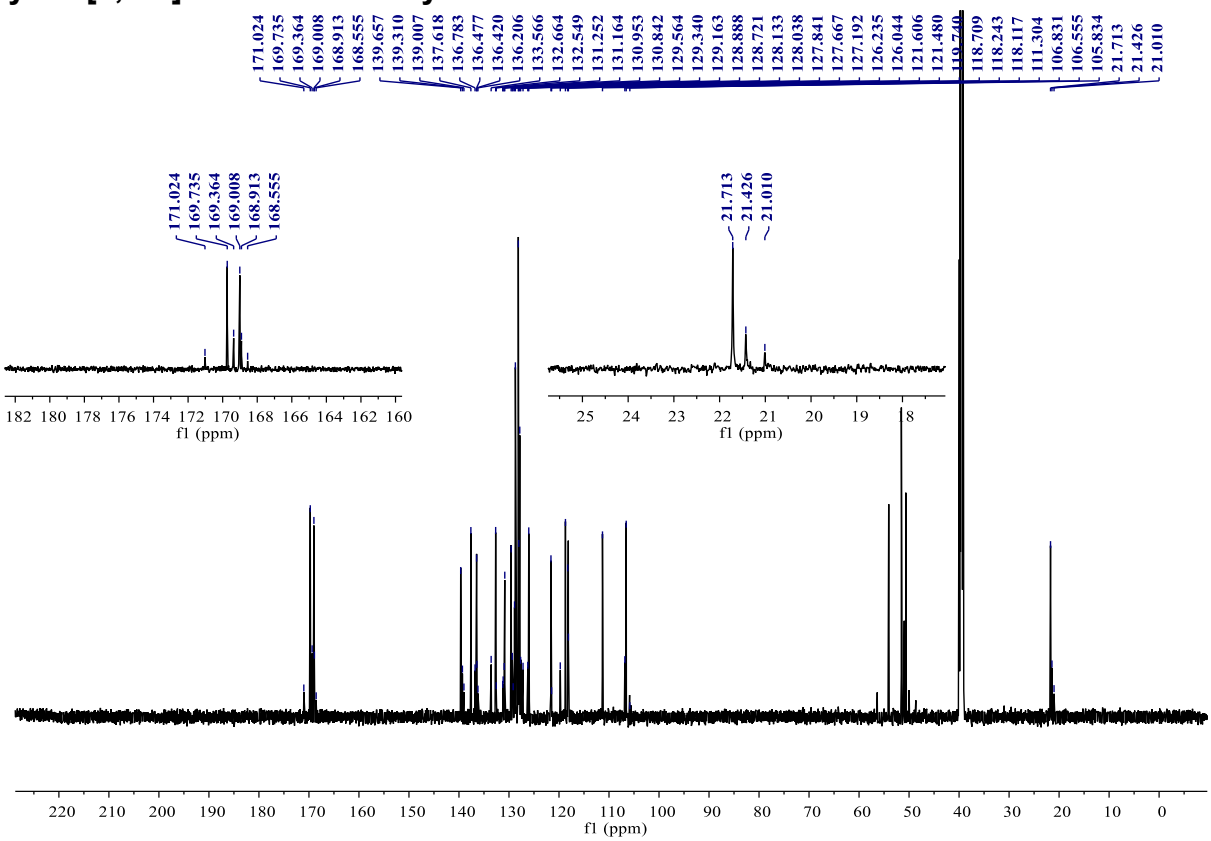

3.15 Synthesis Of methyl (1R,3R)-2-(2-Bromobenzoyl)-1-phenyl-2,3,4,9-tetrahydro-1H-pyrido[3,4-b]indole-3-carboxylate.

Fig.29

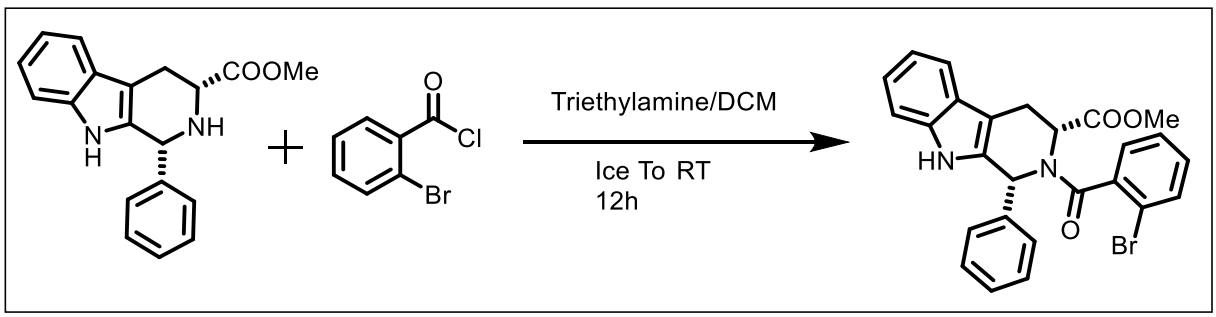

The same general procedure A methyl (1R,3R)-1-phenyl-2,3,4,9-tetrahydro-1H-pyrido[3,4-b]indole-3-carboxylatewas followed with 2-Bromobenzoyl Chloride.(3a) (2.0mmol, 1.0 equiv.), Trethylamine (3mmol, 1.5 equiv.), DCM 30ml,Column chromatography (SiO_2, eluting with 18% ethyl acetate/pet ether) afforded the desired product 4a as White Solid (, 80 %yield).

^{1}H NMR of methyl (1R,3R)-2-(2-Bromobenzoyl)-1-phenyl-2,3,4,9-tetrahydro-1H-pyrido[3,4-b]indole-3-carboxylate.

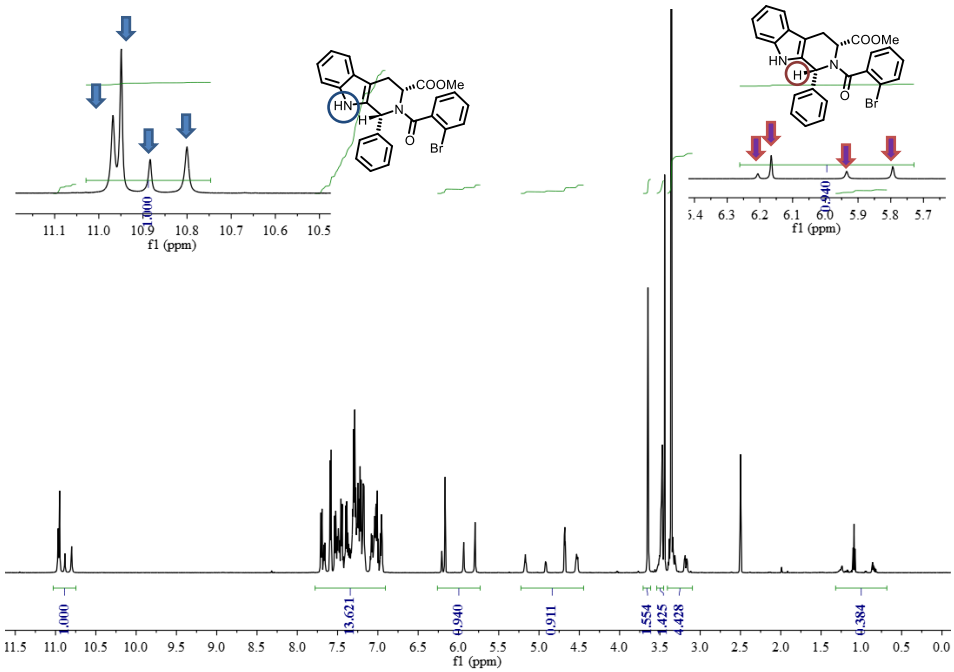

^{13}C NMR of methyl (1R,3R)-2-(2-Bromobenzoyl)-1-phenyl-2,3,4,9-tetrahydro-1H-pyrido[3,4-b]indole-3-carboxylate.

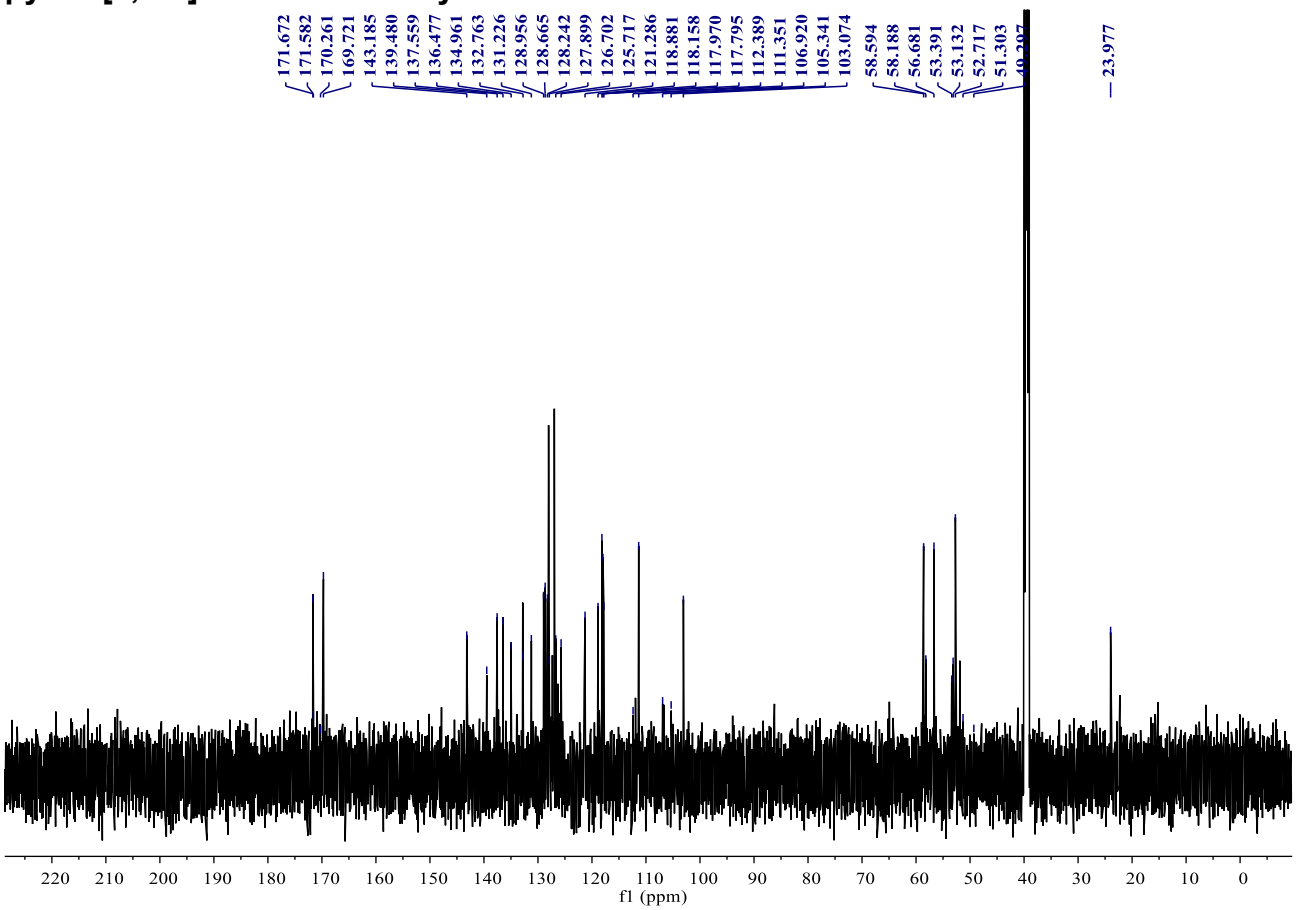

3.16 Synthesis of methyl (1S,3R)-2-(2-Chlorobenzoyl)-1-phenyl-2,3,4,9-tetrahydro-1H-pyrido[3,4-b]indole-3-carboxylate

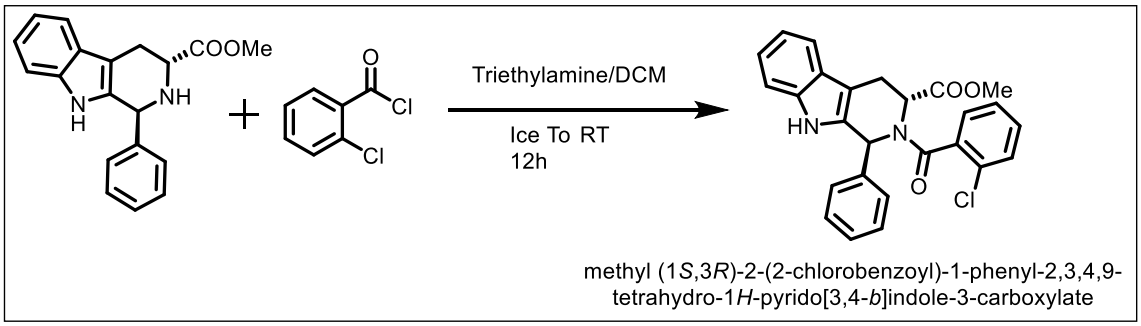

methyl (1*S*,3*R*)-2-(2-chlorobenzoyl)-1-phenyl-2,3,4,9-tetrahydro-1*H*-pyrido[3,4-*b*]indole-3-carboxylate

The same general procedure A methyl (1S,3R)-1-phenyl-2,3,4,9-tetrahydro-1H-pyrido[3,4-b]indole-3-carboxylate was followed with 2-Chlorobenzoyl Chloride.(3a) (2.0mmol, 1.0 equiv.), Trethylamine (3mmol, 1.5 equiv.), DCM 30ml,Column chromatography (SiO_2, eluting with 18% ethyl acetate/pet ether) afforded the desired product 4a as White Solid (, 80 %yield).

^{1}H NMR of methyl (1S,3R)-2-(2-Chlorobenzoyl)-1-phenyl-2,3,4,9-tetrahydro-1H-pyrido[3,4-b]indole-3-carboxylate.

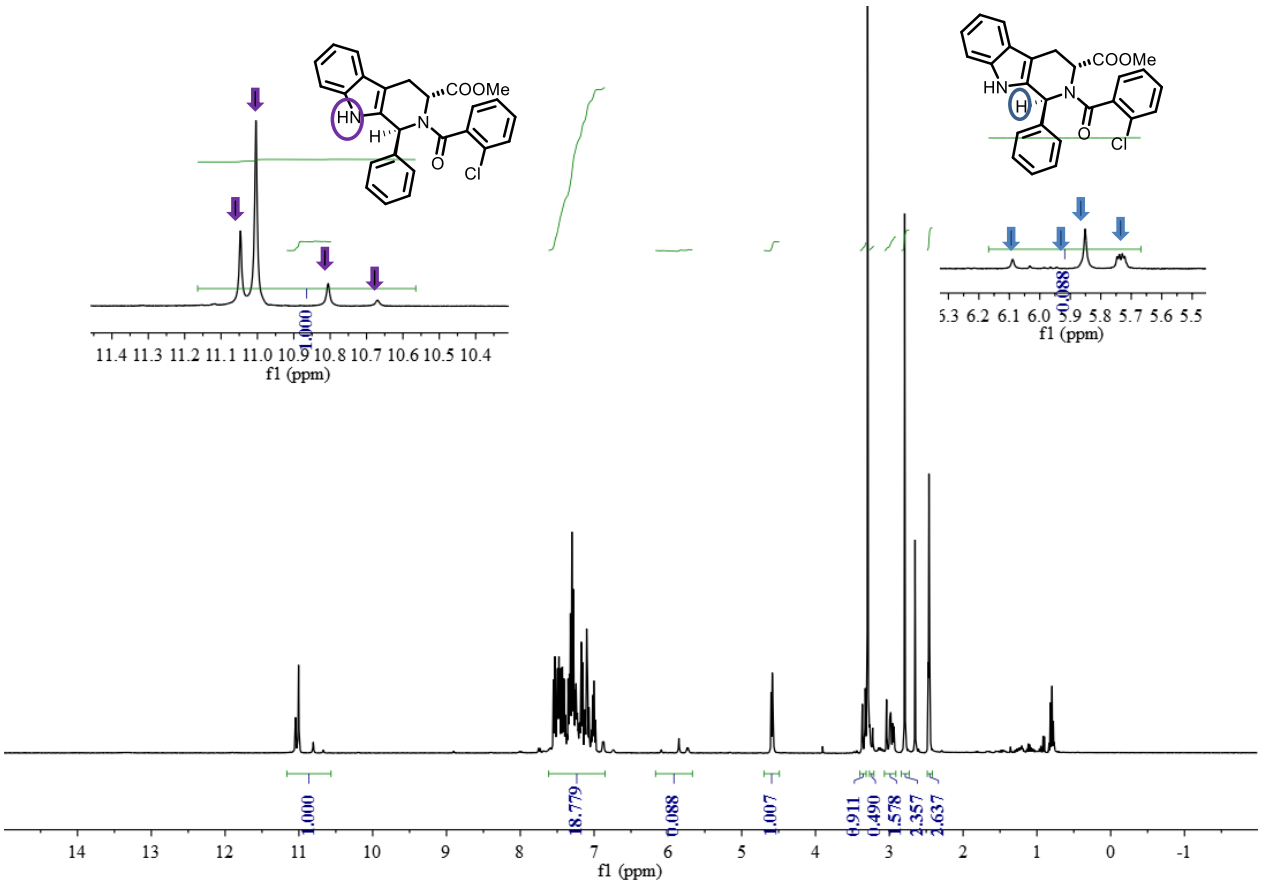

^{13}C NMR of methyl (1S,3R)-2-(2-Chlorobenzoyl)-1-phenyl-2,3,4,9-tetrahydro-1H-pyrido[3,4-b]indole-3-carboxylate.

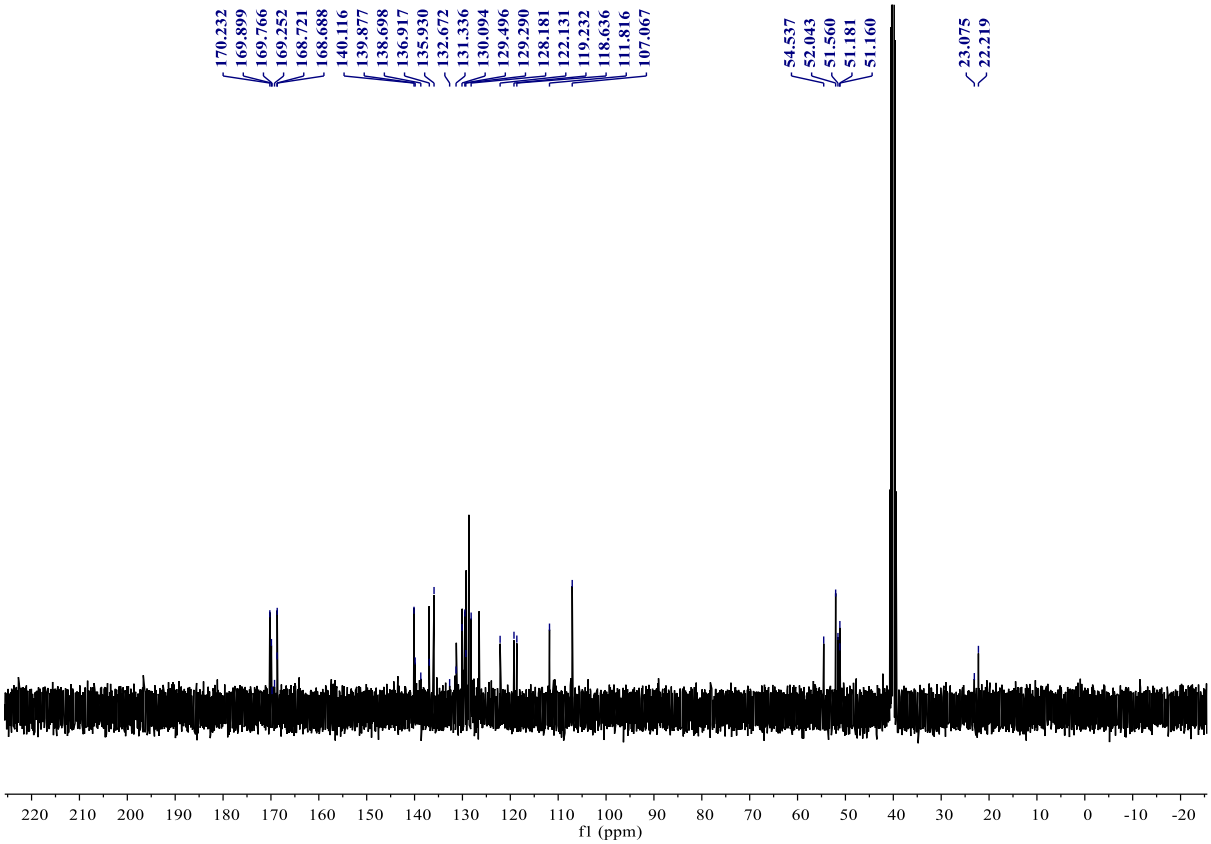

3.17 Synthesis of methyl (1R,3R)-2-(2-Chlorobenzoyl)-1-phenyl-2,3,4,9-tetrahydro-1H-pyrido[3,4-b]indole-3-carboxylate.

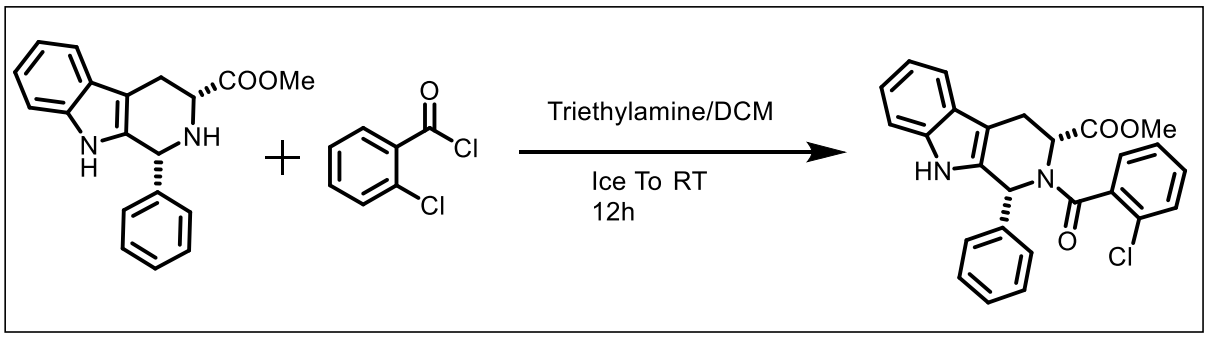

The same general procedure A methyl (1R,3R)-1-phenyl-2,3,4,9-tetrahydro-1H-pyrido[3,4-b]indole-3-carboxylatewas followed with 2-chlorobenzoyl Chloride.(3a) (2.0mmol, 1.0 equiv.), Trethylamine (3mmol, 1.5 equiv.), DCM 30ml,Column chromatography (SiO_2, eluting with 18% ethyl acetate/pet ether) afforded the desired product 4a as White Solid (, 80 %yield).

1H NMR of methyl (1R,3R)-2-(2-Chlorobenzoyl)-1-phenyl-2,3,4,9-tetrahydro-1H-pyrido[3,4-b]indole-3-carboxylate.

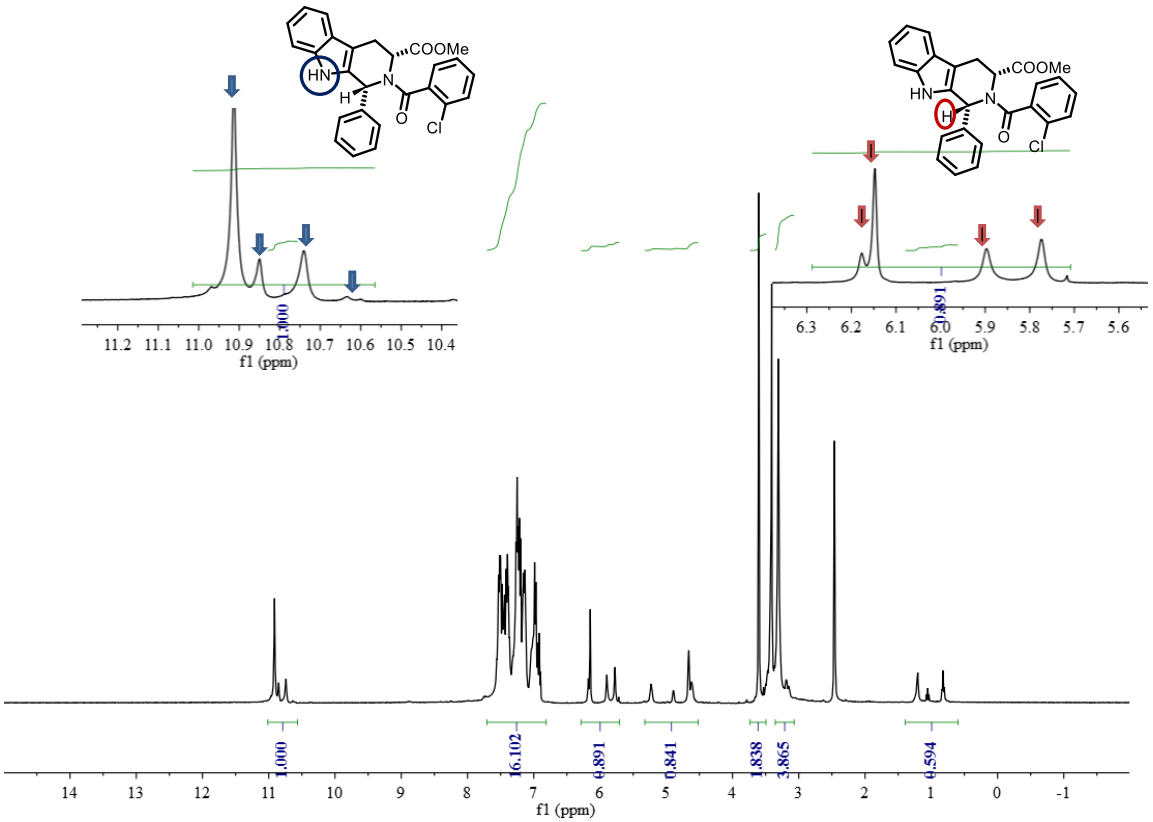

13C NMR of methyl (1R,3R)-2-(2-Chlorobenzoyl)-1-phenyl-2,3,4,9-tetrahydro-1H-pyrido[3,4-b]indole-3-carboxylate.

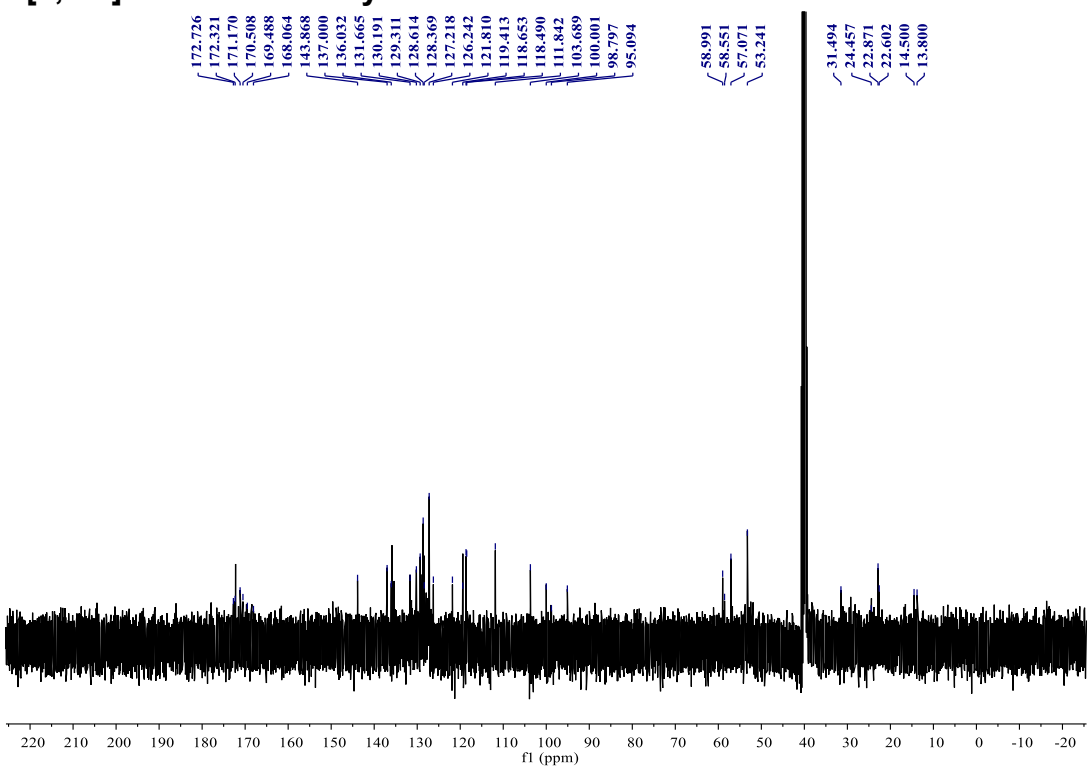

3.18 Synthesis of methyl (1S,3R)-2-(2-fluorobenzoyl)-1-phenyl-2,3,4,9-tetrahydro-1H-pyrido[3,4-b]indole-3-carboxylate.

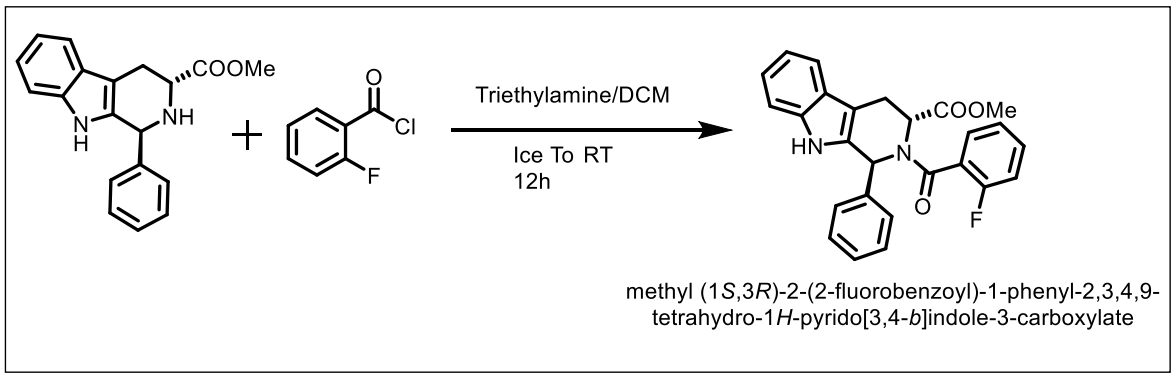

methyl (1*S*,3*R*)-2-(2-fluorobenzoyl)-1-phenyl-2,3,4,9-tetrahydro-1*H*-pyrido[3,4-*b*]indole-3-carboxylate

The same general procedure A methyl (1S,3R)-1-phenyl-2,3,4,9-tetrahydro-1H-pyrido[3,4-b]indole-3-carboxylate was followed with 2-fluorobenzoyl Chloride.(3a) (2.0mmol, 1.0 equiv.), Trethylamine (3mmol, 1.5 equiv.), DCM 30ml,Column chromatography (SiO_2, eluting with 18% ethyl acetate/pet ether) afforded the desired product 4a as White Solid (, 80 %yield).

^{1}H nmr of methyl (1S,3R)-2-(2-fluorobenzoyl)-1-phenyl-2,3,4,9-tetrahydro-1H-pyrido[3,4-b]indole-3-carboxylate

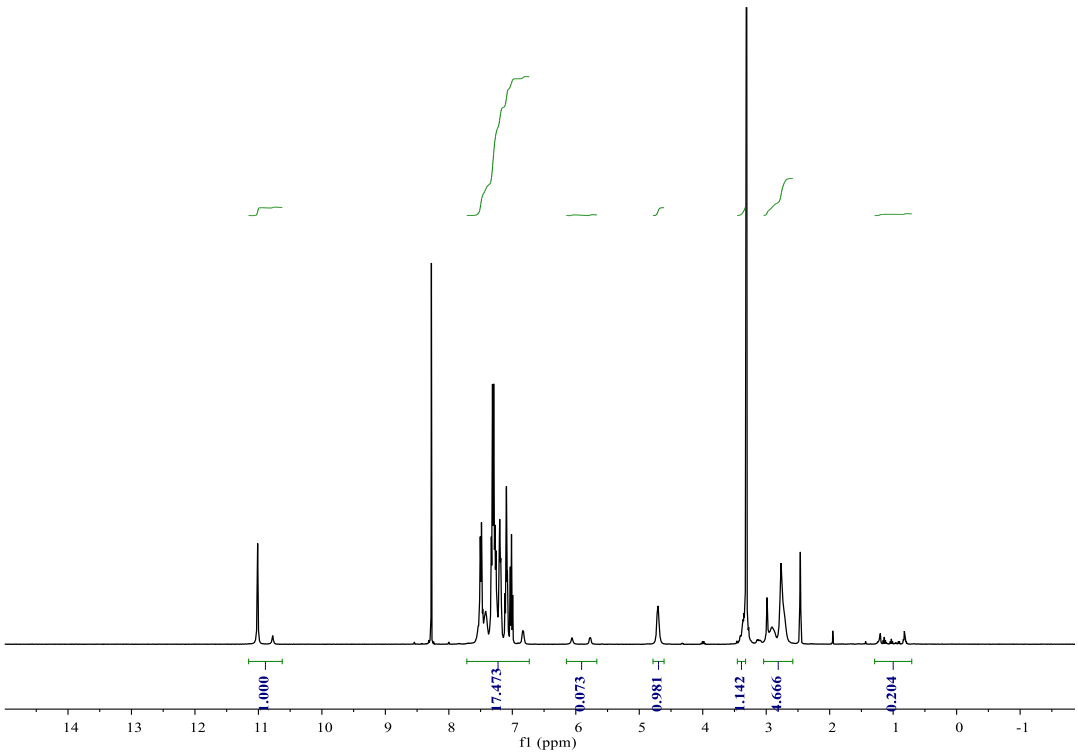

^{13}C nmr of methyl (1S,3R)-2-(2-fluorobenzoyl)-1-phenyl-2,3,4,9-tetrahydro-1H-pyrido[3,4-b]indole-3-carboxylate

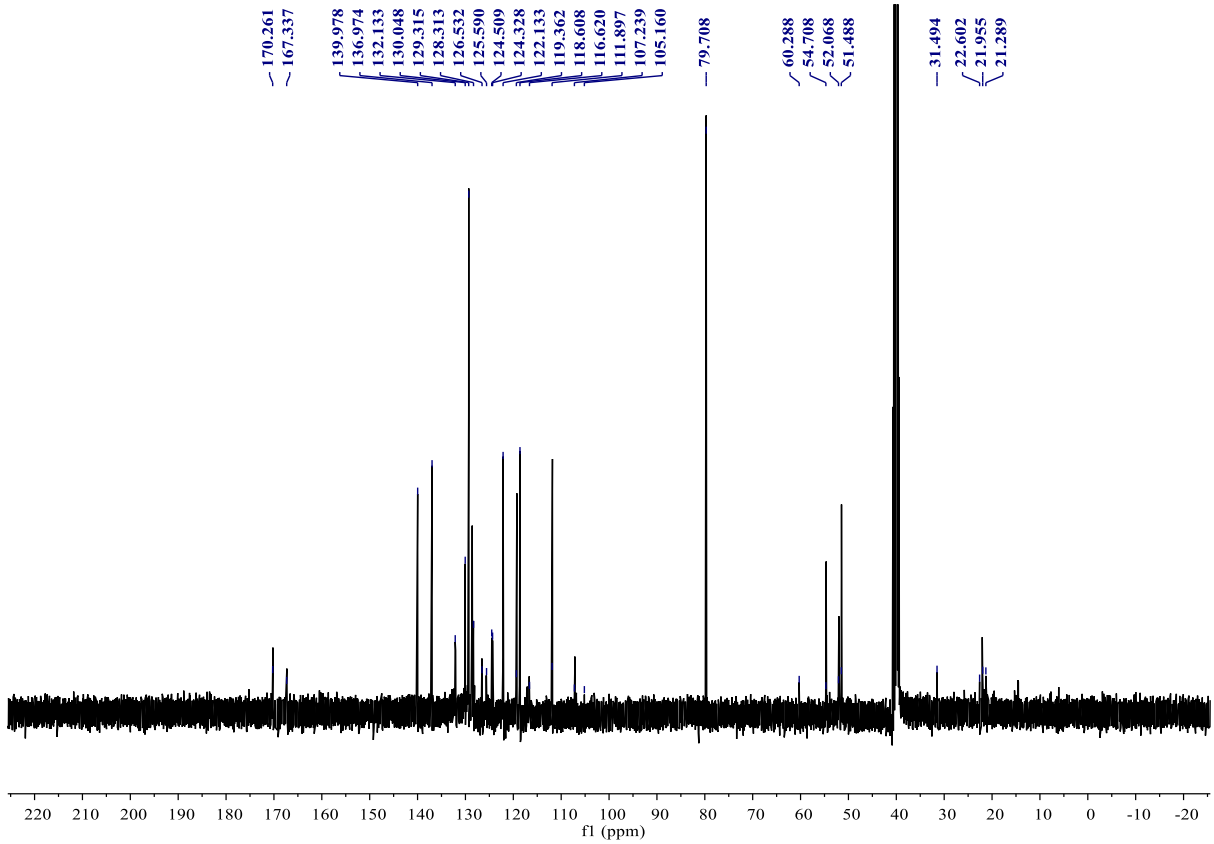

3.19 Synthesis of methyl (1R,3R)-2-(2-fluorobenzoyl)-1-phenyl-2,3,4,9-tetrahydro-1H-pyrido[3,4-b]indole-3-carboxylate.

Fig.32

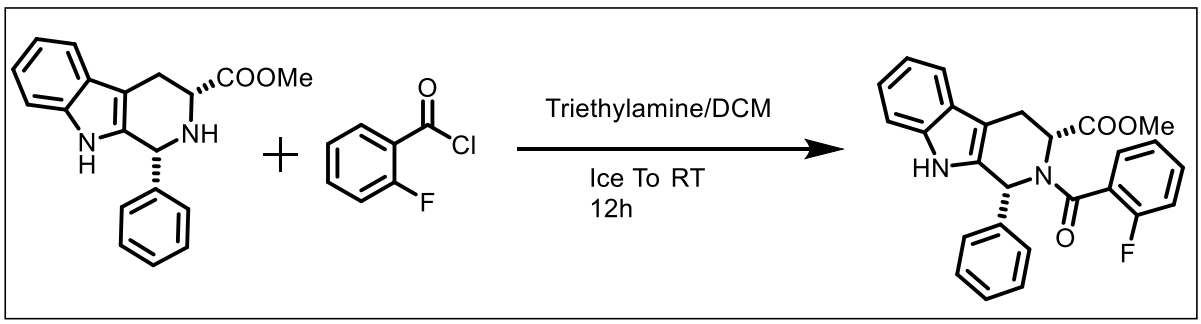

The same general procedure A methyl (1R,3R)-1-phenyl-2,3,4,9-tetrahydro-1H-pyrido[3,4-b]indole-3-carboxylatewas followed with 2-fluorobenzoyl Chloride.(3a) (2.0mmol, 1.0 equiv.), Trethylamine (3mmol, 1.5 equiv.), DCM 30ml,Column chromatography (SiO_2, eluting with 18% ethyl acetate/pet ether) afforded the desired product 4a as White Solid (, 80 %yield).

1H NMR of methyl (1R,3R)-2-(2-fluorobenzoyl)-1-phenyl-2,3,4,9-tetrahydro-1H-pyrido[3,4-b]indole-3-carboxylate

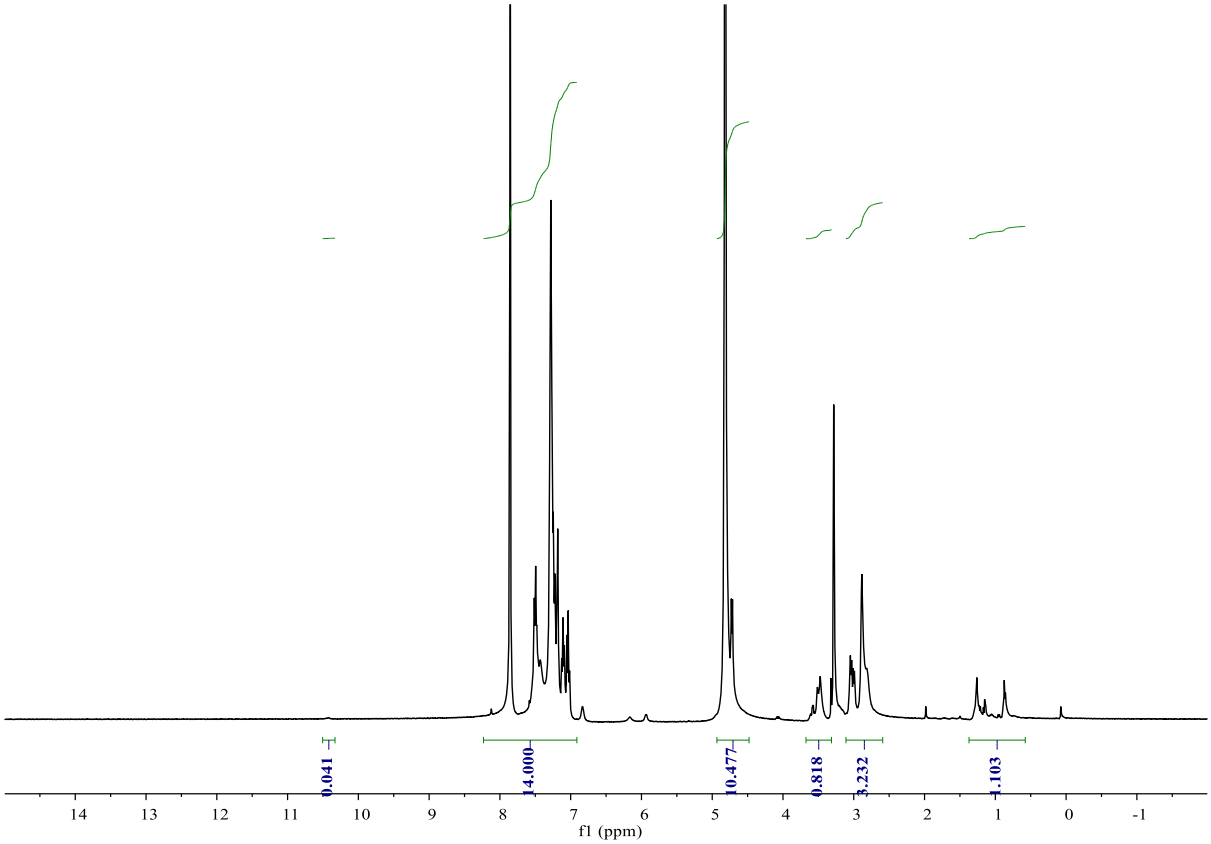

13C NMR of methyl (1R,3R)-2-(2-fluorobenzoyl)-1-phenyl-2,3,4,9-tetrahydro-1H-pyrido[3,4-b]indole-3-carboxylate

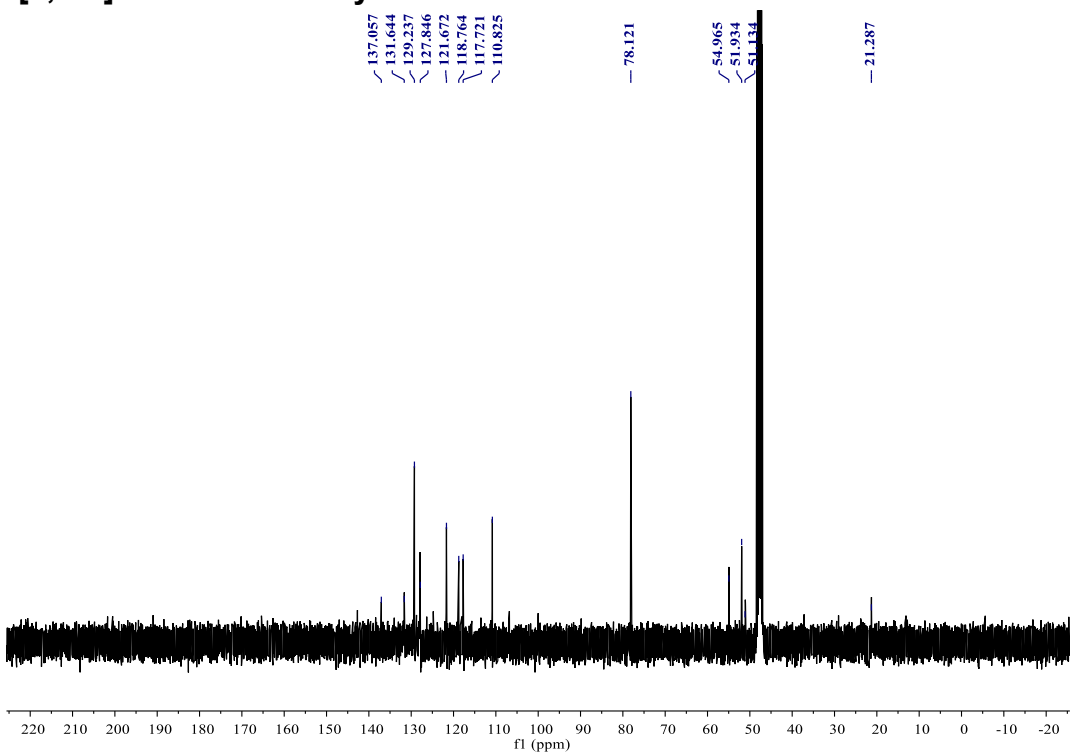

3.20. Synthesis Of methyl (1S,3R)-2-(2-nitrobenzoyl)-1-phenyl-2,3,4,9-tetrahydro-1H-pyrido[3,4-b]indole-3-carboxylate.

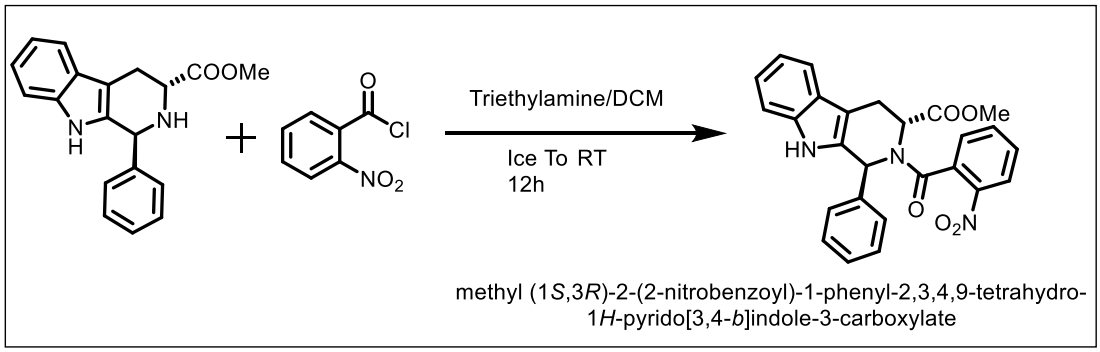

methyl (1*S*,3*R*)-2-(2-nitrobenzoyl)-1-phenyl-2,3,4,9-tetrahydro-1*H*-pyrido[3,4-*b*]indole-3-carboxylate

The same general procedure A methyl (1S,3R)-1-phenyl-2,3,4,9-tetrahydro-1H-pyrido[3,4-b]indole-3-carboxylate was followed with 2-nitrobenzoyl Chloride.(3a) (2.0mmol, 1.0 equiv.), Trethylamine (3mmol, 1.5 equiv.), DCM 30ml,Column chromatography (SiO_2, eluting with 18% ethyl acetate/pet ether) afforded the desired product 4a as White Solid (, 80 %yield).

^{1}H NMR of methyl (1S,3R)-2-(2-nitrobenzoyl)-1-phenyl-2,3,4,9-tetrahydro-1H-pyrido[3,4-b]indole-3-carboxylate.

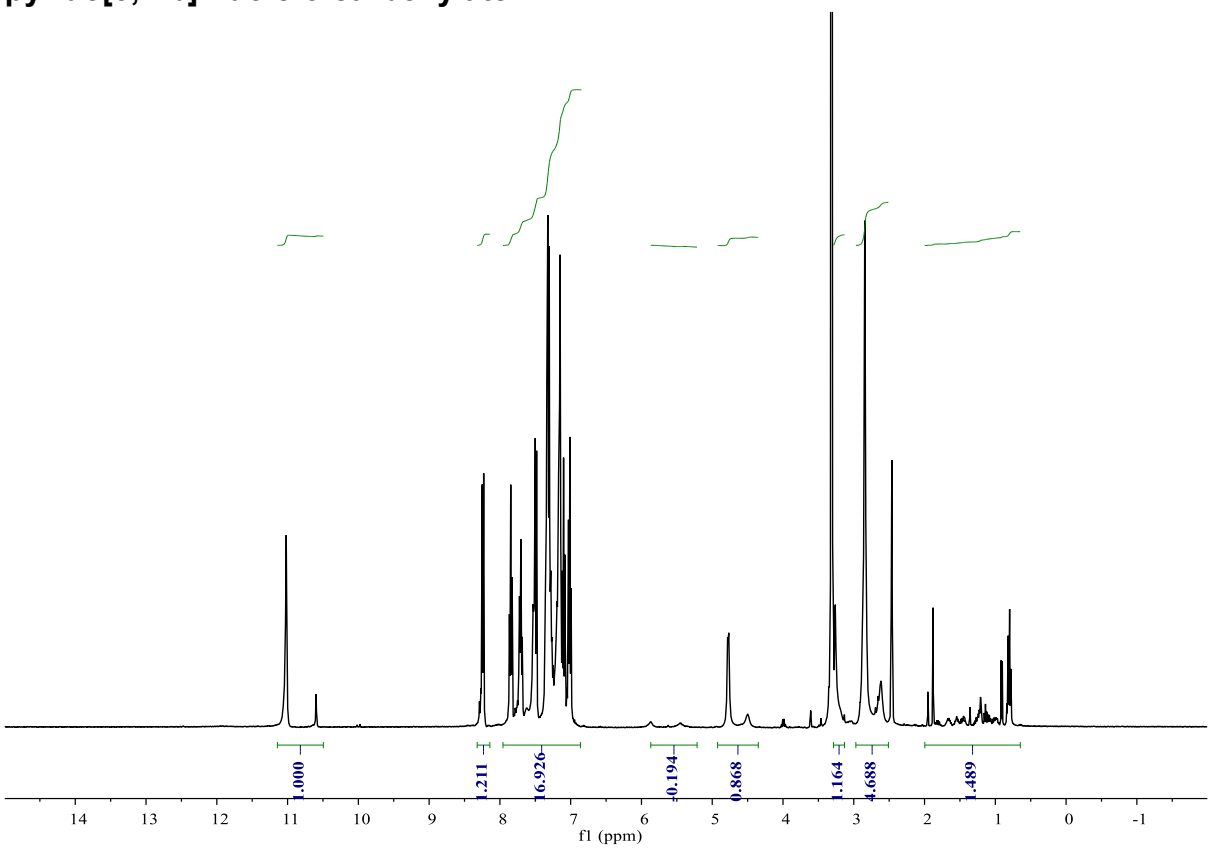

^{13}C NMR of methyl (1S,3R)-2-(2-nitrobenzoyl)-1-phenyl-2,3,4,9-tetrahydro-1H-pyrido[3,4-b]indole-3-carboxylate

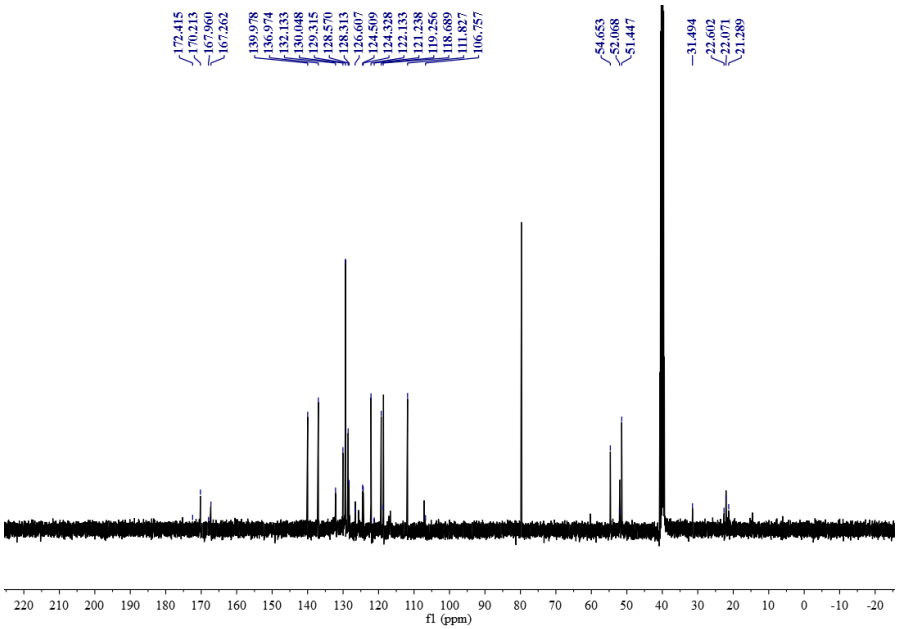

3.21 Synthesis Of methyl (1R,3R)-2-(2-nitrobenzoyl)-1-phenyl-2,3,4,9-tetrahydro-1H-pyrido[3,4-b]indole-3-carboxylate.

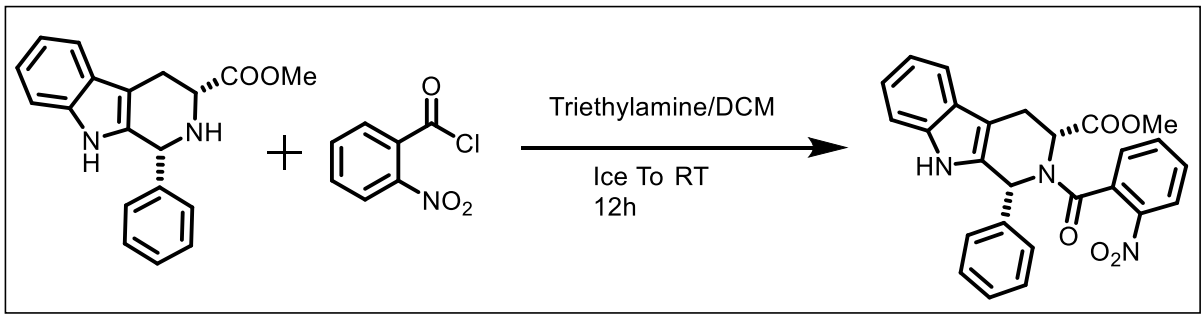

The same general procedure A methyl (1R,3R)-1-phenyl-2,3,4,9-tetrahydro-1H-pyrido[3,4-b]indole-3-carboxylatewas followed with 2-nitrobenzoyl Chloride.(3a) (2.0mmol, 1.0 equiv.), Trethylamine (3mmol, 1.5 equiv.), DCM 30ml,Column chromatography (SiO_2, eluting with 18% ethyl acetate/pet ether) afforded the desired product 4a as White Solid (, 80 %yield).

^{1}H NMR of methyl (1R,3R)-2-(2-nitrobenzoyl)-1-phenyl-2,3,4,9-tetrahydro-1H-pyrido[3,4-b]indole-3-carboxylate in DMSO-D6

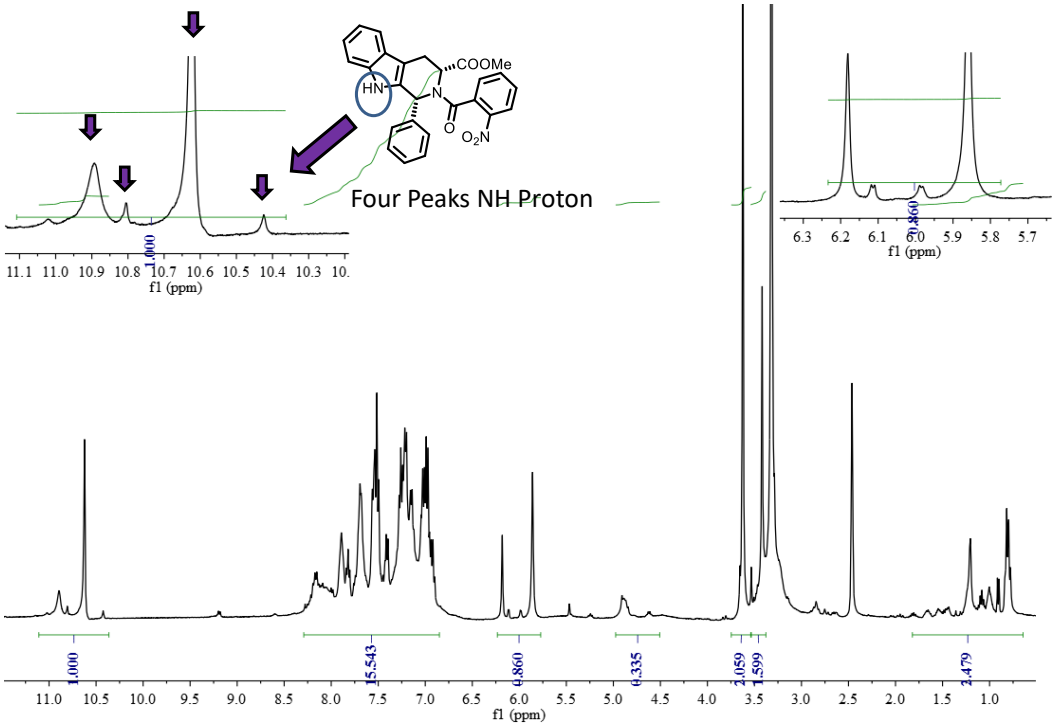

^{13}CNMR of methyl (1R,3R)-2-(2-nitrobenzoyl)-1-phenyl-2,3,4,9-tetrahydro-1H-pyrido[3,4-b]indole-3-carboxylate in DMSO-d$_6$

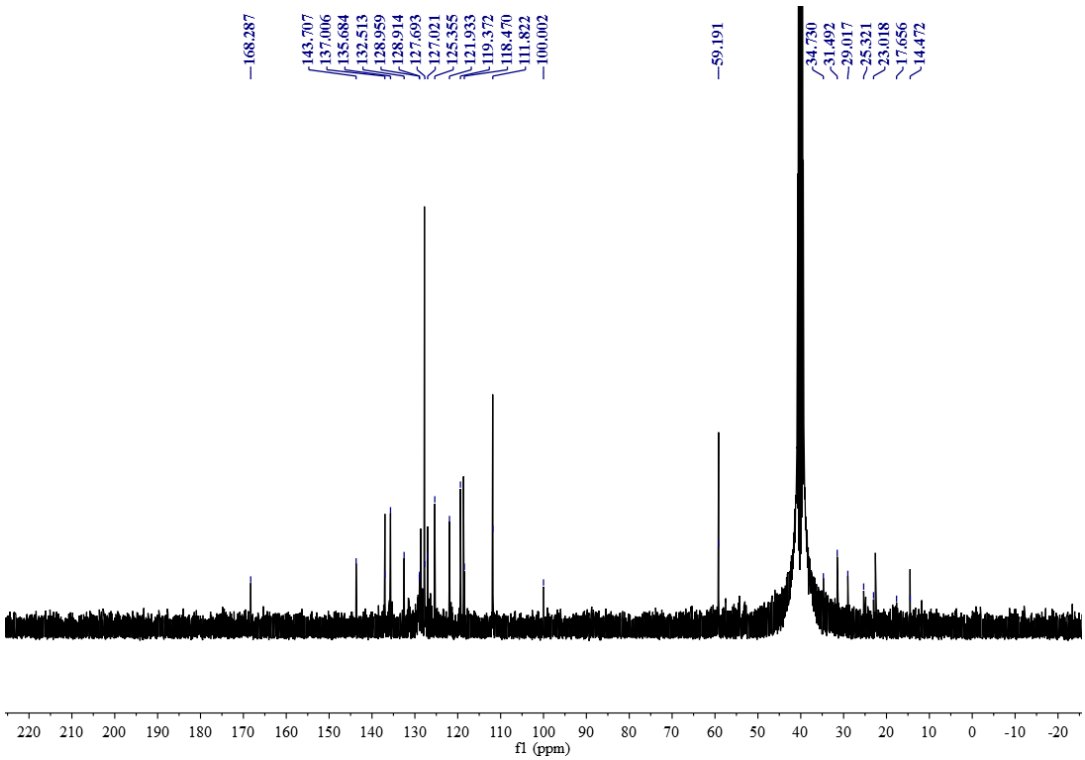

3.22 Synthesis Of methyl (1S,3R)-2-(2-iodobenzoyl)-1-(p-tolyl)-2,3,4,9-tetrahydro-1H-pyrido[3,4-b]indole-3-carboxylate

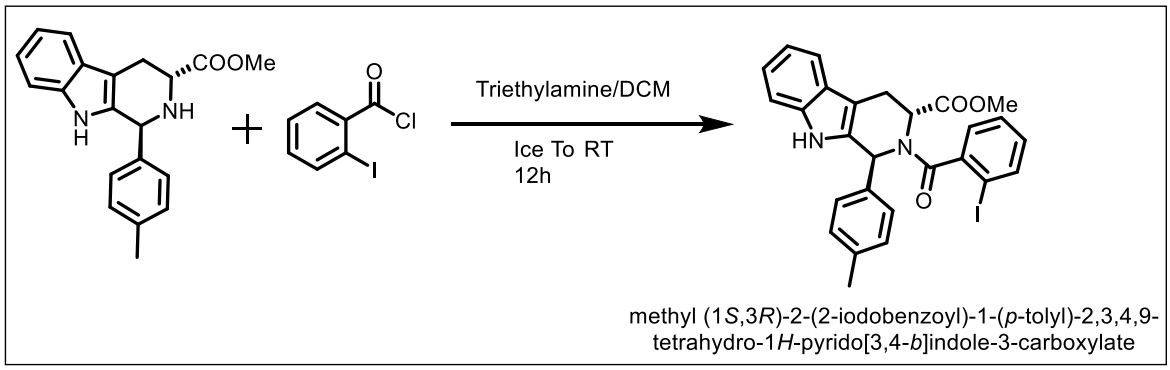

methyl (1*S*,3*R*)-2-(2-iodobenzoyl)-1-(*p*-tolyl)-2,3,4,9-tetrahydro-1*H*-pyrido[3,4-*b*]indole-3-carboxylate

The same general procedure A methyl methyl (1S,3R)-1-(p-tolyl)-2,3,4,9-tetrahydro-1H-pyrido[3,4-b]indole-3-carboxylate was followed with 2-Iodobenzoyl Chloride.(3a) (2.0mmol, 1.0 equiv.), Trethylamine (3mmol, 1.5 equiv.), DCM 30ml,Column chromatography (SiO_2, eluting with 18% ethyl acetate/pet ether) afforded the desired product 4a as White Solid (, 80 %yield).

^{1}H NMR of methyl (1S,3R)-2-(2-iodobenzoyl)-1-(p-tolyl)-2,3,4,9-tetrahydro-1H-pyrido[3,4-b]indole-3-carboxylate in Acetone-D6

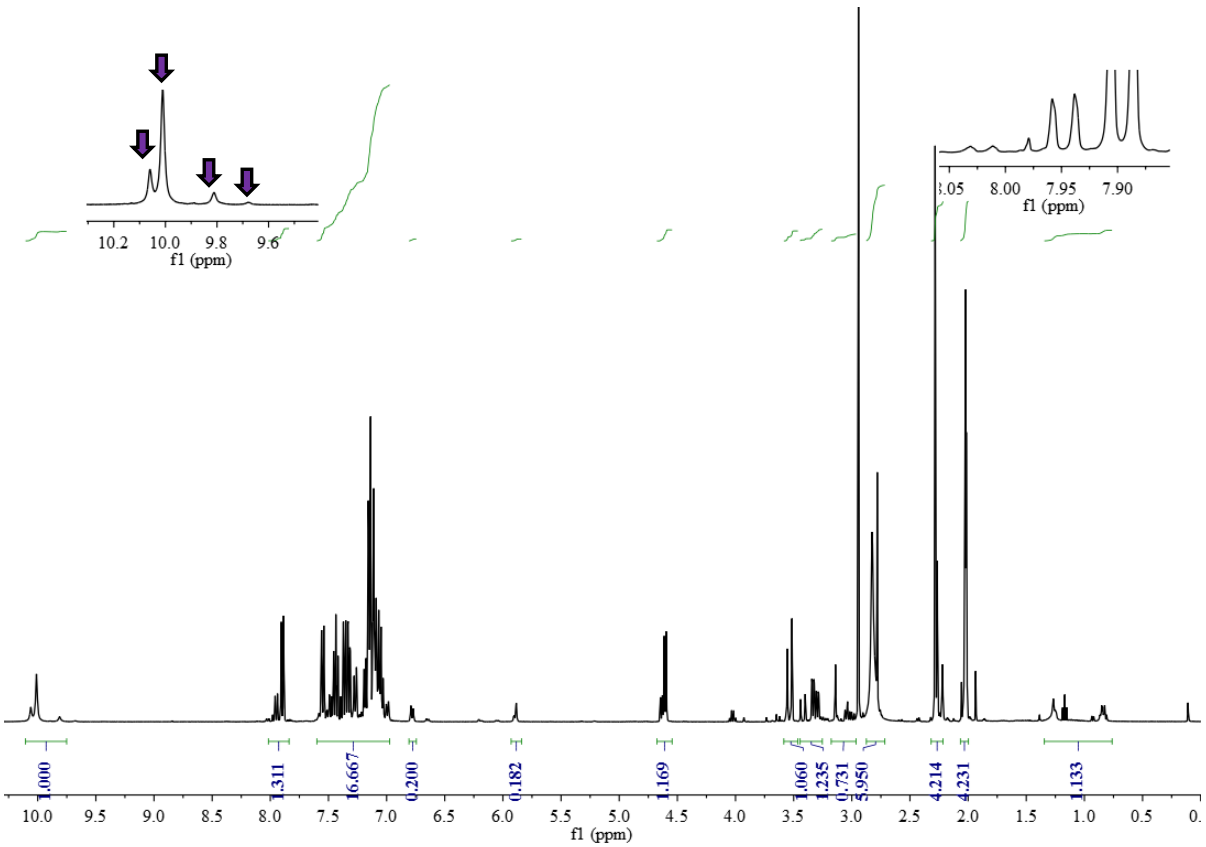

^{13}C NMR of methyl (1S,3R)-2-(2-iodobenzoyl)-1-(p-tolyl)-2,3,4,9-tetrahydro-1H-pyrido[3,4-b]indole-3-carboxylate in Acetone-D$_6$

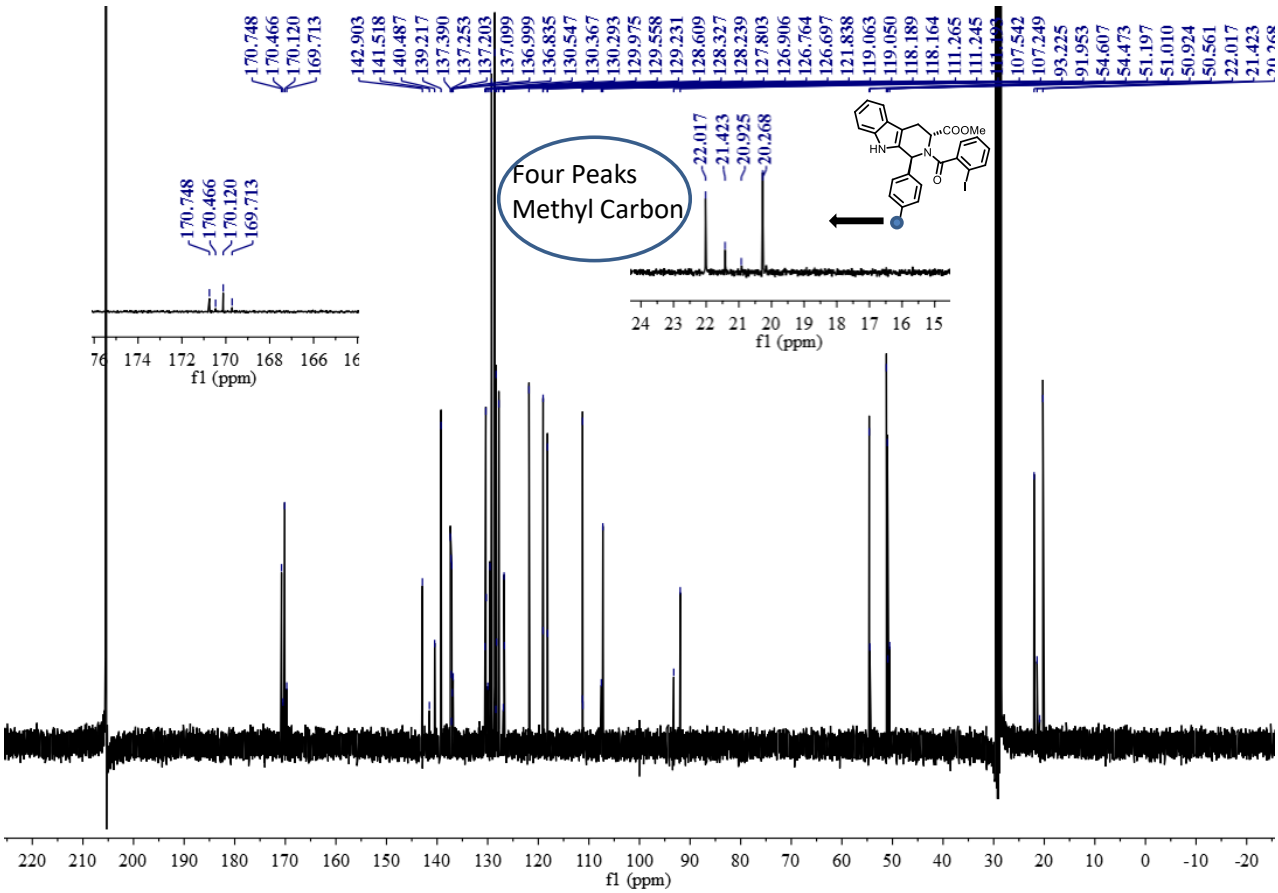

CHAPTER-3

Palladium Catalyzed C(sp^3)-H arylation Followed by De-esterification

3.1. INTRODUCTION:

3.1.1 Carbon-carbon bond forming reactions

This category encompasses reactions specifically designed to forge carbon-carbon (C–C) bonds, which are fundamental transformations in organic chemistry. These processes serve as the corner stone for constructing complex molecular architectures, enabling the synthesis of natural products, pharmaceuticals, agrochemicals, and advanced materials. The ability to form new C–C bonds is critical for extending carbon frameworks, allowing chemists to build molecules with enhanced complexity, functionality, and diversity. Such reactions are indispensable tools in the repertoire of synthetic methodologies, often employing catalytic systems, including transition metals, to achieve high selectivity, efficiency, and sustainability. One of tools of C-C bond formation reaction is palladium-catalyzed C-C bond formation reaction via decarboxylation. [65]

Palladium-catalyzed reductive couplings are among the most important carbon-carbon bond-forming reactions in modern synthetic organic chemistry. Such reactions includes, The π-allyl chemistry (also asymmetric), Stille coupling, Heck reaction, Suzuki reactions, Sonogashira coupling and etc. [66]

3.1.2 Palladium-Catalyzed Decarboxylative Arylation

Palladium-Catalyzed Decarboxylative Arylation is a powerful synthetic method used in organic chemistry to form carbon-carbon bonds by coupling an aryl group with a carbanion derived from a carboxylic acid. This process leverages a palladium catalyst to facilitate the reaction, which involves the loss of carbon dioxide (decarboxylation) from a carboxylic acid or its derivative. Also Pd(0) or Pd(II)-catalyzed protocol for decarboxylative arylation of aromatic C-H bond was developed using aryl acylperoxides as inexpensive aryl sources. Substrates containing pyridyl, oxime, and oxazoline groups undergo effectively ortho-selective C-H arylation with excellent functional group tolerance. [67] Generally, the reactivity of organo-palladium complex is low compared with organo-nickel complexes. However, they have higher chemical stability for oxidations and this makes them easy to use. Therefore, palladium complexes are most commonly used for cross-coupling reactions. Some previous strategic tools for decarboxylative cross coupling reaction. Oxidative decarboxylative cross-couplings have provided a solution to these challenges by offering a more direct pathway that bypasses the need for pre-functionalization of substrates. These reactions enable the incorporation of nitrogen and oxygen nucleophiles without the intermediate oxidation step, streamlining the synthesis process. [68]

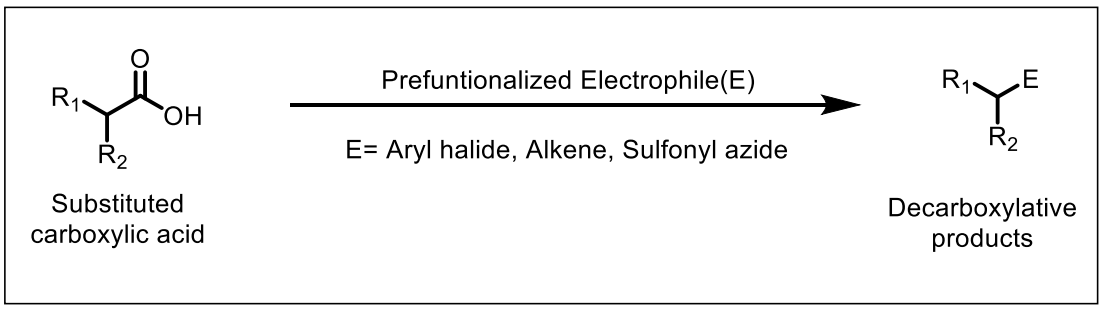

Figure 1: Decarboxylative eletrophillic addition.

Most contemporary strategies for decarboxylative couplings are redox-neutral, which is advantageous as it eliminates the need for additional oxidizing or reducing agents. In these reactions, a carboxylate acts as the pro-nucleophile and is paired with an electrophilic counterpart, such as an organohalide, organosufonyl azides and olefins to form new C–C bonds (Figure 1). Organohalides are commonly chosen due to their established reactivity and effectiveness in various cross-coupling reactions, making this pairing a reliable and efficient approach for constructing complex carbon frameworks. However, when the goal is to form polar C–N and C–O bonds, the reaction strategy often requires modification. Typically, these transformations need the carboxylic acid to be prefunctionalized using an internal oxidant, such as a N-oxyphthalimide (PINO) to facilitate the decarboxylative step (Figure 2). While this prefunctionalization enables subsequent bond formation with nitrogen or oxygen nucleophiles, it also introduces added complexity. The additional step can complicate the synthetic process, necessitate more rigorous purification procedures, and reduce the efficiency of creating large and diverse compound libraries. [68]

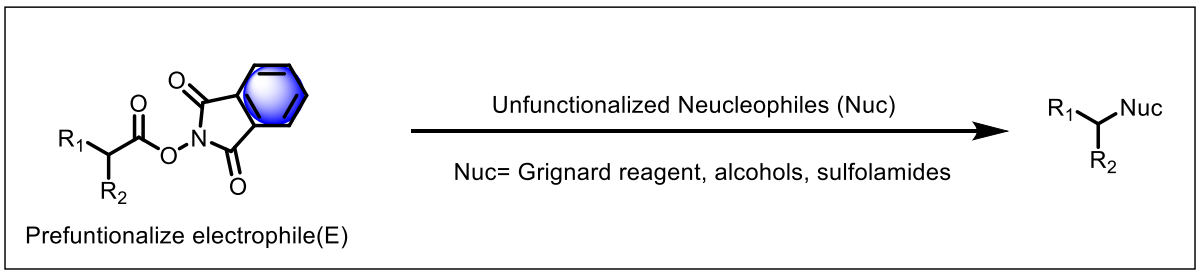

Figure 2: Decarboxylative functionalization with PINO functionalized carboxylic acids.

Another classical example of this type of transformation is decarboxylative Kolbe electrolysis (Figure 3), which allows for the formation of C–C bonds. However, this method often requires a excess amount of the hetero-nucleophile, which acts as a sacrificial oxidant to avoid Kolbe dimerization a competing side reaction that can reduce yields and selectivity [69].

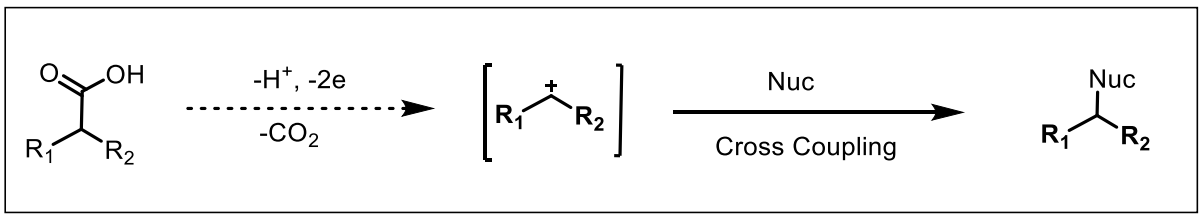

Figure 3: Kolbe electrolysis.

Applications of decarboxylative arylation:

- **Pharmaceutical Synthesis**: Used to create complex molecules for drug discovery.
- **Material Science**: Preparation of functionalized aryl compounds for organic materials.
- **Natural Product Synthesis**: This is a key step in synthesizing molecules with medicinal properties.

3.1.3 Previous decarboxylative cross coupling methodologies

Decarboxylative coupling reaction with alkynyl carboxylic acids and arylsilanes:

A method for decarboxylative coupling of alkynyl carboxylic acids and arylsiloxanes has been developed using a palladium catalyst. The reaction utilizes $Pd(dba)_2$ (1.0 mol %), 1,1-bis(diphenylphosphino)methane (1.0 mol %), and AgF_2 (2.0 equivalents) at 60 °C for 6 hours, yielding the desired coupled products in moderate to good yields. Organosilanes have been utilized as coupling partners in palladium-catalyzed cross-coupling reactions since Hiyama's initial report in 1988 on the coupling of aryl halides with arylsiloxanes. Organosilanes offer several benefits, including stability, non-toxicity, and ease of preparation. Aryl halides are among the most commonly used substrates in reactions involving organosilanes. More recently, a C–H activated substrate has been shown to produce coupled products when reacted with an organosilane in the presence of a nickel catalyst.[1] Triethoxy(4-methylphenyl)silane successfully provided the desired products in moderate to good yields. However, attempts to obtain coupled products using arylsiloxanes like triethoxy-4-nitrophenylsilane and triethoxy-2-thiophenylsilane were unsuccessful (Scheme 1)[75].

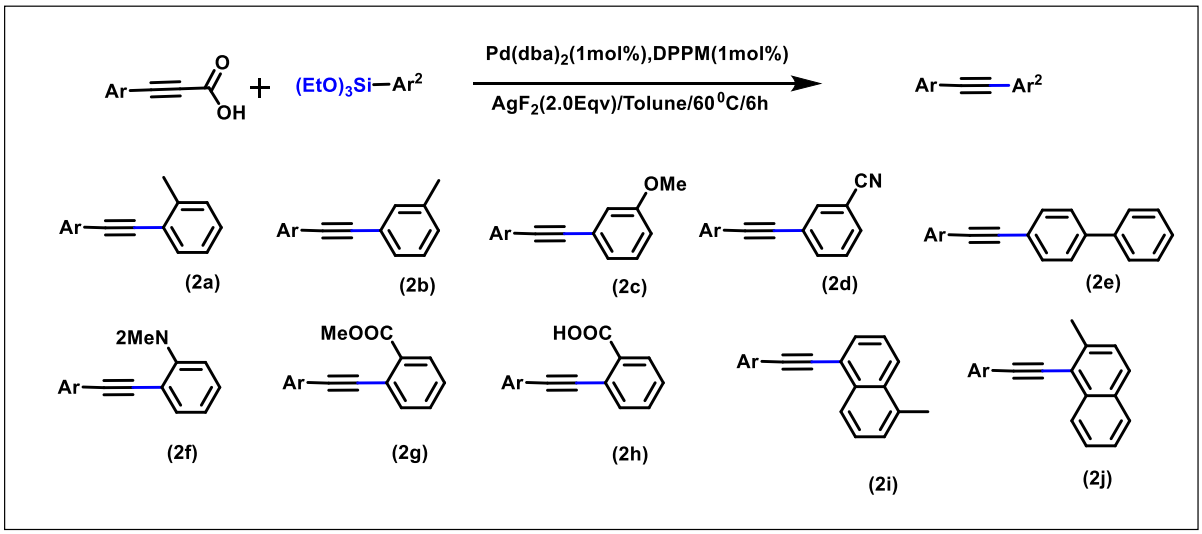

Scheme 1: Decarboxylative coupling reaction with alkynyl carboxylic acids and arylsilanes.

3.1.4 Decarboxylative cross-coupling reactions of 2-picolinic acid:

Novel palladium-catalyzed decarboxylative cross-coupling reactions of 2-picolinic acid with aryl and heteroaryl bromides, including benzenes, naphthalenes, pyridines, and quinolines, have been successfully achieved for C–C bond formation.Arylation of 2-substituted pyridines via Pd-catalyzed decarboxylative cross-coupling reactions of 2-picolinic acid.Derivatives of 2-arylpyridines are significant heterocyclic structural motifs found in numerous natural products, pharmaceuticals, materials, and ligands. Various cross-coupling reactions have been explored for synthesizing 2-arylpyridines using a wide range of aryl halides and organometallic reagents. However, the instability and synthetic challenges associated with 2-pyridyl organometallics limit their use. For instance, while the Suzuki–Miyaura coupling of 2-pyridyl boron derivatives is popular, the inherent instability of 2-pyridyl boronic acid results in limited examples where 2-pyridyl boronates serve as the nucleophilic source in cross-coupling reactions. More recently, Burke's group reported the first identification of 2-pyridyl N-methyliminodiacetic acid (MIDA) boronate, which is air-stable and can be isolated in a chemically pure form. [76] A novel synthetic route to 2-aryl- and heteroaryl-pyridines was discovered and developed using palladium-catalyzed decarboxylative cross-coupling reactions of 2-picolinic acid with aryl- and heteroaryl-bromides. This method features an efficient catalytic system that utilizes commercially available catalyst and ligand components. Additionally, 2-picolinic acid, which is both inexpensive and stable, serves as the starting material in this reaction.

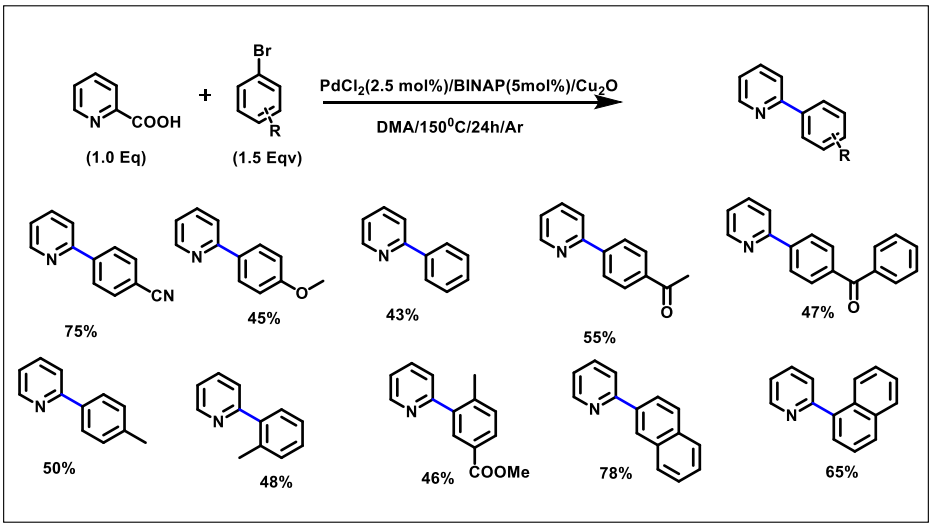

Scheme 2: Decarboxylative cross-coupling reactions of 2-picolinic acid**.**

3.1.4 Stereo selective decarboxylative arylation of unactivated olefins with aryl carboxylic acids:

A palladium(II)-catalyzed, highly regioselective, and stereoselective decarboxylative arylation of unactivated olefins with aryl carboxylic acids has been developed. This method is effective for a variety of unactivated olefins, including allylamides, long-chain functionalized olefins, and purely aliphatic olefins, resulting in the formation of linear E-configured products with high yields. Both electron-rich and electron-deficient aryl carboxylic acids are effective as arylation reagents. The choice of solvent, catalyst precursor, and oxidant was found to significantly influence the reaction efficiency. DMSO, serving as both a co-solvent and ligand, is essential for the catalysis. This method broadens the scope of decarboxylative arylation of olefins with aryl carboxylic acids and offers rapid access to valuable linear arylation products from unactivated Olefins A general and efficient decarboxylative coupling reaction of aryl carboxylic acids with unactivated olefins has been developed under Pd(II) catalysis. This method enables highly regioselective and stereoselective arylation of a wide range of unactivated olefins with variously substituted aryl carboxylic acids, yielding linear products in good to excellent yields with high functional group tolerance. This approach serves as a valuable complement to existing methods for decarboxylative olefination of arene carboxylic acids[77] (Scheme 3).

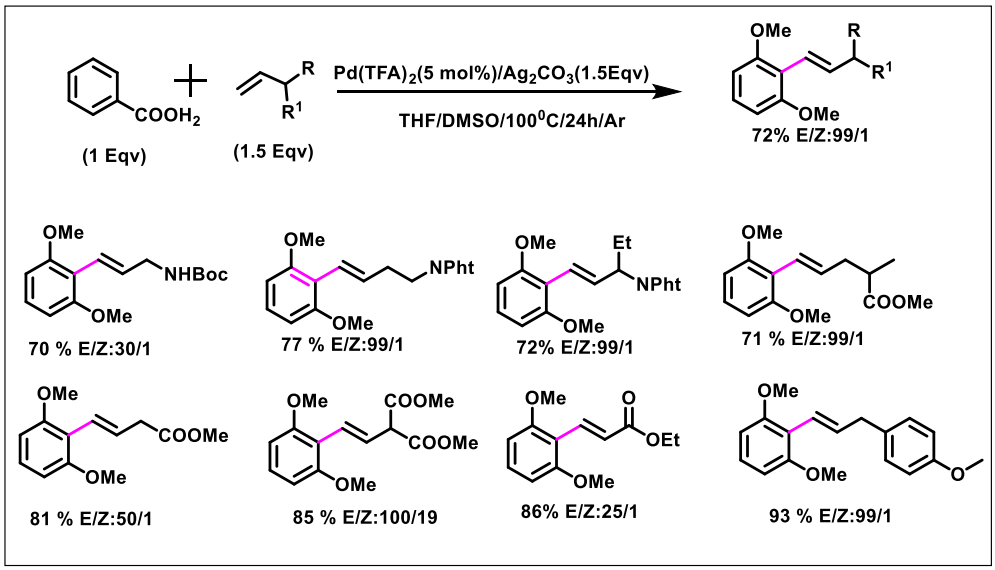

Scheme 3: Stereo selective decarboxylative arylation of unactivated olefins with aryl carboxylic acids.

3.1.5 Decarboxylative γ-Arylation for the Synthesis of Tetrasubstituted Chiral Allenes:

Point-to-axial chirality transfer is accomplished in the decarboxylative γ-arylation of α,α-disubstituted β,γ-alkynoic acids using sterically hindered ortho,ortho′-disubstituted aryl iodides. These palladium-catalyzed reactions proceed with complete enantiospecificity, yielding tetrasubstituted allenes, which are valuable compounds with applications in various fields. An enantiospecific palladium-catalyzed decarboxylative coupling of acyclic β,γ-alkynoic acids with various aryl iodides to form chiral tetrasubstituted allenes is reported. This reaction involves decarboxylative γ-palladation of α,α-disubstituted carboxylic acids, resulting in the formation of tetrasubstituted allenes with complete point-to-axial chirality transfer and excellent yields.Allenes are highly significant as versatile building blocks in organic synthesis. They are also present in natural products, pharmaceutical compounds, and materials science. Although the first synthetic allene was reported by Burton and von Pechmann in 1887, the correct structural assignment came much later. The unique reactivity and inherent chirality (in substituted systems) of allenes stem from the cumulative arrangement of two orthogonal π-bonds. These π-systems participate in various chemical transformations, including cycloaddition and metal-catalyzed addition reactions, and play a role in natural product synthesis. Consequently, substantial efforts have been made to develop synthetic methods for enantiomerically pure allenes. Common approaches include stereospecific formal SN2′ substitutions from enantiopure propargylic precursors and sigmatropic rearrangements, both involving propargylic compounds. Additionally, methods for the stereoselective synthesis of di- and trisubstituted allenes have also been developed. A palladium-catalyzed method has been developed for synthesizing chiral tetrasubstituted allenes from α,α-disubstituted β,γ-alkynoic acids and sterically hindered ortho,ortho′-disubstituted aryl iodides through a decarboxylative coupling reaction, achieving yields

of up to 99%. The γ-arylation proceeds with excellent enantiospecificity, facilitating the formation of highly enantioenriched tetrasubstituted allenes[78] (Scheme 4).

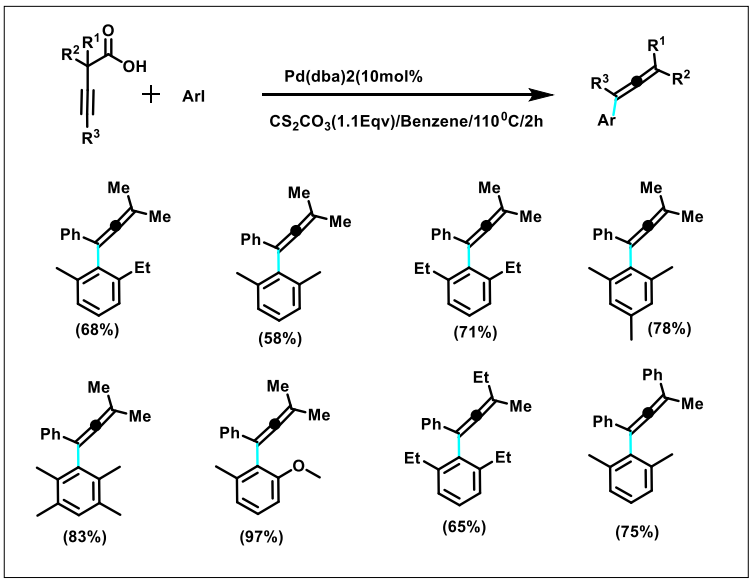

Scheme 4: Decarboxylative γ-Arylation for the Synthesis of Tetrasubstituted Chiral Allenes

3.1.6 Decarboxylative Arylation of C−H Bonds by Aryl Acylperoxides:

A $Pd(OAc)_2$-catalyzed method for decarboxylative arylation of aromatic C−H bonds was developed using aryl acylperoxides as cost-effective aryl sources. Substrates featuring pyridyl, oxime, and oxazoline directing groups undergo highly effective ortho-selective C−H arylation with notable functional group tolerance. The proposed mechanism starts with directing-group-assisted cyclopalladation, followed by the reaction of the resulting palladacycle with aryl radicals that are generated in situ through the thermal decomposition of the acylperoxides. A method for decarboxylative arene C−H arylation was developed using aryl acylperoxides as reagents. These acylperoxides serve as an inexpensive and easily synthesized source of aryl groups from various carboxylic acids, producing CO2 as a harmless byproduct. This findings present a novel strategy for biaryl formation, leveraging cross-coupling reactions between organopalladium complexes and aryl radicals[79] (Scheme 5).

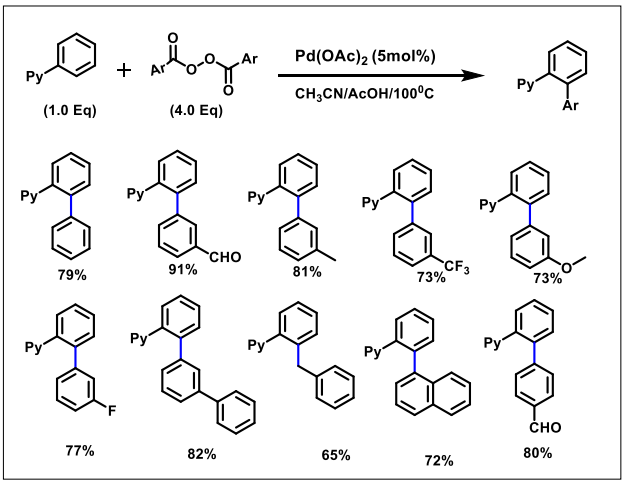

Scheme 5: Decarboxylative Arylation of C−H Bonds by Aryl Acylperoxides.

3.1.7 Decarboxylative Couplings of 2-(2-Azaaryl) acetates withAryl Halides and Triflates:

Pd-catalyzed decarboxylative cross-couplings of 2-(2-azaaryl) acetates with aryl halides and triflates have been discovered, offering potential applications for synthesizing various functionalized pyridines, quinolines, pyrazines, benzoxazoles, and benzothiazoles. Theoretical analysis indicates that, in the decarboxylation transition state, the nitrogen atom at the 2-position of the heteroaromatic compound coordinates directly to Pd(II). Pd-catalyzed decarboxylative cross-coupling of 2-(2-azaaryl) acetates with aryl halides and triflates has been discovered. This reaction holds promise for synthesizing functionalized azaarenes. Theoretical analysis suggests that the nitrogen atom at the 2-position of the heteroaromatics directly coordinates to Pd(II) in the decarboxylation transition state[80] (Scheme 6).

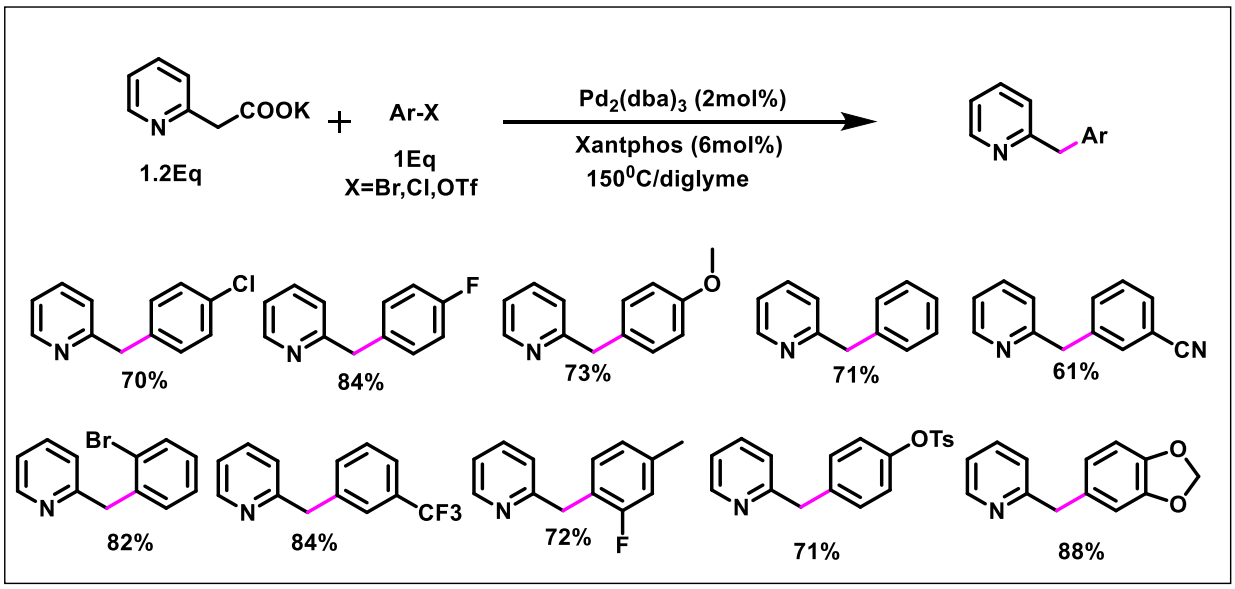

Scheme 6: Decarboxylative Couplings of 2-(2-Azaaryl) acetates withAryl Halides and Triflates.

3.1.8 Results and discussion:

Based on this previous research, we extended this protocol to apply to a broader range of coupling reactions of aryl halide with Sp^3 C-H bond via decarboxylation. A palladium-catalyzed arylation followed by de-esterification is a two-step process widely utilized in organic synthesis due to its efficiency in constructing complex molecular structures. The first step, palladium-catalyzed arylation, involves the formation of a new carbon-carbon (C–C) bond. This step typically utilizes a palladium catalyst, such as Pd(0) or Pd(II), in conjunction with ligands that enhance the reactivity and selectivity of the reaction. The arylation often employs aryl halides or aryl triflates as the coupling partners, allowing for the introduction of various aryl groups onto an ester substrate. The second step, de-esterification, involves the removal of the ester group, converting it to a carboxylic acid or another functional group, depending on the reaction conditions. This step is crucial for unveiling the free acid form or creating functional derivatives necessary for further chemical transformations. De-esterification can be achieved through hydrolysis using either acidic or basic conditions, with the choice depending on the stability of the product and the presence of other functional groups in the molecule. The combination of these steps provides a powerful strategy for generating complex, highly functionalized arylated molecules from simple ester precursors. This method is particularly valuable in medicinal chemistry and materials science, where precise modifications to the molecular framework can lead to compounds with desirable biological or physical properties. The ability to selectively form C–C bonds and subsequently modify the ester group enables chemists to fine-tune molecular architectures for specific applications. Decarboxylative coupling reactions have emerged as essential methodologies in modern synthetic organic chemistry for constructing complex molecular architectures. The primary advantage of these reactions lies in their utilization of carboxylic acids as starting

materials. Carboxylic acids are highly appealing due to their wide availability, stability, and the vast array of structurally diverse options they present. This accessibility makes carboxylic acids ideal feedstock chemicals for building molecular complexity through decarboxylative transformations. Most contemporary strategies for decarboxylative couplings are redox-neutral, which is advantageous as it eliminates the need for additional oxidizing or reducing agents. In these reactions, a carboxylate acts as the pronucleophile and is paired with an electrophilic counterpart, such as an organohalide, to form new C–C bonds. Organohalides are commonly chosen due to their established reactivity and effectiveness in various cross-coupling reactions, making this pairing a reliable and efficient approach for constructing complex carbon frameworks. Recent advancements have refined these electrochemical methods. Baran's development of an electrochemical decarboxylative ether synthesis represents a significant improvement, employing stoichiometric silver(I) as a terminal oxidant to stabilize the nucleophile and facilitate the desired bond formation. Although promising, the scope of electrochemical decarboxylative Ritter reactions remains limited, requiring further exploration and optimization to become broadly applicable. Transition-metal-mediated oxidative decarboxylative couplings conducted under thermal conditions are another viable approach. However, these reactions often require high temperatures, which can lead to poor chemoselectivity and limited functional group tolerance—significant drawbacks when working with sensitive or multifunctional molecules. In response to these limitations, Lundgren introduced a milder copper-catalyzed oxidative decarboxylative C–N bond formation. While effective under less harsh conditions, this method shows optimal results primarily with electron-deficient substrates that enhance anionic decarboxylation. This specificity limits its general applicability, highlighting the ongoing need for versatile, functional-group-tolerant strategies that can accommodate a wider range of substrates and reaction condition. For intra -molecular reaction

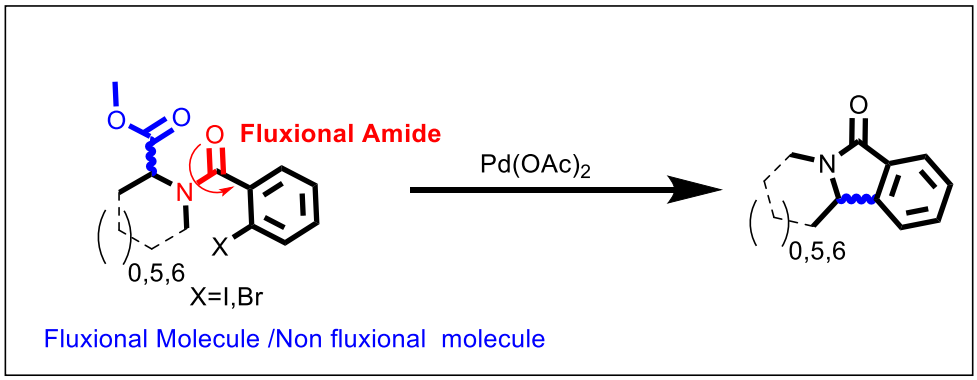

Scheme 7: De-ester arylation (This work)

On the basis of this research, we extended to apply this protocol to a broader range coupling reaction of aryl halide with ester of fluxinal and as well as non fluxional substrates in absence of any oxidant. Consequently, this intramolecular reaction of N-adjacent sp^3 methyl ester with bromo or iodo group was selected as a model reaction. Notably, there has been a rapid emergence of decarboxylative coupling reactions

utilizing carboxylic acids as coupling partners. This development is spurred by the ease of storage and handling of such substrates, which are, in some cases, more readily available compared to halides or alkenes. Various building blocks, including arenecarboxylic, heteroarenecarboxylic, acrylic, propiolic, and α-ketocarboxylic acids, can be harnessed for these promising coupling reactions. While the potential of acrylic acids in these reactions is substantial, their exploration has been relatively limited, in organic synthesis, the establishment of a C-C bond between an aromatic carbon and the carbon alpha to a carbonyl group stands out as one of the most formidable challenges. Notably, there has been a substantial endeavor focused on enhancing and solidifying palladium catalysis methodology as an effective pathway for the synthesis of numerous biologically active indoloisquinoline, isoindolinone, indolinone. An innovative PdII-catalyzed sp^3 C–H arylation process of ester has been devised. This approach leverages a unique indoline-based scaffold, demonstrating its ability to selectively guide C–H bond functionalization. The outcome of this reaction presents a valuable technique for the synthesis of arylated compounds derived from ester, yielding consistently good to excellent yields. Importantly, the newly introduced molecular scaffold allows for facile attachment, removal, and recovery in the process. Building on recent advancements in decarboxylative coupling reactions, we extended this protocol to explore a broader range of coupling reactions between aryl halides and esters, particularly focusing on fluxinal substrates and non-fluxional substrates, all without the need for an external oxidant. For our model reaction, we selected an intramolecular reaction of an N-adjacent sp^3 methyl ester with either a bromo or iodo group. This reaction choice allowed us to evaluate the efficiency and versatility of the coupling protocol in the absence of an added oxidizing agent, which has been a defining feature of many recent decarboxylative strategies. The rapid emergence of decarboxylative coupling reactions using carboxylic acids as coupling partners is largely attributed to the ease with which carboxylic acids can be stored and handled. Unlike halides or alkenes, which may require more stringent conditions or specialized handling, carboxylic acids are often more readily available and less prone to degradation or reactivity issues. This makes carboxylic acids, including arylcarboxylic acids, hetero arylcarboxylic acids, acrylic acids, propiolic acids, and α-ketocarboxylic acids, ideal building blocks for decarboxylative coupling reactions. Despite the promising potential of acrylic acids in these reactions, their application has been somewhat limited, and more exploration is needed to fully unlock their utility in diverse synthetic pathways. Among the many challenges in organic synthesis, establishing a C–C bond between an aromatic carbon and the carbon alpha to a carbonyl group remains one of the most formidable. This bond formation is critical for constructing complex molecules, such as biologically active compounds, yet it requires precise control and often harsh conditions. As such, substantial efforts have been focused on refining palladium-catalyzed methodologies for C–C bond formation, particularly in the synthesis of biologically significant molecules such as indoloisquinolines, isoindolinones, and indolinones. Palladium-catalyzed reactions have become an indispensable tool for such transformations, offering efficient pathways for building complex molecular scaffolds. In line with this, we also developed an innovative PdII-catalyzed sp^3 C–H

arylation process of esters. This new method capitalizes on an indoline-based scaffold, which not only facilitates selective C–H bond functionalization but also serves as a guiding element to ensure high selectivity in the coupling reaction. This selective activation of the C–H bond in the ester substrate leads to the formation of arylated compounds in consistently good to excellent yields. The unique indoline-based scaffold plays a crucial role by enabling easy attachment, removal, and recovery of the catalyst, thereby streamlining the reaction process and enhancing the overall efficiency of the synthetic route. The successful application of this Pd(II)-catalyzed arylation process is a significant advancement in ester functionalization. It provides a reliable and efficient method for generating arylated ester derivatives, with potential applications in the synthesis of complex bioactive molecules. Moreover, this approach demonstrates the versatility of palladium catalysis in overcoming the challenges of functionalizing sp^3 C–H bonds, making it a powerful tool in synthetic organic chemistry.

This reaction achieves sp^3 de-esterification with aryl bromides or iodides, resulting in trisubstituted compounds with excellent yields.

Table 1: Optimization studies

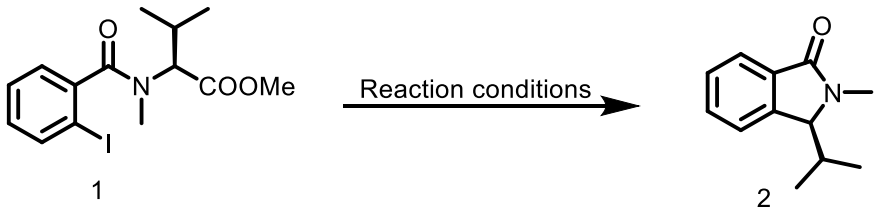

1 2

Entry	Catalyst (p= 2.5mol%) (q=5mol%) (r= 10mol%)	Ligand	Base	Condition/Time(Hours)	Solvent	Temp.	Yield[b] (%) 2
1	-	-		-	Dioxane	100°C	NR
2	$PdCl_2$(p)	PPh_3	K_2CO_3	N_2/24	Dioxane	100°C	NR
3	$Pd(acac)_2$(p)	PPh_3	K_2CO_3	-	Dioxane	100°C	NR
4	$Pd(PPh_3)_4$(p)	PPh_3	K_2CO_3	N_2/24	Dioxane	100°C	NR
5	$Pd(dba)_2$(p)	PPh_3	K_2CO_3	N_2/24	Dioxane	100°C	NR
6	$Pd(OAc)_2$(p)	PPh_3	K_2CO_3	N_2/24	Dioxane	100°C	NR
7	$Pd(OAc)_2$(p)	Xphos	K_2CO_3	N_2/24	Dioxane	100°C	0

8	$Pd(OAc)_2$(p)	PCy_3	K_2CO_3	N_2/24	Dioxane	100°C	Tr
9	$Pd(OAc)_2$(p)	PCy_3	K_3PO_4	N_2/24	Dioxane	100°C	0
10	$Pd(OAc)_2$(p)	PCy_3	KOAc	N_2/24	Dioxane	100°C	0
11	$Pd(OAc)_2$(p)	PCy_3	K_2CO_3	N_2/24	DMSO	100°C	<5
12	$Pd(OAc)_2$(p)	PCy_3	K_2CO_3	O_2/24	DMSO	,,	0
13	,,	PCy_3	K_2CO_3	N_2/24	DMSO	120°C	8
14	,,	PCy_3	K_2CO_3	N_2/24	DMSO	130°C	30
15	,,	PCy_3	K_2CO_3	N_2/24	DMSO	140°C	40
16	,,	PCy_3	K_2CO_3	N_2/24	DMSO:Dioxane 1:1	140°C	55
17	,,	PCy_3	K_2CO_3	N_2/24	DMSO:Dioxane 2:1	,,	58
18[a,b]	**,,**	**PCy_3**	**K_2CO_3**	**N_2/24**	**DMSO:Dioxane 3:1**	**,,**	**77**
19	,,	PCy_3	K_2CO_3	K_2CO_3	DMSO:Dioxane 4:1	,,	71
20	,,	PCy_3	Na_2CO_3	N_2/24	DMSO:Dioxane 3:1	,,	Tr
21	,,	PCy_3	Et_3N	N_2/24	DMSO:Dioxane 3:1	,,	0
22	,,	PCy_3	ACOH	N_2/24	DMSO:Dioxane 3:1	,,	0
23	,,	AgOAc	-	N_2/24	DMSO:Dioxane 3:1	,,	0
24	,,	Ag_2CO_3	-	N_2/24	DMSO:Dioxane 3:1	,,	0
25	,,	$K_2S_2O_8$	-	N_2/24	DMSO:Dioxane 3:1	,,	0
26	,,	BQ	-	N_2/24	DMSO:Dioxane	,,	0

					3:1		
27	,,	AgOAc	-	O_2/24	DMSO:Dioxane 3:1	,,	0
28	,,	Ag_2CO_3	-	O_2/24	DMSO:Dioxane 3:1	,,	0
29	,,	$K_2S_2O_8$	-	O_2/24	DMSO:Dioxane 3:1	,,	0
30	,,	BQ	-	O_2/24	DMSO:Dioxane 3:1	,,	0
31	,,	PCy_3	K_2CO_3	Air	DMSO:Dioxane 3:1	,,	0
32	,,	PCy_3	K_2CO_3	N_2/24	DMSO:DCE 3:1	,,	0
33	,,	PCy_3	K_2CO_3	N_2/24	DMSO:Tolune 3:1	,,	0
34	,,	PCy_3	K_2CO_3	N_2/24	DMSO:DMF 3:1	,,	0
35	,,	PCy_3	K_2CO_3	N_2/24	DMSO:THF 3:1	,,	0
36	,,	PCy_3	K_2CO_3	N_2/24	DMSO:DME 3:1	,,	0
37		PCy_3	K_2CO_3	N_2/24	DMF	,,	0
38	$Ni(OAc)_2$	PCy_3	K_2CO_3	N_2/24	DMSO:Dioxane 3:1	,,	0
39	$Pd(OAc)_2$ (q)	PCy_3	K_2CO_3	N_2/18	DMSO:Dioxane 3:1	,,	75
40[b]	$Pd(OAc)_2$ (r)	PCy_3	K_2CO_3	N_2/12	DMSO:Dioxane 3:1	,,	78

[a]**Standard Reaction Conditions:1a** (0.2 mmol), $Pd(OAc)_2$ (10 mol%), PCy_3 (20 mol%), K_3CO_3(3eqv), DMSO: Dioxane (2mL, 3:1), N_2, 140°C, 12h. [b]Isolated yields, Tr = Traces, NR= No reaction.

The ester-amide-halide 1a was selected as the model substrate to initiate this study, with $Pd(OAc)_2$ as the catalyst and PCy_3 as the ligand (Table 1). Initial solvent screening indicated that 1,4-dioxane and DMSO favored the desired product 2a more effectively than toluene, DMAc, DMF, or DCE (Table 1, entry 6). Increasing the temperature to 130 °C identified DMSO:1,4-dioxane (3:1) as the optimal solvent mixture (Table 1, entry 6). At 140 °C, using DMSO:1,4-dioxane (3:1) resulted in a 75% yield of 2a (Table 1, entry 7). Substitution of $Pd(OAc)_2$ with $Ni(OAc)_2$ resulted in no product formation (Table 1, entry 2), and changing the ligand to Xphos, PPh_3, Xantphos, $P(o\text{-}Tol)_3$ produced only trace amounts of product by TLC (Table 1, entry 3). Increasing $Pd(OAc)_2$ to 20 mol% and PCy_3 to 40 mol% (entry 11) did not improve the yield. Control experiments confirmed the essential roles of both the palladium catalyst and phosphorus ligand in the reaction (entries 11 and 12), as omitting either component led to no conversion of 1a to 2a. Thus, the optimized conditions are as shown in entry.

3.1.9 Substrate Scopes, IsoIndolinone Synthesis by Pd-Catalyzed Arylation and De-esterification Reactions:

To further investigate the applicability of the C–C coupling followed by de-esterification reaction, additional substrates were explored (**Scheme 8**). The initial focus was on substituted β-amide esters (**Scheme 3**, eqn (1)–(3)). Methyl 3-((2-iodophenyl)(methyl)amino)-3-oxopropanoate (**3**) was subjected to standard reaction conditions, yielding the ring-closed product **4**. Notably, under these conditions, simultaneous de-esterification and de-halogenation occurred due to the presence of an group Free N-H rather than a N-methyl group. Product **4** resulted from C1–C2 cleavage, forming a thermodynamically stable enone product that subsequently tautomerized to yield 1-methylindolin-2-one (**3ap**). The successful synthesis of the desired product 1,3-dimethylindolin-2-one (**6**) from methyl 3-((2-iodophenyl)(methyl)amino)-2-methyl-3-oxopropanoate (**5**) under standard conditions suggested that the secondary carbon was not highly reactive in sp^3 C–C coupling. Similarly, methyl 3-((2-iodophenyl)(methyl)amino)-2,2-dimethyl-3-oxopropanoate (**7**) likely exhibits effects comparable to **5** in C–C bond cleavage to form **8**. In conclusion, only sp^3 C units appear to undergo ring-closing followed by de-esterification under standard reaction conditions.

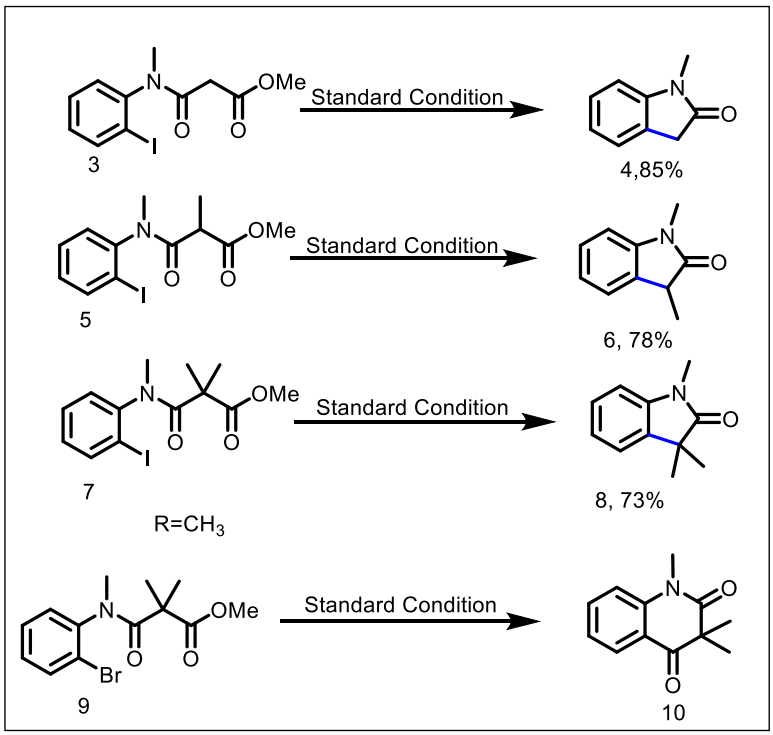

Scheme 8: Substrate scope of beta keto esters

3.1.10 Substrate Scopes, Indolinone Synthesis by Pd Catalyzed De-ester arylation Reaction:

This methodology was also applied to the synthesis of indolinone. (see **Scheme 9**), by varying in different amino acids. Indolinone derivatives (**12**, **14, 16, 18**) were successfully synthesized from the corresponding amino ester derived aryl-amides (**11, 13 ,15, 17**) in moderate to good yields as colorless solids as shown in the **Scheme 9**.

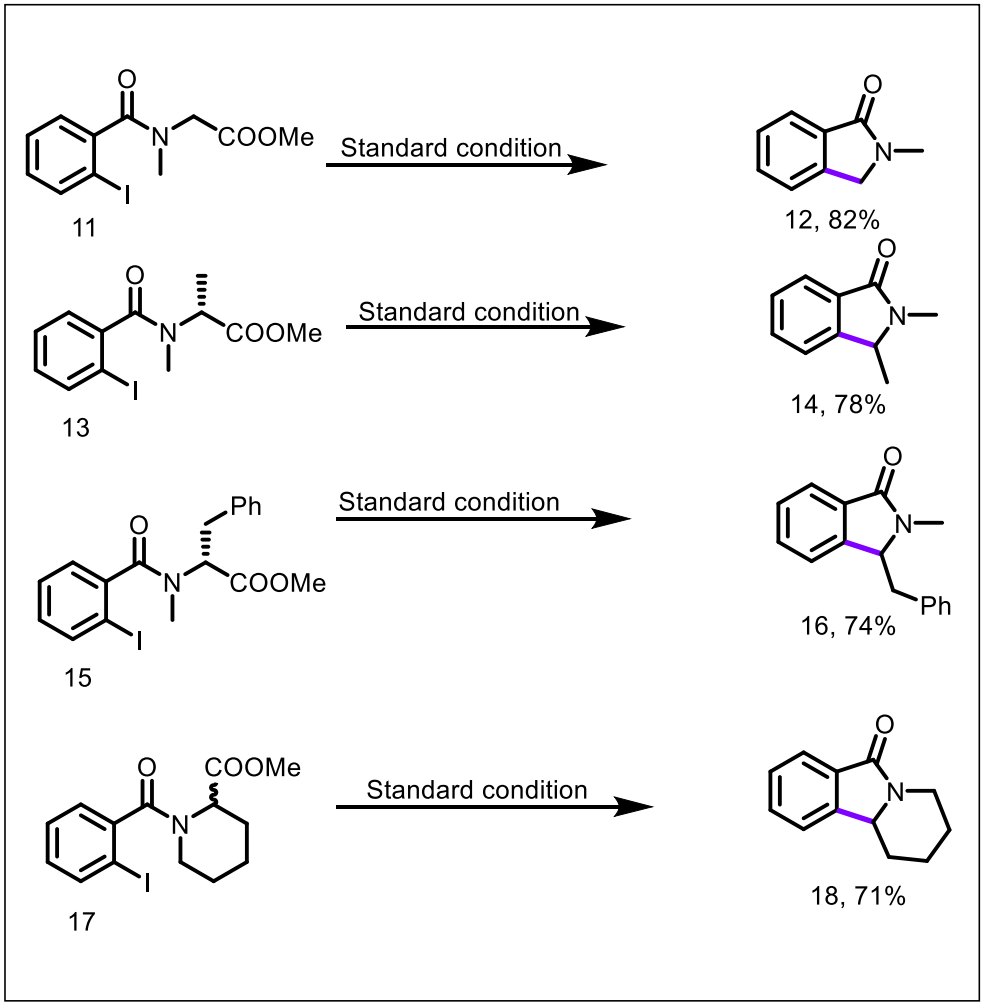

Scheme 9: Substrate scope of N-methyl amino acids

3.1.11 Synthesis of Azatoxin analogues by Pd Catalyzed De-ester arylation Reaction

A substrate scope for biologically active drug molecules such as azatoxin also well explored. It can be seen in the following **Scheme 10**.

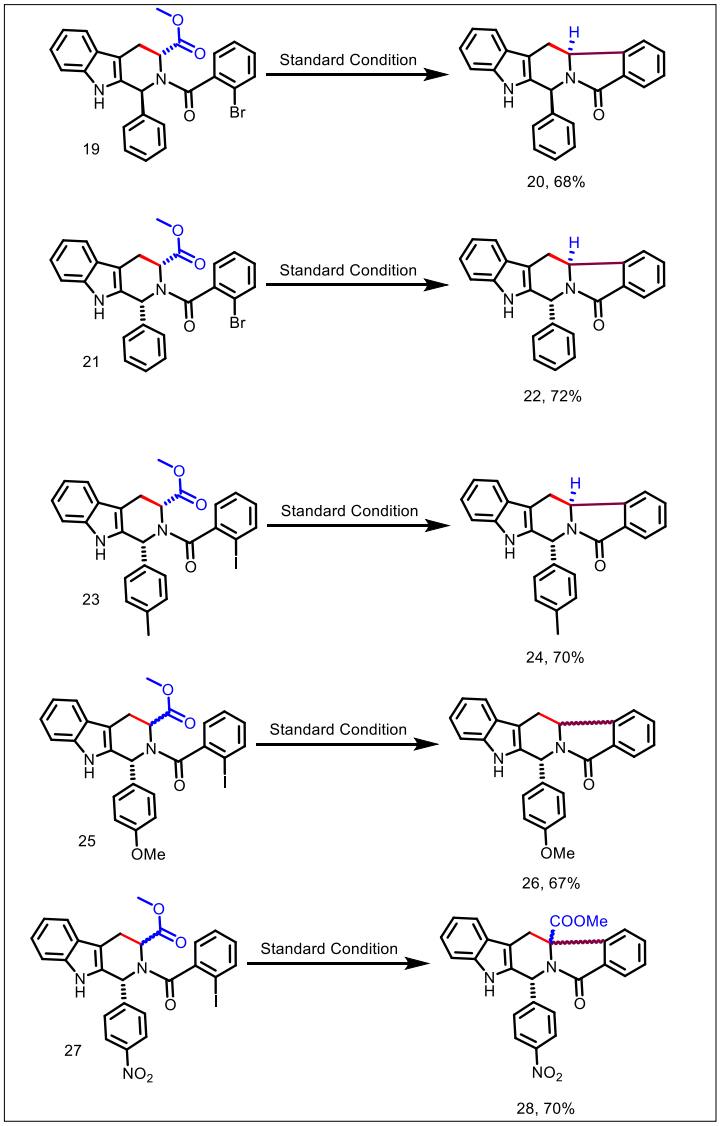

Scheme 10: Substrate scope for complex systems

3.1.12 Probable Mechanism.

Based on some previous literature reports and the control experiment, a mechanism is proposed for the Pd-catalyzed de-ester C–C coupling as illustrated in Scheme **11**. Initially, Pd(0) undergoes oxidative addition with the aryl iodide, leading to the formation of the corresponding aryl Pd(II)-species (I). Subsequent ligand exchange followed by insertion formation of the corresponding aryl six membered Palladacyclic intermediate (II). This species then undergoes reductive elimination generating intermediate (III).

Then ester-methyl abstraction followed by Pd(II) incorporation generating intermediate (IV) and sulfoxonium ylide. Furthermore CO_2 exclusion results in the formation of product **2** and regeneration of Pd(0).

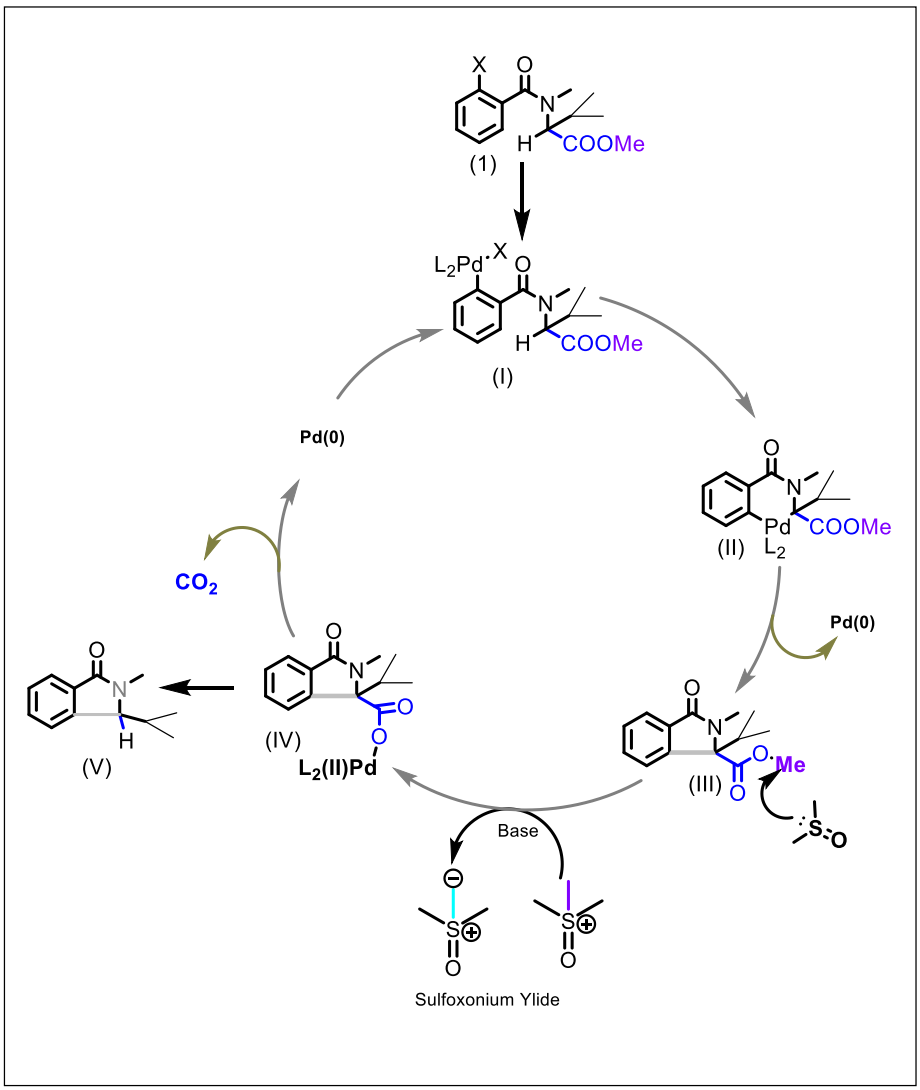

Scheme 11: Plausible reaction pathway A.

3.1.13 Conclusion:

In summary, a Pd-catalyzed process for synthesis of different isoindolinone derivatives are synthesized via intramolecular reaction are reported here. This method involves different amino acid derived tertiary amides as substrate and sterically hindered ortho, ortho'-disubstituted aryl iodides, via a de-ester coupling reaction. The α-arylation generating scope for synthesis of tetrasubstituted indolinone, isoindolinone and indoloisoquinoline.

3.1.14 Supporting Information:

Experimental section:

General Information

All the reagents and solvents used in the present study were purchased from Sigma-Aldrich, TCI and Thermo Fischer Scientific, respectively. All reactions were carried out in an oven-dried reaction tube under an air atmosphere. Silica gel TLC plate were used to perform TLC analysis.All the ^{1}H and ^{13}C NMR spectra were recorded in a 400 MHz and 600 MHz spectrometer. ESI mass spectral analysis was done using the LCQ-ORBITRAP-XL instrument. Bruker Kappa Apex II X-ray crystallography machine was used to solve the crystal structure. Singlet (s), doublet (d), triplet (t), and multiplet (m) were designated as ^{1}H NMR multiplicity patterns. Silica gel (100−200 mesh) and (230−400 mesh) were used for column chromatographic separations. Single crystals of products were obtained through slow evaporation (at room temperature) of a solution in chloroform.

General Synthetic Procedure:

Procedure A: Synthesis of starting Amides

To a dried round bottom flask equipped with a magnetic stir bar was added a solution of the respective aryl carboxylic acid chloride (2.0 mmol, 1 equiv) in DCM (20 Eqv), corresponding amine (2.4 mmol,1.2 equiv.), 0 °C under N_2 atmosphere. The reaction was allowed to stir for 12 h. After completion, the reaction mixture was diluted with DCM (50 mL). The organic layer was washed with aq. $NaHCO_3$ (15 mL), brine (25 mL). Combined organic layer was dried over anhydrousNa_2SO_4, evaporated under *vaccuo*. Resulting crude mixture was purified by column chromatography using EtOAc:Hexane to afford the desired Amide compound.

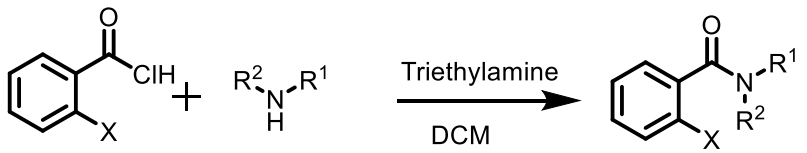

Procedure B: Synthesis of N-methyl amide from their corresponding amide

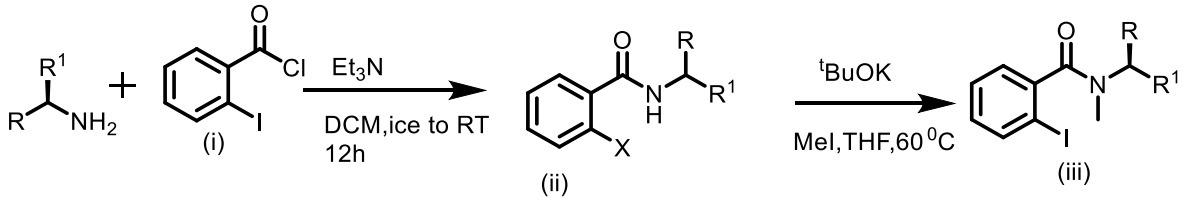

To a dried round bottom flask equipped with a magnetic stir bar was added a solution of the respective Amide(2XX) (1.0mmol, 1 equiv) in Dry THF (20 Eqv), Potassium tertbutoxide (1.5 mmol,1.5 equiv.), 0 °C under N_2 atmosphere, Then methyl iodide (3

mmol, 3 eqv). Was added. The reaction was allowed to stir for 12 hours at 60 ºC. After completion, the reaction mixture was evaporated to dryness & diluted with Ethyl acetate (50 mL). The organic layer was washed with saturated $NaHCO_3$ (15 mL) and brine (25 mL). The combined organic layer was dried over anhydrous Na_2SO_4, evaporated under *vacuum*. The resulting crude mixture was purified by column chromatography using EtOAc: Hexane to afford the desired N-methyl Amide (**3a**).

Procedure C: Synthesis of different alkyl ester from their corresponding methyl ester.

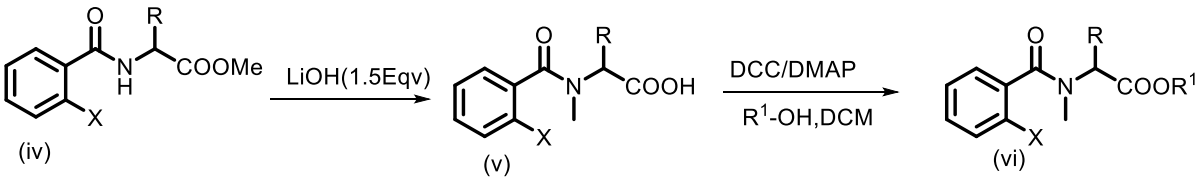

Procedure C (A): To a dried round bottom flask equipped with a magnetic stir bar was added a solution of the respective methyl Ester(**3yy**) (1.0mmol, 1 equiv) in THF: MeOH: Water (1:1:1), Lithium Hydroxide (1.5 mmol,1.5 equiv.), 0 °C under N_2 atmosphere. The reaction was allowed to stir for 12 hours at room temperature. After completion, the reaction mixture was evaporated to dryness & diluted with ethyl acetate (50 ml). The organic layer was washed with saturated aq. Citric Acid (15 mL), brine (25 mL) Combined organic layer was dried over anhydrous Na_2SO_4, evaporated under *vaccuo*. Resulting crude mixture was purified by column chromatography using EtOAc: Hexane to afford the desired Acid compound

Procedure C (B). This Acid(**4zz**) was added in a dried round bottom flask equipped with a magnetic stir bar, Dichloromethane was added at 0^0C. Then alcohol (5Eqv), DCC(1.3Eqv), DMAP(0.1Eqv) was added. The reaction was allowed to stir for 12 hours at Room Temperature.The Reaction mixture was passed through the celite pad,evaporated under *vaccuo*. Resulting crude mixture was purified by column chromatography using EtOAc: Hexane to afford the desired Acid compound

Synthesis of methyl (1S,3R)-1-argio-2,3,4,9-tetrahydro-1H-pyrido[3,4-b] indole-3-carboxylate & methyl (1R,3R)-1-argio-2,3,4,9-tetrahydro-1H-pyrido[3,4-b]indole-3-carboxylate

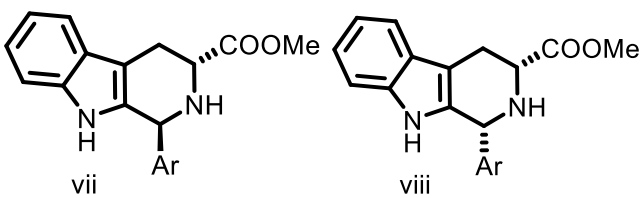

In Accordance with reference number [68] above two beta- carboline compound was Synthesized.

Synthesis of methyl (1R,3R)-2-(2-iodobenzoyl)-1-phenyl-2,3,4,9-tetrahydro-1H-pyrido[3,4-b]indole-3-carboxylate

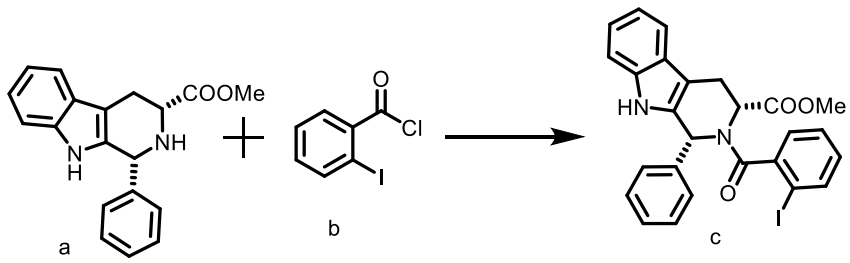

The same general procedure A was followed with 0.25g (2.0mmol, 1.0 equiv.) of corresponding acid. Column chromatography (SiO_2, eluting with 12% ethyl acetate/pet ether) afforded the desired product as white solid.

Synthesis Of methyl (1S,3R)-2-(2-iodobenzoyl)-1-phenyl-2,3,4,9-tetrahydro-1H-pyrido[3,4-b]indole-3-carboxylate

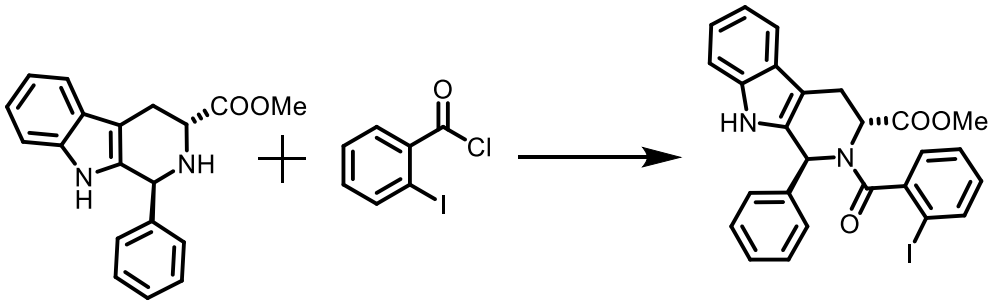

The same general procedure A was followed with 0.25g (2.0mmol, 1.0 equiv.) of corresponding acid. Column chromatography (SiO_2, eluting with 12% ethyl acetate/pet ether) afforded the desired product as white solid.

Synthesis of methyl (1R,3R)-2-(2-iodobenzoyl)-1-(p-tolyl)-2,3,4,9-tetrahydro-1H-pyrido[3,4-b]indole-3-carboxylate

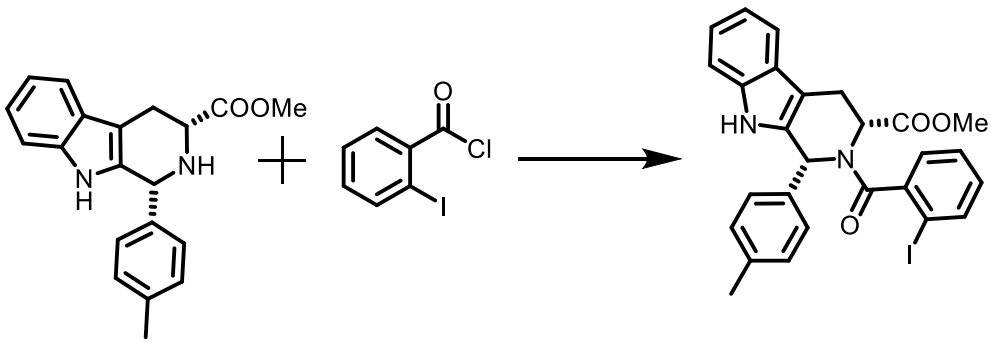

The same general procedure A was followed with 0.25g (2.0mmol, 1.0 equiv.) of corresponding acid. Column chromatography (SiO_2, eluting with 12% ethyl acetate/pet ether) afforded the desired product as white solid.

Synthesis of methyl (3R)-2-(2-iodobenzoyl)-1-(4-methoxyphenyl)-2,3,4,9-tetrahydro-1H-pyrido[3,4-b]indole-3-carboxylate

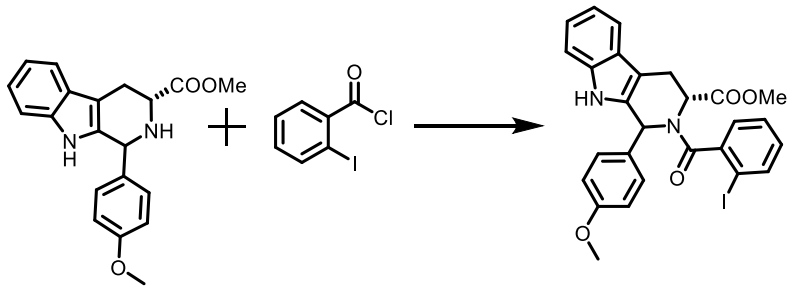

The same general procedure A was followed with 0.25g (2.0mmol, 1.0 equiv.) of corresponding acid. Column chromatography (SiO_2, eluting with 12% ethyl acetate/pet ether) afforded the desired product as white solid.

Synthesis Of methyl (3R)-2-(2-iodobenzoyl)-1-(4-nitrophenyl)-2,3,4,9-tetrahydro-1H-pyrido[3,4-b]indole-3-carboxylate

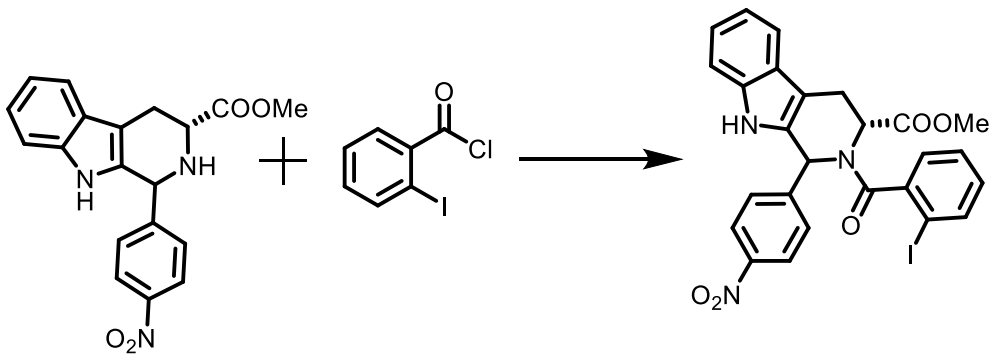

The same general procedure A was followed with 0.25g (2.0mmol, 1.0 equiv.) of corresponding acid. Column chromatography (SiO_2, eluting with 12% ethyl acetate/pet ether) afforded the desired product as light yellow solid.

Synthesis of methyl 3-((2-iodophenyl)(methyl)amino)-3-oxopropanoate.

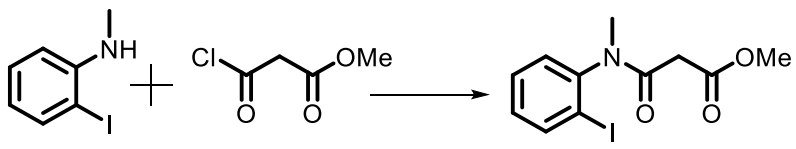

The same general procedure A was followed with 0.25g (2.0mmol, 1.0 equiv.) of corresponding acid. Column chromatography (SiO_2, eluting with 12% ethyl acetate/pet ether) afforded the desired product as light yellow solid.

Synthesis of methyl 3-((2-iodophenyl)(methyl)amino)-2-methyl-3-oxopropanoate

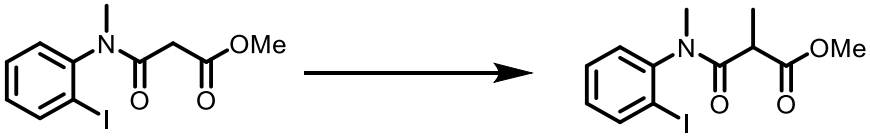

The same general procedure B was followed with 0.25g (2.0mmol, 1.0 equiv.) of corresponding acid. Column chromatography (SiO_2, eluting with 12% ethyl acetate/pet ether) afforded the desired product as light yellow solid.

Synthesis of methyl 3-((2-iodophenyl)(methyl)amino)-2,2-dimethyl-3-oxopropanoate.

The same general procedure B was followed with 0.25g (2.0mmol, 1.0 equiv.) of corresponding acid. Column chromatography (SiO_2, eluting with 12% ethyl acetate/pet ether) afforded the desired product as light yellow solid.

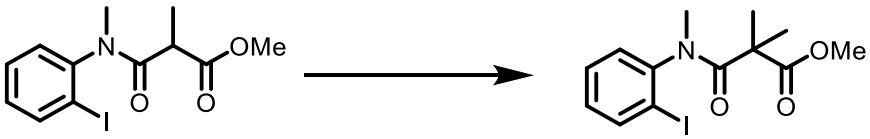

Synthesis of methyl N-(2-iodobenzoyl)-N-methylglycinate

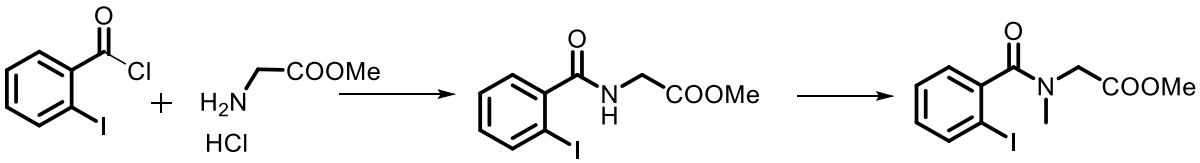

The same general procedure A, B was followed with 0.25 g (2.0mmol, 1.0 equiv.) of corresponding acid. Column chromatography (SiO_2, eluting with 12% ethyl acetate/pet ether) afforded the desired product as light yellow solid.

Synthesis of methyl N-(2-iodobenzoyl)-N-methyl-L-alaninate

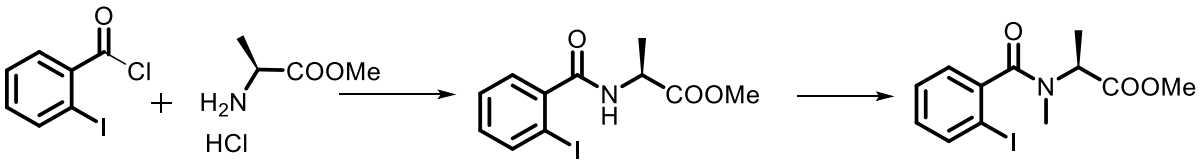

The same general procedure A, B was followed with 0.25g (2.0mmol, 1.0 equiv.) of corresponding acid. Column chromatography (SiO_2, eluting with 12% ethyl acetate/pet ether) afforded the desired product as light yellow solid.

Synthesis of methyl N-(2-iodobenzoyl)-N-methyl-L-valinate.

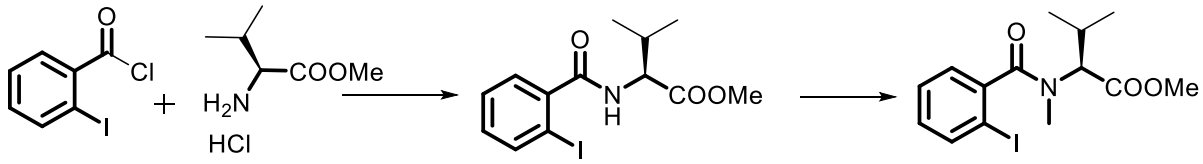

The same general procedure A, B was followed with 0.25g (2.0mmol, 1.0 equiv.) of corresponding acid. Column chromatography (SiO_2, eluting with 12% ethyl acetate/pet ether) afforded the desired product as light yellow solid.

Synthesis of methyl N-(2-iodobenzoyl)-N-methyl-L-phenylalaninate

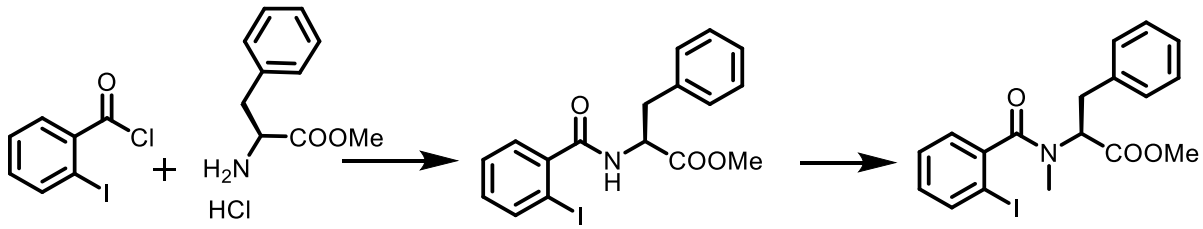

The same general procedure A,B was followed with 0.25g (2.0mmol, 1.0 equiv.) of corresponding acid. Column chromatography (SiO_2, eluting with 12% ethyl acetate/pet ether) afforded the desired product as light yellow solid.

Synthesis of methyl 1-(2-iodobenzoyl)piperidine-2-carboxylate.

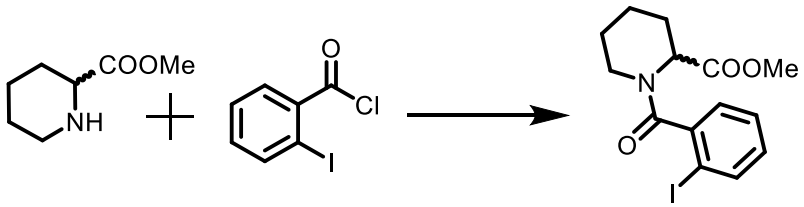

The same general procedure A was followed with 0.25g (2.0mmol, 1.0 equiv.) of corresponding acid. Column chromatography (SiO_2, eluting with 12% ethyl acetate/pet ether) afforded the desired product as light yellow solid.

General procedure D for Pd (II) catalyzed Arylation:

To a Oven dried sealed tube equipped with magnetic bar, Ester conaining 2 halo arylamide (0.2 mmol, 1.0 equiv.), in Dioxane (0.5 mL) was added $Pd(OAc)_2$ (10 mol%), PCy_3 (20 mol%), K_2CO_3(3eqv) were added,Then 1.5 ml of DMSO was added finally purge with N_2 gas,itwas allowed to stir for 12h at 140^{o}C in an oil bath. After completion of the reaction, monitored by TLC, the reaction mixture was diluted with ethyl acetate (2 × 30 mL), filtered through celite bed, and then washed with cold water (2 × 15 mL) and brine (1 × 15 mL). The organic layer was then collected and dried over Na_2SO_4. The organic extract was evaporated under reduced pressure to get crude mixture. It was then

subjected to Flash chromatography (silica gel 230−400 mesh size, ethyl acetate: pet ether) for further purification to get the desired compounds.

3-isopropyl-2-methylisoindolin-1-one (2)

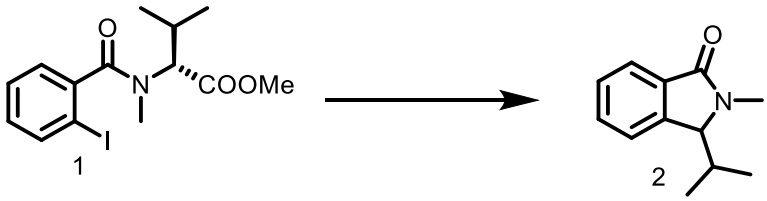

The same general procedure 8 was followed with 0.28g (2.0 mmol, 1.0 equiv.) of corresponding acid compound. Column chromatography (SiO_2, eluting with 18% ethyl acetate/pet ether) afforded the desired product as white solid.

^{1}H NMR (400 MHz, Chloroform-*d*) δ 7.83 – 7.77 (m, 1H), 7.49 – 7.38 (m, 3H), 4.30 (d, 1H), 3.07 (s, 3H), 2.44 – 2.32 (m, 1H), 1.13 (d, 3H), 0.53 (d, 3H).

^{13}C NMR (101 MHz, CHLOROFORM-*D*) δ 168.77, 143.49, 133.34, 130.87, 128.11, 123.52, 122.96, 66.99, 29.38, 28.01, 18.60, 15.49.

1-methylindolin-2-one (4)

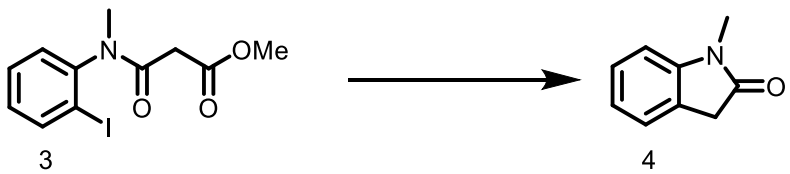

The same general procedure 8 was followed with 0.28g (2.0 mmol, 1.0 equiv.) of corresponding acid compound. Column chromatography (SiO_2, eluting with 18% ethyl acetate/pet ether) afforded the desired product as white solid.

1,3-dimethylindolin-2-one (6)

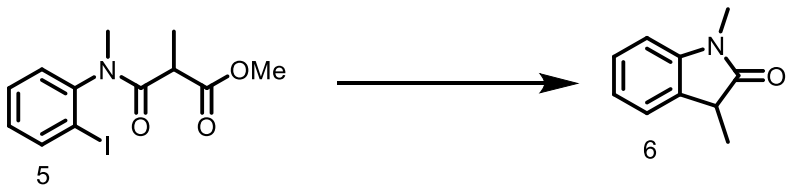

The same general procedure 8 was followed with 0.28g (2.0 mmol, 1.0 equiv.) of corresponding acid compound. Column chromatography (SiO_2, eluting with 18% ethyl acetate/pet ether) afforded the desired product as white solid.

1,3,3-trimethylindolin-2-one

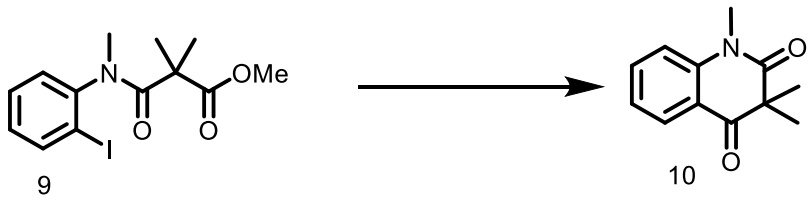

9 10

The same general procedure 8 was followed with 0.28g (2.0 mmol, 1.0 equiv.) of corresponding acid compound. Column chromatography (SiO_2, eluting with 18% ethyl acetate/pet ether) afforded the desired product as white solid.

^{1}H NMR (600 MHz, Chloroform-*d*) δ 7.99 – 7.94 (m, 1H), 7.64 – 7.56 (m, 1H), 7.19 – 7.12 (m, 2H), 3.45 (s, 3H), 1.47 (s, 6H).

^{13}C NMR (151 MHz, DMSO-d_6) δ 197.26, 173.84, 142.64, 135.41, 127.71, 122.58, 119.43, 114.29, 52.66, 29.42, 23.43.

2-methylisoindolin-1-one (12)

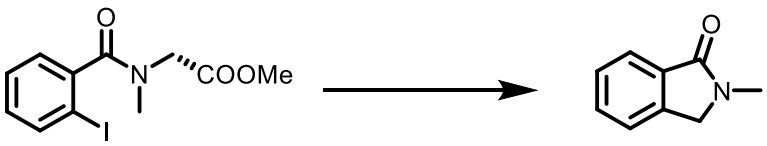

11 12

The same general procedure 8 was followed with 0.28g (2.0 mmol, 1.0 equiv.) of corresponding acid compound. Column chromatography (SiO_2, eluting with 18% ethyl acetate/pet ether) afforded the desired product as white solid.

^{1}H NMR (400 MHz, Chloroform-*d*) δ 7.84 – 7.79 (m, 1H), 7.52 – 7.47 (m, 1H), 7.45 – 7.39 (m, 2H), 4.35 (s, 2H), 3.18 (s, 3H).

^{13}C NMR (101 MHz, $CDCl_3$) δ 168.75, 141.04, 132.96, 131.23, 128.07, 123.65, 122.63, 52.09, 29.52.

2,3-dimethylisoindolin-1-one (14)

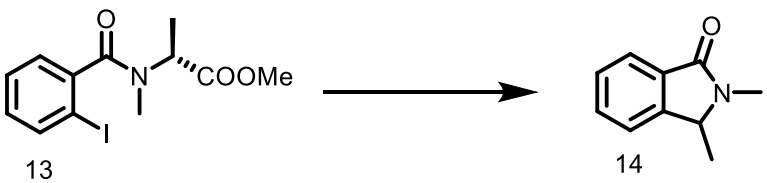

13 14

The same general procedure 8 was followed with 0.28g (2.0 mmol, 1.0 equiv.) of corresponding acid compound. Column chromatography (SiO_2, eluting with 18% ethyl acetate/pet ether) afforded the desired product as white solid.
^{1}H NMR (400 MHz, Chloroform-*d*) δ 7.81 – 7.72 (m, 1H), 7.52 – 7.44 (m, 1H), 7.41 – 7.32 (m, 2H), 4.44 – 4.32 (m, 1H), 3.06 (s, 3H), 1.42 (d, 3H).
^{13}C NMR (101 MHz, Chloroform-*d*) δ 168.19, 146.79, 131.97, 131.40, 128.11, 123.49, 121.85, 57.70, 27.02, 18.00.

3-benzyl-2-methylisoindolin-1-one (16)

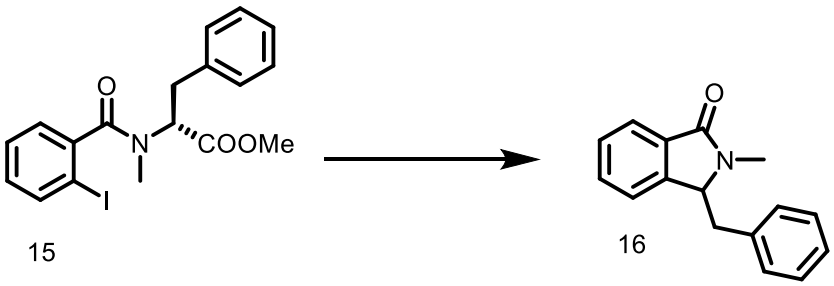

15 16

The same general procedure 8 was followed with 0.28g (2.0 mmol, 1.0 equiv.) of corresponding acid compound. Column chromatography (SiO_2, eluting with 18% ethyl acetate/pet ether) afforded the desired product as white solid.
^{1}H NMR (600 MHz, Chloroform-*d*) δ 7.84 – 7.75 (m, 1H), 7.46 – 7.40 (m, 2H), 7.32 – 7.22 (m, 3H), 7.13 – 7.05 (m, 2H), 7.02 – 6.96 (m, 1H), 4.72 – 4.60 (m, 1H), 3.44 – 3.35 (m, 1H), 3.17 (s, 3H), 2.97 – 2.86 (m, 1H).
^{13}C NMR (151 MHz, $CDCl_3$) δ 168.03, 144.26, 135.50, 131.85, 130.44, 129.01, 128.06, 127.72, 126.56, 123.04, 122.28, 62.31, 38.12, 27.65.

1,3,4,10b-tetrahydropyrido[2,1-a]isoindol-6(2H)-one (18)

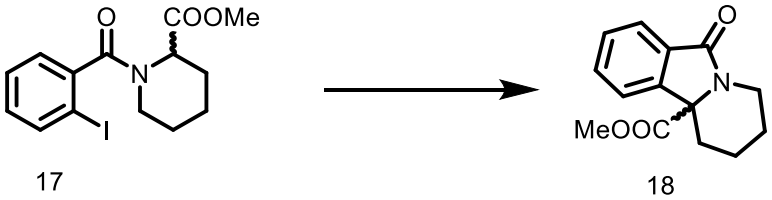

17 18

The same general procedure 8 was followed with 0.28g (2.0 mmol, 1.0 equiv.) of corresponding acid compound. Column chromatography (SiO_2, eluting with 18% ethyl acetate/pet ether) afforded the desired product as white solid.

(6R,12bS)-6-phenyl-5,6,12b,13-tetrahydro-8H-benzo[1,2]indolizino[6,7-b]indol-8-one (20)

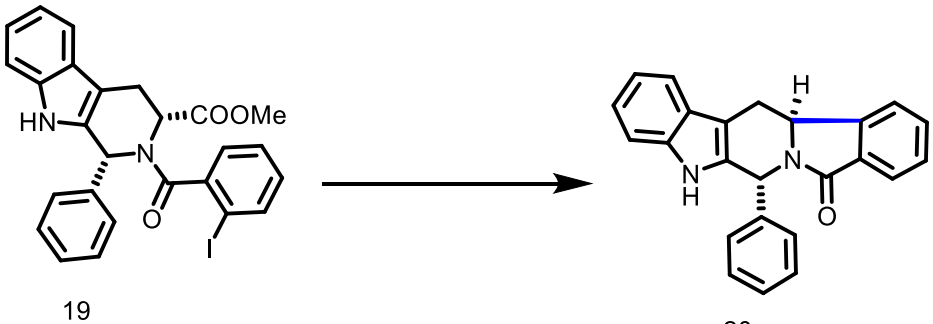

19 20

The same general procedure 8 was followed with 0.28g (2.0 mmol, 1.0 equiv.) of corresponding acid compound. Column chromatography (SiO_2, eluting with 18% ethyl acetate/pet ether) afforded the desired product as white solid.

^{1}H NMR (600 MHz, DMSO-*d*$_6$) δ 11.02 (s, 1H), 7.80 – 7.72 (m, 2H), 7.70 – 7.65 (m, 1H), 7.56 – 7.51 (m, 2H), 7.41 – 7.29 (m, 6H), 7.13 – 7.01 (m, 2H), 6.51 (s, 1H), 5.05 – 4.99 (m, 1H), 3.80 – 3.71 (m, 1H),2.45 (m,1H).

^{13}C NMR (151 MHz, $CDCl_3$) δ 165.51, 146.03, 140.87, 136.98, 131.86, 131.53, 131.49, 128.70, 128.41, 127.97, 127.86, 125.80, 122.96, 121.54, 118.75, 118.05, 111.44, 107.58, 54.12, 51.49, 26.51.

(6S,12bS)-6-phenyl-5,6,12b,13-tetrahydro-8H-benzo[1,2]indolizino[6,7-b]indol-8-one (22)

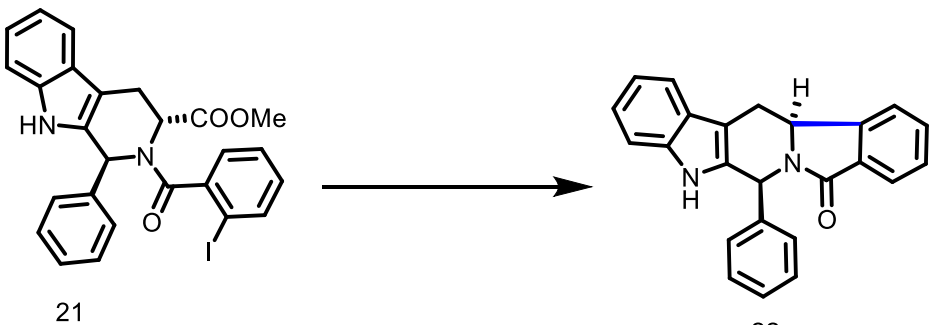

21 22

The same general procedure 8 was followed with 0.28g (2.0 mmol, 1.0 equiv.) of corresponding acid compound. Column chromatography (SiO_2, eluting with 18% ethyl acetate/pet ether) afforded the desired product as white solid.

^{1}H NMR (600 MHz, DMSO-*d*$_6$) δ 11.02 (s, 1H), 7.81 – 7.65 (m, 3H), 7.58 – 7.49 (m, 2H), 7.43 – 7.25 (m, 6H), 7.15 – 6.99 (m, 2H), 6.51 (s, 1H), 5.08 – 4.96 (m, 1H), 3.80 – 3.68 (m, 1H),2.45(m,1H).

^{13}C NMR (151 MHz, $CDCl_3$) δ 171.19, 146.03, 140.84, 136.93, 131.86, 131.49, 131.47, 128.69, 128.40, 127.96, 127.81, 122.95, 122.91, 121.53, 118.81, 118.05, 111.44, 107.57, 54.12, 51.49, 26.50.

(6R,12bS)-6-(p-tolyl)-5,6,12b,13-tetrahydro-8H-benzo[1,2]indolizino[6,7-b]indol-8-one (24)

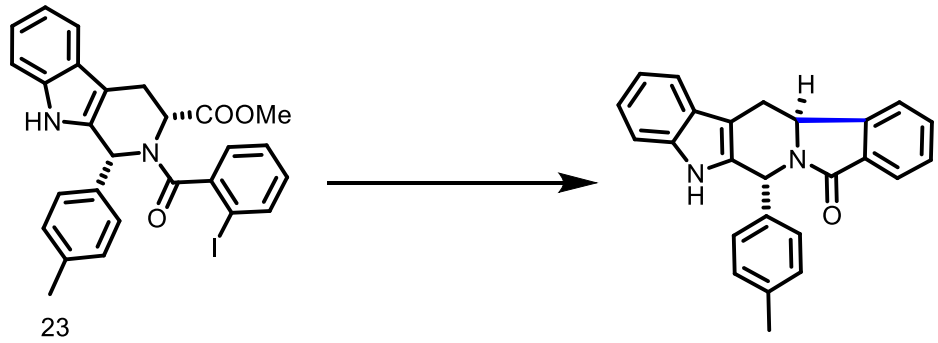

23 24

The same general procedure 8 was followed with 0.28g (2.0 mmol, 1.0 equiv.) of corresponding acid compound. Column chromatography (SiO_2, eluting with 18% ethyl acetate/pet ether) afforded the desired product as white solid.

^{1}H NMR (600 MHz, DMSO-d_6) δ 10.99 (s, 1H), 7.75 (m, 2H), 7.66 (t, *J* = 7.5 Hz, 1H), 7.53 (t, *J* = 6.7 Hz, 2H), 7.29 (m, 3H), 7.16 (d, *J* = 7.7 Hz, 2H), 7.06 (m, 2H), 6.47 (s, 1H), 4.99 (dd, *J* = 10.9, 5.0 Hz, 1H), 3.72 (m, 1H),2.45 (d, 1H), 2.26 (s, 3H).

^{13}C NMR (151 MHz, DMSO-d_6) δ 165.45, 146.01, 137.99, 137.25, 136.92, 131.82, 131.71, 131.60, 129.17, 128.39, 127.80, 125.82, 122.93, 122.89, 121.50, 118.79, 118.03, 111.42, 107.50, 54.07, 51.23, 26.52, 20.66.

(12bS)-6-(4-methoxyphenyl)-5,6,12b,13-tetrahydro-8H-benzo[1,2]indolizino[6,7-b]indol-8-one (26)

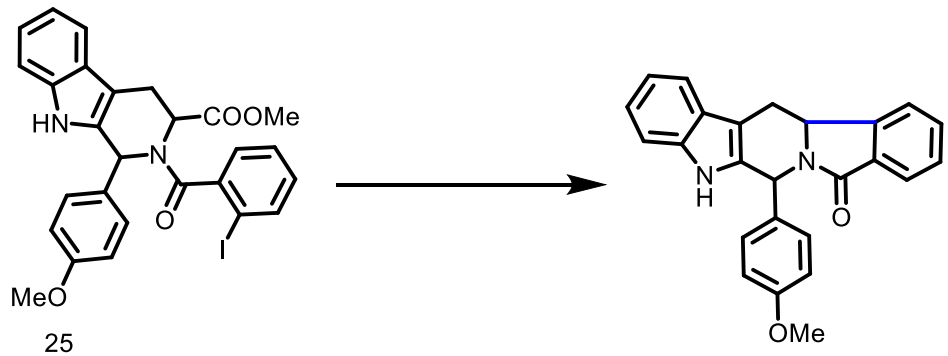

25 26

The same general procedure 8 was followed with 0.28g (2.0 mmol, 1.0 equiv.) of corresponding acid compound. Column chromatography (SiO_2, eluting with 18% ethyl acetate/pet ether) afforded the desired product as white solid.

^{1}H NMR (400 MHz, DMSO-d_6) δ 10.96 (s, 1H), 7.77 – 7.67 (m, 2H), 7.65 – 7.59 (m, 1H), 7.52 – 7.46 (m, 2H), 7.31 – 7.23 (m, 3H), 7.09 – 7.05 (m, 1H), 7.02 – 6.97 (m, 1H), 6.90 – 6.84 (m, 2H), 6.43 (s, 1H), 4.95 (d, *J* = 10.4 Hz, 1H), 3.91 – 3.82 (m, 0H), 3.72 – 3.68 (m, 1H), 3.68 – 3.66 (m, 3H).

^{13}C NMR (101 MHz, DMSO-d_6) δ 165.93, 159.51, 146.54, 137.44, 133.60, 132.36, 132.32, 132.19, 129.66, 128.91, 126.36, 123.43, 123.41, 122.01, 119.31, 118.55, 108.07, 55.71, 54.46, 51.46, 27.05.

methyl 6-(4-nitrophenyl)-8-oxo-6,13-dihydro-5H-benzo[1,2]indolizino[6,7-b]indole-12b(8H)-carboxylate (28)

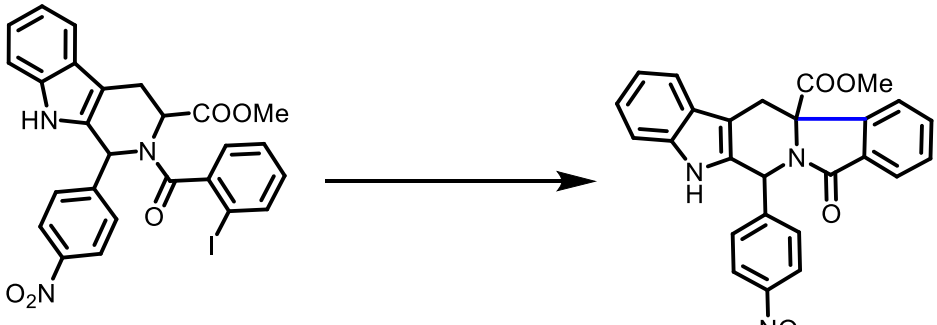

The same general procedure 8 was followed with 0.28g (2.0 mmol, 1.0 equiv.) of corresponding acid compound. Column chromatography (SiO_2, eluting with 18% ethyl acetate/pet ether) afforded the desired product as white solid.

^{1}H NMR (400 MHz, DMSO-*d*$_6$) δ 11.54 (s, 1H), 8.19 – 8.04 (m, 2H), 7.99 – 7.92 (m, 1H), 7.93 – 7.84 (m, 1H), 7.76 – 7.68 (m, 1H), 7.66 – 7.57 (m, 1H), 7.57 – 7.46 (m, 1H), 7.47 – 7.35 (m, 1H), 7.19 – 7.09 (m, 1H), 7.07 –7.00 (m, 1H), 7.01 – 6.93 (m, 2H), 5.62 (d, 1H), 3.40 (d, *J* = 16.3 Hz, 1H), 3.13 (s, 0H), 2.93 (dd, *J* = 16.2, 7.4 Hz, 1H), 2.77 (s, 3H).

^{13}C NMR (101 MHz, DMSO-*D*$_6$) δ 170.31, 168.26, 149.07, 147.61, 137.29, 134.17, 130.17, 129.88, 129.84, 129.62, 126.20, 124.45, 124.36, 123.79, 123.07, 119.83, 119.32, 112.11, 108.57, 66.75, 51.83, 48.97, 21.87.

4.0

Spectral Data (^{1}H, ^{13}C NMR):

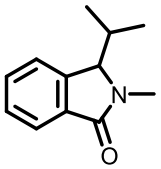

^{1}H NMR Spectra of 3-isopropyl-2-methylisoindolin-1-one (2)

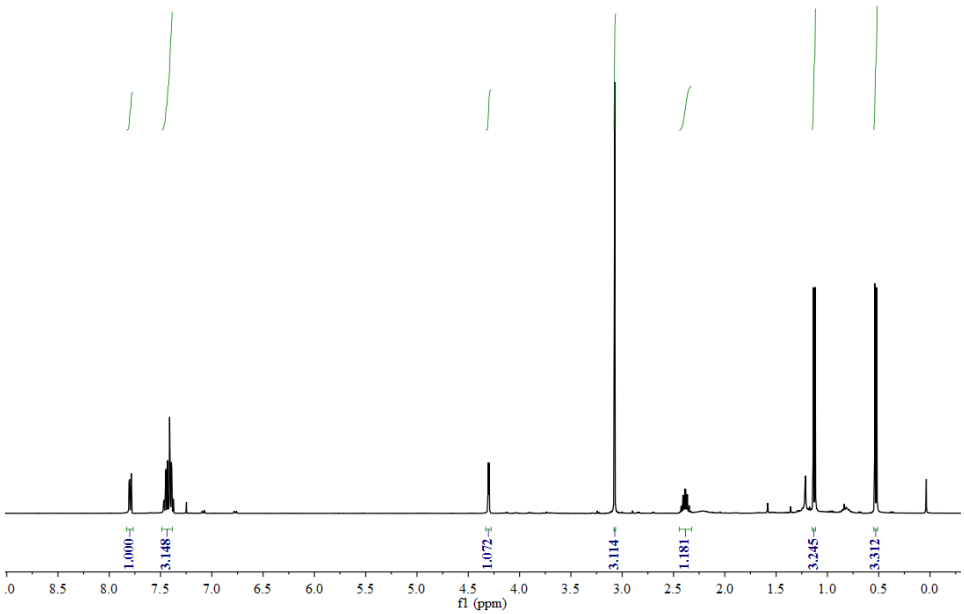

^{13}C NMR Spectra of 3-isopropyl-2-methylisoindolin-1-one (2)

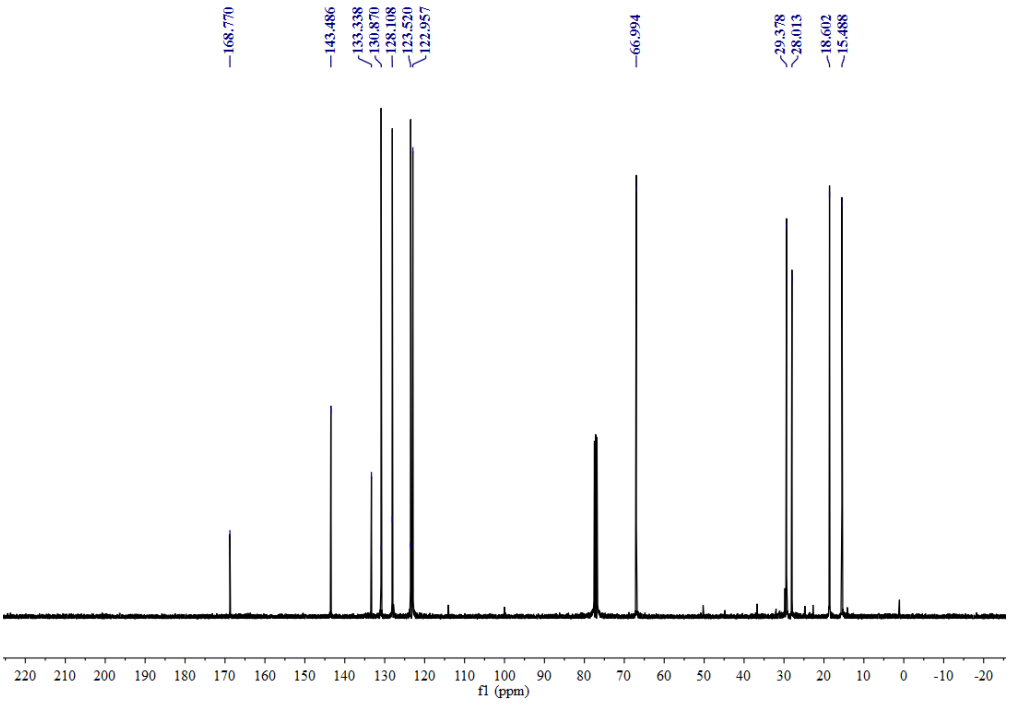

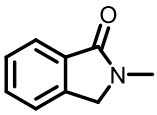

^{1}H NMR Spectra of 2-methylisoindolin-1-one (12)

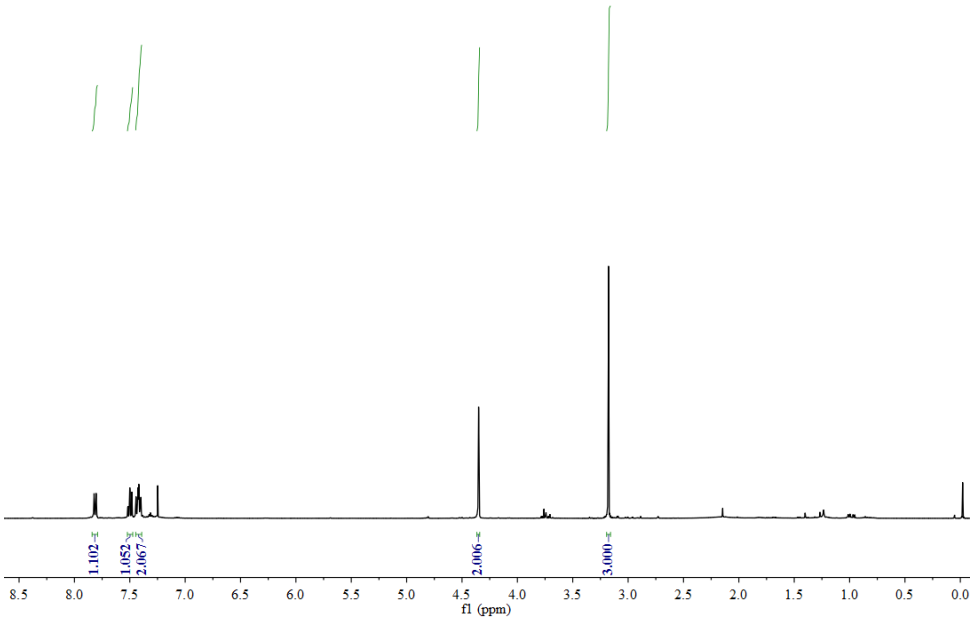

^{13}C NMR Spectra of 2-methylisoindolin-1-one (12)

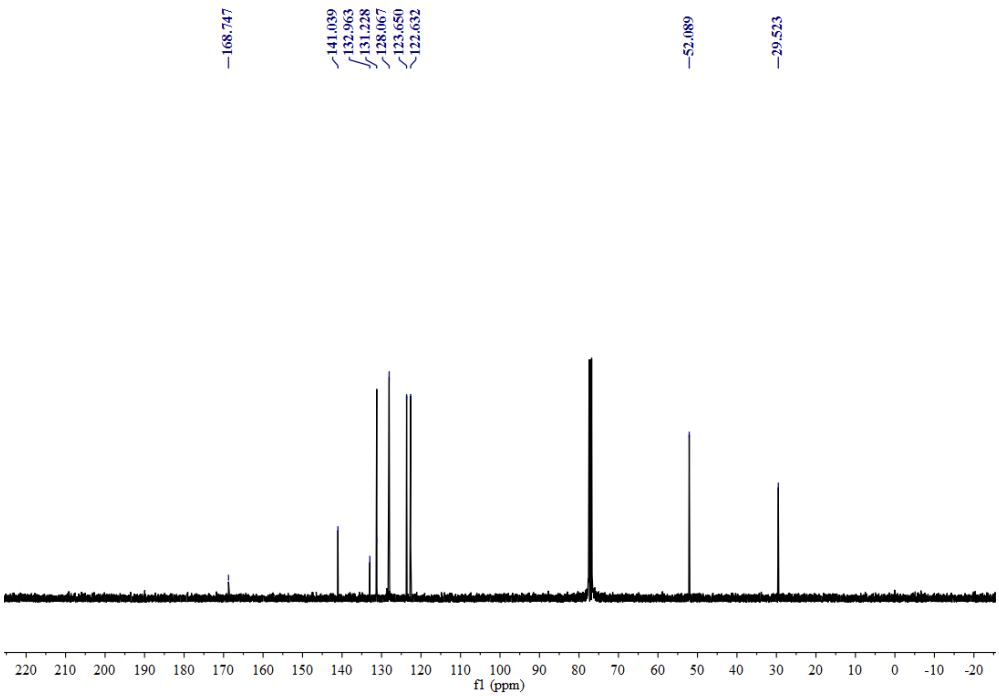

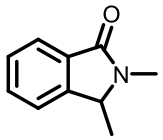

^{1}H NMR Spectra of 2,3-dimethylisoindolin-1-one (14)

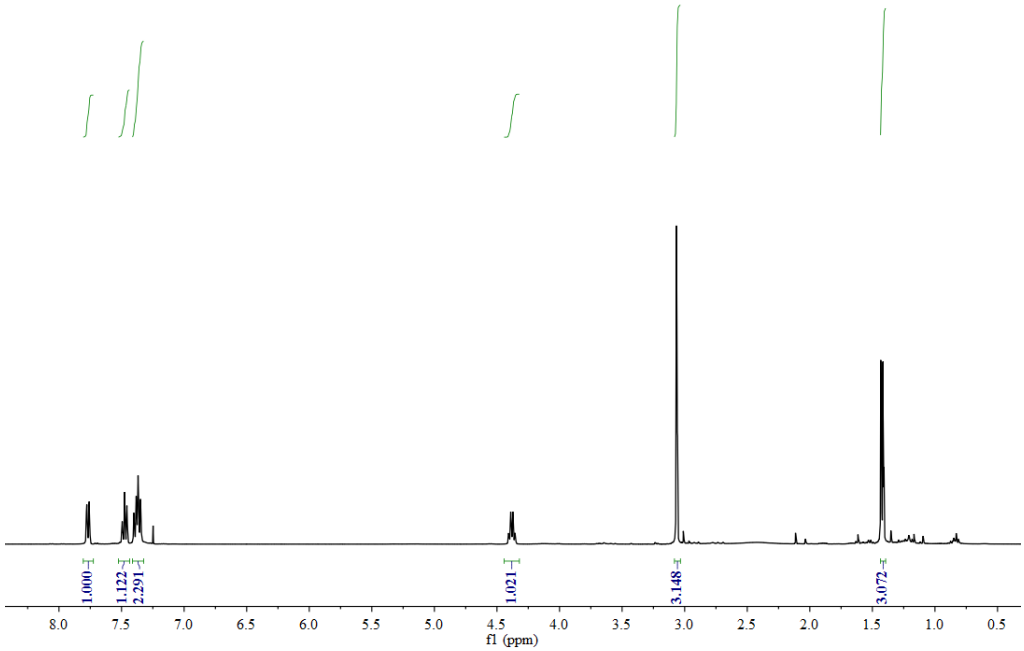

^{13}C NMR Spectra of 2,3-dimethylisoindolin-1-one (14)

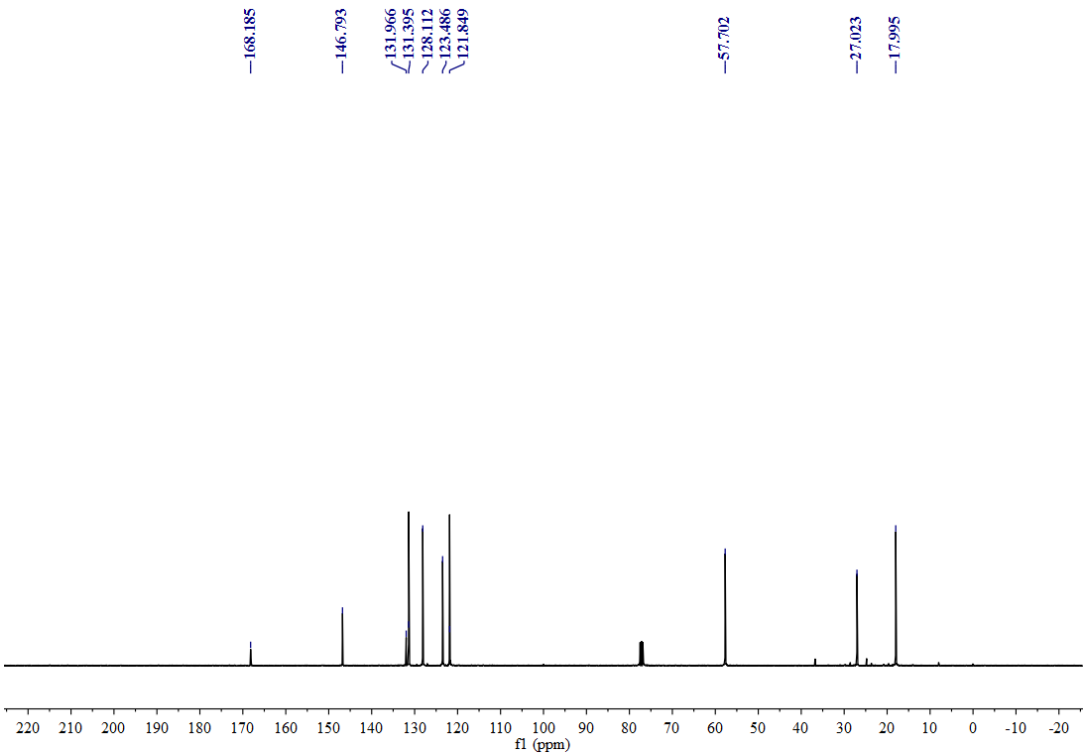

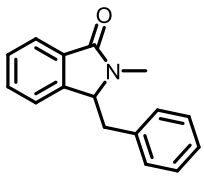

^{1}H NMR Spectra of 3-benzyl-2-methylisoindolin-1-one (16)

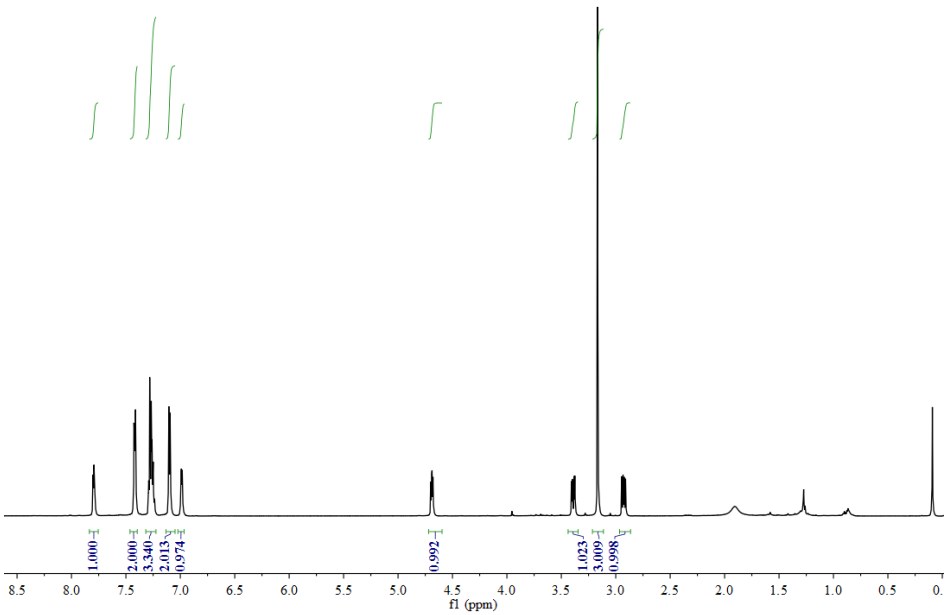

^{13}C NMR Spectra of 3-benzyl-2-methylisoindolin-1-one (16)

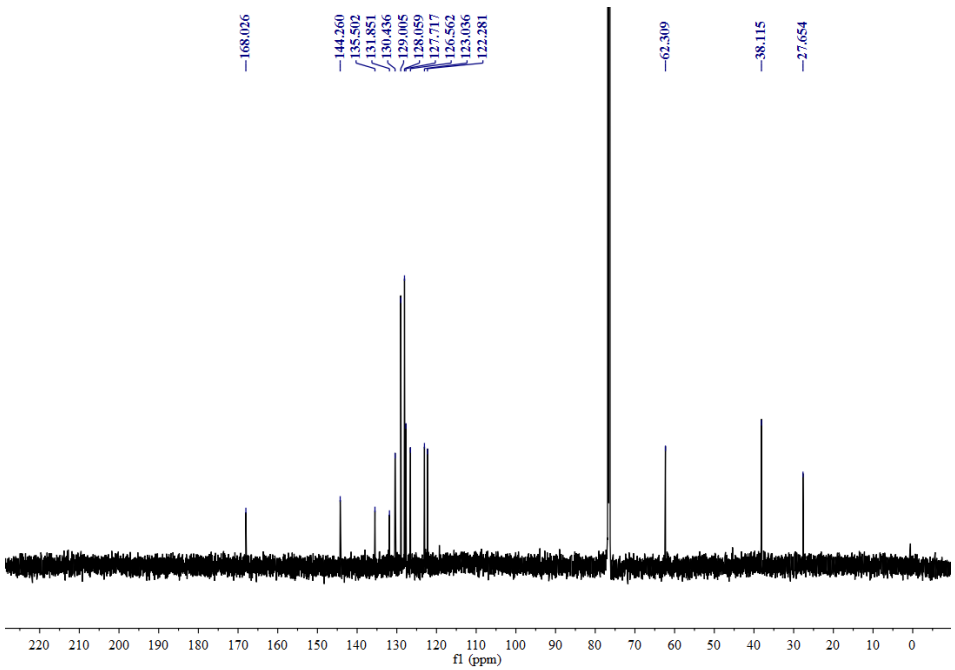

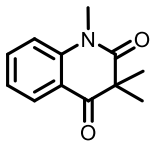

^{1}H NMR Spectra of 1,3,3-trimethylquinoline-2,4(1H,3H)-dione (10)

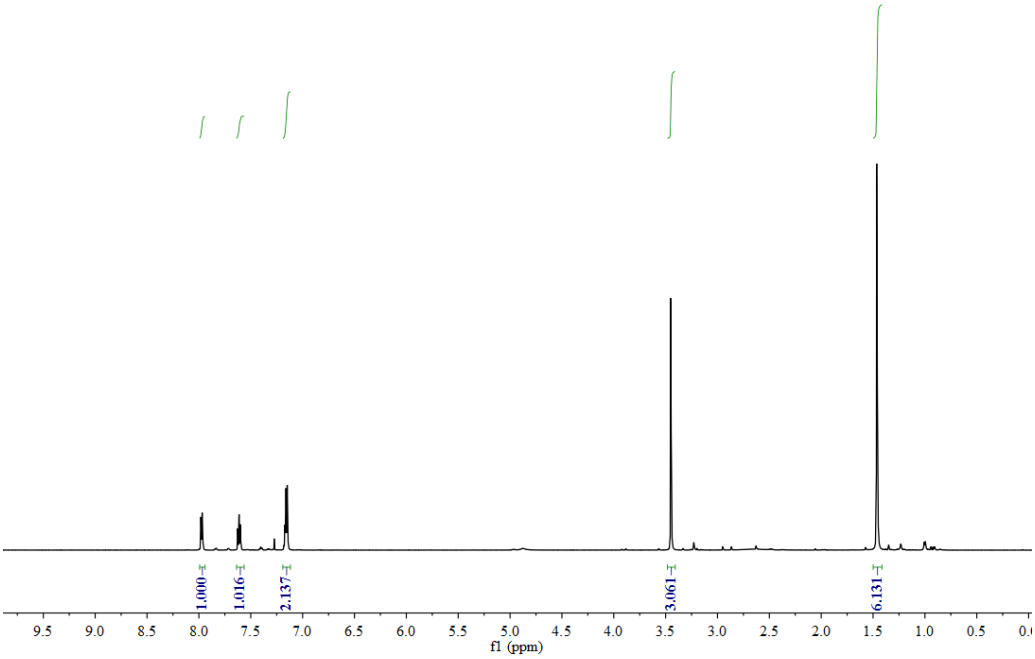

^{13}C NMR Spectra of 1,3,3-trimethylquinoline-2,4(1H,3H)-dione (10)

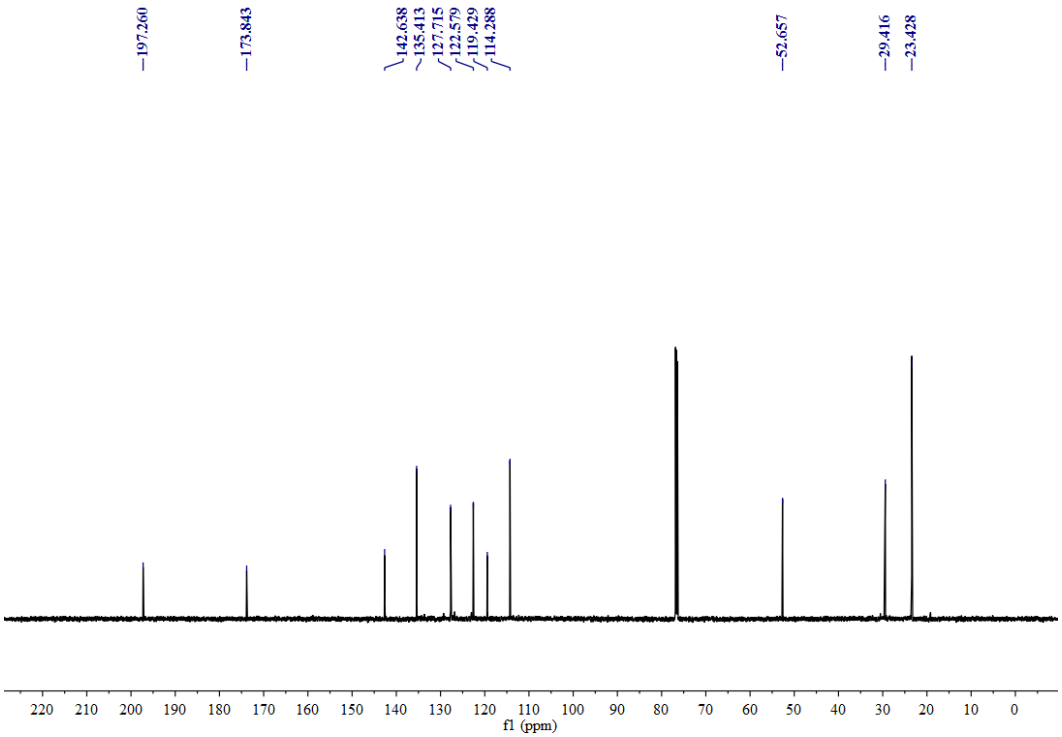

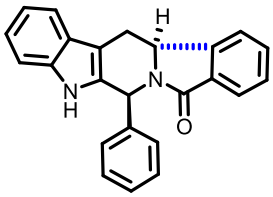

^{1}H NMR Spectra of (6S)-6-phenyl-5,6,12b,13-tetrahydro-8H-benzo[1,2]indolizino[6,7-b]indol-8-one (20)

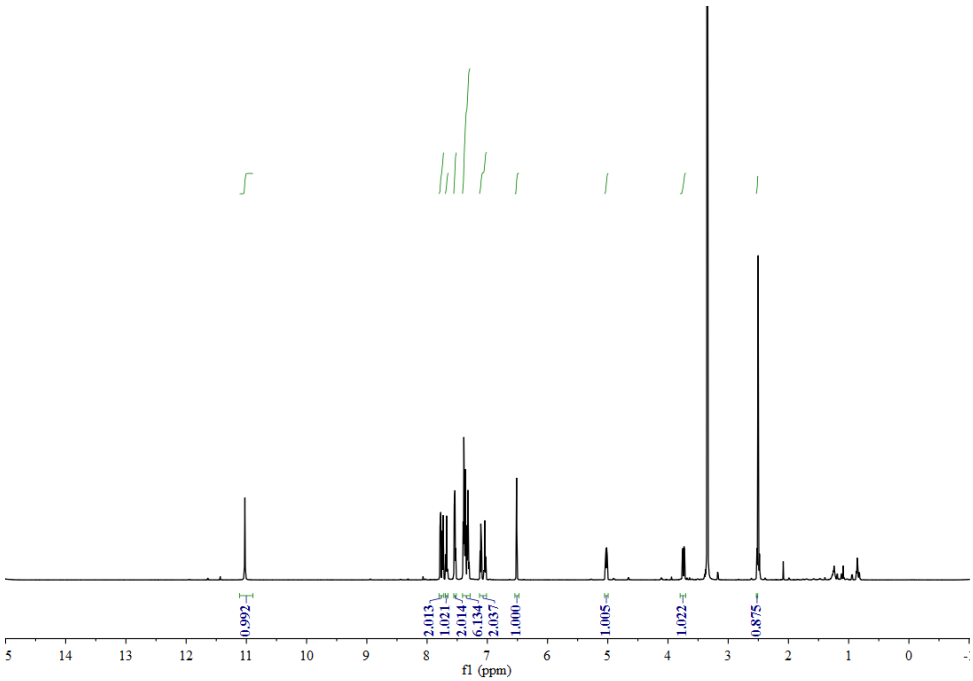

^{13}C NMR Spectra of (6S)-6-phenyl-5,6,12b,13-tetrahydro-8H-benzo[1,2]indolizino[6,7-b]indol-8-one (20)

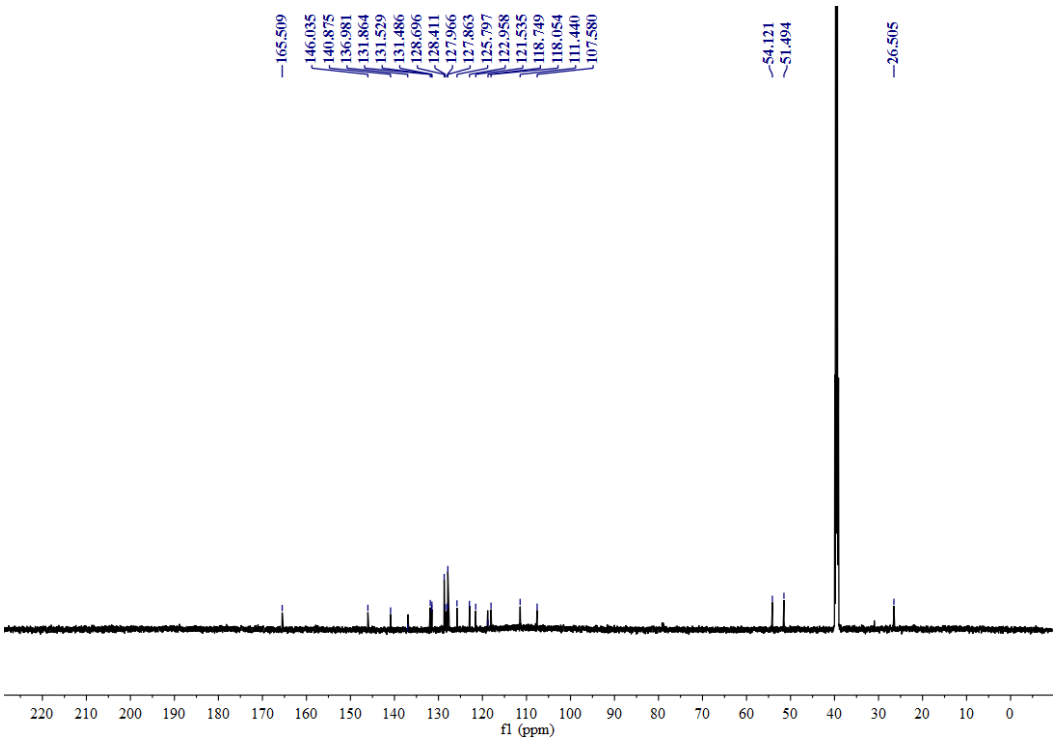

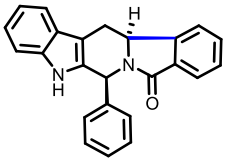

^{1}H NMR Spectra of (6S,12bS)-6-phenyl-5,6,12b,13-tetrahydro-8H-benzo[1,2]indolizino[6,7-b]indol-8-one (22)

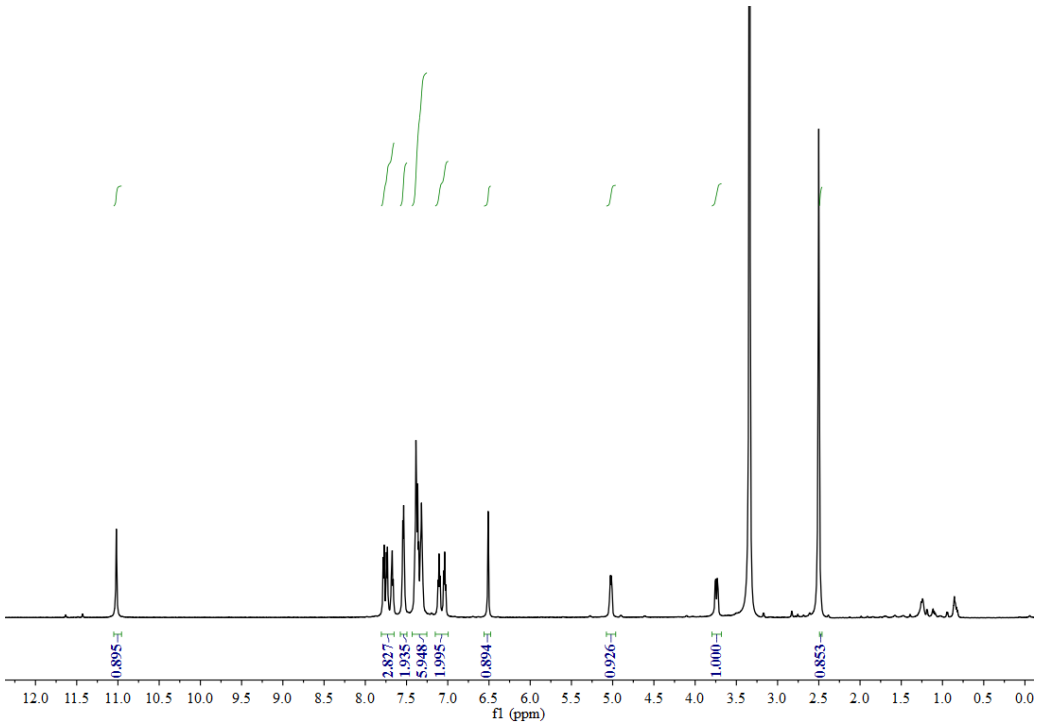

^{13}C NMR Spectra of (6S,12bS)-6-phenyl-5,6,12b,13-tetrahydro-8H-benzo[1,2]indolizino[6,7-b]indol-8-one (22)

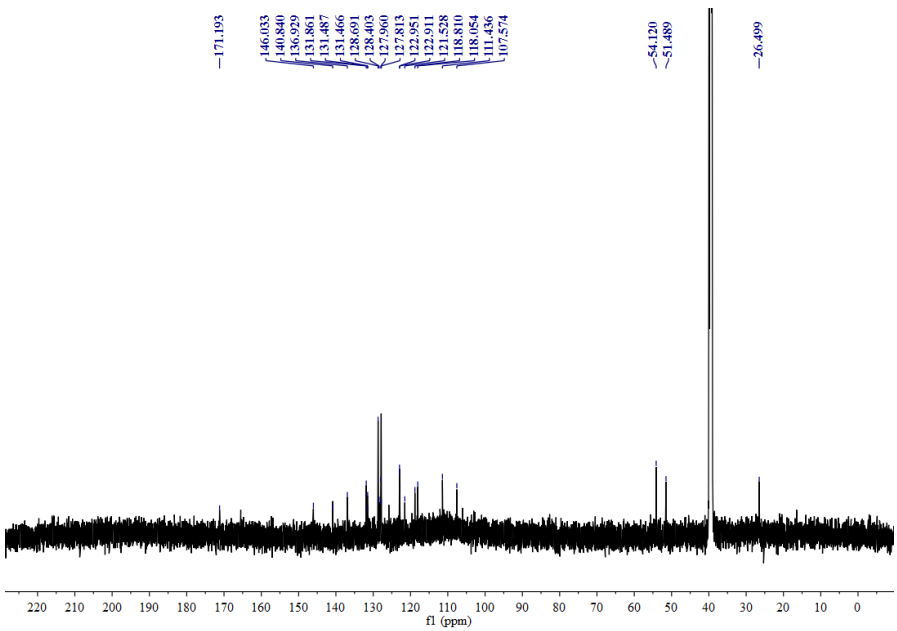

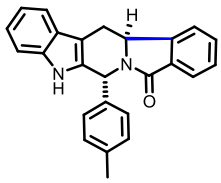

^{1}H NMR Spectra of (6R,12bS)-6-(p-tolyl)-5,6,12b,13-tetrahydro-8H-benzo[1,2]indolizino[6,7-b]indol-8-one (24)

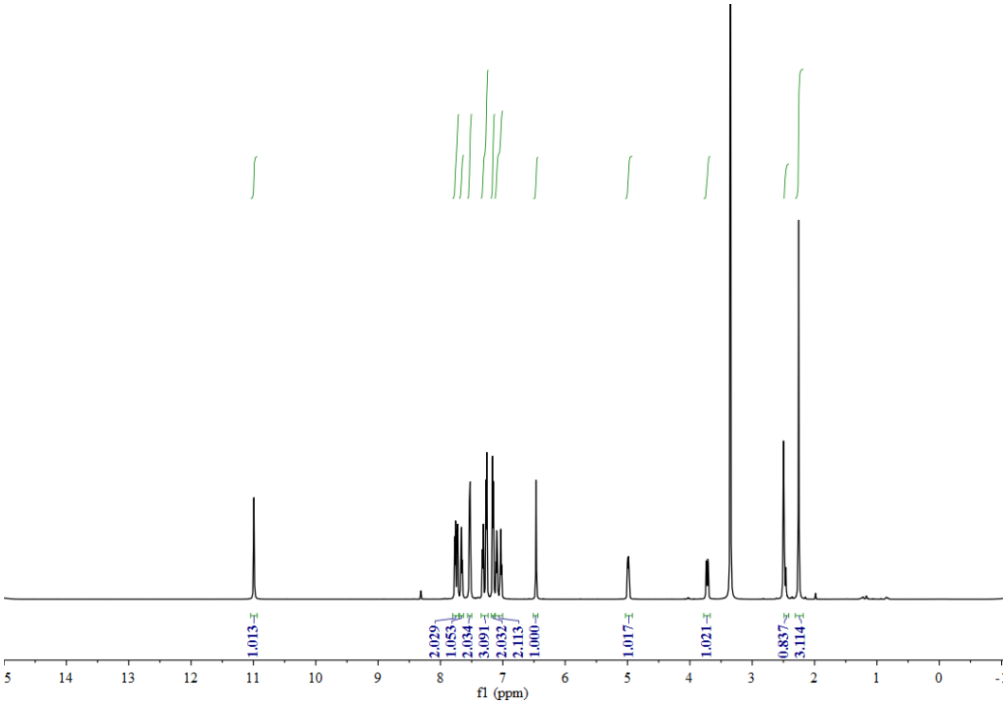

^{13}C NMR Spectra of (6R,12bS)-6-(p-tolyl)-5,6,12b,13-tetrahydro-8H-benzo[1,2]indolizino[6,7-b]indol-8-one (24)

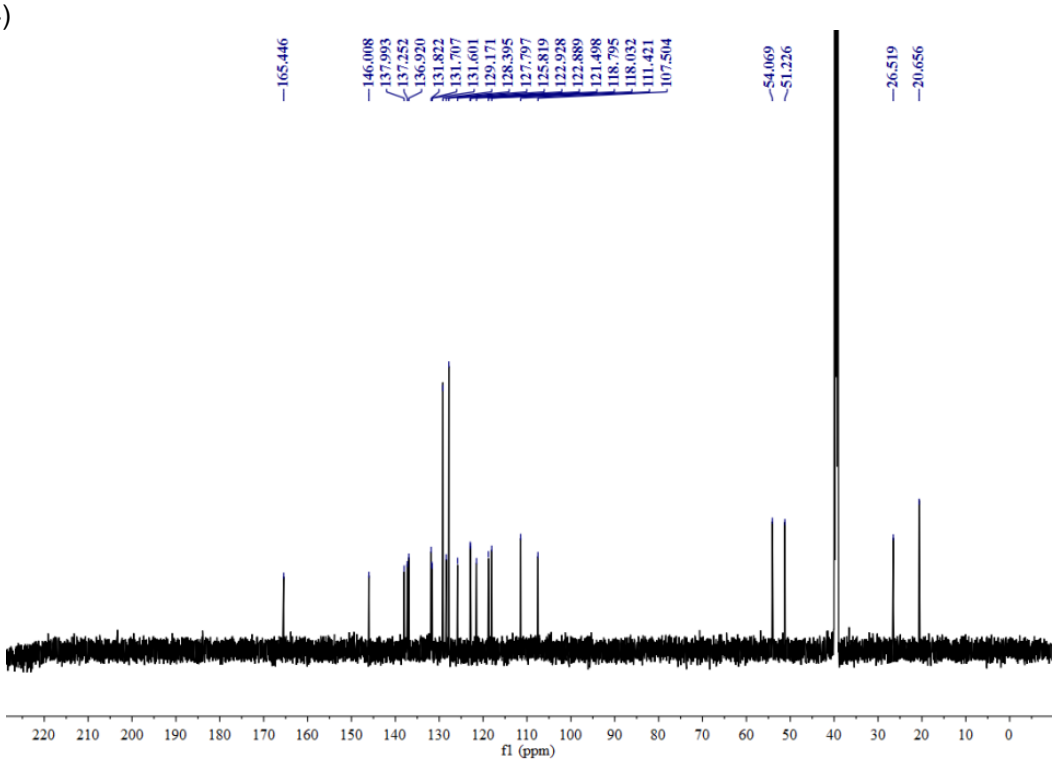

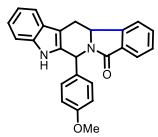

^{1}H NMR Spectra of 6-(4-methoxyphenyl)-5,6,12b,13-tetrahydro-8H-benzo[1,2]indolizino[6,7-b]indol-8-one (26)

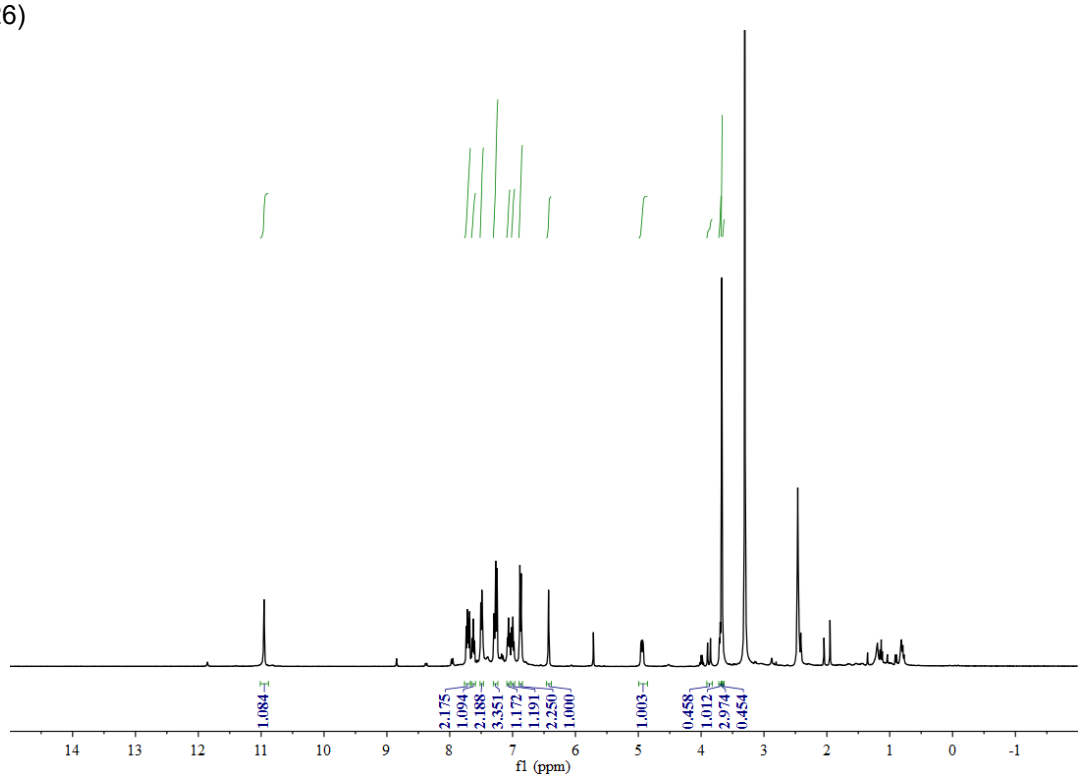

^{13}C NMR Spectra of 6-(4-methoxyphenyl)-5,6,12b,13-tetrahydro-8H-benzo[1,2]indolizino[6,7-b]indol-8-one (26)

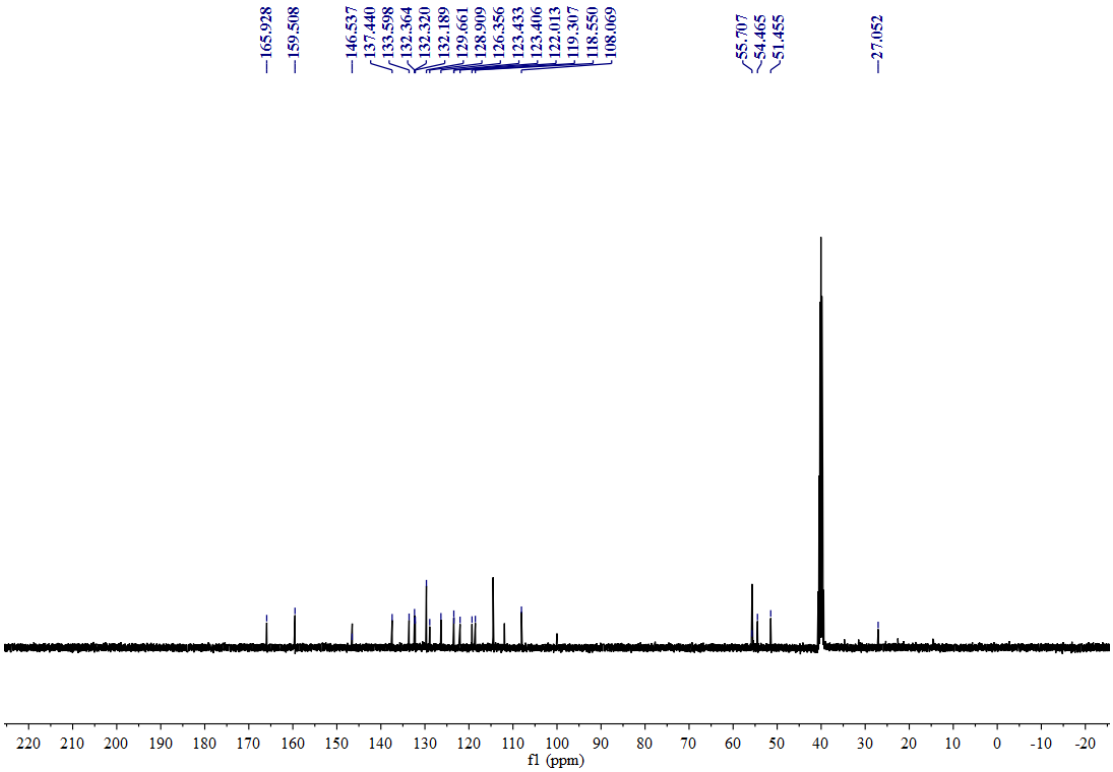

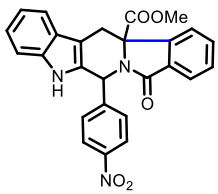

^{1}H NMR Spectra of methyl 6-(4-nitrophenyl)-8-oxo-6,13-dihydro-5H-benzo[1,2]indolizino[6,7-b]indole-12b(8H)-carboxylate (28)

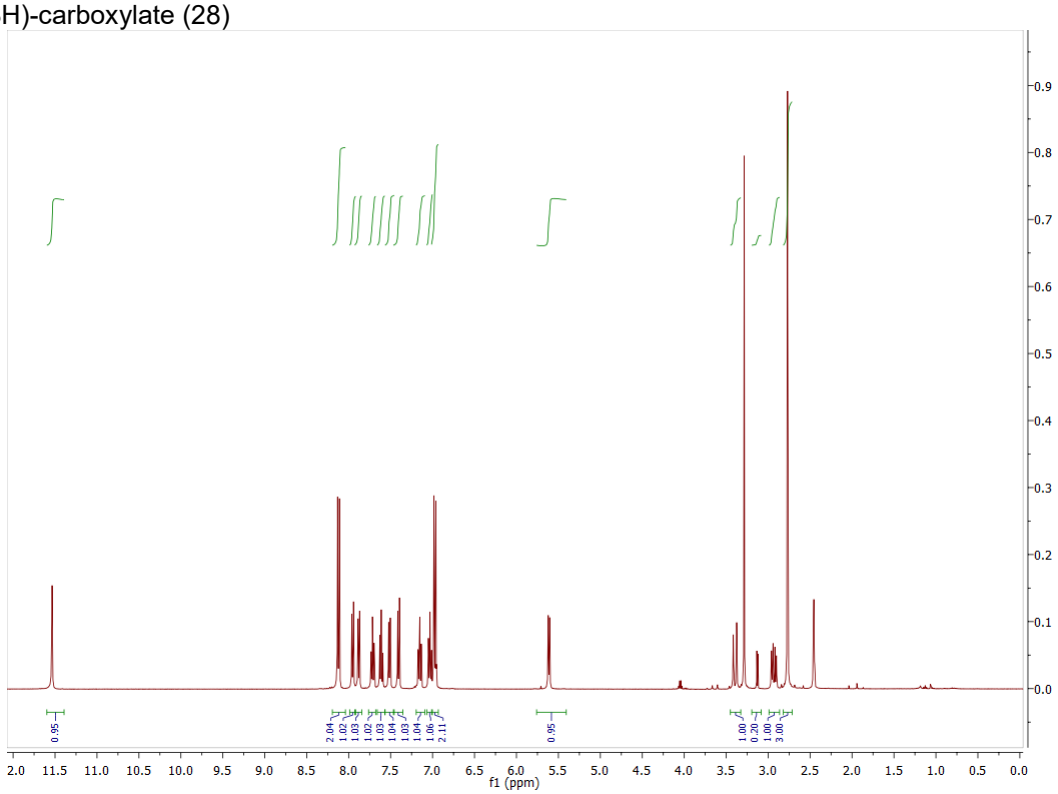

^{13}C NMR Spectra of methyl 6-(4-nitrophenyl)-8-oxo-6,13-dihydro-5H-benzo[1,2]indolizino[6,7-b]indole-12b(8H)-carboxylate (28)

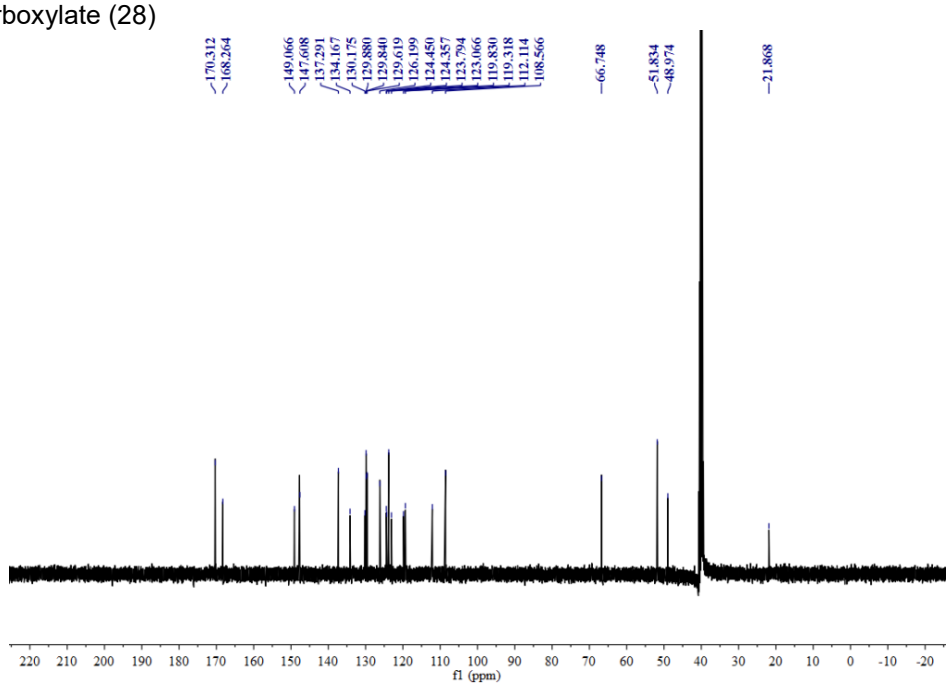

CHAPTER-4

Effect of Inhibition of Liquid-liquid Phase Separation by Small Zwitter ionic Molecules on α-synuclein Aggregation.

4.0 INTRODUCTION

4.1 Parkinson's disease (PD):

Parkinson's disease is a chronic, progressive neurodegenerative disorder that predominantly affects motor function and arises due to the loss of dopaminergic neurons within the substantia nigra pars compacta. This brain region plays a crucial role in the production of dopamine, a neurotransmitter essential for the regulation of smooth, controlled, and coordinated voluntary movements. The progressive degeneration of these neurons leads to a marked reduction in dopamine levels, disrupting communication within the basal ganglia, a network of brain structures critical for motor control[86].

The cardinal motor symptoms of Parkinson's disease include

- **Resting tremors** (involuntary rhythmic shaking, often beginning in one hand),
- **Rigidity** (muscle stiffness that can affect movement and posture)
- **Bradykinesia** (slowness and difficulty in initiating movements)
- **Postural instability** (impaired balance, increasing the risk of falls). These motor impairments can significantly reduce an individual's ability to perform routine activities and contribute to a decline in physical independence.

Beyond motor symptoms, Parkinson's disease frequently involves a range of **non-motor symptoms** that can emerge at different stages of the disease. These include **neuropsychiatric manifestations** such as depression, anxiety, apathy, and cognitive decline, which may progress to Parkinson's disease dementia in some individuals[87]. Autonomic dysfunctions, such as constipation, orthostatic hypotension, and urinary incontinence, are also common, alongside sensory abnormalities like anosmia (loss of smell) and pain[88].

The exact etiology of Parkinson's disease remains incompletely understood, but it is believed to result from a multifactorial interplay of genetic and environmental factors. Genetic predispositions involve mutations in specific genes, such as *LRRK2*, *PARK7*, *PINK1*, and *SNCA*, which are implicated in familial and sporadic cases of the disease. Environmental factors, such as exposure to pesticides, heavy metals, or a history of head trauma, are also considered potential contributors. Although Parkinson's disease is currently incurable, a combination of treatments aims to alleviate symptoms and improve quality of life[89].

- **Pharmacological interventions** primarily focus on restoring dopamine function or mimicking its effects. The gold standard treatment is levodopa, often combined with carbidopa to enhance efficacy and reduce side effects. Additional medications include dopamine agonists, MAO-B inhibitors, and COMT inhibitors.
- **Non-pharmacological approaches**, such as tailored physical therapy, occupational therapy, and speech therapy, help manage motor and non-motor symptoms. In advanced cases,
- **surgical interventions**, such as deep brain stimulation (DBS), may provide significant relief by modulating dysfunctional neural circuits.

Ongoing research is exploring disease-modifying therapies targeting the underlying neurodegeneration, including approaches to slow or halt neuronal loss, reduce α-synuclein aggregation (a hallmark pathological feature), and promote neuronal repair. These efforts aim to not only alleviate symptoms but also alter the disease trajectory in the future.

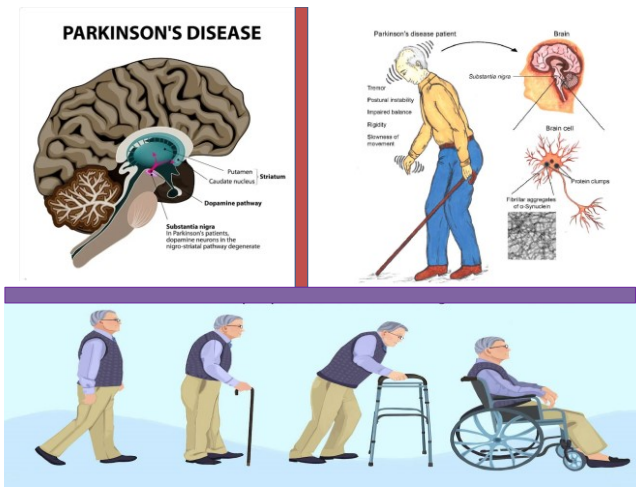

Figure 1: Movement disorder in PD patients (Google, very well health, News medical life-science, Chakraborti et.al)

4.2 α-synuclein Protein (α-syn), responsible for PD:

The discovery of α-synuclein's (α-syn) pivotal role in the pathogenesis of Parkinson's disease (PD) 25 years ago represents a landmark achievement, fundamentally shaping and understanding of neurodegenerative disorders. This small, highly conserved protein, primarily localized to presynaptic terminals, is now recognized as a central player in the molecular cascades driving neurodegeneration. Pathological α-syn undergoes misfolding and aggregation, forming insoluble fibrils that are deposited as Lewy bodies and Lewy neurites, hallmarks of PD pathology. These aggregated forms of α-syn are toxic and implicated in neuronal loss through mechanisms including mitochondrial dysfunction, impairment of autophagic and lysosomal pathways, and disruptions in calcium signalling, all of which compromise cellular homeostasis and viability[90].

The pathological influence of α-syn is not restricted to PD; it extends to a broader group of disorders collectively termed synucleinopathies. These include dementia with Lewy bodies (DLB), multiple system atrophy (MSA), pure autonomic failure (PAF), and REM sleep behaviour disorder (RBD). Despite the heterogeneity in clinical presentation, these disorders share the common feature of abnormal α-syn aggregation, underscoring its broad pathological significance. Emerging evidence emphasizes the role of α-syn in early synaptic dysfunction and plasticity changes, even before the manifestation of significant neuronal loss[91]. Synaptic deficits induced by toxic α-syn species disrupt neurotransmitter release and synaptic connectivity, contributing to early functional impairments observed in PD and related disorders. These alterations may serve as precursors to widespread neurodegeneration, highlighting the importance of studying these early events[92].

A growing body of research points to a critical role of neuro inflammation in the early stages of α-syn pathology. In experimental models and human studies, inflammatory responses, including activation of microglia and astrocytes, are detectable before the accumulation of α-syn aggregates. This early inflammation, potentially triggered by oligomeric α-syn or other stress signals, appears to exacerbate synaptic and neuronal damage, suggesting a bidirectional relationship between inflammation and α-syn pathology. Understanding this interplay could reveal new opportunities for therapeutic intervent. The elucidation of these early-stage mechanisms is crucial for advancing PD research. Identifying and characterizing reliable biomarkers that reflect early pathological changes, such as synaptic dysfunction, inflammation, or initial α-syn aggregation, could transform early diagnosis and enable monitoring of disease progression. Furthermore, therapeutic strategies targeting these initial events hold promise for altering the disease trajectory. Approaches such as immunotherapy to clear toxic α-syn species, small molecules to stabilize synaptic function, and anti-inflammatory agents to modulate neuro inflammation are actively under investigation[93].

Key Facts:

- α-synuclein aggregates disrupt dopaminergic transmission, leading to both presynaptic and postsynaptic dysfunctions.
- In preclinical studies, different cell types show varied susceptibility to α-synuclein aggregates as the disease progresses.
- The immune response triggered by misfolded α-synuclein contributes to the advancement of the disease.
- Synuclein-related neuro inflammation is observed in Parkinson's Disease (PD), Dementia with Lewy Bodies (DLB), Multiple System Atrophy (MSA), Pure Autonomic Failure (PAF), and REM Sleep Behavior Disorder (RBD). These conditions share common clinical, neurochemical, and morphological characteristics.

- ❖ Novel therapeutic approaches targeting α-synuclein include both passive and active immunization strategies, as well as compounds that modulate protein aggregation.

α-synuclein (α-syn) is a small (14 KDa) acidic protein found in neurons of the central and peripheral nervous systems, as well as in blood cells and other tissues. Historically, α-syn was considered a 'natively unfolded' monomer, but it has been shown that the protein largely exists in a folded tetramer form (~58 KDa) with minimal potential for amyloid-like aggregation. The monomer and tetramer forms coexist, and an imbalance in their ratio can favour the formation of aggregation-prone forms. Structurally, α-syn is divided into three primary regions, each contributing unique molecular and biological properties. The N-terminus (residues 1–60) features amphipathic repeats that form an α-helix structure, crucial for membrane interaction. The NAC region (residues 61–95) is the most prone to aggregation. The C-terminus (residues 96–140) is negatively charged and plays roles in calcium (Ca^{2+}) binding and chaperone-like activities. Recent findings indicate that Ca^{2+} binding to the C-terminus also modulates α-syn's interaction with synaptic membranes.

In Parkinson's Disease (PD), Dementia with Lewy Bodies (DLB), and Pure Autonomic Failure (PAF), α-synmisfolds into a pathological β-sheet structure, recruiting additional monomers to form oligomers and amyloid fibrils. These inclusions localize in axons as Lewy neurites or in neuron bodies as Lewy bodies (LB). In Multiple System Atrophy (MSA), α-syn aggregates primarily form glial cytoplasmic inclusions known as Papp-Lantos bodies, which are argyrophilic inclusions found in the cytoplasm of oligodendrocytes. Neuronal cytoplasmic inclusions are also present in MSA but exhibit different distributions, commonly seen in regions like the putamen, pontine nuclei, and inferior olivarynuclei. The phenomenon of liquid–liquid phase separation (LLPS) in biological polymers, such as proteins and RNA, has gained recognition as a pivotal process in the formation of intracellular membrane less organelles. Notable examples of such organelles include nucleoli, Cajal bodies, and promyelocyticleukemia bodies within the nucleus, as well as stress granules in the cytoplasm. These liquid condensates act as concentrated hubs for biomolecules (proteins and nucleic acids) at specific cellular sites, enabling various cellular functions. Due to the absence of physical barriers, these condensates can exchange their components rapidly with the surrounding environment[85].

Common features of liquid condensates include high mobility and a spherical shape that deforms upon physical contact, only to fuse and return to their spherical form. Proteins that undergo LLPS often contain intrinsically disordered regions (IDRs) associated with prion-like and low-complexity domains (LCDs), where amino acid variability is minimal. These IDRs facilitate LLPS through weak, multivalent interactions, allowing diverse interactions among proteins and other biomolecules. Over time, many proteins forming mobile liquid condensates become more viscoelastic and rigid, transitioning into a gel-like state that no longer exchanges components with the surroundings. This state may result from polymer entanglement or stronger protein associations, leading to fibril

formation, as seen with proteins such as FUS, TDP-43, tau, and hnRNPA1. Phase separation could thus enhance the nucleation rate for aggregation into amyloid-like fibrils. α-synuclein (α-Syn), an unstructured protein linked to Parkinson's disease (PD), is known for its cytotoxic aggregation into oligomers and amyloid fibrils. Mutations associated with familial PD are known to influence α-Syn aggregation, emphasizing its role in PD pathogenesis. Although significant research has explored α-Syn aggregation, the early events in this process remain poorly defined. The primary structure of α-Syn consists of an N-terminal region, an aggregation-prone non-amyloid-β component (NAC), and a flexible C-terminal domain. While the NAC region drives aggregation, most familial mutations occur in the N-terminus, underscoring its significance in misfolding and aggregation. Given that α-Syn contains two LCDs, we hypothesized that it could undergo LLPS under suitable conditions. Reports show that α-Syn indeed undergoes LLPS in the presence of a molecular crowder, a process further enhanced by PD-related conditions. We demonstrate that the N-terminal and hydrophobic NAC domain are key drivers of α-Syn LLPS. Remarkably, α-Syn droplets transition from a liquid state to a solid-like state, forming hydrogels with fibrillary aggregates and oligomers. Furthermore, α-Syn forms liquid droplets within cells that later evolve into solid-like aggresomes, a process regulated by microtubules. These results indicate that phase separation is a precursor to α-Syn aggregation, implicating it in PD pathology.

In Parkinson’s Disease (PD), Dementia with Lewy Bodies (DLB), and Pure Autonomic Failure (PAF), the pathological transformation of α-synuclein (α-syn) into a β-sheet-rich structure initiates a cascade of events that lead to neurodegeneration. This misfolding event triggers the recruitment of additional α-syn monomers, resulting in the formation of toxic oligomers and amyloid fibrils. These aggregates are deposited in neurons as Lewy bodies (LB) within the soma or as Lewy neurites in axons. Conversely, in Multiple System Atrophy (MSA), α-syn aggregates predominantly within oligodendrocytes as glial cytoplasmic inclusions (Papp-Lantos bodies), which are argyrophilic and represent a hallmark of the disease. While neuronal cytoplasmic inclusions are also observed in MSA, their distribution is distinct, typically localized to the putamen, pontine nuclei, and inferior olivary nuclei, reflecting unique patterns of pathology across synucleinopathies.

The phenomenon of liquid–liquid phase separation (LLPS) has emerged as a critical mechanism in the biophysics of intracellular organization. LLPS facilitates the assembly of membrane less organelles, including nuclear structures like nucleoli, Cajal bodies, and promyelocyticleukemia (PML) bodies, as well as cytoplasmic stress granules. These liquid-like condensates concentrate specific proteins and RNAs at distinct cellular sites, enabling localized biochemical activities without physical barriers. LLPS-derived structures are dynamic, allowing rapid exchange of molecules with their surroundings, and are characterized by spherical morphology, which can deform and coalesce upon interaction. Proteins driving LLPS typically contain intrinsically disordered regions (IDRs) enriched with low-complexity domains (LCDs), which mediate multivalent, weak interactions essential for condensate formation. Over time, liquid condensates may transition into viscoelastic or gel-like states due to polymer entanglement or

strengthened intermolecular interactions, often leading to the formation of amyloid fibrils, as observed with proteins like FUS, TDP-43, tau, and hnRNPA1.α-Syn, an intrinsically disordered protein linked to PD, plays a central role in disease pathogenesis due to its inherent aggregation propensity. Familial PD-associated mutations, particularly in the N-terminal region, enhance α-syn aggregation, underscoring the significance of this domain in misfolding and fibrillization. The α-syn protein consists of three distinct regions: An N-terminal domain that governs interactions, a highly aggregation-prone non-amyloid-β component (NAC) domain, and a flexible C-terminal domain that modulates structural dynamics. The NAC domain is the primary driver of aggregation, forming the core of amyloid fibrils, while the N-terminal region significantly influences the misfolding process[96].

Recent studies have demonstrated that α-syn undergoes LLPS under physiological and pathological conditions, particularly in the presence of molecular crowders or other factors mimicking the intracellular environment of PD. LLPS of α-syn is primarily mediated by its N-terminal and hydrophobic NAC domains. Once formed, α-syn liquid droplets exhibit a progressive transition into solid-like states, resulting in the formation of hydrogels enriched with oligomers and fibrils. Within cells, α-syn phase separates to form liquid droplets that later evolve into aggresomes—solid-like aggregates associated with cytoskeletal structures, a process dependent on microtubules. These findings suggest that LLPS acts as an upstream event in α-syn aggregation, serving as a nucleation platform that promotes fibril formation. The dynamic nature of LLPS and its eventual transition into pathological aggregates implicate this process as a critical step in PD pathogenesis. Understanding the molecular determinants of α-syn LLPS offers a novel framework for identifying therapeutic targets. Modulating LLPS or preventing its pathological progression could potentially disrupt the aggregation cascade, providing new avenues for intervention in PD and related synucleinopathies [85] (Figure 2).

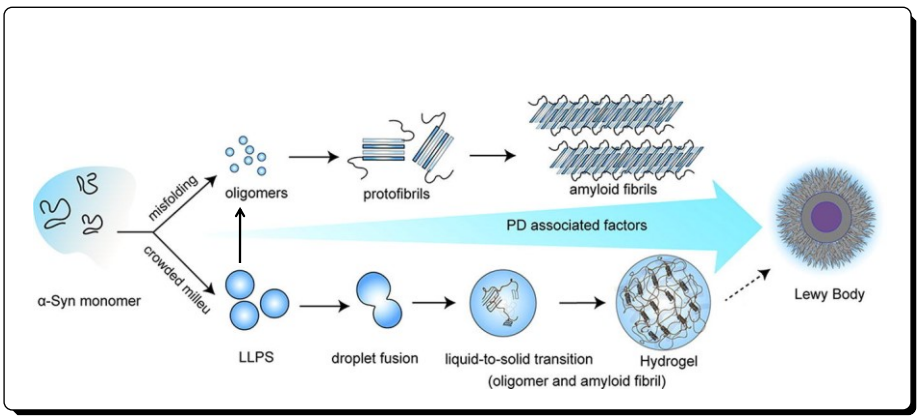

Figure 2: α-syn fibrillation/amydolysis landscape (picture taken and modified Maji et. al).

Canonical subcellular organelles, including mitochondria, the endoplasmic reticulum, and lysosomes, are defined by lipid bilayer membranes that create distinct microenvironments necessary for executing specialized cellular functions. These

structures maintain their integrity and function through the spatial separation provided by their membranes. In contrast, membrane less organelles (MLOs) are cellular compartments that lack a surrounding membrane but still compartmentalize specific biomolecules, including proteins and nucleic acids, to regulate cellular processes. Prominent examples of MLOs include the nucleolus, Cajal bodies, P granules, stress granules, and nuclear speckles. Despite their lack of a physical boundary, MLOs are capable of maintaining their structural integrity, concentrating biomolecules at specific sites, and facilitating specialized biochemical reactions.

Emerging evidence has revealed that MLOs are formed and maintained through liquid–liquid phase separation (LLPS), a biophysical process whereby biomolecules demix from the surrounding cytoplasm or nucleoplasm to form dynamic, liquid-like droplets. These droplets are characterized by their ability to deform, fuse, and coalesce into larger structures, while retaining the capacity for rapid molecular exchange with the surrounding milieu. LLPS-based organization enables MLOs to act as hubs for biochemical reactions, respond to cellular signals, and transiently sequester or release specific proteins and RNAs based on cellular needs. Proteins involved in LLPS often contain intrinsically disordered regions (IDRs) and low-complexity domains (LCDs), which feature repetitive amino acid motifs and exhibit conformational flexibility. These domains enable weak, multivalent interactions critical for phase separation. Initially, LLPS-derived droplets exhibit fluid-like properties, maintaining dynamic molecular rearrangements and rapid exchange with their environment. However, over time, these droplets can undergo transitions to more viscoelastic or gel-like states, ultimately progressing to solid-like structures. These transitions are mediated by enhanced molecular interactions, such as polymer entanglement or the formation of stable multimolecular networks, which reduce the dynamic properties of the droplets[87].

While liquid-to-solid transitions can be beneficial in certain physiological contexts-for instance, in the assembly of the Balbiani body during oocyte development or in the organization of heterochromatin—aberrant transitions are associated with pathological outcomes. Dysfunctional transitions often result in the accumulation of toxic protein aggregates implicated in neurodegenerative diseases, including Alzheimer’s disease (AD), amyotrophic lateral sclerosis (ALS), and Parkinson’s disease (PD). For example, mutations in the RNA-binding protein FUS are linked to aberrant LLPS and the formation of insoluble amyloid-like fibrils. Similar pathological behaviour has been observed with TDP-43, hnRNPA1, and tau protein, which are associated with ALS, AD, and related disorders.

Understanding the dynamics of liquid–liquid phase separation (LLPS) and its implications in cellular physiology and disease pathogenesis is pivotal for elucidating the molecular mechanisms underlying normal and pathological processes. This knowledge provides a foundation for developing therapeutic strategies to regulate LLPS, prevent aberrant phase transitions, and mitigate the formation of toxic aggregates associated with neurodegenerative disorders. In the context of Parkinson's disease (PD), α-

synuclein (α-Syn) is a central protein that aggregates into amyloid fibrils, driving neurotoxicity and neuronal death. Recent research has revealed that α-Syn can undergo LLPS to form liquid-like droplets both in vitro and within cellular environments, with its non-amyloid-β component (NAC) domain serving as the primary driver of this phase separation. Over time, these droplets transition into more rigid, solid-like states containing fibrillar aggregates and oligomers, processes integral to PD pathology. Using purified α-Syn obtained through established protocols, we systematically examined the effects of various experimental conditions on its ability to undergo LLPS. Our findings demonstrated that salt concentration plays a crucial role in modulating α-Syn LLPS. Different salts, counter ions, and low pH environments, along with multivalent cations relevant to PD, significantly accelerated the kinetics of LLPS, reducing initiation times from days to immediate onset. These conditions also lowered the critical concentration of α-Syn required for phase separation. Furthermore, we observed that N-terminal acetylation of α-Syn, a post-translational modification, increased the critical concentration for LLPS, suggesting that acetylation may act as a regulatory mechanism.[85]

From Majhi et al Interestingly proposed some salt like molecule can stop LLPS, their studies showed that α-Syn droplets undergo liquid to solid-like transition, forming hydrogel containing oligomeric structures. Surewicz et al proposed that identification of small molecule modulators of LLPS, which can disrupt phase transitions while maintaining functional integrity of LLPS, might be very important therapeutically. In an ongoing project in the laboratory on the search of new therapeutics against neurodegenerative diseases, mainly on Parkinson's disease, we were interested to design and synthesize small molecule modulators of LLPs, in order to inhibit α-Syn aggregation and hence the early events of aggregations.[94] This study how the experimental conditions affected the progression of LLPS-mediated aggregation and amyloid fibril formation. While the kinetics of LLPS initiation and progression varied based on environmental factors, the involvement of specific domains within α-Syn, such as the NAC region and the N-terminus, remained consistent. These domains appear to orchestrate both the initial phase separation and subsequent transitions to solid-like states.

Their findings provide critical insights into the mechanisms underlying α-Syn LLPS and its liquid-to-solid transition, emphasizing its relevance in PD pathogenesis. The acceleration of LLPS by specific salts and environmental conditions aligns with pathological settings where α-Syn aggregation is observed, such as regions with disrupted ion homeostasis or altered cellular environments.[98],[99] Understanding these transitions enhances our comprehension of how α-Syn aggregation and fibril formation occur in vivo, offering potential targets for therapeutic intervention.

4.3 Bioinformatics of α-Syn protein:

The intricate function of LLPS in propelling the fibrillation process makes the identification of α-synuclein LLPS modulators imperative. To predict the disorder and probability of phase separation of α-synuclein we used several sequence-based bioinformatics tools. PONDR score was used to predict the naturally occurring disordered region in the α-synuclein sequence. PONDR predicted four disorder regions in the sequence stretching from amino acids 1-10, 75-76, 78-80 and 104-140 (Fig. 4). Importantly, the last segment which is C-terminal domain (CTD) is highly disordered and the overall score of CTD was also high (0.885) compared to others. We confirm our disorder prediction with another tool namely IUPred3.IUPred3 also predicted the similar results, that CTD of α-synuclein is extremely disordered (Fig. 4E). Our next focus was to predict the phase separation propensity on the basis of another tool, Fuzrop. The tool predicted that, the overall probability of phase separation of α-synuclein is 0.62 which is consistent with the other phase separating proteins (Fig. 4F). The residue-specific propensity revealed that the C-terminal domain has a high probability of phase separation. **[104],[105],[106]**

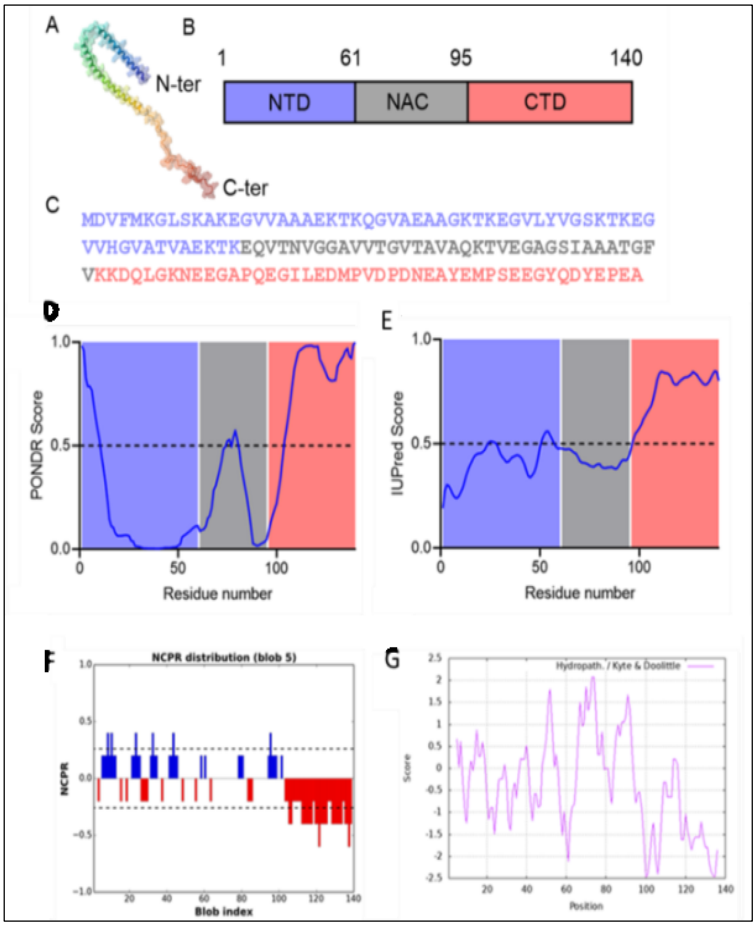

Figure 4. Structure and sequence of α-synuclein: Model structure of membrane bound α-synuclein (PDB ID- 1XQ8). N-ter denotes N-terminal domain andC-ter denotes C-terminal domain. (B) Domain structure of α-synuclein. (C) Linear amino acid sequence of α-Synuclein; Blue denotes N-terminal domain, Grey denotes NAC domain,crimson red denotes C-terminal domain. (D) PONDR prediction from the linear sequence of α-synuclein predicts that C-terminal domain of the protein has disordered region. (E) IUPred3 analysis from the linear sequence of α-synuclein predicts similar to PONDR. (F) Comparison of cat

GRANUALE scores of different phase separating proteins with α-synuclein. (G) Net charge per residue (NCPR) distribution of α-synuclein. Red: Negatively charged amino acids, Blue: Positively charged amino acids. The CTD of α-Synuclein is entirely negatively charged. (H) Kyte-Doolittle hydropathy plot of α-Synuclein indicates the NAC domain of α-Synuclein is enrich in hydrophobic residues.

4.4. Objectives of the present work:

Recent studies have shown that small charged molecules bind to the α-Syn protein weakly. Chattopadhyay et al have reported that arginine amino acid having a guanidine group (positively charged) binds to α-Syn and inhibits fibrillation/aggregation process. They have also shown that glutamate on the other hand did not inhibit. They showed that while arginine binds to the protein, glutamate was excluded from the core of the protein and remained on the surface. Interestingly they have also shown similar positive charged amino acid lysine did not bind to the protein and hence did not also have any effect on the protein aggregations.

Encouraged by all this data a small series of charged molecules were designed and synthesized in this project. Hence the major objectives of the present work:

(i) A small series of pyridine derived amino acid based zwitter ionic molecules will be designed and synthesized.
(ii) Different spectroscopic, bio-chemical and bio-physical experiments will be carried out to establish the inhibition of α-Syn aggregations through LLPS inhibition by these newly synthesized zwitter ionic molecules.

4.5. Results:

4.6: Synthesis of pyridine derived amino-acids based zwitter ionic molecules:

CTD of α-synuclein is the major driver for phase separation. The cat GRANULE score for phase separation was comparable with other proteins. Consequently, we then focused on the charge and hydrophobic pattering in the sequence of α-synuclein. Therefore, the charge scanning by the CIDER tool revealed that the N-terminal domain of α-synuclein has a mixture of positively and negatively charged amino acids, whereas the C-terminal domain is mostly acidic in nature (Fig. 4F). So, positively charged ligands can bind primarily with the CTD. Hydrophobicity and charge pattering are significant among other factors that can influence phase separation. On the other hand, we employed ExPASy tool to probe the hydrophobic regions in the α-synuclein. It suggested that most of the amino acids in the NAC domain of the sequence are hydrophobic in nature (Fig. 4G). This hydrophobic core may interact with another hydrophobic chain of the small molecule to cause self-coacervation. Majhi et al has reported that phase separation acts as an initial step towards α-Syn aggregation associated with PD pathogenesis.

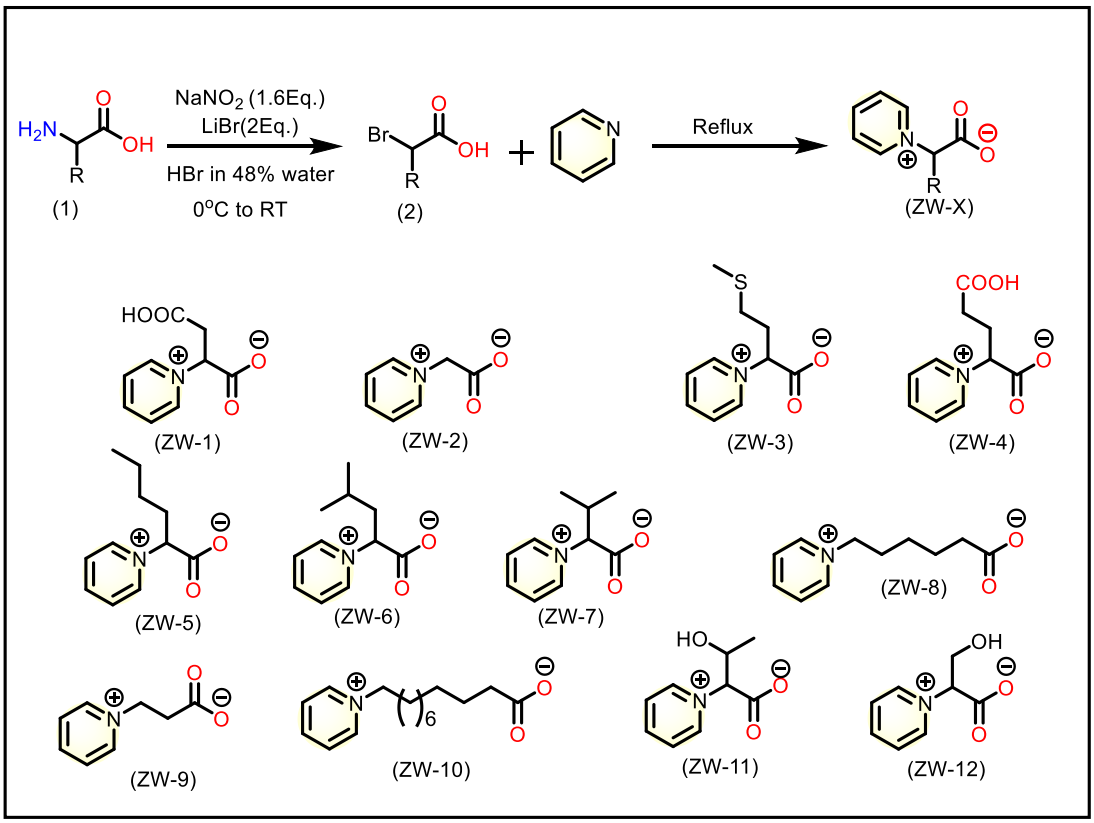

Figure 5: Synthetic Scheme

All the zwitter ionic molecules were synthesized from their corresponding amino acid derivatives in the presence of LiBr (1.5 equiv.) and 42% HBr (4 equiv.). The mixture was stirred for 10 minutes at 0°C. Then, an aqueous solution of $NaNO_2$ (1.6 equiv. in 10 ml water) was added dropwise, converting the amino acid derivatives to their corresponding bromo derivatives. Finally, the zwitter ionic molecules were formed when the bromo derivative was refluxed in presence of pyridine in DCM solvents.

Next, the hydrophobicity scale of these synthesized zwitter ionic molecules was measured by determining their concentration in octanol and water through absorbance measurements using a UV spectrophotometer.

4.7 Hydrophobicity Measurements:

4.7.1. Molar absorption coefficient (ε) measurement of each synthesized molecules in water:

The molar absorption coefficient(ε) was measured by dissolving individual zwitterionic compounds in deionized water at concentrations of 10 μM, 5 μM, 2.5 μM, and 1.225 μM. Absorbance measurements were then taken using a UV spectrophotometer. Molar absorption coefficient(ε) values were calculated from the individual plot of absorbance versus concentration. by Beer–Lambert law.

4.7.2. Molar absorption coefficient(ε) of zwitter ionic molecules in octanol:

Each zwitter ionic compounds were dissolved in octanol & heated until fully solubilisation and kept 12 hours at room temperature. Individual zwitterionic compounds in Octanol solutions were prepared at concentrations of 10 μM, 5 μM, 2.5 μM, and 1.225 μM. Absorbance measurements were then taken using a UV spectrophotometer. The molar absorption coefficient(ε) values were calculated from the individual plot of absorbance versus concentration by Beer–Lambert law.

4.7.3. Hydrophobicity measurements from partition:

To the solutions of individual zwitter ionic compounds in water, an equal volume of octanol was added. The mixtures were then shaken for 1 hour. The concentrations of each zwitter ionic compound in both octanol and water phases were measured using a UV spectrophotometer.

Table1.

Compound name	molar absorption coefficient in Octanol(ε_{oct} $M^{-1}cm^{-1}$)	molar absorption coefficient in Water ($\varepsilon_w M^{-1}cm^{-1}$)	From Partition coefficient concentration in Octanol(C_{oct} M)	From Partition coefficient concentration in water (C_w M)	$\log P = \log \frac{C_{oct}}{C_w}$
ZW-1	410.1	900.00	0.01545	0.1572	-1.009
ZW-2	430.1	900.00	0.02110	0.2170	-0.693
ZW-3	452.1	912.00	0.07812	0.2577	-0.5183
ZW-4	422.2	910.00	0.01928	0.2316	-0.831
ZW-5	432.1	919.00	0.02557	0.2135	-0.9253
ZW-6	461.2	920.00	0.06026	0.2424	-0.6045
ZW-7	490.0	923.00	0.08022	0.2390	-0.4741
ZW-8	607.5	930.00	0.80080	0.1917	+0.6209
ZW-9	510.1	912.00	0.16620	0.2345	-0.7089
ZW-10	710.0	936.00	1.02800	0.2190	+0.671

ZW-11	432.0	928.00	0.01468	0.2420	-1.217
ZW-12	433.9	919.00	0.05460	0.2399	-0.6420

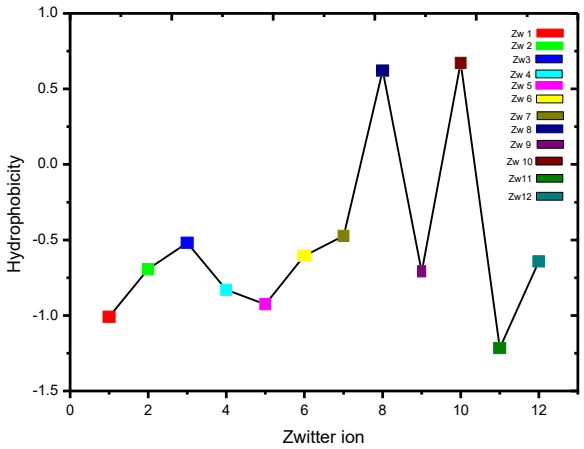

Figure 6. Hydrophobicity Order of zwitterionic molecules.

4.7.4 Turbidity and Microscopy Studies of α-synuclein with zwitterionic ligands:

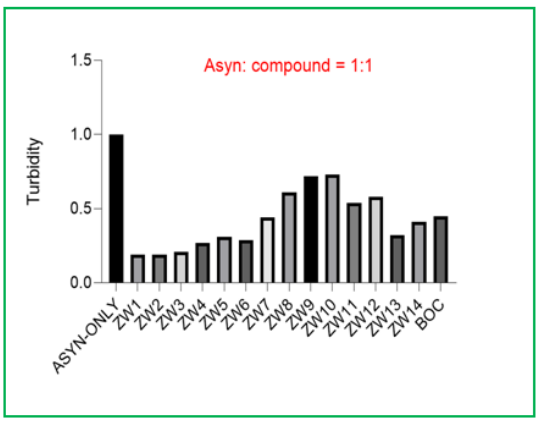

Figure 7. Turbidity (absorbance at 350 nm) screening of synthesized compounds in the presence of 100 μM α-syn incubated at 37°C, 180 rpm for 4 hours. Here additionally Boc- protected amino acids i,e tyrosine, phenyl alinine , glycine which is represented as **ZW-13, ZW-14**, and BOC respectively.

To test the effect of these compounds on LLPS of α-synuclein, light scattering was used as a probe to screen the phase behaviour. 100uM of α-syn was incubated in 10% PEG-8000 and 100 mM NaCl in the presence and absence of synthesized molecules (50 uM) under 37°C and 180 rpm shaking conditions and measured the turbidity (at 350nm) of the solutions. The turbidity was found to be minimum for compound **ZW-2** and highest for **ZW-10** among them (Figure 7). Therefore, it may be concluded that inhibition of droplet formation was maximum by **ZW-2** and the inhibitory power gradually decreased with increasing hydrocarbon chain length as well as hydrophobicity of the side chain in the zwitter ionic compounds (Figure 7)

Fig. 8a

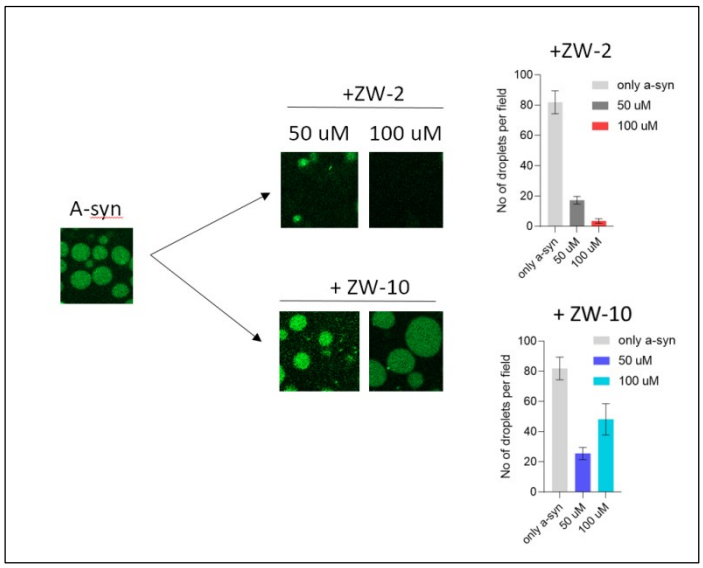

Fig. 8b

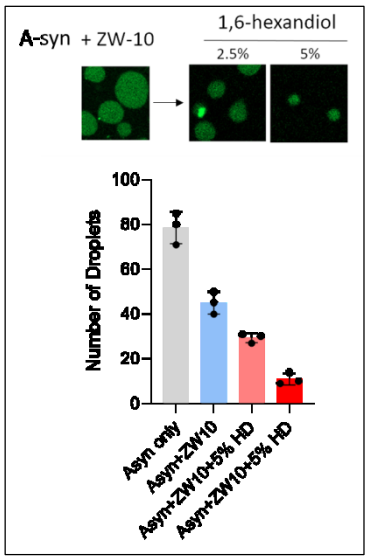

Figure 8a. (A) Confocal microscopy images of liquid droplets in the presence and absence of **ZW-2** and **ZW-10**, Corresponding number of droplets obtained from microscopy. Scale bar:10μm; **Figure 8b.** (A) Confocal microscopy images of liquid droplets in the presence and absence of **ZW-2** and **ZW-10** and Corresponding number of droplets obtained from microscopy (scale bar:10 μm)

The long hydrocarbon chain of the small molecule can interact with the hydrophobic NAC core of the protein and it can induce the droplet formation. This type of increase was also observed in other compounds which have hydrophobic side chain. To further confirm our observations, we used 1% Alexa-488 maleimide labelled α-syn along with unlabelled one and observed under confocal microscopy under similar experimental conditions. We observed a concentration dependent inhibition of droplets in the presence of **ZW-2** which is similar to our turbidity experiments. In the presence of 50 μM **ZW-2**, there was a decrease in number of droplets from only α-syn sample. A further ~16-fold decrease was observed in the presence of 100μM of **ZW-2**, indicates the potential inhibiting power against bimolecular condensates of a-syn. On the contrary, in the case of **ZW-10** though the number of droplets decreased but the extent of inhibition was less compared to **ZW-10**, which further confirms the potential involvement of hydrophobic interaction in the droplet formation (Figure 8a, and 8b). To test this interaction (between long hydrophobic chain present in the compound **ZW-10** with the NAC-hydrophobic core of α-synuclein) we used a common chemical probe 1,6-hexanediol. It has been shown to disrupt LLPS. When introduced to a system undergoing LLPS, 1,6-hexanediol (1,6-HD) can dissolve the liquid-like droplets, effectively reversing the phase separation. This property of 1,6-hexanediol is often used in research to study the role of LLPS in cellular processes and to investigate the behaviour of proteins and nucleic acids in the context of phase separation. Furthermore, 1,6-hexanediol has the ability to interfere with droplet formation through hydrophobic interactions. We added 5% and 10% 1,6 hexandiol to the reacting mixture (α-syn+**ZW-10**), there was a decrease in the number of droplets observed by confocal microscopy, confirmed the hydrophobic interactions present within the system

(Figure 8a & 8b). It is known that the liquid droplets of α-synuclein can mature into toxic amyloid fibrils for a longer incubation time.

4.7.5 MTT Assay & Citotoxicity assay of selective Zwiiter ionic Molecules

SH-SY5Y cells were seeded in a 96-well plate at a density of 10^4–10^5 cells/well in 100 µL of medium containing various compounds at a concentration of 100 µM. The cells were incubated in a CO_2 incubator for 24 hours. Following incubation, the media was discarded, and the cells were washed with PBS. Fresh medium (100 µL) was added to each well, along with 10 µL of MTT stock solution (12 mM), and the plate was incubated for 4 hours. Afterward, 75 µL of the medium was removed, and 50 µL of DMSO was added to each well. The contents were mixed thoroughly, incubated at 37°C for 10 minutes, and mixed again. Absorbance was then measured at 540 nm using a plate reader (Figure 9).

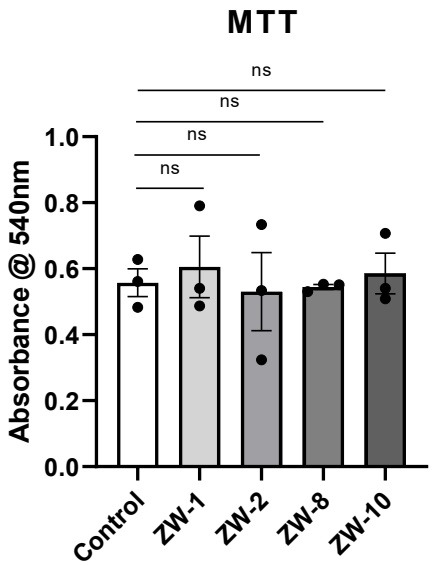

Figure 9: Cell viability assay of selected compounds

SHSY-5Y cells were treated with different compounds (**ZW-1**, **ZW-2**, **ZW-8** and **ZW-10**) at a concentration of 100 µM showed non-significant change in cell viability as compared with control group. ns= non-significant as against untreated cells with respect to treatment with different compounds. Values shown are mean ± sem of three independent experiments.

4.7.6 Cell viability assay result

To check the toxicity of different compounds (**ZW-1**, **ZW-2**, **ZW-8**, and **ZW-10**) MTT assay was performed on SHSY-5Y cell line. Cells were treated with 100 µM of compounds (dissolved in milliQ water) and incubated for 24 h in a CO_2 incubator at 37

ºC. When incubated with MTT active mitochondria of viable cells converts soluble MTT (yellow color) to insoluble formazan product (purple color). Treatment with different compounds (**ZW-1**, **ZW-2**, **ZW-8**, and **ZW-10**) showed non-significant change in cell viability as compared with control group where no treatment was made. Hence it can be stated that these compounds do not possess any adverse effect on the viability of neuronal cells.

4.7.7 Cytotoxicity Assay

Cytotoxicity assay was performed using flow cytometry with Annexin V-FITC and Propidium iodide (PI). Briefly SHSY-5Y cells were seeded in a 6 well plate at a density of 1 x 10^6 cells/well. Cells were incubated for 24 h in a CO_2 incubator with different compounds to be tested (**ZW-1**, **ZW-2**, **ZW-8** and **ZW-10**). After 24 h treatment, media was discarded and cells were washed with PBS. The percentage of live/dead cells was determined using Invitrogen Dead Cell Apoptosis Kit following manufacturer protocol. Briefly, after treatment with compounds cells were harvested and re-suspended in 100 µL of 1X Annexin binding buffer. 5 µL of Annexin V-FITC and 1 µL of PI solution (100 µg/mL) was added to the cell suspension and the cells were incubated for 15 min at room temperature. 400 µL of fresh 1X Annexin binding buffer was added and cells were analyzed by flow cytometry with appropriate filters.

4.7.8 Cytotoxicity Assay result

Cytotoxic effect of the compounds (**ZW-1**, **ZW-2**, **ZW-8,** and **ZW-10**) was tested by measuring the percentage of live/dead cells after treatment for 24 h using flow cytometry. A typical live/dead panel shows live cells with low fluorescence for both FITC and PI (quadrant 3), early apoptotic cells with high FITC fluorescence and low PI fluorescence (quadrant 4) while late apoptotic cells with high fluorescence for both FITC and PI (quadrant 1) and necrotic cells with low FITC fluorescence and high PI fluorescence (quadrant 2). When SHSY-5Y cells were treated with 100 µM of compounds (ZW-1, ZW-2, ZW-8 and ZW-10), they showed non-significant change in cell viability as compared with control group where no treatment was made. Hence these compounds do not have any cytotoxic effect on the neuronal cells (Fig.10).

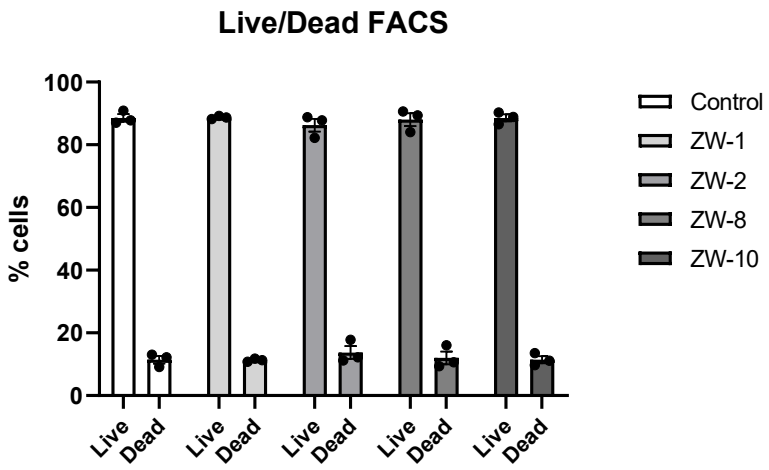

Figure 10: Cytotoxicity assay using flow cytometry with Annexin V-FITC and Propidium iodide (PI). SHSY-5Y cells were treated with different compounds (**ZW-1**, **ZW-2**, **ZW-8**, and **ZW-10**) at a concentration of 100 µM showed non-significant change in cell viability as compared with control group. ns = non-significant as against untreated cells with respect to treatment with different compounds. Values shown are mean ± sem of three independent experiments.

4.7.9. Binding Studies of ligands with α-Synuclein Protein by ^{1}H NMR spectroscopy:

To understand the binding of the synthesized ligands with α-syn protein to stop the phase separation phenomenon, ^{1}H NMR studies of the native protein were performed with and without incubating the ligands externally. Figure 11(a) shows ^{1}H NMR of the wild-type α-syn protein 1mm in D_2O solvent. The down-field proton signals are due to the aromatic residues present in aromatic amino acids like phenylalanine, histidine, etc. However, to confirm the identity of these peaks within the protein, we had taken ^{1}H NMR of histidine amino acids in D_2O solvent, which corroborated that these down-field peaks were due to imidazole protons present in the side chains. On gradually adding **ZW-1** ligand (0 to 93 µM) into α-syn protein solution, the overall ^{1}H NMR spectra of the protein did not change. The two protons at δ 7.7 ppm and 6.9 ppm were found to have shifted very marginally (Figure 11b). However, when increasing concentration of compound **ZW-2** (0 to 93 µM) was added in D_2O solution of α-synuclein appreciable change in position of these peakes were observed. There was a significant shift of these two protons to δ 8.2 ppm and 7.1 ppm from δ 7.7 ppm and 6.9 ppm (native protein), in the 1H NMR spectra. The downfield chemical shift difference of 0.5 ppm of proton at δ 7.7 ppm to δ 8.2 ppm on the addition of **ZW-2** was significant and indicates a strong binding interaction of ligand to the protein (Figure 12a). Next, we chose a compound **ZW-8**, which showed poor effect in the turbidity assay. Interestingly, the stack-plot of ^{1}H NMR spectra of **ZW-8** ligand showed less affinity towards the binding of the protein (Figure 12.b). Marginal down field shift of protons at δ7.7 ppm and 6.9 ppm was observed and on addition of **ZW-8** upto 93 µM these two peaks had disappeared completely (Figure 11).

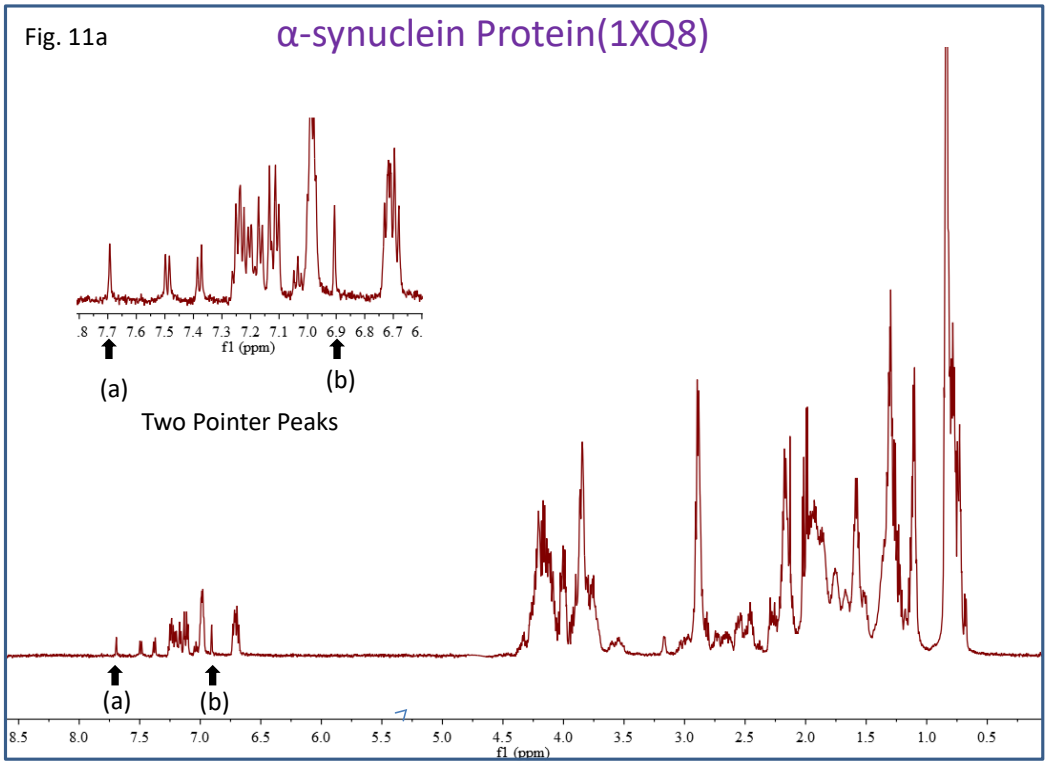

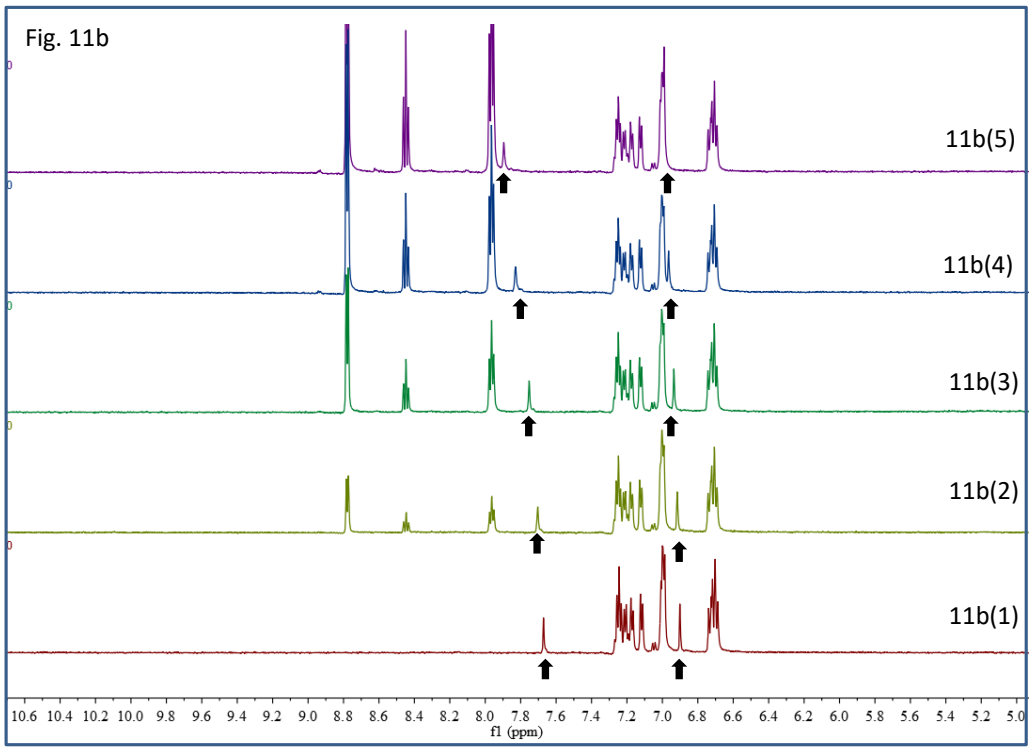

Figure 11: (a) ^{1}H NMR of α-synuclein protein (1.0 mM) in D_2O. (b) ^{1}H NMR of α -synuclein protein (1.0 mM) in D_2O with gradual increasing concentration of **ZW-1** ligand (1.0 M stalk solution) from 0 to 93 μM where 11b (1) 1H NMR spectra of only α-synuclein protein 11b (2) 18 μM, 11b(3) 32 μM, 11b(4) 55 μM, 11b(5) 93 μM of ligand **ZW-1** addition.

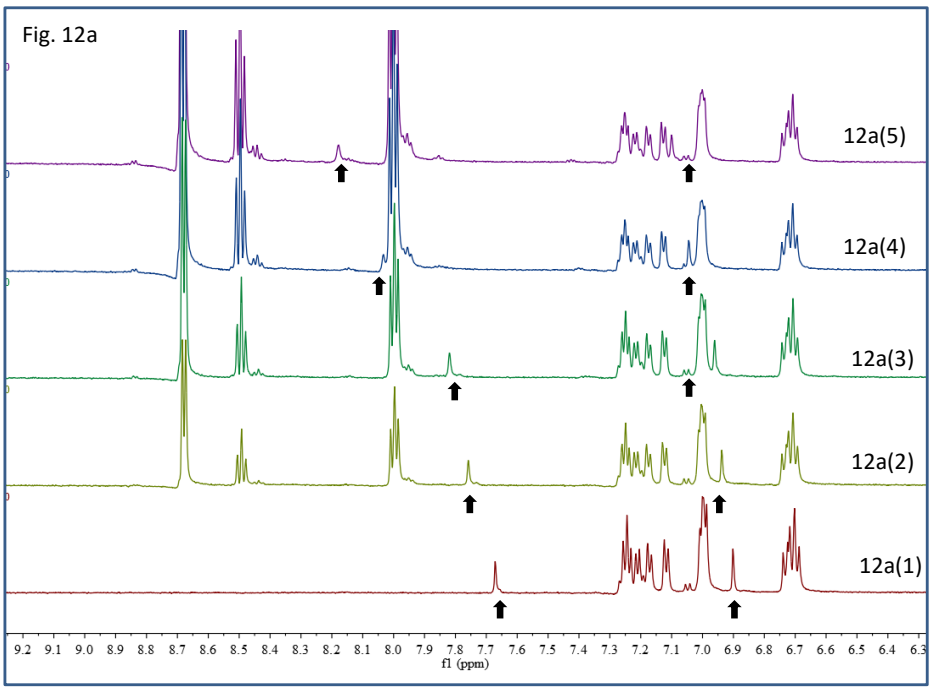

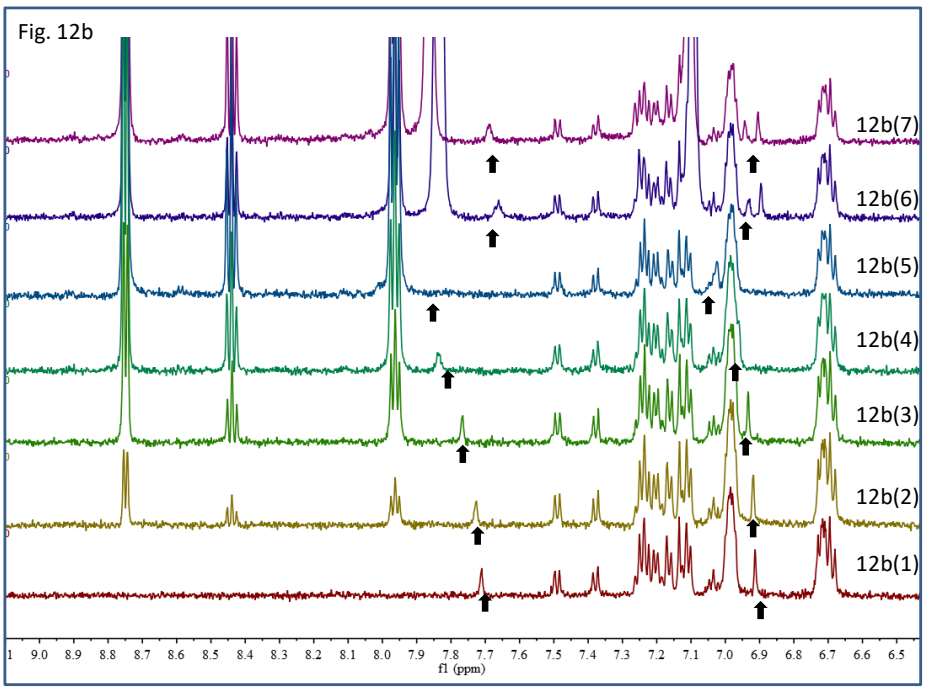

Figure 12: (a) ^{1}H of α-synuclein protein(1.0mM) NMR in D_2O with different concentration **ZW-2** ligand from 0 to 93 μM where 12a(1) only α-synuclein protein 12a(2) 18 μM of ligand **ZW-2**, 12a(3) 32 μM of ligand **ZW-2**, 12a(4) 55 μM of ligand **ZW-2**, 12a(5) 93 μM of ligand **ZW-2**. (b) ^{1}H NMR of α-synucleinprotein (1.0 mM) in D_2O with gradually increasing concentration of **ZW-8** ligand where 12b(1) only α-synuclein protein 12b(2) 18 μM of ligand zw-2, 12b(3) 32 μM of ligand **ZW-2**, 12b(4) 55 μM of ligand **ZW-2**, 12b(5) 93 μM of ligand **ZW-2**. & then aqueous solution of histidine was added 12b(6) 90 μM of histidine, 12b(7) 155 μM of histidine.

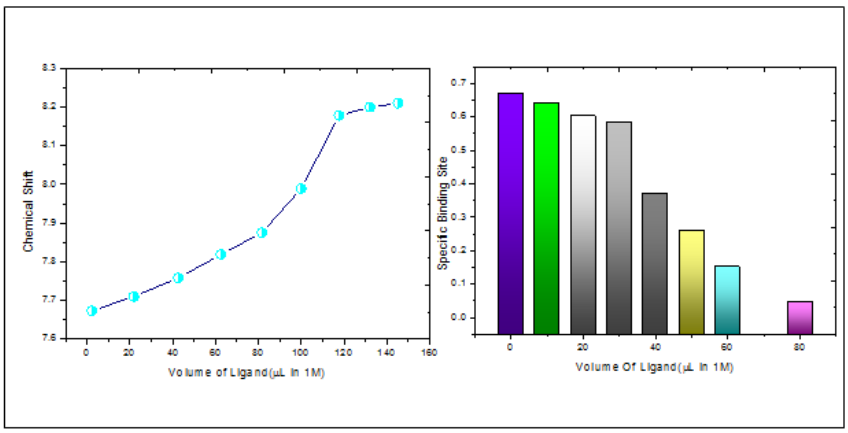

Figure 13 (a): Chemical shift as a function of zwitter ion **(ZW-2)** concentration. This figure shows the chemical shift variations observed at different concentrations of zwitter ion (3b), illustrating the effect on the spectral properties of the sample. (b): Availability of specific binding sites i,e the pointer sites of α-synuclein at different zwitter ion **(ZW-8)** concentrations. This figure displays how the availability of binding sites in α-synuclein changes with varying concentrations of zwitter ion (3h), demonstrating potential interactions and binding affinities.

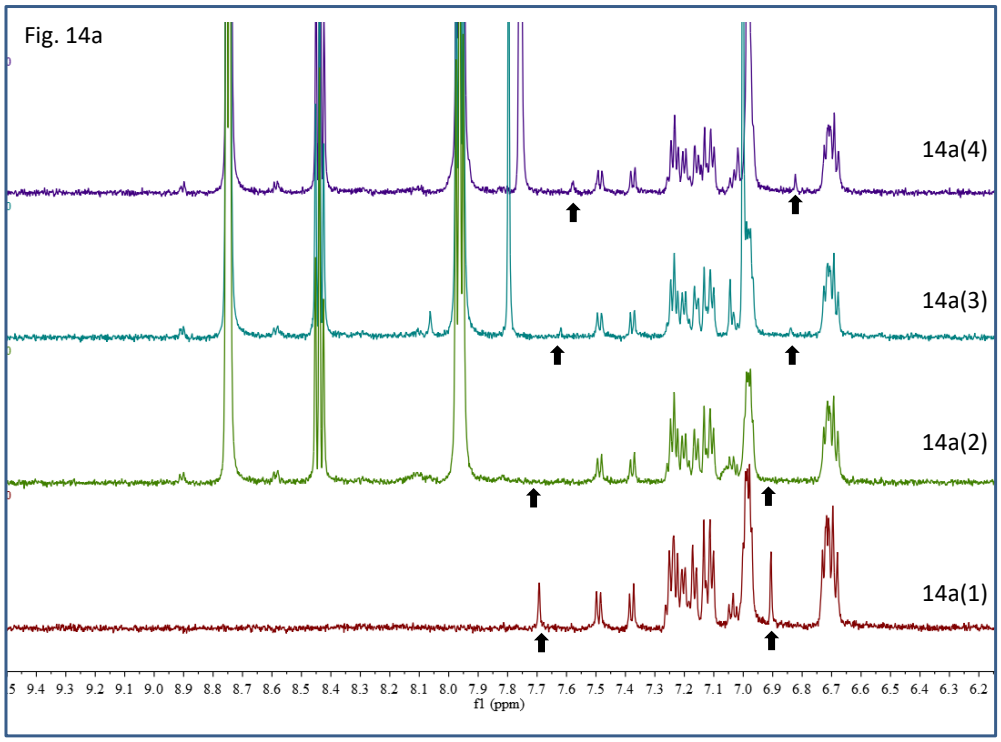

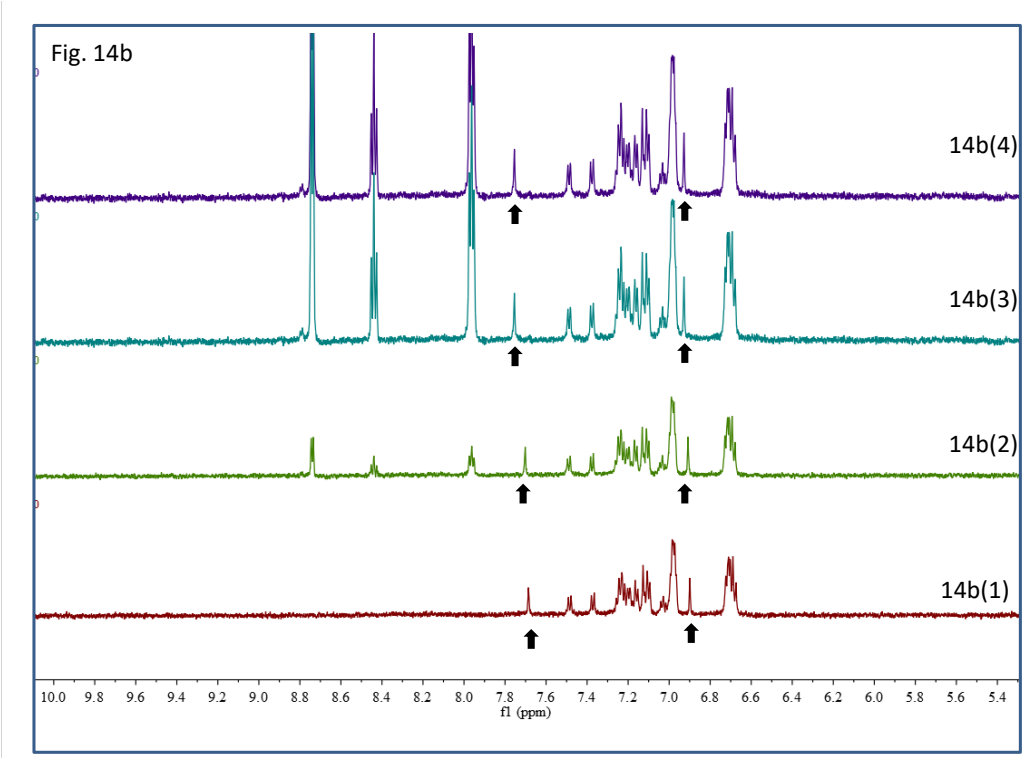

Figure 14. (a) ^{1}H NMR in D_2O of a-synuclein protein (1mM) with different concentration (**ZW-8**) ligand ^{1}H NMR of α-synuclein protein (1.0 mM) in D_2O with gradually increasing concentration of **ZW-8** ligand where a(1) only α-synuclein protein, a(2) 100μM of ligand **ZW-8**, then aqueous solution of imidazole was added, a(3) 90 μM of imidazole, a(4) 155μM of imidazole, (b) ^{1}H NMR in D_2O of a-synuclein protein (1mM) with different concentration (**ZW-10**) ligand ^{1}H NMR of α-synuclein protein (1.0 mM) in D_2O with gradually increasing concentration of **ZW-10** ligand where, b(1) only α-synuclein protein, b(2) 18 μM of ligand zw-10, b(3) 90 μM of ligand **ZW-10**, b(4) 160 μM of ligand **ZW-10**.

when free histidine amino acids were added in a portion of 90 μM into the same solution and ^{1}H NMR was recorded, the same peaks at δ 7.7 ppm and 6.9 ppm reappeared. This study unambiguously proved that **ZW-2** and **ZW-8** have strong binding interactions with histidine residue (H_{50}) at the N-terminal region of α-synuclein protein. By repeating the experiment with different doses of ligand **(ZW-8**), the diminished peaks became sharper in the presence of different concentrations of imidazole (90μM to 155μM) in **fig.14a** it is most likely that these zwitter ionic molecules may form salt-bridge interactions with the imidazole protons, which is responsible for their binding with N-H_{50}. No significant changes were observed for the **(ZW-10)** ligand **fig.14b.** the most hydrophobic (hydrophobic scale +0.74) zwitterionic molecule in this study, up to a concentration of 90 μM. However, upon increasing the ligand concentration beyond 90 μM, slight changes were noted, with a minor decrease in the chemical shift of both characteristic proton peaks.

4.7.9 MALDI Mass Spectroscopy.

MALDI mass spectrum was used to study the binding of small molecule with the α-syn protein. The standard protein sample gave a mass of 14535.1973. The α-syn protein was incubated separately with the zwitter ionic compounds **ZW-2** (molecular mass 137.0477), **ZW-8** and **ZW-10** respectively and mass spectra was recorded. In the mass spectra of compound **ZW-2**, we observed a mass peak at 14672.4336 (14535+137), which corresponded to the small molecule bound protein. This spectrum unambiguously confirmed that **ZW-2** binds with α-syn protein. Only very feeble mass was observed for the other two compounds **ZW-8** and **ZW-10**, which were earlier shown in the NMR spectra to bind weakly.

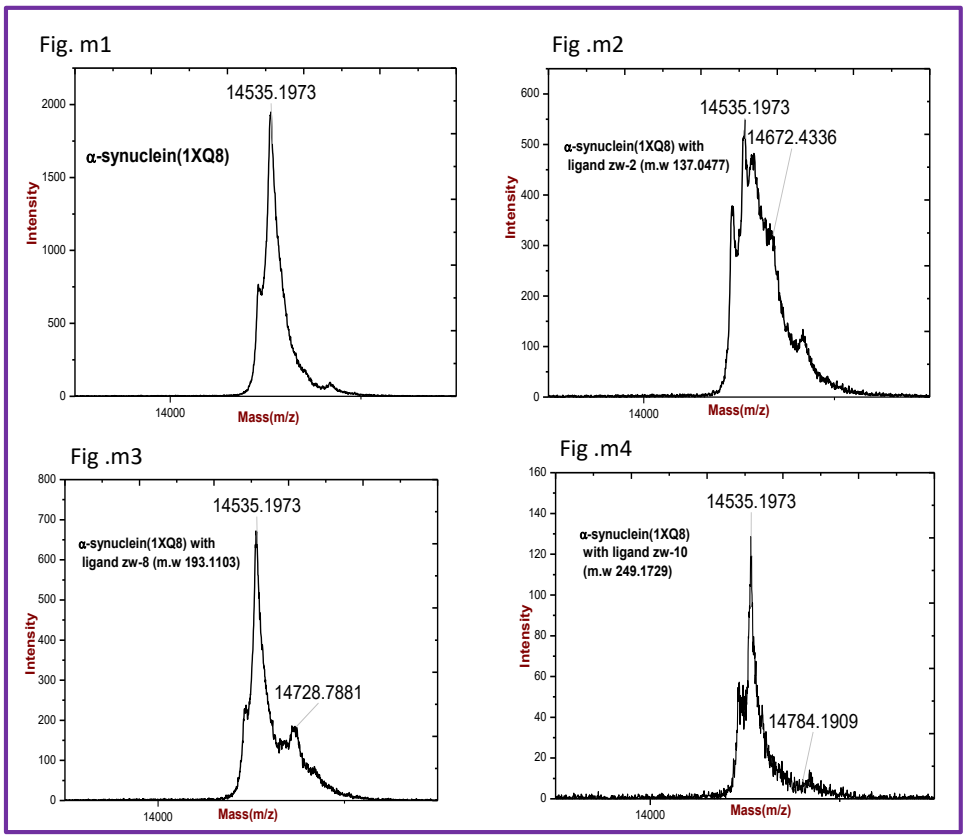

Figure 15. MALDI spectroscopy was used to study the binding of small molecule with α-syn protein

4.7.10 Isothermal Calorimetry (ITC) study

It is known that salt bridge interactions may play a crucial role in stabilizing a protein's three-dimensional structure and are particularly important in protein-ligand binding. It contributes to the overall stability and function of proteins by reducing the entropy of disordered proteins. In our study (Figure.16a), the entropy change (ΔS) for α-synuclein binding with the zwitter ionic ligand **ZW-2** is -27 $J.mol^{-1}K^{-1}$, indicating a decrease in disorder, On the other hand, the entropy changes due to the binding with **ZW-10** (Figure b), is calculated to be +167.4 $J.K^{-1}.mol^{-1}$, suggesting less stability. At a higher

concentration of ligand **ZW-10** (Figure 16c), the entropy change due to binding is -245.9 $J.K^{-1}.mol^{-1}$. Additionally, the dissociation constant, K_d for **ZW-2** is 5×10^{-8} M (for a ligand concentration of 0.25 μM and α-synuclein concentration of 0.05 μM), which is higher than the dissociation constant for **zw-10** ($K_d=1\times10^{-9}$ M) at low concentration (0.25 μM ligand, 0.05 μM α-synuclein). However, the dissociation constant for **ZW-10** increases to 2.11×10^{-5} M at higher ligand concentration (1.25 μM ligand, 0.05 μM α-synuclein). This result highlights that **ZW-2** binds to α-syn with the greater efficiency, which may be explained due to more favourable with stronger electrostatic interactions. The entropy change (ΔS) for α-synuclein binding with the zwitter ionic ligand **ZW-2** is -27 $J.K^{-1}.mol^{-1}$, indicating a decrease in disorder, whereas the entropy changes for binding with **ZW-10** is +167.4 $J.K^{-1}.mol^{-1}$, suggesting less stability. At a higher concentration of ligand **ZW-10**, the entropy change for binding is -245.9 $J.K^{-1}.mol^{-1}$

(a)

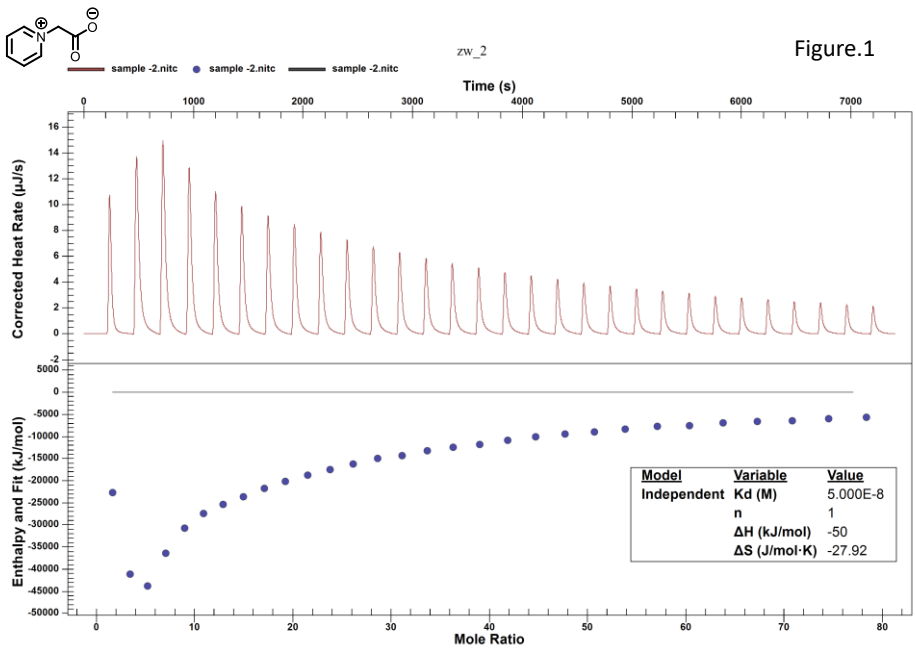

Figure.1

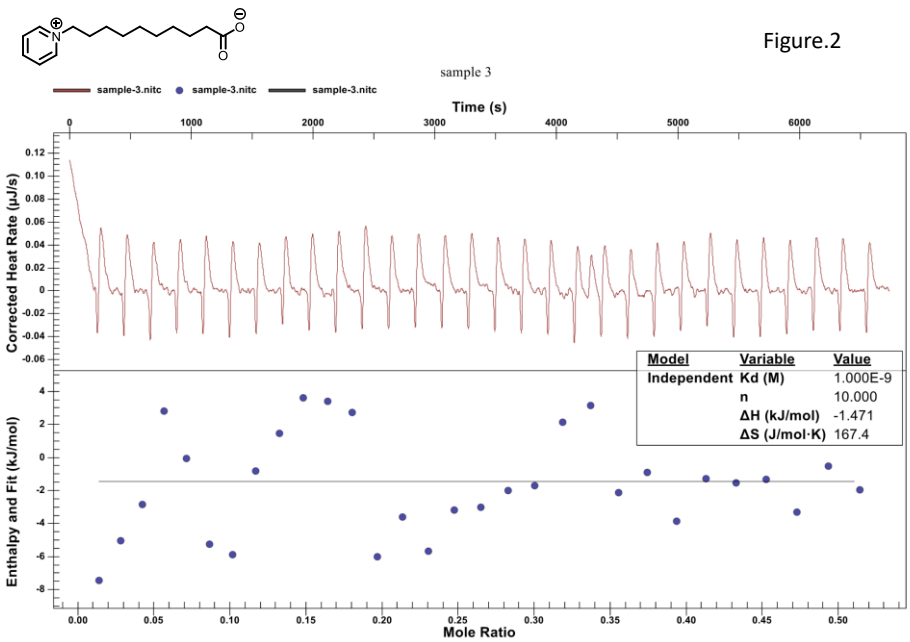

Figure.2

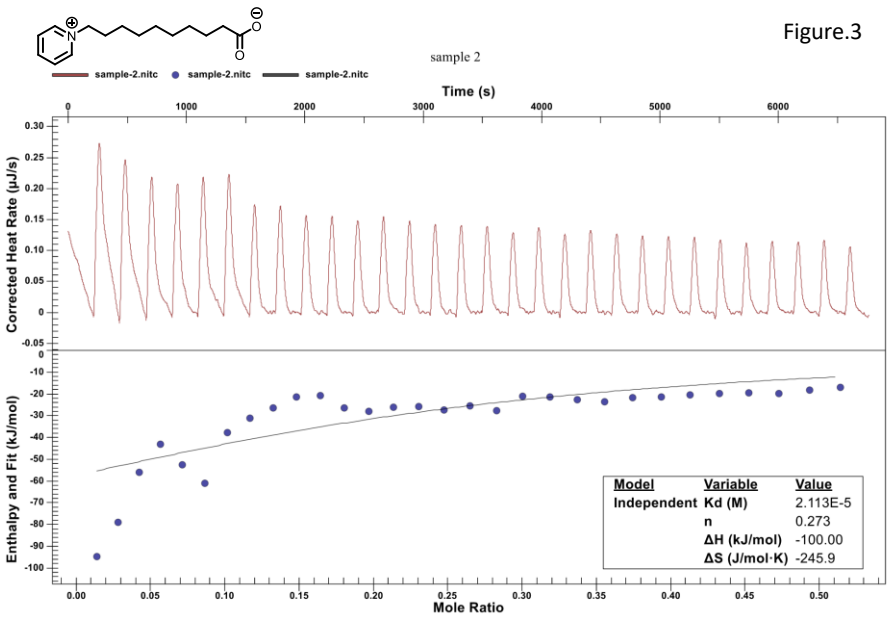

Figure.3

Table 2. The values from the ITC data:

Condition Number	For ZW-2 (figure 1)	For ZW-10 (figure. 2)	For ZW-10 (figure. 3)
Syringe Concentration in water	0.25μM	0.25 μM	1.25 μM
Cell Concentration in Water	0.05 μM	0.05 μM	0.05 μM
Temperature	298K	298K	298K
No. of Injection	30	30	30
Volume per Injection	5 μM	5 μM	5 μM
RPM	200	200	200
Delay	60 Seconds	60 Seconds	60 Seconds
Injection Interval	240 Seconds	240 Seconds	240 Seconds

4.7.11 Circular Dichroism (CD) Study & DSC Studies:

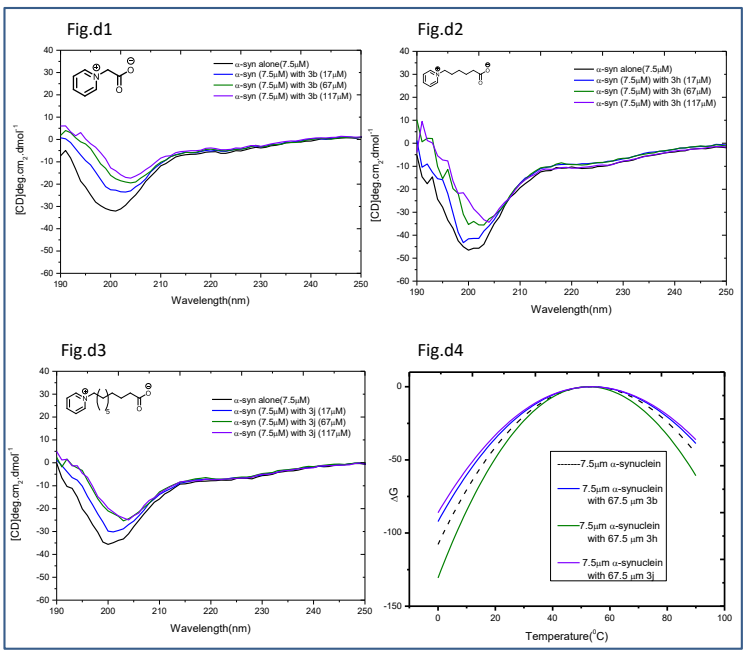

Figure 18. d1: ITC binding study of α-syneuclein protein with ligand **ZW-2**; **d2**: ITC binding study of α-syneuclein protein with ligand **ZW-8**; **d3**: ITC binding study of α-syneuclein protein with ligand ZW-10; **d4**: DSC study of α-syneuclein protein with ligand **ZW-2**, **ZW-8**, **ZW-10**.

Circular dichroism (CD) spectroscopy & Differential Scannning Calorimetry (DSC) studies was utilized to investigate the conformational changes of α-synuclein protein in aqueous solution. The CD spectrum of α-synuclein in deionized water exhibited a characteristic negative minimum at 198 nm, indicative of the monomeric conformation of the protein. The CD measurements were conducted in deionized water without incubation, as shown in Figure 18, along with varying concentrations of ligands.

Upon increasing ligand concentrations, the characteristic negative minima at 208 nm and 218 nm, typically associated with α-helix and β-sheet-rich structures, respectively, were not observed. This suggests that the presence of ligands did not induce significant conformational changes in α-synuclein in the aqueous solution. However, with increasing concentrations of ligand **ZW-2**, the peak at 198 nm became broader, indicating a higher binding efficiency of ligand **ZW-2** compared to other zwitter ionic ligands. The findings suggest that the α-synuclein protein maintains a highly stable conformation in the presence of zwitter ionic ligands.

4.7.12 Plausible Mechanism of binding of ZW-2 with α-Syn protein

From the experimental data……

- **MALDI Massspectrometry.** The turbidity results support the MALDI mass measurements. In the presence of a fivefold excess of ligand, binding was observed only at a 1:1 ratio of ligand to protein. This indicates that a single ligand molecule binds specifically to one protein molecule.

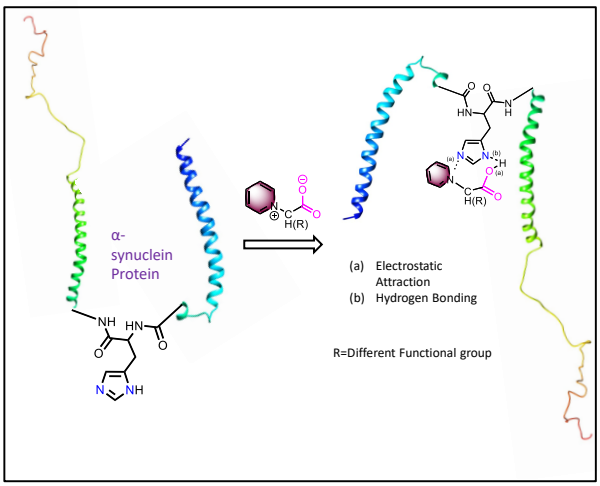

Figure 19. Hydrogen bonding and salt bridge interaction between zwitter ion and a-synuclein protein.

ITC Experiments: This experiment demonstrates that the coefficient value (n=1) is lowest for **ZW-2** at low concentrations, indicating that binding occurs at a single site.

- **NMR Experiments:** NMR titration confirms that the histidine residues of the α-synuclein protein interact with the ligand.

❖ **CD Experiments:** From the CD experiment, with increasing concentrations of ligand **ZW-2**, the peak at 198 nm became broader, indicating a higher binding efficiency of ligand **ZW-2** compared to other zwitter ionic ligands which also support like NMR experiment.

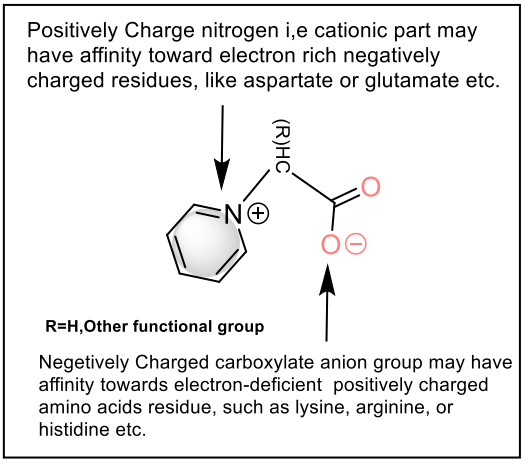

Figure 20: Donor-acceptor sites via electrostatic interaction in zwitter ions.

Salt bridge interactions between proteins and ligands are electrostatic attractions between oppositely charged groups. These interactions typically form between a positively charged residue, such as lysine, arginine, or histidine, with the carboxylate ion of a zwitter-ionic ligand. Conversely, they also occur between a negatively charged residue, like aspartate or glutamate, with the pyridinium group of a zwitter-ionic ligand.

Also L-histidine, a key amino acid, is characterized by its aromatic side chain i,e imidazole which pK_b of approximately 6.5. This property provides significant buffering capacity in biological systems, allowing histidine to act as both a proton donor and acceptor, thereby stabilizing protein-ligand interactions. Salt bridges play a crucial role in stabilizing a protein's three-dimensional structure and are particularly important in protein-ligand binding, contributing to the overall stability and function of protein molecules by reducing the entropy of disordered proteins.

The docking study in (Fig. 19) revealed that molecules **ZW-2** and **ZW-8** interacted with a similar region of the α-synuclein protein, displaying comparable binding affinities. Molecule 3b interacted with residues 38, 39, 40, 43, 44, 45, and 48 of α-synuclein, with a calculated binding affinity of -3.8 kcal/mol. Similarly, molecule **ZW-8** bound to residues 32, 35, 38, 39, 40, 43, 44, 45, and 48, showing a slightly higher binding affinity of -3.9 kcal/mol. In contrast, molecule 3j interacted with residues 39, 40, 43, 45, and 48, but exhibited a lower binding affinity of -3.1 kcal/mol. Additionally, ^{1}H NMR studies and MALDI mass spectrometry suggest that residues 50, 54, and 58 of α-synuclein may play a particularly significant role in ligand binding, with a binding affinity of -3.19 kcal/mol

4.7.13 Discussion:

In the present study, small zwitter ionic molecules can inhibit liquid droplets forming due to α-syn phase separation. Turbidity (a direct proof of the formation of aggregates in solution by the α-syn protein) assay was performed with the synthesized molecules, and light scattering experiments were done. This experiment resulted in ligand **ZW-2**, which efficiently inhibited droplet formation. Confocal microscopy images of liquid droplets in the presence and absence of **ZW-2** also confirmed the ability of the said ligand to inhibit droplet formations. Cell viability and cytotoxicity assays were performed with **ZW-2** and other ligands in the series, which showed no toxicity in the normal cell lines up to 100 μM concentrations. In all these studies, we compared our results with another ligand, **ZW-10**, which is not a good LLPS inhibitor. To find out the possible reason of **ZW-2**, inhibiting α-syn phase separation and hence LLPS formation, concentration-dependent ^{1}H NMR studies were performed with **ZW-2** and other derivatives with α-syn protein. The shift of protons of the sidechain imidazole residue of histidine in N-terminal region towards more down field in the ^{1}H NMR spectra, clearly indicates that ligand **ZW-2** strongly interacts with it. The binding of **ZW-2** at the N-terminal pocket of α-syn by forming a possible six/seven membered salt-bridge interaction might have disrupted the geometry of the protein. This structural change at the N-terminal histidine residue may be inhibited the protein to undergo droplet formation and aggregations. The same has not reflected in case of **ZW-8** or **ZW-10** which is a poor binder of α-syn. Structurally, **ZW-2** contains a glycine residue (single methylene in between the positive and negative charges) and our experimental results indicated that substitution at the α-carbon of the inhibitor molecule is not tolerated. Moreover increase in methylene chain length i,e hydrophobicity was also not permitted as reflected in the droplet formation studies.

Despite these findings, prior studies, including our own, have identified critical barriers to the LLPS of α-Syn under physiological conditions. Specifically, the protein concentrations required for LLPS were higher than those typically observed in biophysical study, and the process often required prolonged incubation periods. These observations suggested the presence of kinetic hurdles that diverged from classical phase transition dynamics. The objective of our current study was to investigate how environmental factors influence the LLPS behavior of α-Syn, with the goal of understanding the conditions that promote or inhibit this process.

5.0 Supporting Information for Synthesis:

5.1 General Information:

All reactions were carried out in oven-dried glassware. Reagents were purchased from Sigma-Aldrich, Acros, Alfa Aesar or TCI. Reactions were monitored by thin layer chromatography (TLC) carried outon silica gel plates (Merck silica gel 60, f254); the spots were visualized with UV light (254 and 365nm). Flash column chromatography was performed using 230-400 mesh silica gel. Silica gel (230-400 mesh) was used for column chromatographic separations. Yields refer to isolated yields after chromatographic purification. 1H NMR (400 MHz) and ^{13}C spectra were recorded in CD_3OD solvent using TMS as the internal standard and are reported relative to the residual solvent signal. The following abbreviations were used to explain NMR peak multiplicities: s = singlet, d = doublet, t =triplet, q = quartet, m = multiplet, br = broad. High resolution mass spectra (HRMS, m/z) were recorded using ESI (Q-TOF and Orbitrap, positive ion) EI mode.

5.2 Experimental Procedures and Spectral data:

5.2.1 General procedure for ZW-1 to ZW-12:

To different amino acid derivatives (1 equiv), LiBr (1.5 equiv.), and 42% HBr (4 equiv.) was added and the reaction mixture was stirred at 0°C for 10 minutes. After that, an aqueous solution of $NaNO_2$ (1.6 equiv. in 10 mL water) was added dropwise using a dropping funnel. Once the reaction was complete (monitored by TLC), the mixture was washed with ethyl acetate and water (3 x10 mL). The ethyl acetate layer was dried over anhydrous sodium sulphate, and the solvent was removed under reduced pressure to obtain the corresponding bromo derivatives. It was then refluxed with pyridine (10 equiv.) for 12 hours, followed by evaporation to dryness. The final compounds were purified via column chromatography using silica gel, yielding the corresponding zwitter ionic compound.

5.2.2 Spectra Interpretations (^{1}H, ^{13}C, HRMS) of synthesized compounds:

Compound ZW-1:

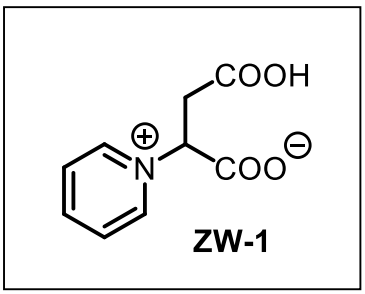

ZW-1

Aspartic acid (2.66g, 20.0mmol, 1.0 equiv.), lithium bromide (2.6g, 30.0mmol,1.5 equiv.) sodium nitrite (2.2g, 32.0 mmol,1.6 equiv.) were used.
Yield (90% yield, Brown solid), Column chromatography (silica gel, eluting with 35% methanol/ethyl acetate with).
^{1}H NMR (400 MHz, Methanol-*d*$_4$): δ 9.12 (d, *J* = 6.5 Hz, 2H), 8.62 (t, *J* = 7.8 Hz, 1H), 8.13 (t, *J* = 6.8 Hz, 2H), 4.94 (t, *J* = 6.4 Hz, 1H), 3.24 – 3.11 (m, 2H).
^{13}C NMR (101 MHz, Methanol-*d*$_4$): δ 171.7, 145.9, 145.3, 127.9, 57.2, 34.1.
HRMS (ESI) m/z: $[M+H]^+$ Calcd for $C_9H_9NO_4$: 196.0610; Found 196.0722.

Compound ZW-2:

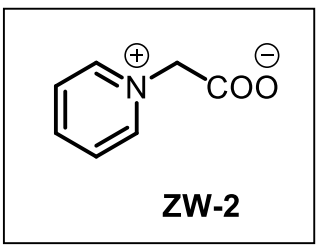

ZW-2

Glycine (1.5 g, 20.0 mmol, 1.0 equiv.), Lithium Bromide (2.6 g, 30.0 mmol,1.5 equiv.), sodium nitrite (2.2 g, 32.0 mmol,1.6 equiv.) were used.

Yield (95% yield, white solid), Column chromatography (silica gel, eluting with 35% methanol/ethyl acetate with).
^{1}H NMR (400 MHz, Methanol-*d*$_4$): δ 9.13 – 8.89 (m, 2H), 8.78 – 8.57 (m, 1H), 8.26 – 8.04 (m, 2H), 5.65 (s, 1H), 4.48 (s, 1H).
^{13}C NMR (100 MHz, Methanol-*d*4): δ 167.47, 146.56, 146.23, 145.32, 127.99, 61.16.
HRMS (ESI) m/z: [M+H] Calcd. for $C_7H_8NO_2$: 138.0555; Found 138.0560.

Compound ZW-3:

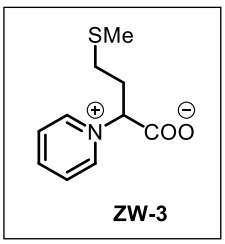

Methionine (1.5 g, 20.0 mmol, 1.0 equiv.), lithium bromide (2.6 g, 30.0 mmol,1.5 equiv.) Sodium Nitrite (2.2 g, 32.0 mmol,1.6 equiv.) were used.

Yield (85% yield, Grey liquid), Column chromatography (silica gel, eluting with 35% methanol/ ethyl acetate).
^{1}H NMR (400 MHz, Methanol-*d*$_4$): δ 9.29 – 8.80 (m, 2H), 8.73 – 8.56 (m, 1H), 8.23 – 8.06 (m, 2H), 5.91 – 5.82 (m, 1H), 4.82 – 4.73 (m, 1H), 4.29 – 4.06 (m, 0H), 3.74 – 3.62 (m, 0H), 3.47 – 2.94 (m, 1H), 2.86 – 1.75 (m, 3H).
^{13}C NMR (100 MHz, Methanol-*d*$_4$): δ 175.69, 172.84, 146.97, 146.61, 145.90, 144.96, 141.73, 127.51, 68.45, 68.26, 63.06, 59.48, 43.73, 33.40, 31.36, 29.92, 29.66, 26.98, 13.85, 12.49.
HRMS (ESI) m/z: $[M+H]^+$ Calcd for $C_{10}H_{14}NO_2S$: 212.0745; Found 212.0753.

Compound ZW-4:

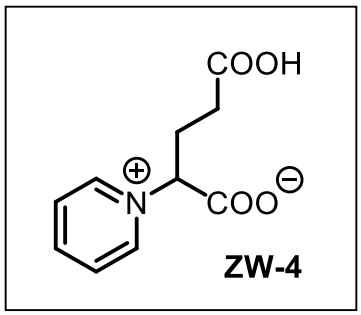

Glutamic Acid (2.940 g, 20.0 mmol, 1.0 equiv.), lithium bromide (2.6 g, 30.0 mmol,1.5 equiv.), sodium nitrite (2.2 g, 32.0 mmol,1.6 equiv.) were used.

^{1}H NMR (400 MHz, Methanol-*d*$_4$): δ 9.80 – 8.73 (m, 2H), 8.71 – 8.50 (m, 1H), 8.44 – 7.95 (m, 2H), 4.93 – 4.60 (m, 1H), 4.14 – 3.96 (m, 0H), 3.66 – 3.49 (m, 0H), 3.42 – 3.12 (m, 0H), 2.98 – 1.75 (m, 3H), 1.68 – 0.96 (m, 0H).
^{13}C NMR (100 MHz, Methanol-*d*$_4$): δ 198.74, 178.42, 178.37, 172.59, 142.73, 127.86, 100.00, 78.60, 76.24, 60.75, 30.22, 27.13, 26.75, 26.54, 26.41, 25.94, 25.86, 25.55, 13.36.
HRMS (ESI) m/z: $[M+H]^+$ Calcd for $C_{10}H_{12}NO_4$ 210.0766; Found 194.1163.

Compound ZW-5:

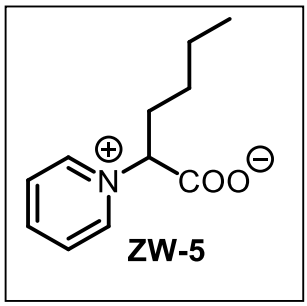

Nor leucine (2.620 g ,20.0 mmol, 1.0 equiv.), lithium bromide (2.6 g, 30.0 mmol,1.5 equiv.), and sodium nitrite (2.2 g, 32.0 mmol, 1.6 equiv.) were used.

^{1}H NMR (400 MHz, Methanol-d_4): δ 9.06 – 8.88 (m, 2H), 8.69 – 8.56 (m, 1H), 8.17 – 8.10 (m, 2H), 4.67 – 4.62 (m, 1H), 2.22 – 1.85 (m, 2H), 1.51 – 1.21 (m, 4H), 1.00 – 0.80 (m, 3H).

^{13}C NMR (100 MHz, Methanol-d_4): δ 147.42, 145.89, 145.25, 141.97, 128.62, 127.88, 62.28, 31.20, 28.15, 22.00, 13.09.

HRMS (ESI) m/z: $[M+H]^+$ Calcd. for $C_{11}H_{16}NO_2$: 194.1181 found 194.1172

Compound ZW-6:

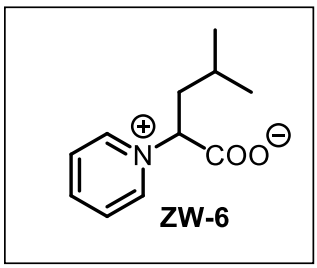

Leucine (2.620 g, 20.0 mmol, 1.0 equiv.) lithium bromide (2.6 g, 30.0 mmol,1.5 equiv.), sodium nitrite (2.2 g, 32.0 mmol,1.6 equiv.) were used.

Yield (95% yield, white solid), Column chromatography (silica gel, eluting with 35% methanol/ethyl acetate).

^{1}H NMR (400MHz, Methanol-d_4): δ 9.17 (t, *J*=4.7Hz, 2H), 8.66 (m,1H), 8.18 (t, *J*=6.7Hz,2H), 4.77 (dt, *J*=7.2, 2.5Hz, 2H), 2.00–1.89 (m, 2H), 1.71 (dd, 1H), 1.02 (dd, *J* = 6.7, 1.5 Hz, 6H).

^{13}C NMR (100 MHz, Methanol-d_4): δ 173.57, 145.64, 144.83, 128.37, 60.42, 40.03, 25.71, 21.47.

HRMS (ESI) m/z: $[M+H]^+$ Calcd. for $C_{11}H_{16}NO_2$: 194.1181; Found 194.1173

Compound ZW-7:

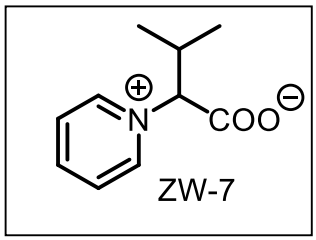

Valine (2.620g, 20.0 mmol, 1.0 equiv.), lithium bromide (2.6g, 30.0 mmol, 1.5 equiv.) sodium nitrite (2.2 g, 32.0 mmol,1.6 equiv.) were used.
Yield (95% yield, white solid), Column chromatography (silica gel, eluting with 35% methanol/ethyl acetate).
^{1}H NMR (400 MHz, Methanol-*d*$_4$): δ 9.04 (d, *J* = 6.0 Hz, 2H), 8.64 (t, *J* = 7.8 Hz, 1H), 8.21 – 8.11 (m, 2H), 4.52 (d, *J* = 9.1 Hz, 1H), 2.31 (m,1H), 0.99 (d, *J* = 7.5 Hz, 6H).
^{13}C NMR (100 MHz, Methanol-*d*$_4$): δ 177.70, 145.79, 144.82, 128.19, 68.02, 30.56, 18.17.
HRMS (ESI) m/z: $[M+H]^+$ Calcd. for $C_{10}H_{14}NO_2$ Exact Mass: 180.1025; Found 180.1020.

Compound ZW-8:

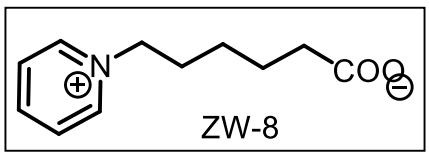

6-Amino caproic Acid (2.62 g ,20.0 mmol, 1.0 equiv.), lithium bromide (2.6 g, 30.0 mmol,1.5 equiv.), sodium nitrite (2.2 g, 32.0 mmol,1.6 equiv.) were used.
Yield (95% yield, white solid), Column chromatography (silica gel, eluting with 35% methanol/ethyl acetate)
^{1}H NMR (400 MHz, Methanol-*d*$_4$) δ 9.05 (d, 2H), 8.60 (t, *J* = 7.6 Hz, 1H), 8.13 (t, *J* = 6.6 Hz, 2H), 4.67 (t, *J* = 7.5 Hz, 2H), 2.25 (t, *J* = 8.1 Hz, 2H), 2.14 – 1.94 (m, 2H), 1.66 – 1.48 (m, 2H), 1.33 (t, *J* = 31.8 Hz, 12H).
^{13}C NMR (100 MHz, Methanol-*d*$_4$) δ 175.69, 145.66, 144.76, 128.29, 61.52, 33.22, 30.85, 25.24, 23.99.

Compound ZW-9:

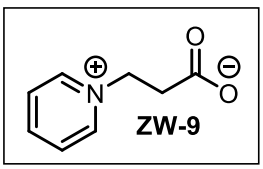

β-alanine (1.780 g, 20.0 mmol, 1.0 equiv.), lithium bromide (2.6 g, 30.0 mmol,1.5 equiv.), sodium nitrite (2.2 g, 32.0 mmol,1.6 equiv.) were used.
^{1}H NMR (400 MHz, Methanol-d4): δ 9.15 (d, J = 6.3 Hz, 2H), 8.64 (t, J = 8.4 Hz, 1H), 8.14 (t, J = 7.0 Hz, 2H), 4.93 (s, 2H), 3.20 (t, J = 6.4 Hz, 2H).
^{13}C NMR (100 MHz, Methanol-d4): δ 171.78, 146.00, 145.39, 128.03, 57.28, 34.29.

HRMS (ESI) m/z: [M+H] Calcd. for $C_8H_{10}NO_2$:152.0712 found 152.0717.
Compound ZW-10:

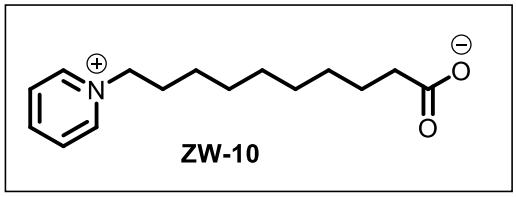

ZW-10

Yield (95% yield, white solid), Column chromatography (silica gel, eluting with 35% methanol ethyl acetate).

^{1}H NMR (400 MHz, Methanol-*d*4): δ 9.06 (s, 2H), 8.61 (d, *J* = 7.6 Hz, 1H), 8.13 (s, 2H), 4.67 (s, 2H), 2.25 (s, 2H), 2.02 (s, 2H), 1.56 (s, 2H), 1.33 (d, *J* = 31.3 Hz, 12H).
^{13}C NMR (100 MHz, Methanol-*d*4): δ 176.24, 145.57, 144.59, 128.24, 61.80, 33.64, 31.19, 29.05, 29.03, 28.98, 28.84, 28.71, 25.80, 24.74.
HRMS (ESI) m/z: $[M+H]^+$ Calcd. for $C_{16}H_{26}NO_2$: 264.1969 found 264.1945

5.2.3 Spectra (^{1}H, ^{13}C) of synthesized compounds:

^{1}H NMR of **ZW-1** in CD_3OD

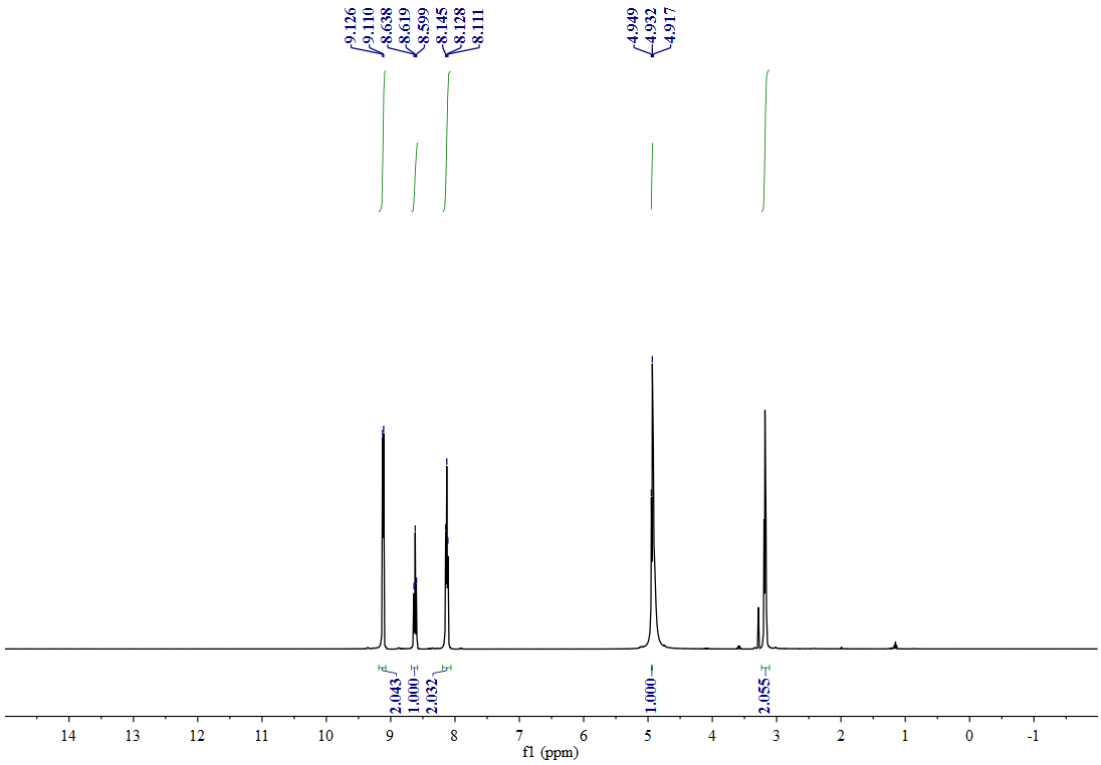

^{13}C NMR of **ZW-1** in CD_3OD

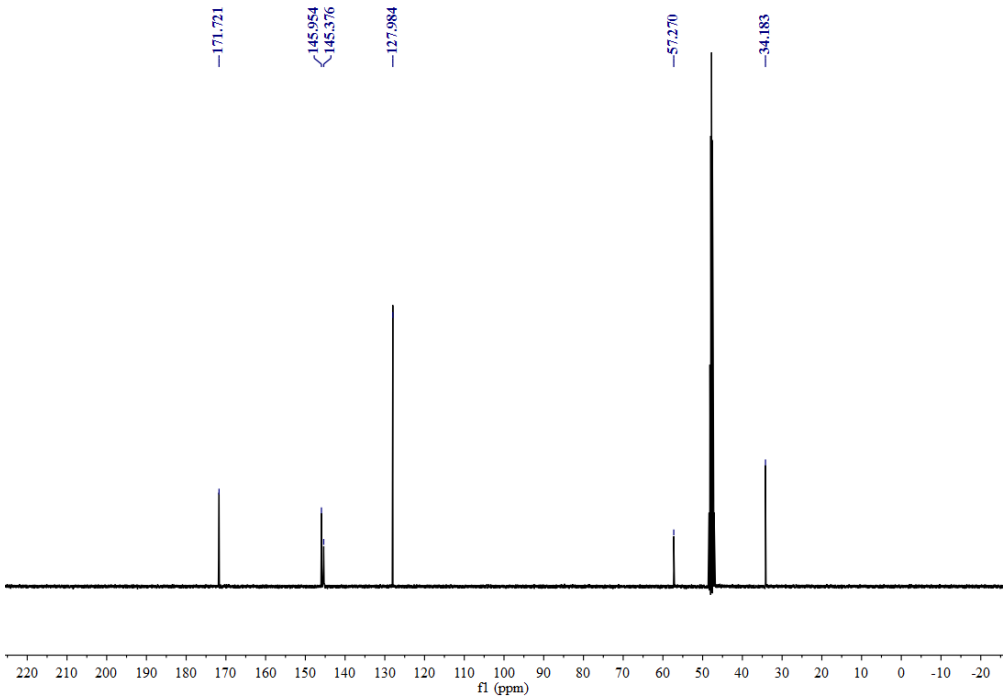

^{1}H NMR of **ZW-2** in CD3OD

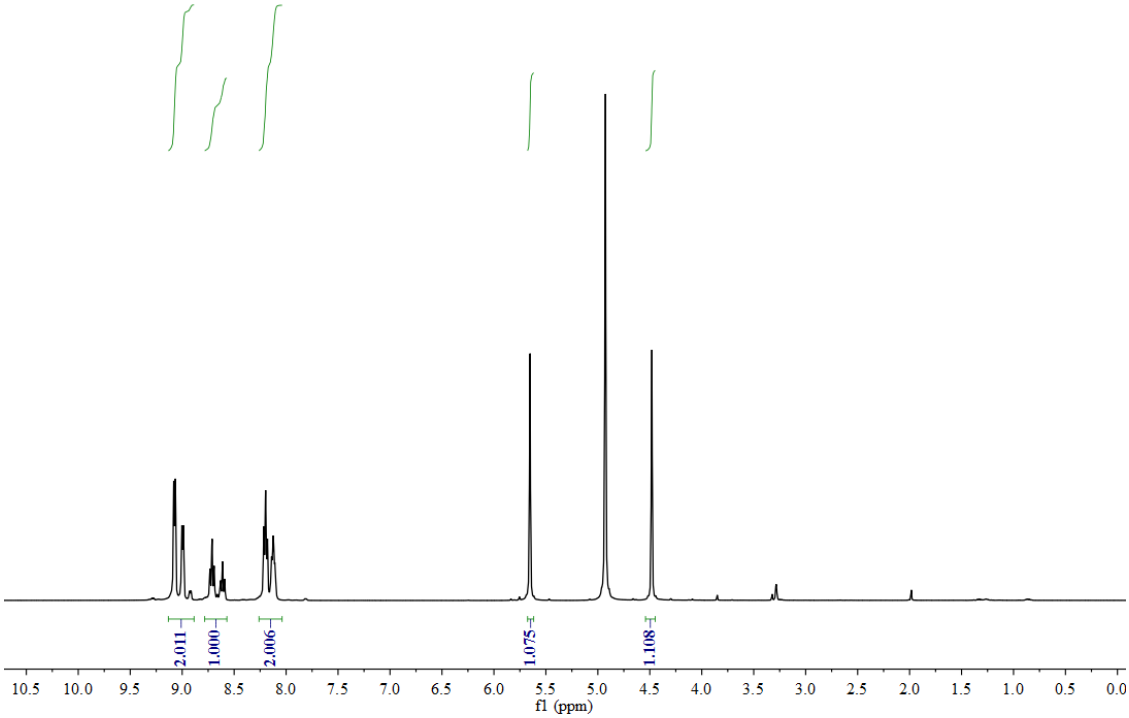

^{13}C NMR of **ZW-2** in CD_3OD

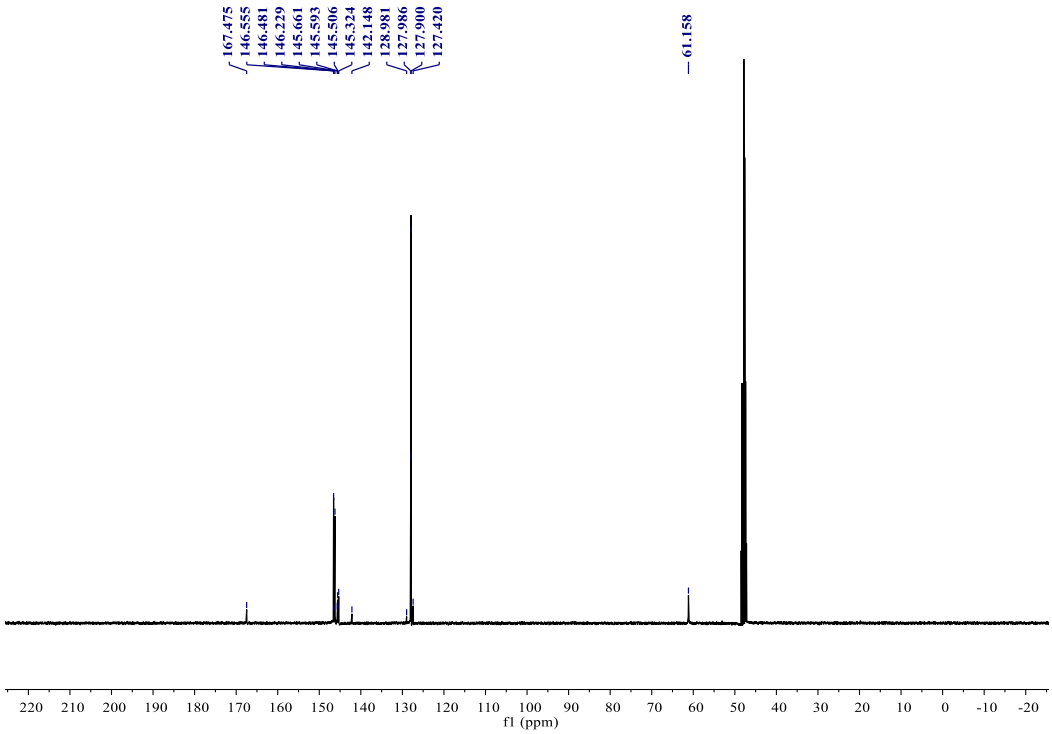

^{1}H NMR **ZW-3** in CD_3OD

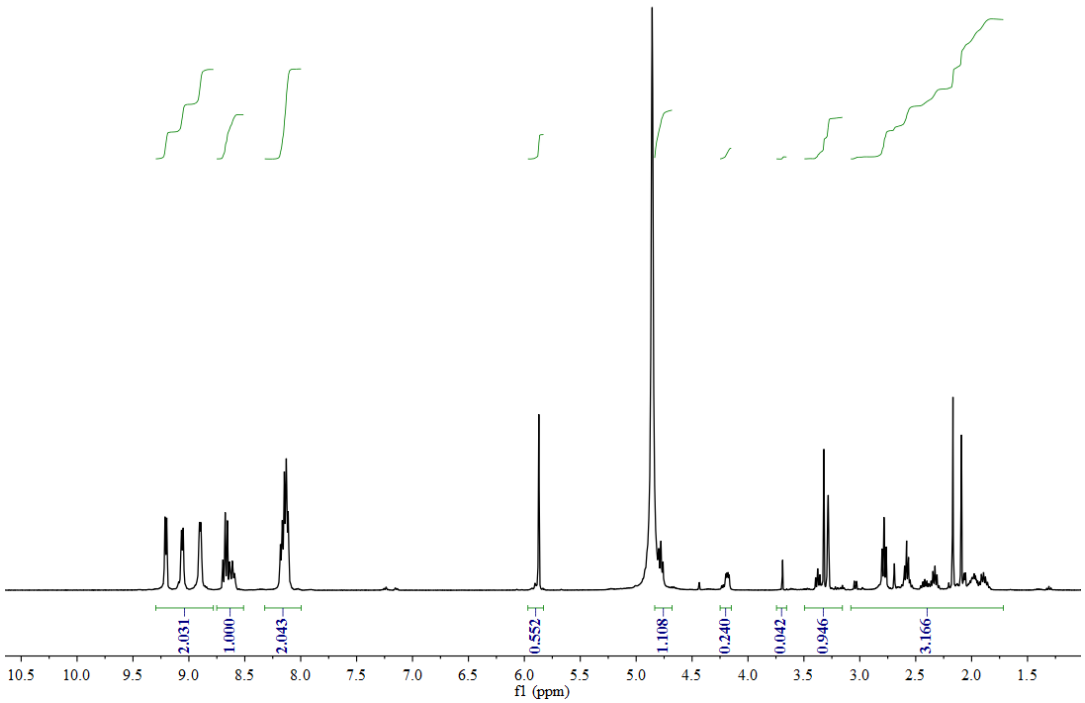

^{13}C NMR of **ZW-3** in CD_3OD

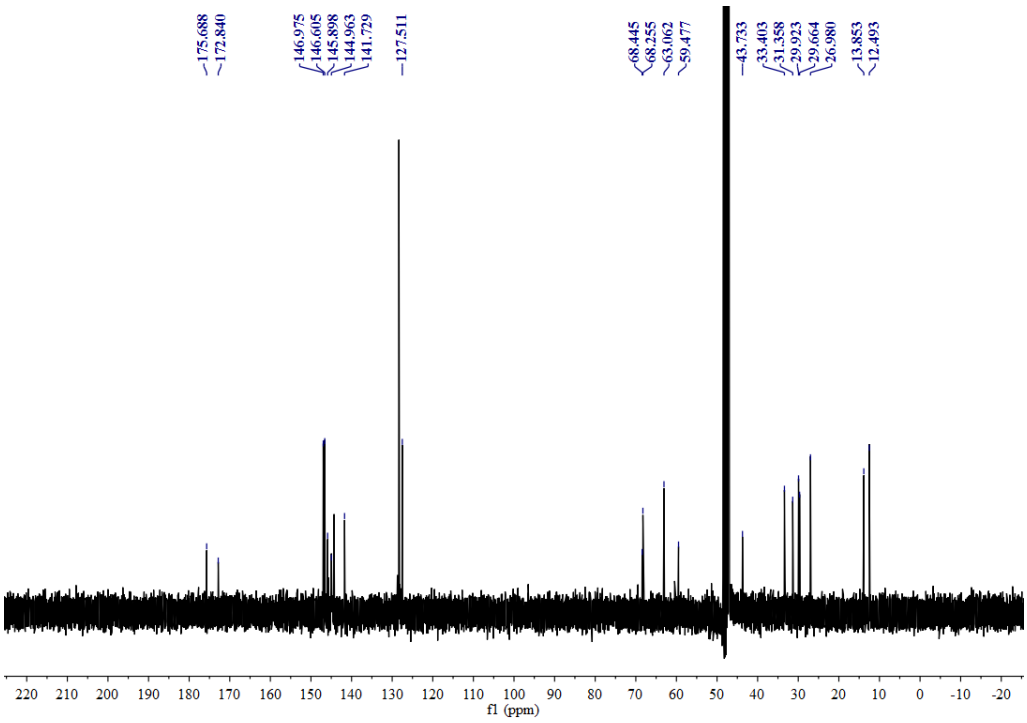

^{1}H NMR of **ZW-4** in CD_3OD

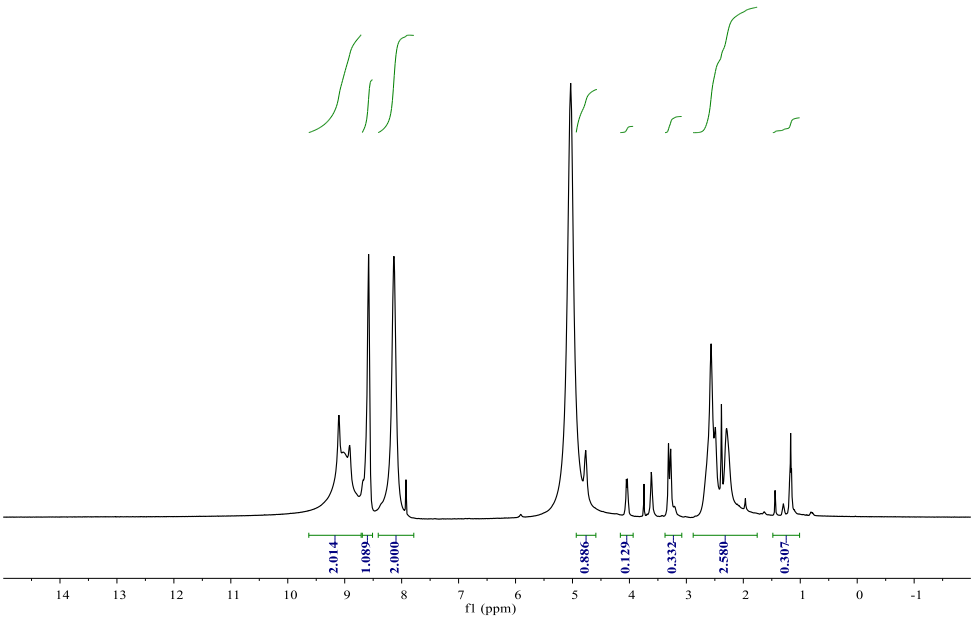

^{13}C NMR of **ZW-4** in CD_3OD

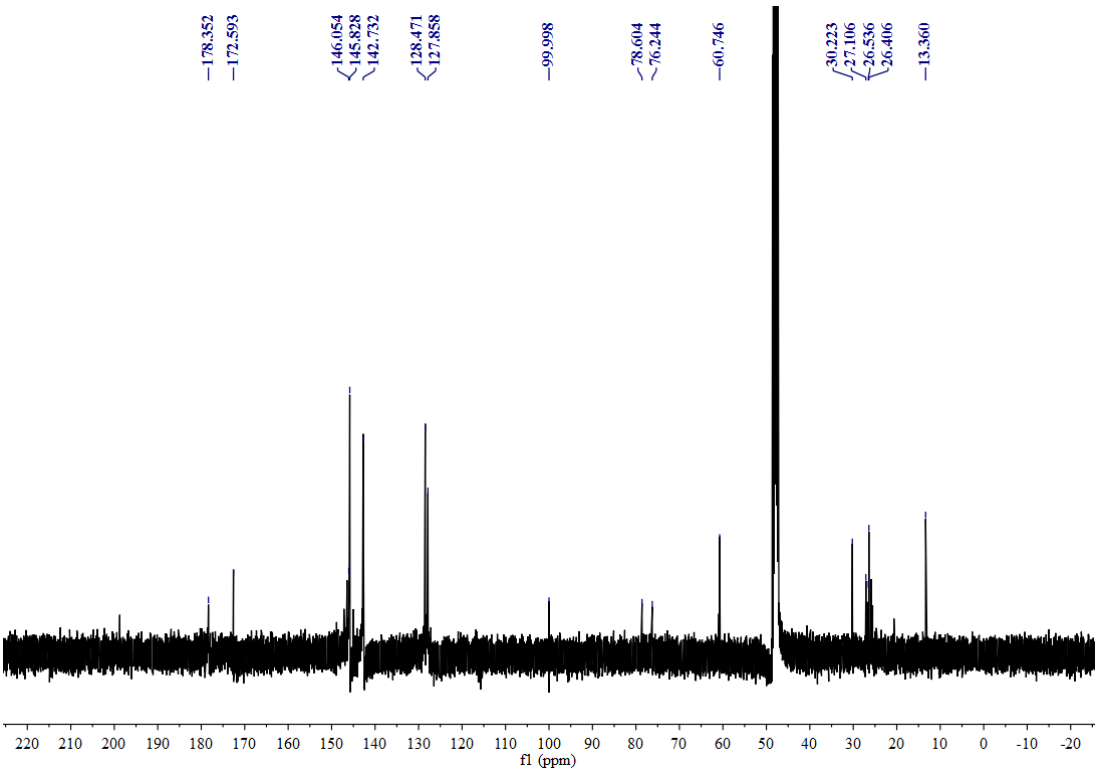

^{1}H NMR of **ZW-5** in CD_3OD

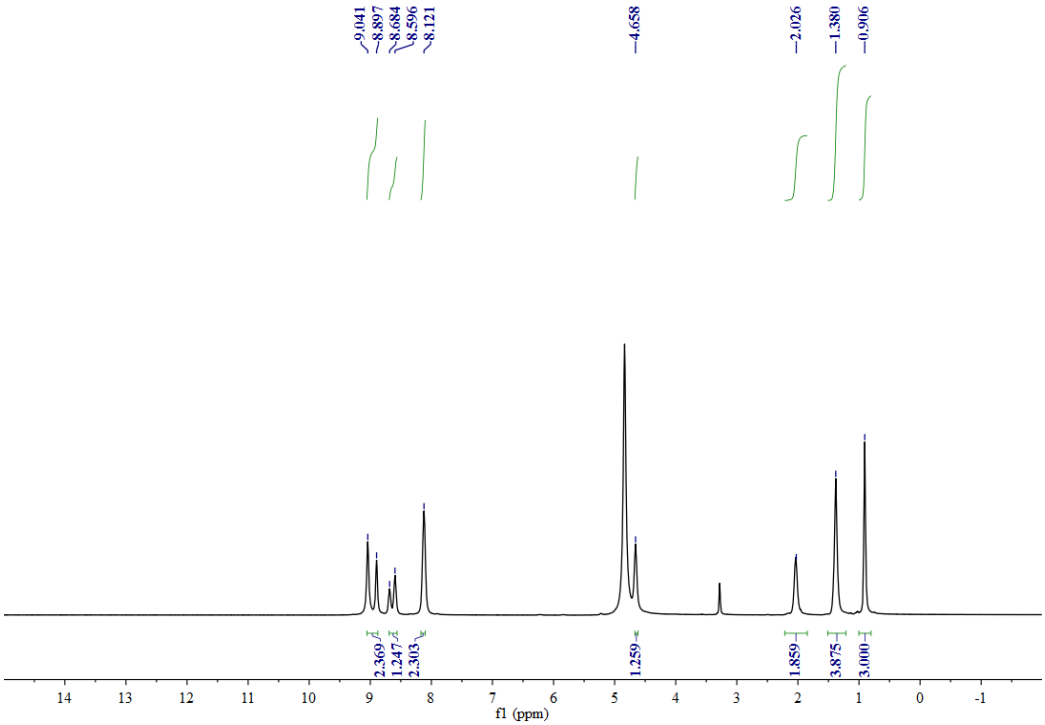

^{13}C NMR of **ZW-5** in CD_3OD

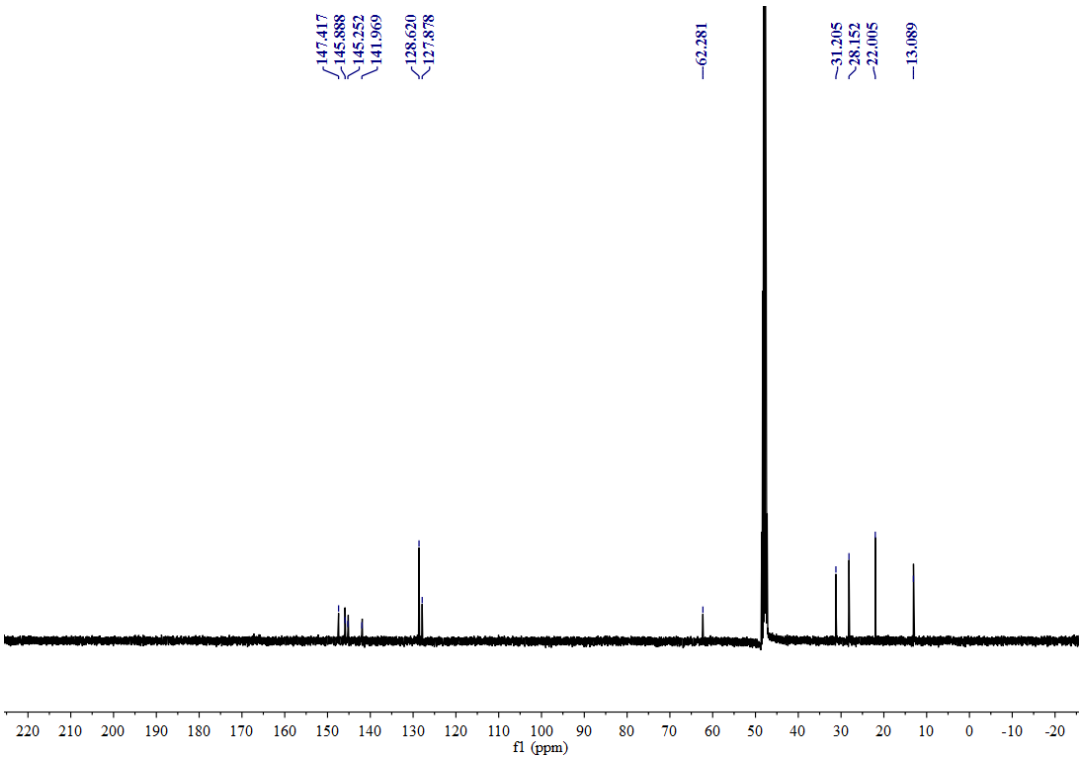

^{1}H NMR of **ZW-6** in CD_3OD

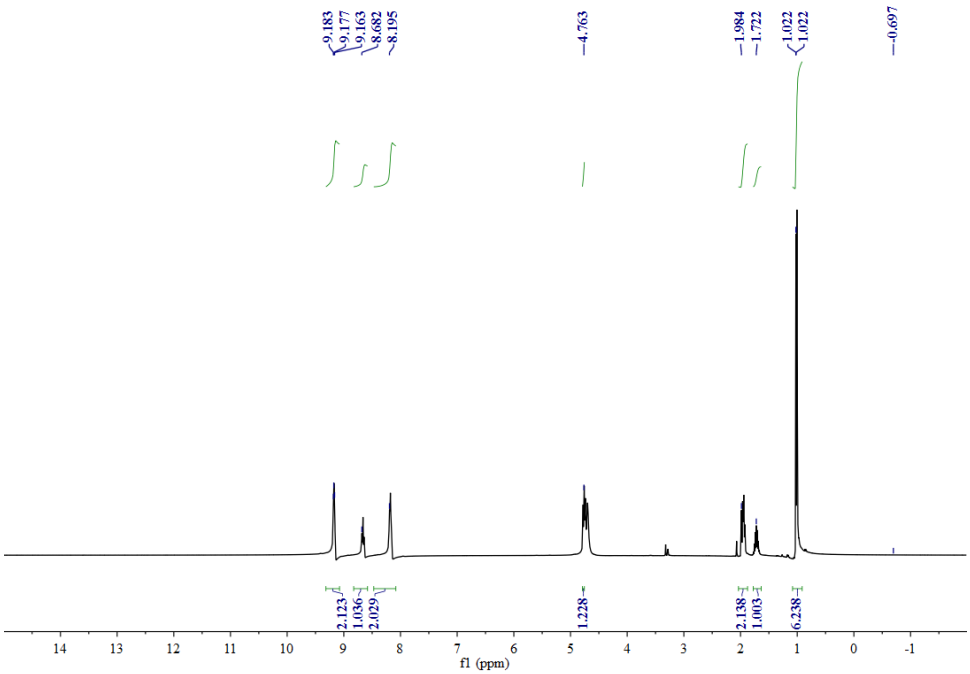

^{13}C NMR of **ZW-6** in CD_3OD

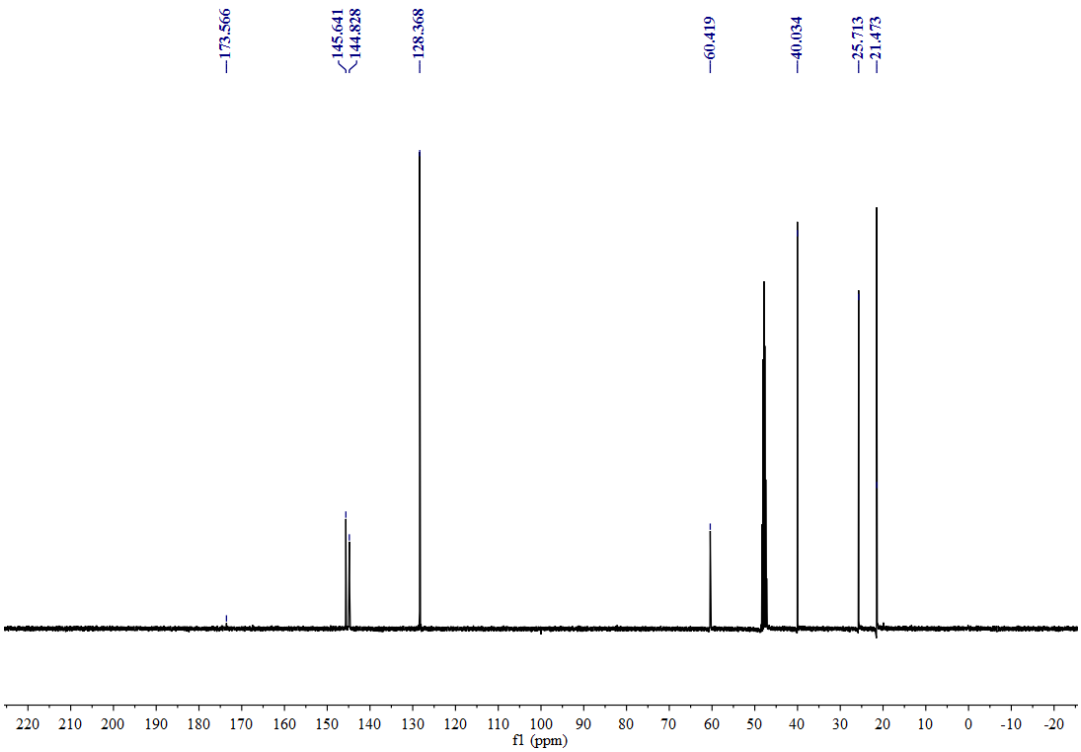

^{1}H NMR of **ZW-7** in CD_3OD

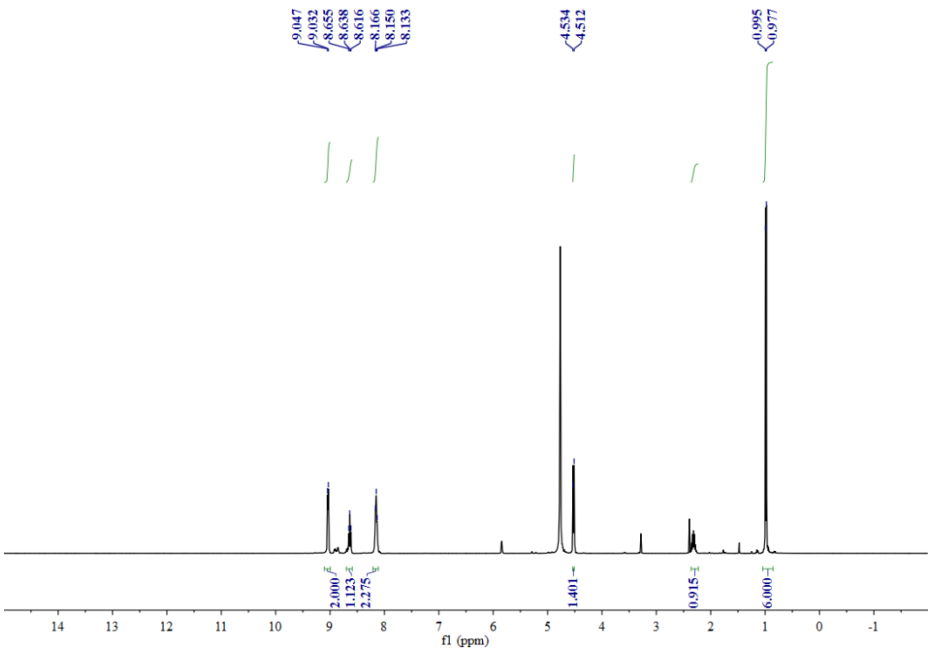

^{13}C NMR of **ZW-7** in CD_3OD

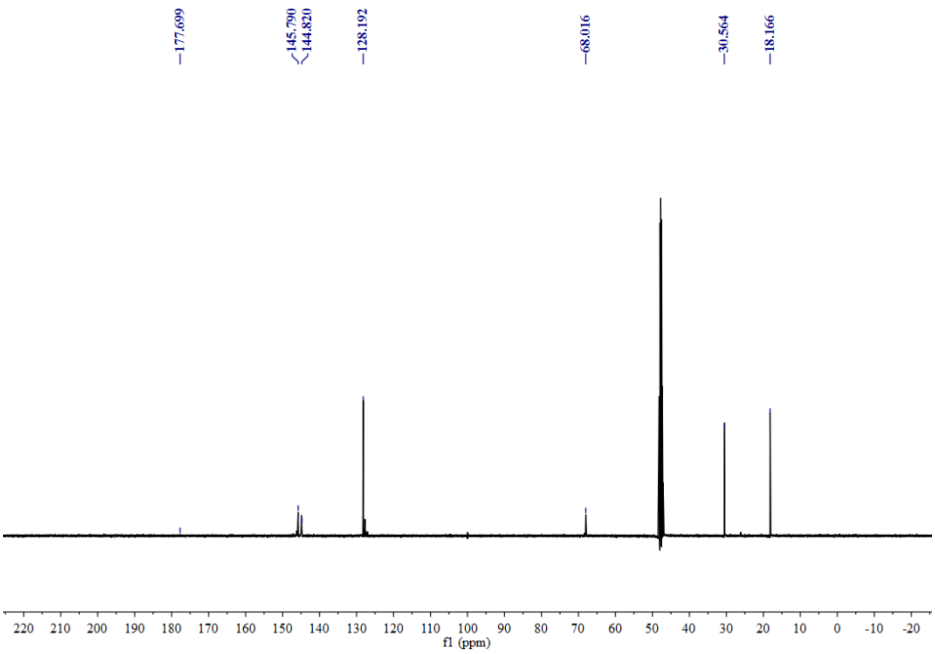

^{1}H NMR of **ZW-8** in CD_3OD

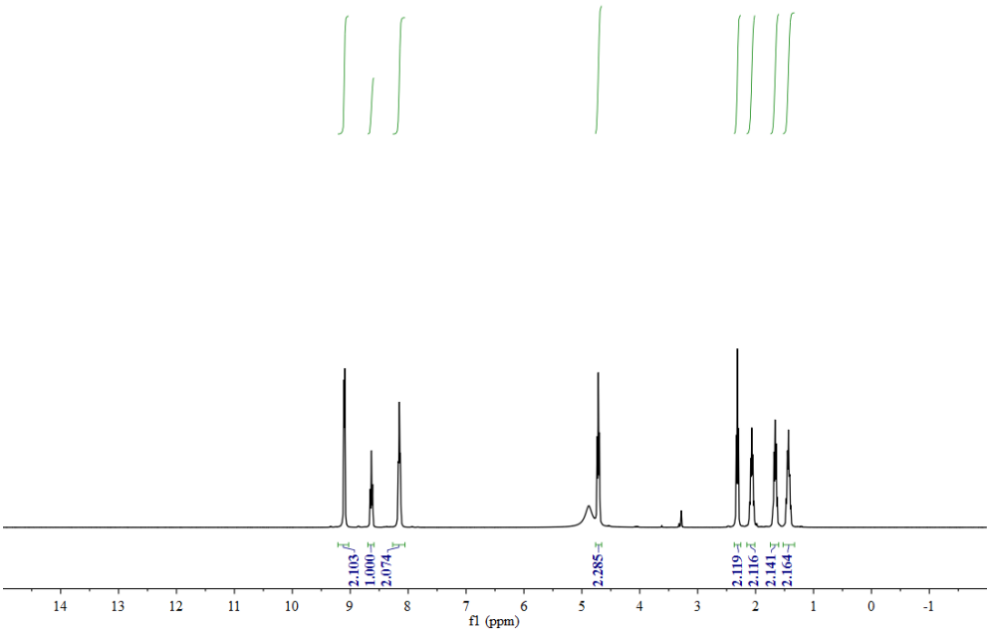

^{13}C NMR of **ZW-8** in CD_3OD

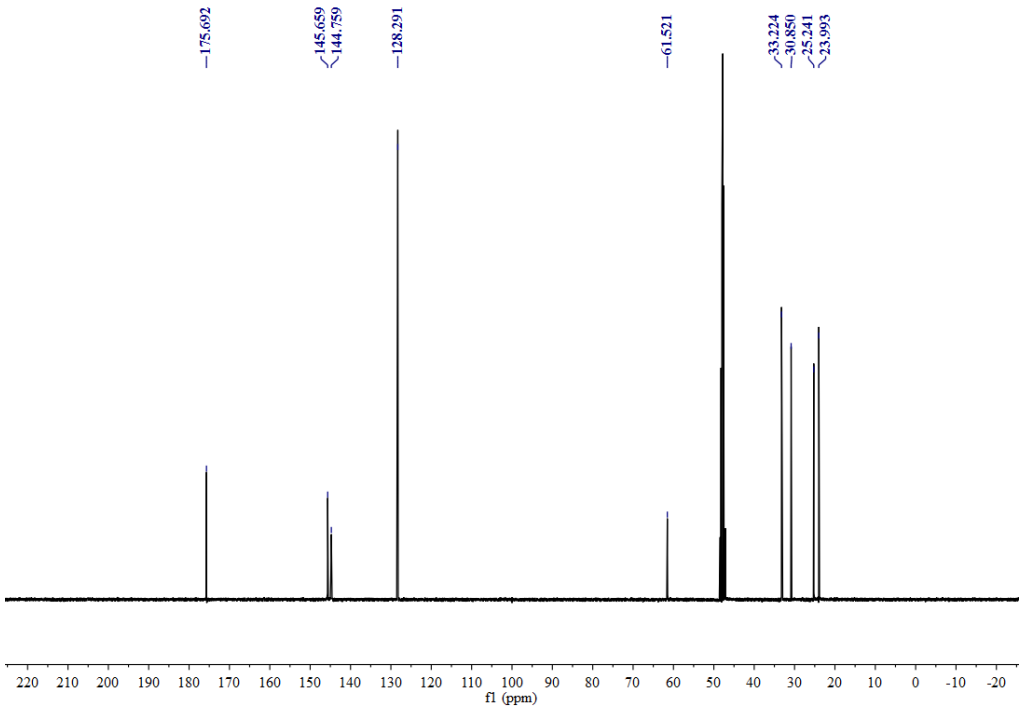

^{1}H NMR of **ZW-9** in CD_3OD

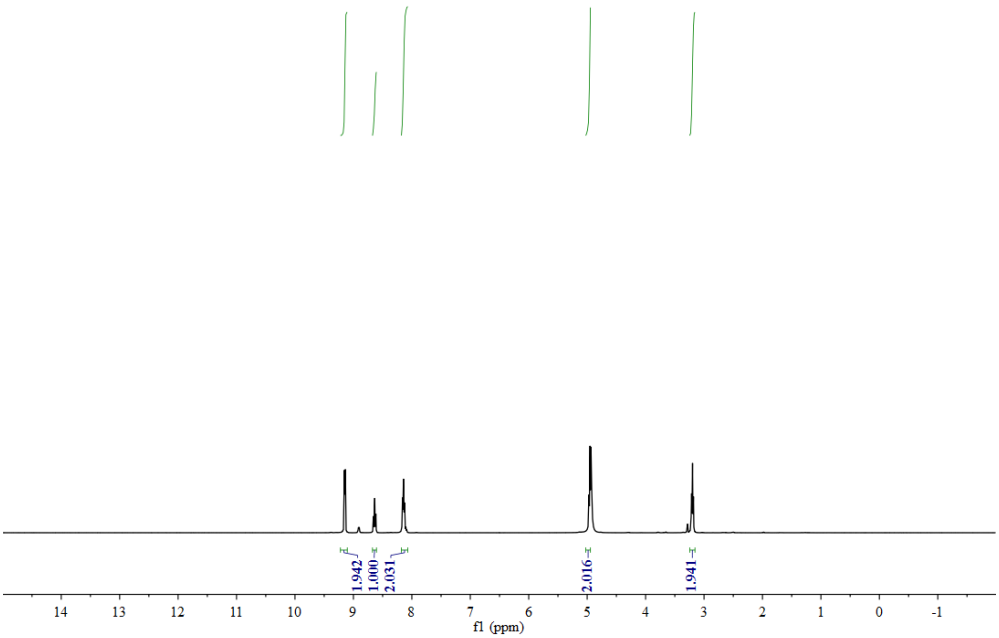

^{13}C NMR of **ZW-9** in CD_3OD

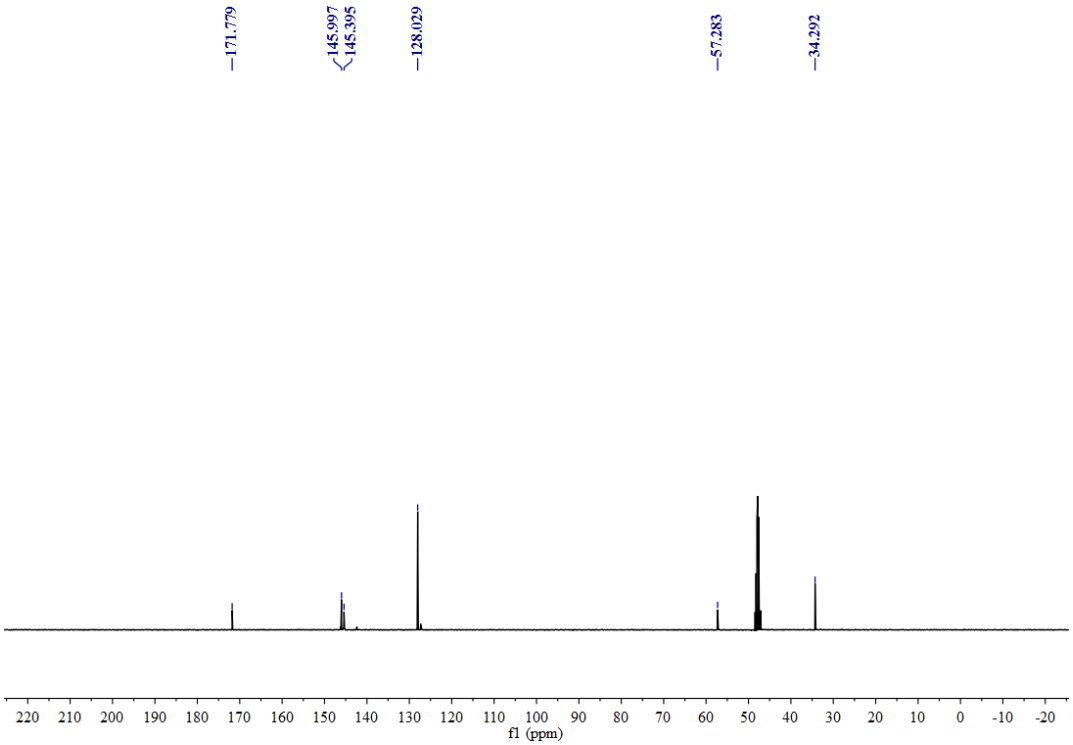

^{1}H NMR of **ZW-10** in CD_3OD

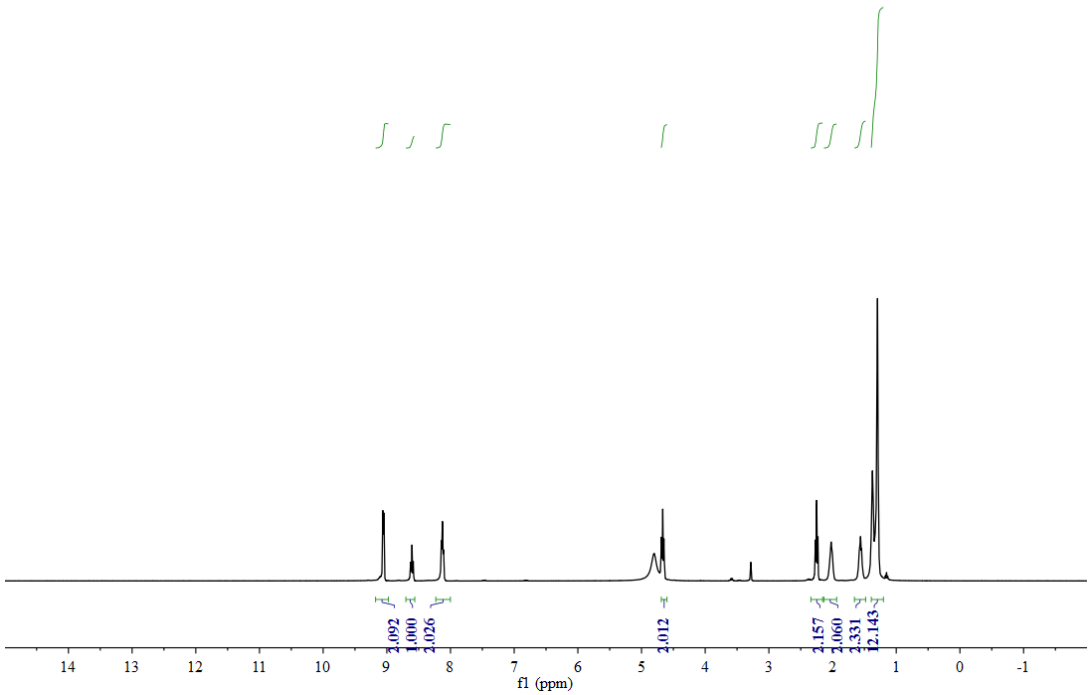

^{13}C NMR of **ZW-10** in CD_3OD

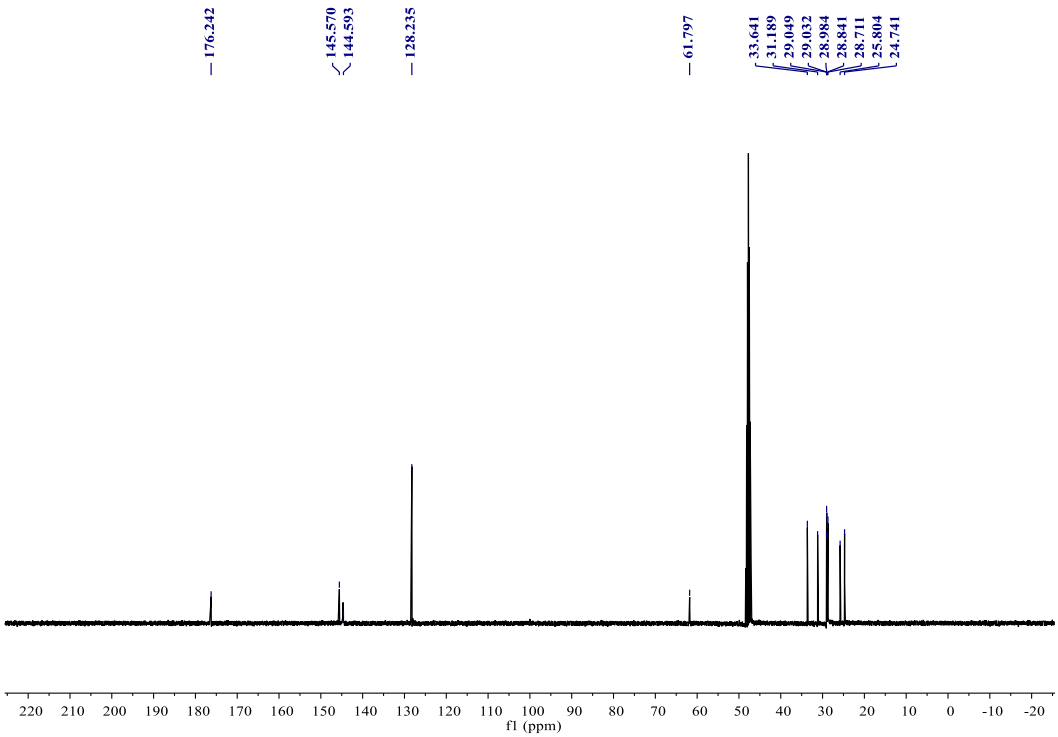

5.3 HPLC purity data of synthesized compounds:

HPLC data of **ZW-1**

Data File C:\HPLC Da...DS_ZW1_Dr_BBanerjee_IICB_030123\BBDS_ZW1_Dr_BBanerjee_IICB_030123.D
Sample Name: BBDS_ZW1_Dr_BBanerjee_IICB_030123

```
    ======================================================================
    Acq. Operator   : SYSTEM
    Sample Operator : SYSTEM
    Acq. Instrument : 1290 Infinity II Prep LC       Location :     -
    Injection Date  : 04-01-2023 17:35:03                 Inj :   1
                                                  Inj Volume : Manually
    Acq. Method     : C:\HPLC DATA\SAN.M
    Last changed    : 04-01-2023 16:21:57 by SYSTEM
                      (modified after loading)
    Analysis Method : C:\HPLC DATA\SAN.M
    Last changed    : 07-12-2022 17:07:01 by SYSTEM
    Additional Info : Peak(s) manually integrated
```

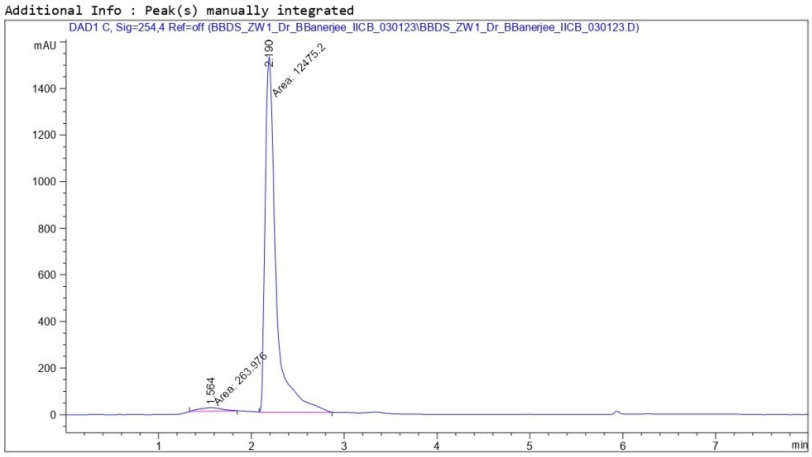


```
    ================================================================================
                               Fraction Information
    ================================================================================
    No Fractions found.
    ================================================================================
    ================================================================================
    ================================================================
                           Area Percent Report
    ================================================================

    Sorted By             :      Signal
    Multiplier            :      1.0000
    Dilution              :     10.0000
    Sample Amount:        :      1.00000  [ng/ul]   (not used in calc.)
    Use Multiplier & Dilution Factor with ISTDs
```

```
Data File C:\HPLC Da...DS_ZW1_Dr_BBanerjee_IICB_030123\BBDS_ZW1_Dr_BBanerjee_IICB_030123.D
Sample Name: BBDS_ZW1_Dr_BBanerjee_IICB_030123


    Signal 1: DAD1 C, Sig=254,4 Ref=off

    Peak RetTime Type  Width     Area      Height     Area
      #   [min]        [min]   [mAU*s]     [mAU]       %
    ----|-------|----|-------|----------|----------|--------|
       1   1.564 PM    0.2857  263.97604   15.39782   2.0722
       2   2.190 MM    0.1361 1.24752e4  1527.51624  97.9278

    Totals :                  1.27392e4  1542.91406


    ===================================================================
                              *** End of Report ***
```

HPLC data of **ZW-2**

```
Data File C:\Users\P...2_50ul-ori_DrBBanerjee_09623\BBDS-ZW-2_50ul-ori_DrBBanerjee_09623.D
Sample Name: BBDS-ZW-2_50ul-ori_DrBBanerjee_09623

    ===================================================================
    Acq. Operator   : SYSTEM
    Sample Operator : SYSTEM
    Acq. Instrument : HPLC                          Location :     -
    Injection Date  : 6/9/2023 3:13:16 PM                Inj :   1
                                                   Inj Volume : Manually
    Acq. Method     : C:\Users\Public\Documents\ChemStation\1\Methods\DEF_LC.M
    Last changed    : 6/9/2023 2:02:47 PM by SYSTEM
                      (modified after loading)
    Analysis Method : C:\Users\Public\Documents\ChemStation\1\Methods\DEF_LC.M
    Last changed    : 6/23/2014 1:43:01 AM by SYSTEM
    Additional Info : Peak(s) manually integrated
```

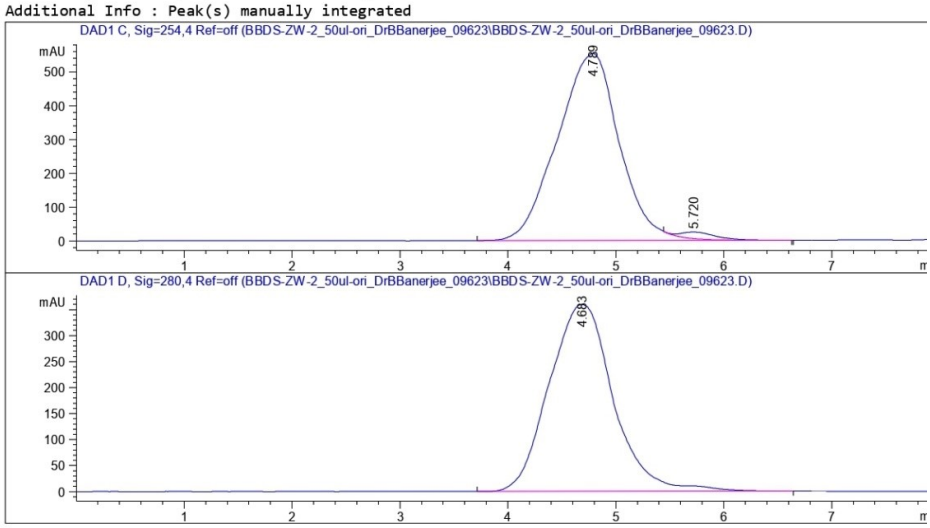


```
    ===================================================================================
                                Fraction Information
    ===================================================================================
    No Fractions found.
    ===================================================================================
    ===================================================================================
    ===================================================================
                              Area Percent Report
    ===================================================================

    Sorted By             :      Signal
    Multiplier            :      1.0000
    Dilution              :      1.0000
    Use Multiplier & Dilution Factor with ISTDs
```

```
Data File C:\Users\P...2_50ul-ori_DrBBanerjee_09623\BBDS-ZW-2_50ul-ori_DrBBanerjee_09623.D
Sample Name: BBDS-ZW-2_50ul-ori_DrBBanerjee_09623

    Signal 1: DAD1 C, Sig=254,4 Ref=off

    Peak RetTime Type  Width     Area      Height     Area
      #   [min]        [min]   [mAU*s]     [mAU]       %
    ----|-------|----|-------|----------|----------|--------|
       1   4.789 BV R  0.5929 2.20113e4   552.32037  98.0262
       2   5.720 VB E  0.3470  443.20981   19.22313   1.9738

    Totals :                  2.24545e4   571.54351


    Signal 2: DAD1 D, Sig=280,4 Ref=off

    Peak RetTime Type  Width     Area      Height     Area
      #   [min]        [min]   [mAU*s]     [mAU]       %
    ----|-------|----|-------|----------|----------|--------|
       1   4.683 BB    0.6175 1.48423e4   359.65955 100.0000

    Totals :                  1.48423e4   359.65955

    ===================================================================
                              *** End of Report ***
```

HPLC data of **ZW-3**

```
Data File C:\HPLC Da...DS_ZW3_Dr_BBanerjee_IICB_030123\BBDS_ZW3_Dr_BBanerjee_IICB_030123.D
Sample Name: BBDS_ZW3_Dr_BBanerjee_IICB_030123

    ===================================================================
    Acq. Operator   : SYSTEM
    Sample Operator : SYSTEM
    Acq. Instrument : 1290 Infinity II Prep LC        Location :     -
    Injection Date  : 04-01-2023 16:24:40                  Inj :   1
                                                    Inj Volume : Manually
    Acq. Method     : C:\HPLC DATA\SAN.M
    Last changed    : 04-01-2023 16:21:57 by SYSTEM
                      (modified after loading)
    Analysis Method : C:\HPLC DATA\SAN.M
    Last changed    : 05-01-2023 12:14:08 by SYSTEM
                      (modified after loading)
    Additional Info : Peak(s) manually integrated
```

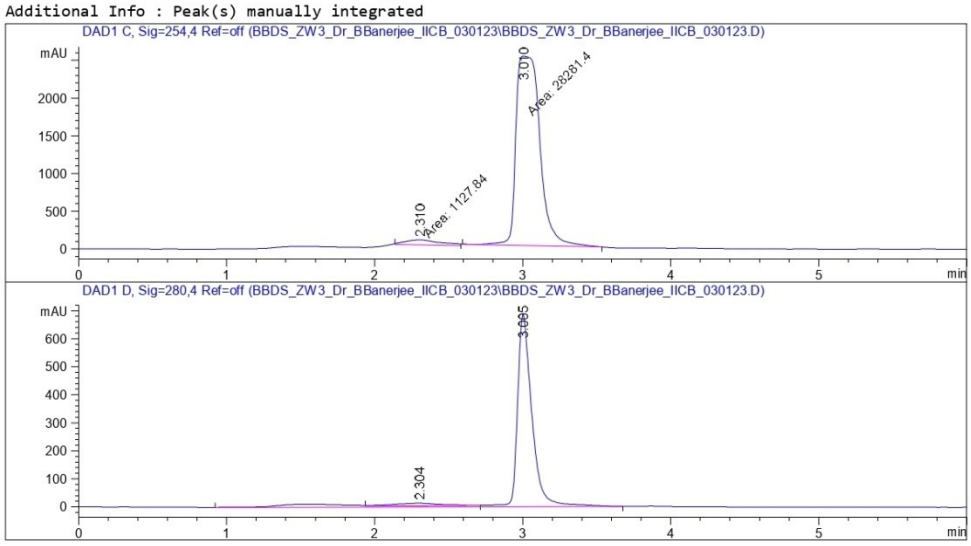


```
    ===================================================================================
                                Fraction Information
    ===================================================================================
    No Fractions found.
    ===================================================================================
    ===================================================================================
    ===================================================================
                             Area Percent Report
    ===================================================================

    Sorted By             :      Signal
    Multiplier            :      1.0000
    Dilution              :     10.0000
    Sample Amount:        :      1.00000  [ng/ul]   (not used in calc.)
    Use Multiplier & Dilution Factor with ISTDs
```

```
Data File C:\HPLC Da...DS_ZW3_Dr_BBanerjee_IICB_030123\BBDS_ZW3_Dr_BBanerjee_IICB_030123.D
Sample Name: BBDS_ZW3_Dr_BBanerjee_IICB_030123


    Signal 1: DAD1 C, Sig=254,4 Ref=off

    Peak RetTime Type  Width     Area      Height     Area
      #   [min]       [min]   [mAU*s]     [mAU]       %
    ----|-------|----|-------|----------|----------|--------|
       1   2.310 MM    0.2881 1127.83545   65.24479   3.8350
       2   3.010 MM    0.1879 2.82814e4  2508.73242  96.1650

    Totals :                  2.94093e4  2573.97721


    Signal 2: DAD1 D, Sig=280,4 Ref=off

    Peak RetTime Type  Width     Area      Height     Area
      #   [min]       [min]   [mAU*s]     [mAU]       %
    ----|-------|----|-------|----------|----------|--------|
       1   2.304 VV E  0.3255  213.24046    9.16483   3.9606
       2   3.005 VB R  0.1038 5170.81543  686.69202  96.0394

    Totals :                  5384.05589  695.85684


    ===================================================================
                               *** End of Report ***
```

HPLC data of **ZW-4**

```
Data File C:\Users\P...4_50ul-ori_DrBBanerjee_09623\BBDS-ZW-4_50ul-ori_DrBBanerjee_09623.D
Sample Name: BBDS-ZW-4_50ul-ori_DrBBanerjee_09623

    ===================================================================
    Acq. Operator   : SYSTEM
    Sample Operator : SYSTEM
    Acq. Instrument : HPLC                          Location :     -
    Injection Date  : 6/9/2023 3:02:20 PM                Inj :   1
                                                   Inj Volume : Manually
    Acq. Method     : C:\Users\Public\Documents\ChemStation\1\Methods\DEF_LC.M
    Last changed    : 6/9/2023 2:02:47 PM by SYSTEM
                      (modified after loading)
    Analysis Method : C:\Users\Public\Documents\ChemStation\1\Methods\DEF_LC.M
    Last changed    : 6/23/2014 1:43:01 AM by SYSTEM
    Additional Info : Peak(s) manually integrated
```

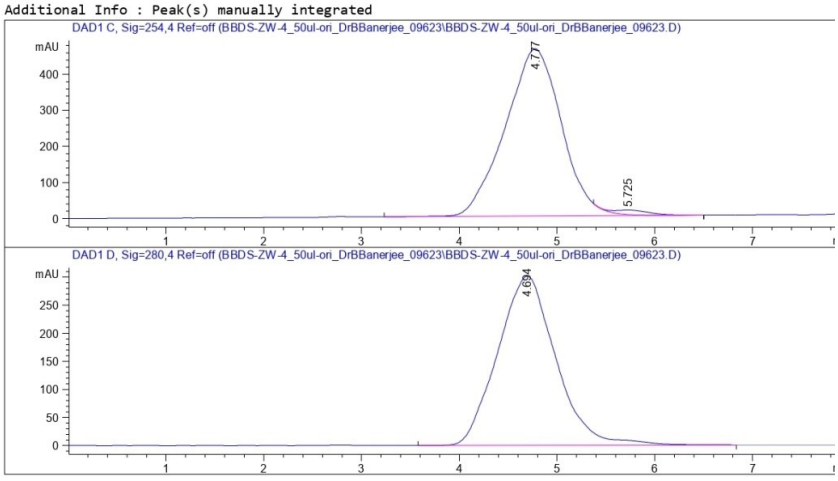


```
    ================================================================================
                                Fraction Information
    ================================================================================
    No Fractions found.
    ================================================================================
    ================================================================================
    ===================================================================
                            Area Percent Report
    ===================================================================

    Sorted By             :      Signal
    Multiplier            :      1.0000
    Dilution              :      1.0000
    Use Multiplier & Dilution Factor with ISTDs
```

```
Data File C:\Users\P...4_50ul-ori_DrBBanerjee_09623\BBDS-ZW-4_50ul-ori_DrBBanerjee_09623.D
Sample Name: BBDS-ZW-4_50ul-ori_DrBBanerjee_09623


    Signal 1: DAD1 C, Sig=254,4 Ref=off

    Peak RetTime Type  Width     Area      Height     Area
      #   [min]        [min]   [mAU*s]     [mAU]       %
    ----|-------|----|-------|----------|----------|--------|
       1   4.777 BV R  0.5890 1.86006e4   464.69214  98.2893
       2   5.725 VB E  0.3454  323.74124   12.70178   1.7107

    Totals :                 1.89243e4   477.39391


    Signal 2: DAD1 D, Sig=280,4 Ref=off

    Peak RetTime Type  Width     Area      Height     Area
      #   [min]        [min]   [mAU*s]     [mAU]       %
    ----|-------|----|-------|----------|----------|--------|
       1   4.694 BB    0.5507 1.24761e4   301.56595 100.0000

    Totals :                 1.24761e4   301.56595


    ===================================================================
                               *** End of Report ***
```

HPLC data of **ZW-5**

```
Data File C:\Users\P...5_50ul-ori_DrBBanerjee_09623\BBDS-ZW-5_50ul-ori_DrBBanerjee_09623.D
Sample Name: BBDS-ZW-5_50ul-ori_DrBBanerjee_09623

    ===================================================================
    Acq. Operator   : SYSTEM
    Sample Operator : SYSTEM
    Acq. Instrument : HPLC                          Location :     -
    Injection Date  : 6/9/2023 2:17:06 PM                Inj :   1
                                                   Inj Volume : Manually
    Acq. Method     : C:\Users\Public\Documents\ChemStation\1\Methods\DEF_LC.M
    Last changed    : 6/9/2023 2:02:47 PM by SYSTEM
                      (modified after loading)
    Analysis Method : C:\Users\Public\Documents\ChemStation\1\Methods\DEF_LC.M
    Last changed    : 6/23/2014 1:43:01 AM by SYSTEM
```

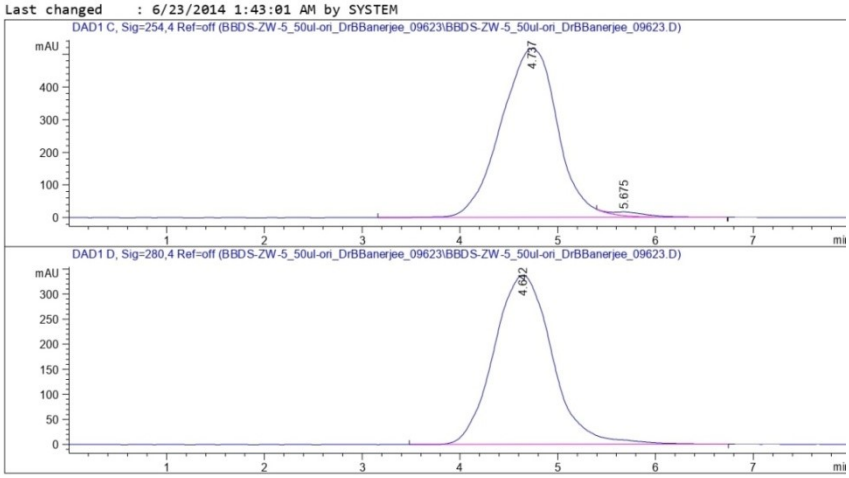


```
    ===================================================================================
                                Fraction Information
    ===================================================================================
    No Fractions found.
    ===================================================================================
    ===================================================================================
    ===================================================================
                            Area Percent Report
    ===================================================================

    Sorted By             :      Signal
    Multiplier            :      1.0000
    Dilution              :      1.0000
    Use Multiplier & Dilution Factor with ISTDs


    Signal 1: DAD1 C, Sig=254,4 Ref=off
```

Data File C:\Users\P...5_50ul-ori_DrBBanerjee_09623\BBDS-ZW-5_50ul-ori_DrBBanerjee_09623.D
Sample Name: BBDS-ZW-5_50ul-ori_DrBBanerjee_09623

Peak #	RetTime [min]	Type	Width [min]	Area [mAU*s]	Height [mAU]	Area %
1	4.737	BV R	0.5969	2.08863e4	517.47681	98.5899
2	5.675	VB E	0.3509	298.72137	11.13670	1.4101
Totals :				2.11850e4	528.61351	

Signal 2: DAD1 D, Sig=280,4 Ref=off

Peak #	RetTime [min]	Type	Width [min]	Area [mAU*s]	Height [mAU]	Area %
1	4.642	BB	0.6029	1.39630e4	337.32626	100.0000
Totals :				1.39630e4	337.32626	

*** End of Report ***

HPLC data of **ZW-6**

Data File C:\Users\P...6_50ul-ori_DrBBanerjee_09623\BBDS-ZW-6_50ul-ori_DrBBanerjee_09623.D
Sample Name: BBDS-ZW-6_50ul-ori_DrBBanerjee_09623

Acq. Operator : SYSTEM
Sample Operator : SYSTEM
Acq. Instrument : HPLC Location : -
Injection Date : 6/9/2023 2:07:54 PM Inj : 1
Inj Volume : Manually
Acq. Method : C:\Users\Public\Documents\ChemStation\1\Methods\DEF_LC.M
Last changed : 6/9/2023 2:02:47 PM by SYSTEM
(modified after loading)
Analysis Method : C:\Users\Public\Documents\ChemStation\1\Methods\DEF_LC.M
Last changed : 6/23/2014 1:43:01 AM by SYSTEM

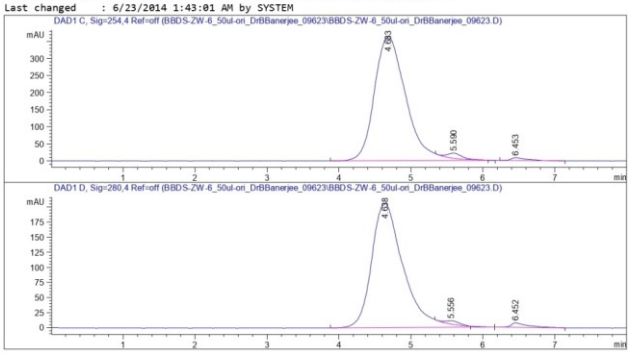

Fraction Information

No Fractions found.

Area Percent Report

Sorted By : Signal
Multiplier : 1.0000
Dilution : 1.0000
Use Multiplier & Dilution Factor with ISTDs

Signal 1: DAD1 C, Sig=254,4 Ref=off

Data File C:\Users\P...6_50ul-ori_DrBBanerjee_09623\BBDS-ZW-6_50ul-ori_DrBBanerjee_09623.D
Sample Name: BBDS-ZW-6_50ul-ori_DrBBanerjee_09623

Peak #	RetTime [min]	Type	Width [min]	Area [mAU*s]	Height [mAU]	Area %
1	4.683	BV R	0.4589	1.11079e4	365.10886	96.9843
2	5.590	VB E	0.2137	215.14600	14.78883	1.8785
3	6.453	BB	0.2093	130.25513	8.38104	1.1373
Totals :				1.14533e4	388.27873	

Signal 2: DAD1 D, Sig=280,4 Ref=off

Peak #	RetTime [min]	Type	Width [min]	Area [mAU*s]	Height [mAU]	Area %
1	4.638	BV R	0.4563	6325.81592	205.97469	96.8737
2	5.556	VB E	0.2077	78.27068	5.44487	1.1986
3	6.452	BB	0.2225	125.87662	7.54974	1.9277
Totals :				6529.96321	218.96930	

*** End of Report ***

HPLC data of **ZW-7**

Data File C:\HPLC Da...DS_ZW7_Dr_BBanerjee_IICB_030123\BBDS_ZW7_Dr_BBanerjee_IICB_030123.D
Sample Name: BBDS_ZW7_Dr_BBanerjee_IICB_030123

Acq. Operator : SYSTEM
Sample Operator : SYSTEM
Acq. Instrument : 1290 Infinity II Prep LC Location : -
Injection Date : 04-01-2023 17:25:26 Inj : 1
Inj Volume : Manually
Acq. Method : C:\HPLC DATA\SAN.M
Last changed : 04-01-2023 16:21:57 by SYSTEM
(modified after loading)
Analysis Method : C:\HPLC DATA\SAN.M
Last changed : 05-01-2023 12:30:33 by SYSTEM
(modified after loading)
Additional Info : Peak(s) manually integrated

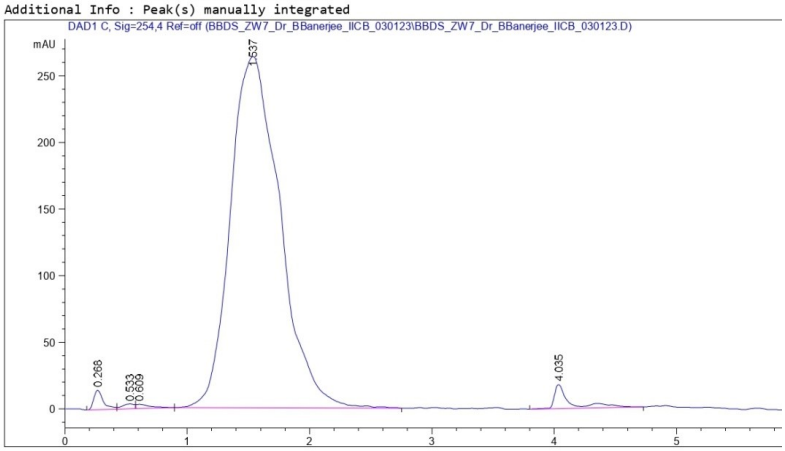

Fraction Information

No Fractions found.

Area Percent Report

Sorted By : Signal
Multiplier : 1.0000
Dilution : 10.0000
Sample Amount: : 1.00000 [ng/ul] (not used in calc.)
Use Multiplier & Dilution Factor with ISTDs

```
Data File C:\HPLC Da...DS_ZW7_Dr_BBanerjee_IICB_030123\BBDS_ZW7_Dr_BBanerjee_IICB_030123.D
Sample Name: BBDS_ZW7_Dr_BBanerjee_IICB_030123

    Signal 1: DAD1 C, Sig=254,4 Ref=off

    Peak RetTime Type  Width     Area      Height     Area
      #   [min]       [min]   [mAU*s]     [mAU]       %
    ----|-------|----|-------|----------|----------|--------|
       1   0.268 BV    0.0832   79.34888   14.64669   1.0292
       2   0.533 VV    0.1076   25.69477    3.67147   0.3333
       3   0.609 VB    0.1173   26.88915    3.22431   0.3488
       4   1.537 BV R  0.4043 7420.18359  263.68491  96.2435
       5   4.035 BV R  0.0927  157.68858   18.01508   2.0453

    Totals :                  7709.80497  303.24244

    ========================================================================
                              *** End of Report ***
```

HPLC data of **ZW-8**

```
Data File C:\HPLC Da...DS_ZW8_Dr_BBanerjee_IICB_030123\BBDS_ZW8_Dr_BBanerjee_IICB_030123.D
Sample Name: BBDS_ZW8_Dr_BBanerjee_IICB_030123

    ========================================================================
    Acq. Operator   : SYSTEM
    Sample Operator : SYSTEM
    Acq. Instrument : 1290 Infinity II Prep LC        Location :     -
    Injection Date  : 04-01-2023 15:42:03                  Inj :   1
                                                    Inj Volume : No inj
    Acq. Method     : C:\HPLC DATA\SAN.M
    Last changed    : 04-01-2023 15:49:36 by SYSTEM
                      (modified after loading)
    Analysis Method : C:\HPLC DATA\SAN.M
    Last changed    : 05-01-2023 12:32:25 by SYSTEM
                      (modified after loading)
    Additional Info : Peak(s) manually integrated
```

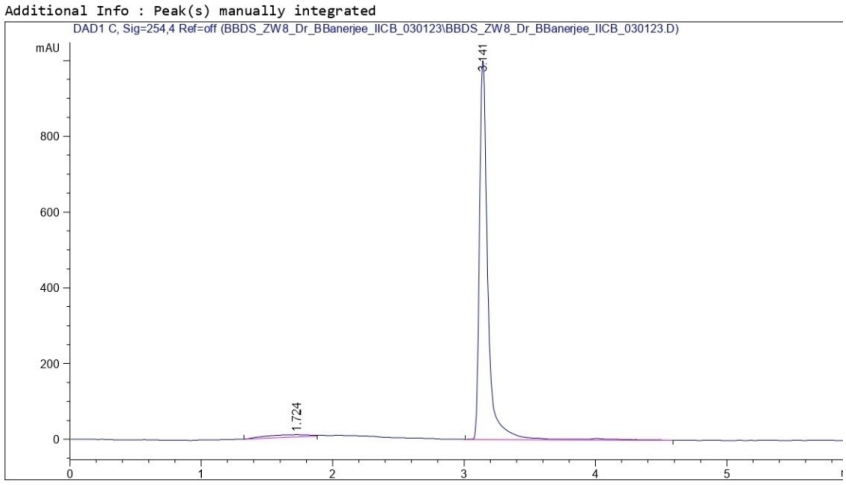


```
    ============================================================================
                              Fraction Information
    ============================================================================
    No Fractions found.
    ============================================================================
    ============================================================================
    ========================================================================
                             Area Percent Report
    ========================================================================

    Sorted By             :      Signal
    Multiplier            :      1.0000
    Dilution              :     10.0000
    Sample Amount:        :      1.00000  [ng/ul]   (not used in calc.)
    Use Multiplier & Dilution Factor with ISTDs
```

```
Data File C:\HPLC Da...DS_ZW8_Dr_BBanerjee_IICB_030123\BBDS_ZW8_Dr_BBanerjee_IICB_030123.D
Sample Name: BBDS_ZW8_Dr_BBanerjee_IICB_030123


    Signal 1: DAD1 C, Sig=254,4 Ref=off

    Peak RetTime Type  Width     Area      Height     Area
      #   [min]        [min]   [mAU*s]     [mAU]       %
    ----|-------|----|-------|----------|----------|--------|
       1   1.724 BV    0.3175  146.36337    5.66451   3.1733
       2   3.141 BV R  0.0652 4465.92188 1007.54968  96.8267

    Totals :                   4612.28525 1013.21419


    ===================================================================
                               *** End of Report ***
```

HPLC data of **ZW-9**

```
Data File C:\HPLC Da...DS_ZW9_Dr_BBanerjee_IICB_030123\BBDS_ZW9_Dr_BBanerjee_IICB_030123.D
Sample Name: BBDS_ZW9_Dr_BBanerjee_IICB_030123

    ===================================================================
    Acq. Operator   : SYSTEM
    Sample Operator : SYSTEM
    Acq. Instrument : 1290 Infinity II Prep LC        Location :     -
    Injection Date  : 04-01-2023 15:52:42                 Inj :   1
                                                    Inj Volume : No inj
    Acq. Method     : C:\HPLC DATA\SAN.M
    Last changed    : 04-01-2023 15:49:36 by SYSTEM
                      (modified after loading)
    Analysis Method : C:\HPLC DATA\SAN.M
    Last changed    : 05-01-2023 12:25:39 by SYSTEM
                      (modified after loading)
    Additional Info : Peak(s) manually integrated
```

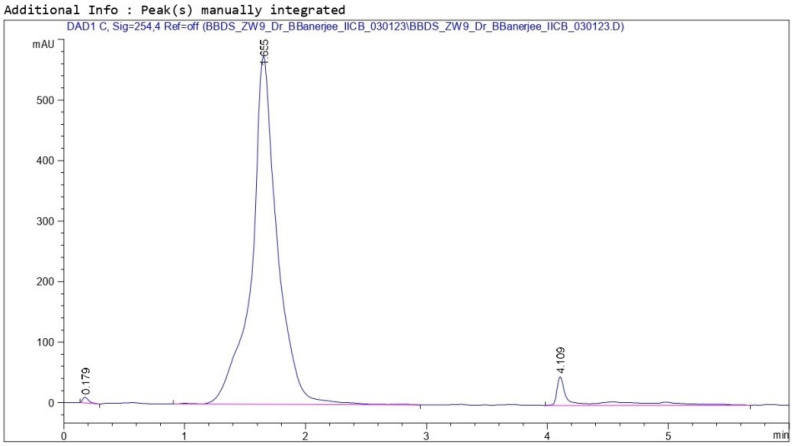


```
    ===============================================================================
                              Fraction Information
    ===============================================================================
    No Fractions found.
    ===============================================================================
    ===============================================================================
    ===================================================================
                             Area Percent Report
    ===================================================================

    Sorted By             :      Signal
    Multiplier            :      1.0000
    Dilution              :     10.0000
    Sample Amount:        :      1.00000  [ng/ul]   (not used in calc.)
    Use Multiplier & Dilution Factor with ISTDs
```

```
Data File C:\HPLC Da...DS_ZW9_Dr_BBanerjee_IICB_030123\BBDS_ZW9_Dr_BBanerjee_IICB_030123.D
Sample Name: BBDS_ZW9_Dr_BBanerjee_IICB_030123


    Signal 1: DAD1 C, Sig=254,4 Ref=off

    Peak RetTime Type  Width     Area      Height     Area
      #   [min]        [min]   [mAU*s]     [mAU]       %
    ----|-------|----|-------|----------|----------|--------|
       1   0.179 BB    0.0527   32.28741    9.72110   0.3574
       2   1.655 VV R  0.2029 8532.75586  575.02740  94.4514
       3   4.109 BV R  0.0679  468.97150   47.42759   5.1912

    Totals :                  9034.01476  632.17609


    ===================================================================
                              *** End of Report ***
```

5.4 Supporting data for biochemical and biophysical studies:

Materials and Methods for Biological Assay

5.4.1 Materials

In the purification process of α-syncline, LB media, isopropyl-1-thio-β-d-galactopyranoside (IPTG), sodium phosphate monobasic, sodium phosphate dibasic from Sigma Aldrich, St. Louis, USA was used. For the LLPS study Polyethyleneglycol-8000was purchased from Sigma Aldrich, MO, USA, India. For protein labeling, Alexa 488 maleimide fromThermo Fisher Scientific, MA, USA, and Sigma Aldrich, MO, USA was used respectively. Small molecules were purchased from Sigma Aldrich, St. Louis, USA. Poly(U) RNA was purchased from Sigma Aldrich, St. Louis, USA Glass slides and coverslips were purchased from Rivera, India, and Blue Star, India respectively. AFM experiment muscovite mica was purchased from Sigma Aldrich, MO, USA. Size exclusion chromatography was done by using Sephadex G-25 superfine from Sigma Aldrich, MO, USA.

5.4.2 Experimental Methods

5.4.3 ^{1}H NMR

^{1}H NMR was recorded in 600MHz NMR instruments by using D_2O as solvent. All NMR spectra reported here are recorded by water suppression techniques.

5.4.4 MALDI-TOF.

The purified and lyophilized proteins were dissolved in 1.5 ml centrifuge tubes after the purification process. The protein samples were then solidified in -80^{0}C for lyophilisation. The lyophilized samples were dissolved in Milli Q water and the molecular weight of the purified protein was determined by Matrix Assisted Laser Desorption/Ionization (MALDI)

mass spectrometer (4800 MALDI-TOF/TOF Analyzer, Applied Bio systems/ MDS SCIEX, USA).

5.4.5 Sodium dodecyl sulfate-polyacrylamide gel electrophoresis (SDS-PAGE)

The most popular gel electrophoretic method for protein analysis, SDS-PAGE, depends on dividing proteins according to size and figuring out their relative molecular mass. Proteins are strongly bound to SDS, an anionic detergent, which denatures the proteins to produce linear polypeptide chains. One SDS molecule is present for every two amino acids on average. β-Mercaptoethanol decreases disulfide bonds, which helps in the denaturation of proteins. At a constant ratio of roughly 1.4 g of SDS per gm of protein, the detergent binds to the hydrophobic portion of the denatured protein. Because the protein-SDS complex has a net negative charge, it migrates in the direction of the anode, with protein size determining how they separate. On the basis of the molecular weight of the protein, the gel is prepared. The molecular weights of the model proteins were within 14-30 KDa. So, we used 15% gel for SDS-PAGE. The composition for different gel and buffer solution are as follows.

Stacking gel buffer (0.5M Tris HCl, pH 6.8), Resolving gel buffer (1.5M Tris HCl, pH 8.8), 1000ml SDS running buffer (3g Tris, 14.4g Glycine, 1g SDS, and 1000ml double distilled water), SDS loading dye (0.25 mM Tris HCl, 8% w/v SDS, 0.2% bromophenol blue, 40% glycerol, and 20% β-mercaptoethanol), staining solution (40% methanol, 10% glacial acetic acid, 50% double distilled water, and 500mg Coomassie Brilliant Blue (R250)/500ml staining solution) and destaining solution (40% w/v methanol, 10% glacial acetic acid, and 50% double distilled water).A separating gel is layered on top of a stacking gel to create the structure of the polyacrylamide gel. Proteins from the sample are concentrated into a small band at the top of the separating gel by the stacking gel. Isotachophoresis, a phenomenon whereby ionic strength and pH differences between the resolving buffer and the stacking gel are utilized, was used to accomplish this. The protein solution was mixed with loading dye solution and it was heated at 90^0C for 10 minutes. The sample was then loaded into the well along with the protein ladder marker. The tank was filled with SDS-PAGE running buffer. The current used for the experiment was 120mA. Then the gel was transferred into a staining box containing staining solution and kept for 30 minutes under shaking conditions. Then the staining solution was replaced by destaining solution (20% (v/v) ethanol and 5% (v/v) acetic acid). The detained gel was washed with Milli-Q water and imaged in a BIORAD GelDoc Go Gel imaging system.

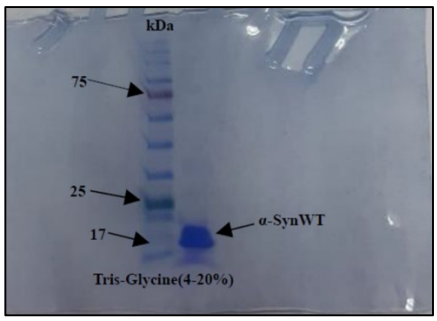

Figure 21. SDS-PAGE image of purified α-synclein protein. Molecular weight (in kDa) of the marker proteins are indicated in the left.

5.4.6 Fluorescence labeling of α-syn

Fluorescence labeling of the protein is necessary to visualize under fluorescence and confocal microscopy. The α-synclein protein was labeled with bright green fluorescence dye Alexa 488-C4 maleimide. The dye solution was dissolved in DMSO. while, the lyophilized protein samples were dissolved in 20 mM NaP buffer (pH-7.4). The concentration of the protein was determined as described before using a UV spectrophotometer. Then protein was mixed with dye such as the ratio of protein and dye was 1:5. This mixture was then kept at 4^0C overnight in the dancing shaker. The labeled protein was separated from the dye by using Sephadex gel filtration column, and pooled. The concentration was measured in a UV-VIS spectrometer to obtain the percentage of labeling. The labeling percentage was ~40% for Alexa 488 conjugated α-synuclein.

5.4.7 In-vitro phase separation assay

The lyophilized protein sample was mixed in NaP (pH= 7.4) buffer and concentration was measured in a UV-VIS spectrophotometer. Phase separation reaction mixtures were prepared by mixing unlabelled protein at different concentrations along with 1% labelled protein, 100 mM NaCl and 10% PEG-8000 was used under experimental conditions. For incubation periods and time points, the Eppendorf tubes were kept in a moist chamber at a temperature of 37°C with shaking at 180 rpm. The solution was then drop casted on a clean glass slide and sandwiched by a clean cover slip to visualize under the microscope. The phase separation was confirmed by turbidity measurement (Absorbance at 600 nm) in a UV-VIS spectrophotometer and corresponding images were taken in a confocal or fluorescence microscope in DIC or fluorescence mode.

5.4.8 Turbidity assay

Turbidity or light scattering is one of the most common assays to determine the phase separation. Turbidity refers to the cloudiness or haziness of a fluid caused by the presence of suspended particles, often microscopic in size, that scatter light as it passes through the substance. If the protein phase separates, then the droplets will scatter more

light compared to the solution where there is no phase separation. The turbidity measurement was done at a wavelength of 350 nm in a UV-VIS spectrometer (Thermos Scientific, USA). The protein solution was incubated for the required time for phase separation and then the absorbance was measured under different conditions.

5.4.9 Circular dichroism (CD) Spectroscopy

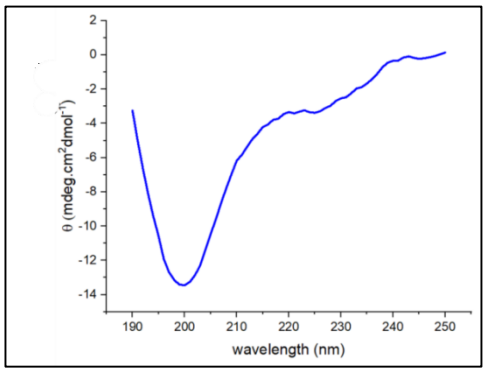

Figure 22. CD spectrum of native α-Syn protein.

Circular dichroism (CD) spectroscopy is a powerful analytical technique employed in biochemistry, chemistry, and structural biology to study the secondary structure of molecules, particularly proteins and nucleic acids. When light interacts with chiral molecules, circular dichroism measures the difference in absorption of light that is circularly polarized—left-handed versus right-handed. When used to proteins, CD spectroscopy can provide details about secondary structural components including alpha helices, beta sheets, and random coils by identifying distinctive absorption bands in the far-ultraviolet spectrum (usually ranging from 170 to 250 nm). A JASCO J815 CD equipment was used to monitor secondary structure change by CD, with scan speeds of 100 nm/min, integration times of 1 s, and an equal number of acquisitions of 3. For the best signal-to-noise ratio, CD measurements were performed between195 and 250 nm using the allowed HT voltage. The far UV CD measurements were performed with a conventional CD cuvette with a 0.1 cm route length

5.4.10 Bioinformatics analysis of α- synuclein

Intrinsically disordered proteins (IDPs) have a general tendency to phase separate under crowded conditions. Recent literatures suggest that, there is a very strong correlation between the disordered region and phase separation of any protein. It is also to be noted that globular proteins like BSA and lysozyme can also undergo phase separation under suitable conditions. To predict the disorder and probability of phase separation we used several sequence based bioinformatics tools. PONDR score (http://www.pondr.com/) was used to predict the naturally occurring disordered region in the α-synuclein sequence. PONDR predicted four disorder regions in the sequence stretching from amino acids 1-10, 75-76, 78-80 and 104-140 (Fig. 4.5A-C). Importantly, the last segment

which is C-terminal domain (CTD) is highly disordered and the overall score of CTD was also high (0.885) compared to others. We confirm our disorder prediction with another tool namely IUPred3 (https://iupred3.elte.hu/). IUPred3 also predicted the similar results, that CTD of α-synuclein is extremely disordered (Fig. 4.5D). Our next focus was to predict the phase separation propensity on the basis of another tool, Fuzrop (https://fuzdrop.bio.unipd.it/predictor). The tool predicted that, the overall probability

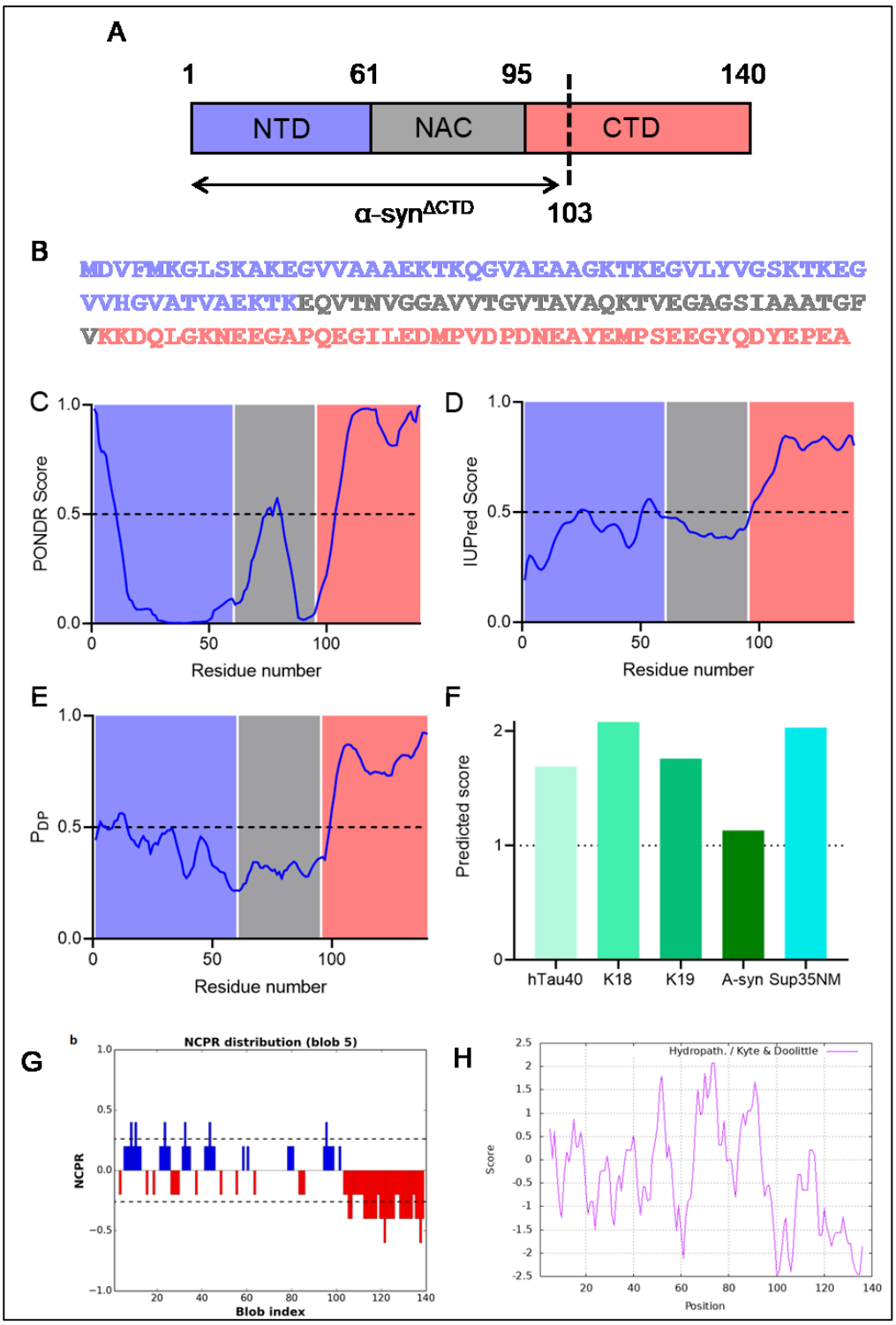

Figure 23. Bioinformatics analysis of α-synuclein:(A) Domain structure of full length and C-terminal truncated version of α-synuclein. (B) Linear sequence of α-synuclein. (C) Linear amino acid sequence of α-Synuclein; Blue denotes N-terminal domain, Grey denotes NAC domain, crimson red denotes C-terminal domain. (C) PONDR prediction from the linear sequence of α-synuclein. (D) IUPred3 analysis from the linear sequence of α-synuclein. (E) Probability of phase separation calculated from FuzDrop. (F) Comparison of cat GRANUALE scores of different phase separating proteins with α-synuclein. (G) Net charge per residue (NCPR) distribution of α-synuclein. Red: Negatively charged amino acids, Blue: Negatively charged amino acids. (H) Kyte-Doolittle hydropath plot of α-synuclein of phase separation of α-synuclein is 0.62 which is consistent with the other phase separating proteins (Fig. 4.5E). The residue-specific propensity revealed that the C-terminal domain has a high probability of phase separation. This data is well connected to our disorder prediction data. Taken together from our bioinformatics study we can conclude that CTD of α-synuclein is the major driver for phase separation. The cat GRANULE score for phase separation was comparable with other proteins (Fig. 4.5F). Consequently, we then focused on the charge and hydrophobic pattering in the sequence of α-synuclein. Therefore, the charge scanning by the CIDER tool (https://pappulab.wustl.edu/CIDERinfo.html) revealed that the N-terminal domain of α-synuclein has a mixture of positively and negatively charged amino acids, whereas the C-terminal domain is mostly acidic in nature (Fig. 4.5G)[28]. So, positively charged ligands can bind primarily with the CTD. Our in silico analyses were further confirmed by experimental techniques. Hydrophobicity and charge pattering are significant among other factors that can influence phase separation. On the other hand, we employed ExPASy tool to probe the hydrophobic regions in the α-synuclein. It suggested that most of the amino acids in the NAC domain of the sequence are hydrophobic in nature (Fig. 4.5H). This hydrophobic core may interact with another hydrophobic core of the polypeptide chain to cause self-coacervation.

6.0 References

1. Reddy, P. V. G., Kiran, Y. B. R., Reddy, C. S., and Reddy, C. D. **(2004)** Synthesis andAntimicrobial Activity of Novel Phosphorus Heterocycles with Exocyclic P–C Link, *Chemical and pharmaceutical bulletin 52*, 307-310.
2. Wang, B. J., and Groziak, M. P. **(2016)** Recent developments in the chemistry of boronheterocycles, In *Advances in Heterocyclic Chemistry*, pp 47-90, Elsevier.
   Abdel-Hafez, S. H. **(2008)**
3. (a) Selenium containing heterocycles: Synthesis, anti-inflammatory, analgesic and anti-microbial activities of some new 4-cyanopyridazine-3 (2H) selenone derivatives, *European journal of medicinal chemistry 43*, 1971-1977.
   (b) Brown, E. G. **(2012)** *Ring nitrogen and key biomolecules: The biochemistry of Nheterocycles*, Springer Science & Business Media.
4. Chin, Y.-W., Balunas, M. J., Chai, H. B., and Kinghorn, A. D. **(2006)** Drug discovery from natural sources, *The AAPS journal 8*, E239-E253.
5. Cordell, G. A., Quinn-Beattie, M. L., and Farnsworth, N. R. **(2001)** The potential ofalkaloids in drug discovery, *Phytotherapy Research: An International Journal Devoted to Pharmacological and Toxicological Evaluation of Natural Product Derivatives 15*,183-205.
6. Hughes, E. H., and Shanks, J. V. **(2002)** Metabolic engineering of plants for alkaloid production, *Metabolic Engineering 4*, 41-48.
7. Rohini, R., Shanker, K., Reddy, P. M., Ho, Y.-P., and Ravinder, V. **(2009)** Mono and bis-6-arylbenzimidazo [1, 2-c] quinazolines: A new class of antimicrobial agents, *European journal of medicinal chemistry 44*, 3330-3339.
8. Chen, Q., Zhu, X.-L., Jiang, L.-L., Liu, Z.-M., and Yang, G.-F. **(2008)** Synthesis, antifungal activity and CoMFA analysis of novel 1, 2, 4-triazolo [1, 5-a] pyrimidine derivatives, *European Journal of Medicinal Chemistry 43*, 595-603.
9. Danac, R., and Mangalagiu, I. I. **(2014)** Antimycobacterial activity of nitrogen heterocycles derivatives: Bipyridine derivatives. Part III [13, 14],
   European journal ofmedicinal chemistry 74, 664-670.
10. Miert, S. V.; Hostyn, S.; Maes, B. U. M.; Cimanga, K.; Brun, R.; Kaiser, M.; Matyus, P.; Dommisse, R.; Lemiere, G.; Vlietinck, A.; Pieters, L. J. *Nat. Prod*., **2005**, 68, 674.
11. Cimanga, K.; De Bruyne, T.; Pieters, L.; Vlietinck, A. J.; Turger, C. A. J. *Nat. Prod*., **1997**, 60, 688.
12. Molina, A.; Vaquero, J. J.; Garcia-Navio, J. L.; Alvarez-Builla, J.; de PascualTeresa, B.; Gago, F.; Rodrigo, M. M.; Ballesteros, M. *J. Org. Chem*., **1996,** 61, 5587.
13. Paulo, A.; Gomes, E. T.; Steele, J.; Warhurst, D. C.; Houghton, P. *J. Planta Med*., **2000**, 66, 30. 2.
14. Cimanga, K.; De Bruyne, T.; Pieters, L.; Claeys, M.; Vlietinck, A. *Tetrahedron Lett.*, **1996,** 37, 1703.
15. Gellert, E.; Hamet, R.; Schlitter, E. Helv. Chim. Acta, 1951, 34, 642; (c) Pousset, J. L.; Martin, M. T.; Jossang, A.; Bodo, B. *Phytochemistry*, **1995**, 39, 735.

16. Dwuma-Badu, D.; Ayim, J. S. K.; Fiagbe, N. Y. Y.; Knapp, J. E.; Schiff, P. L. Jr.; Slatkin, D. J. *J. Pharm. Sci.*, **1978**, 67, 433; (e) Tackie, A. N.; Boye, G. L.; Sharaf, M. H. M.; Schiff, P. L. Jr.; Crouch, R. C.; Spitzer, T. D.; Johnson, R. L.; Dunn, J.; Minick, D.; Martin, G. E. *J. Nat. Prod*., **1993**, 56, 653.
17. Ablordeppey, S. D.; Hufford, C. D.; Bourne, R. F.; Dwama-Badu, D. *Planta Med*., **1990**, 56, 416.
18. Spitzer, T. D.; Crouch, R. C.; Martin, G. E.; Sharaf, M. H. M.; Schiff, P. L. Jr.; Tackie, A. N.; Boye, G. L. J. *Heterocycl. Chem*., **1991**, 28, 2065.
19. Tackie, A. N.; Sharaf, M. H. M.; Schiff, P. L. Jr.; Boye, G. L.; Crouch, R. C.; Martin, G. E. *J. Heterocycl. Chem*., **1991**, 28, 1429.
20. Paulo, A.; Gomes, E. T.; Hougton, P. J*. J. Nat. Prod*., **1995**, 58, 1485.
21. Cimanga, K.; DeBruyne, T.; Lasure, A.; Poel, B. V.; Pieters, L.; Claeys, M.; Berghe, D. V.; Vlietinck, A. *J. Planta Med*., **1996**, 62, 22.
22. Crouch, R. C.; Davis, A. O.; Spitzer, T. D.; Martin, G. E.; Sharaf, M. H. M.; Schiff, P. L. Jr.; Phoebe, C. H. Jr.; Tackie, A. N. *J. Heterocycl. Chem*., **1995,** 32, 1077.
23. Hadden, C. E.; Sharaf, M. H. M.; Guido, J. E.; Robins, R. H.; Tackie, A. N.; Phoebe, C. H. Jr.; Schiff, P. L. Jr. Martin, G. E. *J. Nat. Prod*., **1999**, 62, 238.
24. Fort, D. M.; Litvak, J.; Chen, J. L.; Lu, Q.; Phuan, P. W.; Cooper, R.; Bierer, D. E. *J. Nat. Prod*., **1998**, 61, 1528.
25. Blinov, K.; Elyashberg, M.; Martirosian, E. R.; Molodtsov, S. G.; Williams, A. J. A. J.; Tackie, A. N.; Sharaf, M. H. M.; Schiff, P. L. Jr.; Crouch, R. C.; Martin, G. E.; Hadden, C. E.; Guido, J. E.; Mills, K. A. Magn. *Reson. Chem*., **2003**, 41, 577.
26. Boye, G. L.; Ampofo, O. Proceedings of the First International Symposium on Cryptolepine, Ghana, University of Science and Technology: Kumasi, Ghana, 1983, 37.
27. Oliver-Bever, B. Medicinal Plants in Tropical West Africa, *Cambridge University Press*: 21 Cambridge, UK, **1986**, 41.
28. Boakye-Yiadom, K. J. *Crude Drug Res*.**1979**, 17, 78.
29. Bierer, D. E.; Fort, D. M.; Mendez, C. D.; Luo, J.; Imbach, P. A.; Dubenko, L. G.; Jolad, S. D.; Gerber, R. E.; Litvak, J.; Lu, Q.; Zhang, P.; Reed, M. J.; Waldeck, N.; Bruening, R. C.; Noamesi, B. K.; Hector, R. F.; Carlson, T. J.; King, S. R. *J. Med. Chem*., **1998,** 41, 894.
30. Bisz, E., Piontek, A., Dziuk, B., Szostak, R. and Szostak, M. Barriers to rotation in ortho-substituted tertiary aromatic amides: effect of chloro-substitution on resonance and distortion. *The Journal of Organic Chemistry*, 2**018**, *83*(6), .3159-3163.
31. *The Amide Linkage: Structural Significance in Chemistry, Biochemistry, and Materials Science*; Greenberg, A., Breneman, C. M., Liebman, J. F., Eds.; Wiley: New York, 2000.
32. Tani, K.; Stoltz, B. M. *Nature* **2006**, *441*, 731.
33. Aube, J. *Angew. Chem., Int. Ed.* **2012**, *51*, 3063.
34. For selected reviews, see: (a) Hall, H. K., Jr.; El-Shekeil, A. *Chem. Rev.* 1983, *83*, 549. (b) Yamada, S. *Rev. Heteroat. Chem.* **1999**, *19*, 203.
35. Clayden, J.; Moran, W. J. *Angew. Chem., Int. Ed.* **2006**, *45*, 7118.

36. Szostak, M.; Aubé, J. *Chem. Rev.* **2013**, *113*, 5701.
37. For representative examples, see: (a) Liniger, M.; VanderVelde, D. G.; Takase, M. K.; Shahgholi, M.; Stoltz, B. M. *J. Am. Chem. Soc.* 2016, *138*, 969. (b) Liniger, M.; Liu, Y.; Stoltz, B. *J. Am. Chem. Soc.* 2017, *139*, 13944. (c) Komarov, I. V.; Yanik, S.; Ishchenko, A. Y.; Davies, J. E.; Goodman, J. M.; Kirby, A. J. *J. Am. Chem. Soc.* **2015**, *137*, 926.
38. (d) Golden, J.; Aubé, J. *Angew. Chem., Int. Ed.* 2002, *41*, 4316. (e) Sliter, B.; Morgan, J.; Greenberg, A. *J. Org. Chem.* 2011, *76*, 2770. For a recent synthesis of Tröger's base twisted amides, see: (f) Artacho, J.; Ascic, E.; Rantanen, T.; Karlsson, J.; Wallentin, C. J.; Wang, R.; Wendt, O. F.; Harmata, M.; Snieckus, V.; Warñmark, K. *Chem. - Eur. J.* 2012, *18*, 1038.
39. Meng, G.; Szostak, M. *Org. Lett.* **2015**, *17*, 4364.
40. Holzer, W.; Meng, G.; Shi, S.; Lalancette, R.; Szostak, R.; Szostak, M.*Chem. - Eur. J.* **2016**, *22*, 14494.
41. (a) Clayden, J.; Foricher, Y. J. Y.; Lam, H. K. *Eur. J. Org. Chem.* **2002**, *2002*, 3558. (b) Hutchby, M.; Houlden, C. E.; Haddow, M. F.; Tyler, S. N.; Lloyd-Jones, G. C.; Booker-Milburn, K. I. *Angew. Chem., Int. Ed.* **2012**, *51*, 548. (c) Clayden, *J. Nature* **2012**, *481*, 274.
42. (a) Yamada, S. *Angew. Chem., Int. Ed. Engl.* **1993**, *32*, 1083.
43. (b) Yamada, S. *Angew. Chem., Int. Ed. Engl.* **1995**, *34*, 1113.
44. For recent elegant examples of amide distortion by peripheral metal coordination, see: (a) Adachi, S.; Kumagai, N.; Shibasaki, M. *Chem. Sci.* 2017, *8*, 85. (b) Adachi, S.; Kumagai, N.; Shibasaki, M. *Synlett* **2018**, *29*, 301.
45. For reviews, see: (a) Liu, C.; Szostak, M. *Chem. - Eur. J.* 2017, *23*, 7157. (b) Meng, G.; Shi, S.; Szostak, M. *Synlett* **2016**, *27*, 2530.
46. For a study on isomerization around the C−C(O) axis in benzamides, see: (a) Ahmed, A.; Bragg, R. A.; Clayden, J.; Lai, L. W.;McCarthy, C.; Pink, J. H.; Westlund, N.; Yasin, S. A. *Tetrahedron* **1998**.
47. For selected studies on ortho-substituted benzamides, see: Kessler, H. *Angew. Chem., Int. Ed. Engl.* **1970**, *9*, 219.
48. Mannschreck, A.; Mattheus, A.; Rissmann. *J. Mol. Spectrosc.* 1967,*23*, 15. (c) Jungk, A. E.; Schmidt, G. M. J. *Chem. Ber.* **1971**, *104*, 3289.
49. (d) Leibfritz, D. *Chem. Ber.* **1975**, *108*, 3014. (e) Kleinpeter, E. *J. Mol. Struct.* **1996**, *380*, 139. For a study on solvolysis of ortho-chloro derivatives, see: (f) Park, K. H.; Kevill, D. N. *J. Phys. Org. Chem.* **2012**, *25*, 2.
50. (a) Kayama, S.; Tabata, H.; Takahashi, Y.; Tani, N.; Wakamatsu, S.; Oshitari, T.; Natsugari, H.; Takahashi, H. *Tetrahedron* 2015, *71*, 7046; (b) Kanase, Y.; Kuniyoshi, M.; Tabata, H.; Takahashi, Y.; Kayama, S.; Wakamatsu, S.; Oshitari, T.; Natsugari, H.; Takahashi, H. *Synthesis* 2015, *47*, 3907; (c) Kondo, K.; Kan, K.; Tanada, Y.; Bando, M.; Shinohara, T.; Kurimura, M.; Ogawa, H.; Nakamura, S.; Hirano, T.; Yamamura, Y.; Kido, M.; Mori, T.; Tominaga, M. *J. Med. Chem.* 2002, *45*, 3805. (d) Okaniwa, M.; Imada, T.; Ohashi, T.; Miyazaki, T.; Arita, T.; Yabuki, M.; Sumita, A.; Tsutsumi, S.; Higashikawa, K.; Takagi, T.; Kawamoto, T.; Inui, Y.; Yoshida, S.; Ishikawa, T. *Bioorg.*

Med. Chem. 2012, *20*, 4680.
51. *Science of Synthesis: Cross-Coupling and Heck-Type Reactions*; Molander, G. A., Wolfe, J. P., Larhed, M., Eds.; Thieme: Stuttgart, 2013.
52. Selected examples: (a) Clayden, J.; Lund, A.; Vallverdu, L.; Helliwell, M. *Nature* 2004, *431*, 966. (b) Clayden, J. *Chem. Soc. Rev.* 2009, *38*, 817. (c) Sola, J.; Fletcher, S. P.; Castellanos, A.; Clayden, J. *Angew. Chem., Int. Ed.* 2010, *49*, 6836. (d) Knipe, P. C.; Thompson, S.; Hamilton, A. D. *Chem. Sci.* 2015, *6*, 1630. (e) Barrett, K. T.; Metrano, A. J.; Rablen, P. R.; Miller, S. J. *Nature* 2014, *509*, 71.
53. For bridged lactams, see: (a) Szostak, R.; Aube,́J.; Szostak, M. *Chem. Commun.* 2015, *51*, 6395. (b) Szostak, R.; Aube,́J.; Szostak, M. *J. Org. Chem.* 2015, *80*, 7905. For acyclic amides, see: (c) Szostak, R.; Shi, S.; Meng, G.; Lalancette, R.; Szostak, M. *J. Org. Chem.* 2016, *81*, 8091.
54. Szostak, R.; Meng, G.; Szostak, M. *J. Org. Chem.* 2017, *82*, 6373.
55. Martin, R.; Romea, P.; Tey, C.; Urpi, F.; Vilarrasa, J. *Synlett* 1997,*12*, 1414.
56. For classic computational studies on bridged lactams, see: Greenberg, A.; Venanzi, C. A. *J. Am. Chem. Soc.* 1993, *115*, 6951.
57. Greenberg, A.; Moore, D. T.; DuBois, T. D. *J. Am. Chem. Soc.* 1996, *118*, 8658. See, also: (c) Morgan, J.; Greenberg, A. *J. Chem. Thermodyn.* 2014, *73*, 206.
58. For selected theoretical studies on amide bonds, see: (a) Kemnitz, C. R.; Loewen, M. J. *J. Am. Chem. Soc.* 2007, *129*, 2521. (b) Mujika, J. I.; Mercero, J. M.; Lopez, X. *J. Am. Chem. Soc.* 2005, *127*, 4445. (c) Glover,
59. S. A.; Rosser, A. A. *J. Org. Chem.* 2012, *77*, 5492. (d) Glover, S. A.; Rosser, A. A.; Taherpour, A.; Greatrex, B. W. *Aust. J. Chem.* 2014, *67*,507. (e) Morgan, J.; Greenberg, A.; Liebman, J. F. *Struct. Chem.* 2012, *23*, 197. (f) Morgan, J. P.; Weaver-Guevara, H. M.; Fitzgerald, R. W.; Dunlap-Smith, A.; Greenberg, A. *Struct. Chem.* 2017, *28*, 327.
60. (20) (a) Wiberg, K. B. *Acc. Chem. Res.* 1999, *32*, 922. (b) Cox, C.; Lectka, T. *Acc. Chem. Res.* 2000, *33*, 849.
61. Li, Q.Y., Gockel, S.N., Lutovsky, G.A., DeGlopper, K.S., Baldwin, N.J., Bundesmann, M.W., Tucker, J.W., Bagley, S.W. and Yoon, T.P., 2022. Decarboxylative cross-nucleophile coupling via ligand-to-metal charge transfer photoexcitation of Cu (II) carboxylates. *Nature chemistry*, *14*(1), pp.94-99.
62. Xuan, J., Zhang, Z.-G. & Xiao, W.-J. Visible-light-induced decarboxylative functionalization of carboxylic acids and their derivatives. Angew. Chem. Int. Ed. 54, 15632–15641 (2015).
63. Rodríguez, N. & Goossen, L. J. Decarboxylative coupling reactions: a modern strategy for C–C-bond formation. Chem. Soc. Rev. 40, 5030–5048 (2011).
64. Arshadi, S., Ebrahimiasl, S., Hosseinian, A., Monfared, A. & Vessally, E. Recent developments in decarboxylative cross-coupling reactions between carboxylic acids and N–H compounds. RSC Adv. 9, 8964–8976 (2019).

65. Zeng, Z., Feceu, A., Sivendran, N. & Gooßen, L. J. Decarboxylation-initiated intermolecular carbon–heteroatom bond formation. Adv. Synth. Catal. 363, 2678–2722 (2021).
66. Scott, E., Peter, F. & Sanders, J. Biomass in the manufacture of industrial products—the use of proteins and amino acids. Appl. Microbiol. Biotechnol. 75, 751–762 (2007).
67. Gallezot, P. Conversion of biomass to selected chemical products. Chem. Soc. Rev. 41, 1538–1558 (2012).
68. Bertamino, A., Ostacolo, C., Medina, A., Di Sarno, V., Lauro, G., Ciaglia, T., Vestuto, V., Pepe, G., Basilicata, M.G., Musella, S. and Smaldone, G. Exploration of TRPM8 binding sites by β-carboline-based antagonists and their in vitro characterization and in vivo analgesic activities. *Journal of Medicinal Chemistry*, **2020**, 63(17), 9672-9694.
69. Jang, J., Raja, G.C.E., Lee, J.H., Son, Y., Kim, J. and Lee, S,.Palladium-catalyzed decarboxylative coupling reaction with alkynyl carboxylic acids and arylsiloxanes. *Tetrahedron Letters*, **2016**, 57(41), 4581-4584.
70. Li, X., Zou, D., Leng, F., Sun, C., Li, J., Wu, Y. and Wu, Y. Arylation of 2-substituted pyridines via Pd-catalyzed decarboxylative cross-coupling reactions of 2-picolinic acid. *Chemical Communications*, **2013**, 49(3), 312-314.
71. Qin, X., Chen, C., Zhang, L., Xu, J., Pan, Y., Zhao, H., Han, J., Li, H. and Xu, L. Palladium-catalyzed highly regioselective and stereoselective decarboxylative arylation of unactivated olefins with aryl carboxylic acids. *Tetrahedron*, **2017**, 73(16),2242-2249.
72. Scheipers, I., Mück-Lichtenfeld, C. and Studer, A. Palladium-Catalyzed Decarboxylative γ-Arylation for the Synthesis of Tetrasubstituted Chiral Allenes. *Angewandte Chemie International Edition*, 2019, 58(20), 6545-6548.
73. Yu, W.Y., Sit, W.N., Zhou, Z. and Chan, A.S.C. Palladium-catalyzed decarboxylative arylation of C− H bonds by aryl acylperoxides. *Organic Letters*, **2009**, 11(15), 3174-3177.
74. Shang, R., Yang, Z.W., Wang, Y., Zhang, S.L. and Liu, L. Palladium-catalyzed decarboxylative couplings of 2-(2-azaaryl) acetates with aryl halides and triflates. *Journal of the American Chemical Society*, **2010**, 132(41),14391-14393.
75. Dennington, R., Keith, T.A. and Millam, J.M. (**2016**) GaussView 6.0. 16. *Semichem Inc*., Shawnee Mission.
76. Weigend, F.; Ahlrichs, R., Balanced basis sets of split valence, triple zeta valence and quadruple zeta valence quality for H to Rn: Design and assessment of accuracy. *Physical Chemistry Chemical Physics* **2005,***7* (18), 3297-3305.
77. Lee, C.; Yang, W.; Parr, R. G., Development of the Colle-Salvetti correlation-energy formula into a functional of the electron density. *Physical Review B* **1988,***37* (2), 785-789.
78. Rassolov, V. A.; Pople, J. A.; Ratner, M. A.; Windus, T. L., 6-31G* basis set for atoms K through Zn. *The Journal of Chemical Physics* **1998,***109* (4), 1223-1229.

Mukherjee, S., Sakunthala, A., Gadhe, L., Poudyal, M., Sawner, A.S., Kadu, P. and Maji, S.K., Liquid-liquid phase separation of α-synuclein: a new mechanistic insight for α-synuclein aggregation associated with Parkinson's disease pathogenesis. *Journal of molecular biology*, **2023**, *435*(1), p.167713.

79. Ghosh, S., Kundu, A. and Chattopadhyay, K., Small molecules attenuate the interplay between conformational fluctuations, early oligomerization and amyloidosis of alpha synuclein. *Scientific Reports*, **2018**, 8(1), p.5481.
80. Peng PH, Hsu KW, Wu KJ. Liquid-liquid phase separation (LLPS) in cellular physiology and tumor biology. *Am J Cancer Res*. **2021**, 11(8):3766-3776.
81. 4.Wu W, Tan Y, Yin H, Jiang M, Jiang Y, Ma X, Yin T, Li Y, Zhang H, Cai X, Meng G. Phase separation is required for PML nuclear body biogenesis and function. *FASEB J*. **2023** Jun;37(6): e22986.
82. Peng PH, Hsu KW, Wu KJ. Liquid-liquid phase separation (LLPS) in cellular physiology and tumor biology. *Am J Cancer Res*. **2021**, 11(8):3766-3776.
83. Wu W, Tan Y, Yin H, Jiang M, Jiang Y, Ma X, Yin T, Li Y, Zhang H, Cai X, Meng G. Phase separation is required for PML nuclear body biogenesis and function. *FASEB J*. **2023**, 37(6): e22986.
84. Rodriguez-Lopez G, O'Neil Williams Y, Toro-Mendoza J. Individual and Collective Behavior of Emulsion Droplets Undergoing Ostwald Ripening. *Langmuir*. **2019**, 35(15):5316-5323.
85. Inoue S, Kimura Y, Uematsu Y. Ostwald ripening of aqueous microbubble solutions. *J Chem Phys*. **2022**, 157(24):244704.
86. Martin EW, Holehouse AS, Peran I, Farag M, Incicco JJ, Bremer A, Grace CR, Soranno A, Pappu RV, Mittag T. Valence and patterning of aromatic residues determine the phase behavior of prion-like domains. *Science.* **2020**, 367(6478):694-699
87. Henderson MX, Trojanowski JQ, Lee VM. α-Synuclein pathology in Parkinson's disease and related α-synucleinopathies. *Neurosci Lett*. **2019**, 709:134316.
88. Protter D, Lang C, Cooper AA. αSynuclein and Mitochondrial Dysfunction: A Pathogenic Partnership in Parkinson's Disease? Parkinsons Dis. **2012**,2012: 829207.
89. Villar-Piqué A, Lopes da Fonseca T, Outeiro TF. Structure, function and toxicity of alpha-synuclein: the Bermuda triangle in synucleinopathies. *J Neurochem*. **2016**, 139 Suppl 1:240-255.
90. Taschenberger G, Garrido M, Tereshchenko Y, Bähr M, Zweckstetter M, Kügler S. Aggregation of αSynuclein promotes progressive in vivo neurotoxicity in adult rat dopaminergic neurons. *ActaNeuropathol*. **2012**, 123(5):671-83
91. Pinto-Costa R, Harbachova E, La Vitola P, Di Monte DA. Overexpression-Induced α-Synuclein Brain Spreading. *Neurotherapeutics.* **2023**, 20(1):83-96.
92. Ray S, Singh N, Kumar R, Patel K, Pandey S, Datta D, Mahato J, Panigrahi R, Navalkar A, Mehra S, Gadhe L, Chatterjee D, Sawner AS, Maiti S, Bhatia S, Gerez JA, Chowdhury A, Kumar A, Padinhateeri R, Riek R, Krishnamoorthy G, Maji SK. α-

Synuclein aggregation nucleates through liquid-liquid phase separation. *Nat Chem.* **2020**,12(8):705-716.
93. Sawner AS, Ray S, Yadav P, Mukherjee S, Panigrahi R, Poudyal M, Patel K, Ghosh D, Kummerant E, Kumar A, Riek R, Maji SK. Modulating α-Synuclein Liquid-Liquid Phase Separation. *Biochemistry.* **2021** ,60(48):3676-3696.
94. Sorrentino ZA, Vijayaraghavan N, Gorion KM, Riffe CJ, Strang KH, Caldwell J, Giasson BI. Physiological C-terminal truncation of α-synuclein potentiates the prion-like formation of pathological inclusions. *J Biol Chem.* **2018**, 293(49):18914-18932.
95. Farzadfard A, Pedersen JN, Meisl G, Somavarapu AK, Alam P, Goksøyr L, Nielsen MA, Sander AF, Knowles TPJ, Pedersen JS, Otzen DE. The C-terminal tail of α-synuclein protects against aggregate replication but is critical for oligomerization. *Commun Biol.* **2022**, 5(1):123.
96. Li S, Wang Y, Lai L. Small molecules in regulating protein phase separation. *ActaBiochimBiophys Sin (Shanghai)*. **2023**, 55(7):1075-1083.
97. Su Y, Maimaitiyiming Y, Wang L, Cheng X, Hsu CH. Modulation of Phase Separation by RNA: A Glimpse on N6-Methyladenosine Modification. *Front Cell Dev Biol*. **2021**, 9:786454.
98. Ruff KM, Dar F, Pappu RV. Ligand effects on phase separation of multivalent macromolecules. *Proc Natl AcadSci U S A.* **2021**, 118(10):e2017184118.
99. Abbas M ,Lipiński WP , Wang J , Spruijt E . Peptide-based coacervates as biomimetic protocells. *ChemSoc Rev.* **2021**, 50(6):3690-3705.
100. Dang M, Song J. A review of the effects of ATP and hydroxychloroquine on the phase separation of the SARS-CoV-2 nucleocapsid protein. *Biophys Rev.* 2022, 14(3):709-715.
101. Richard J. Wheeler, Hyun O. Lee, Ina Poser, Arun Pal, Thom Doeleman, Satoshi Kishigami, SukhleenKour, Eric Nathaniel Anderson, Lara Marrone, Anastasia C. Murthy, Marcus Jahnel, Xiaojie Zhang, Edgar Boczek, Anatol Fritsch, Nicolas L. Fawzi, Jared Sterneckert, Udai Pandey, Della C. David, Benjamin G. Davis, Andrew J. Baldwin, Andreas Hermann, Marc Bickle, Simon Alberti, Anthony A. Hyman Small molecules for modulating protein driven liquid-liquid phase separation in treating neurodegenerative disease. *bioRxiv* 721001.
102. Poudyal M, Sakunthala A, Mukherjee S, Gadhe L, Maji SK. Phase separation and other forms of α-Synuclein self-assemblies. *Essays Biochem.* **2022**, 66(7):987-1000
103. Rodríguez LC, Foressi NN, Celej MS. Modulation of α-synuclein phase separation by biomolecules. *BiochimBiophysActa Proteins Proteom*. **2023**,1871(2):140885. doi: 10.1016/j.bbapap.2022.140885
104. Babinchak WM, Dumm BK, Venus S, Boyko S, Putnam AA, Jankowsky E, Surewicz WK. Small molecules as potent biphasic modulators of protein liquid-liquid phase separation. *Nat Commun.* **2020** ,11(1):5574.
105. Xu B, Chen J, Liu Y. Curcumin Interacts with α-Synuclein Condensates to Inhibit Amyloid Aggregation under Phase Separation. *ACS Omega*. **2022**, 7(34):30281-30290.

106. Tsang B, Pritišanac I, Scherer SW, Moses AM, Forman-Kay JD. Phase Separation as a Missing Mechanism for Interpretation of Disease Mutations. *Cell.* **2020**, 183(7):1742-1756.
107. Holehouse AS, Das RK, Ahad JN, Richardson MO, Pappu RV. CIDER: Resources to Analyze Sequence-Ensemble Relationships of Intrinsically Disordered Proteins. *Biophys J*. **2017**, 112(1):16-21.
108. Vrijsen S, Houdou M, Cascalho A, Eggermont J, Vangheluwe P. Polyamines in Parkinson's Disease: Balancing Between Neurotoxicity and Neuroprotection. *Annu Rev Biochem.* **2023**, 92:435-464.
109. Nitani A, Muta H, Adachi M, So M, Sasahara K, Sakurai K, Chatani E, Naoe K, Ogi H, Hall D, Goto Y. Heparin-dependent aggregation of hen egg white lysozyme reveals two distinct mechanisms of amyloid fibrillation. *J Biol Chem.* **2017**, 292(52):21219-21230.
110. Vijayan B, Raj V, Nandakumar S, Kishore A, Thekkuveettil A. Spermine protects alpha-synuclein expressing dopaminergic neurons from manganese-induced degeneration. *Cell BiolToxicol*. **2019**, 35(2):147-159.
111. Antony T, Hoyer W, Cherny D, Heim G, Jovin TM, Subramaniam V. Cellular polyamines promote the aggregation of alpha-synuclein. *J Biol Chem.* **2003**, 278(5):3235-40.
112. Vijayan B, Raj V, Nandakumar S, Kishore A, Thekkuveettil A. Spermine protects alpha-synuclein expressing dopaminergic neurons from manganese-induced degeneration. *Cell BiolToxicol*. **2019**, 35(2):147-159.
113. Büttner S, Broeskamp F, Sommer C, Markaki M, Habernig L, Alavian-Ghavanini A, Carmona-Gutierrez D, Eisenberg T, Michael E, Kroemer G, Tavernarakis N, Sigrist SJ, Madeo F. Spermidine protects against α-synuclein neurotoxicity. *Cell Cycle.* **2014**,13(24):3903-8.
114. Moritz L, Hammoud SS. The Art of Packaging the Sperm Genome: Molecular and Structural Basis of the Histone-To-Protamine Exchange. *Front Endocrinol (Lausanne).* **2022**,13:895502.
115. 36.Francis S, Yelumalai S, Jones C, Coward K. Aberrant protamine content in sperm and consequential implications for infertility treatment. *Hum Fertil (Camb)*. **2014**,17(2):80-9.
116. de Mateo S, Ramos L, de Boer P, Meistrich M, Oliva R. Protamine 2 precursors and processing. *Protein Pept Lett*. **2011**, 18(8):778-85.
117. 38.Thachil J. Protamine-The Journey from DNA to Heparin Neutralization to Gene therapy. *SeminThrombHemost.* **2022**, 48(2):240-243.
118. Goers J, Uversky VN, Fink AL. Polycation-induced oligomerization and accelerated fibrillation of human alpha-synuclein in vitro. *Protein Sci.* **2003**,12(4):702-7.
119. Lee JE, Sang JC, Rodrigues M, Carr AR, Horrocks MH, De S, Bongiovanni MN, Flagmeier P, Dobson CM, Wales DJ, Lee SF, Klenerman D. Mapping Surface Hydrophobicity of α-Synuclein Oligomers at the Nanoscale. *Nano Lett*. **2018**,

18(12):7494-7501.
120. Düster R, Kaltheuner IH, Schmitz M, Geyer M. 1,6-Hexanediol, commonly used to dissolve liquid-liquid phase separated condensates, directly impairs kinase and phosphatase activities. *J Biol Chem*. **2021**, 296:100260.
121. Sonawane SK, Uversky VN, Chinnathambi S. Baicalein inhibits heparin-induced Tau aggregation by initializing non-toxic Tau oligomer formation. *Cell Commun Signal*. **2021**, 19(1):16.
122. Wu Y, Ma L, Cai S, Zhuang Z, Zhao Z, Jin S, Xie W, Zhou L, Zhang L, Zhao J, Cui J. RNA-induced liquid phase separation of SARS-CoV-2 nucleocapsid protein facilitates NF-κB hyper-activation and inflammation. *Signal Transduct Target Ther.* **2021**, 6(1):167.
123. Saiki S, Sasazawa Y, Fujimaki M, Kamagata K, Kaga N, Taka H, Li Y, Souma S, Hatano T, Imamichi Y, Furuya N, Mori A, Oji Y, Ueno SI, Nojiri S, Miura Y, Ueno T, Funayama M, Aoki S, Hattori N. A metabolic profile of polyamines in parkinson disease: A promising biomarker. *Ann Neurol*. **2019**, 86(2):251-263.

7.0 List of Published papers:

1. Bera, S., Mondal, P., **Sarkar, D**., Pathi, V.B., Pakrashy, S., Datta, A. and Banerji, B., **2021**. Synthetic and Computational Studies on RhIII-Catalyzed Redox-Neutral Cascade of Carbenoid Functionalization and Dephosphonylative Annulation. ***The Journal of Organic Chemistry***, *86*(10), 7069-7077.

2. Bera, S., Chandrasekhar, K., Chatterjee, S., Killi, S.K., **Sarkar, D**. and Banerji, B., 2019. RhIII-Catalyzed Decarboxylative o-Acylation of Arenes Bearing an Oxidizing Directing Group. ***European Journal of Organic Chemistry***, ***2019***(24), 3877-3881.

3. Patra, A.S., Ghorai, S., **Sarkar, D**., Das, R., Sarkar, S. and Pal, S., **2017**. Anionically functionalized guar gum embedded with silica nanoparticles: an efficient nanocomposite adsorbent for rapid adsorptive removal of toxic cationic dyes and metal ions. ***Bioresource technology***, *225*, 367-376.

4. Fluxionality of Both Amides and Esters Reveals the Presence of Four Rotational Isomers at Room Temperature *(Manuscript under preparation)*

5. Synthesis of Azatoxin Analog Palladium Catalyzed C(sp^3)-H arylation Followed by De-esterification**.** *(Manuscript under preparation)*

6. Chemoproteomic Profiling of Zwitterion Interactions Reveals Modulation of α-Synuclein Phase Separation. *(Manuscript under preparation)*

JOC The Journal of Organic Chemistry

pubs.acs.org/joc Article

Synthetic and Computational Studies on Rh^{III}-Catalyzed Redox-Neutral Cascade of Carbenoid Functionalization and Dephosphonylative Annulation

Suvankar Bera, Partha Mondal, Debabrata Sarkar, Vijay Babu Pathi, Sourav Pakrashy, Ayan Datta,* and Biswadip Banerji*

Cite This: J. Org. Chem. 2021, 86, 7069−7077 Read Online

ACCESS | Metrics & More | Article Recommendations | Supporting Information

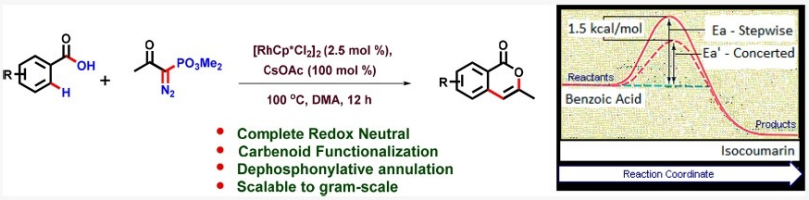

ABSTRACT: A Rh(III)-catalyzed regioselective redox-neutral cascade process of carbenoid functionalization followed by dephosphonylative annulation of benzoic acids with α-diazo-β-keto phosphonate has been realized, which led to the direct synthesis of a privileged 3-substituted isocoumarin scaffold. To the best of our knowledge, this is the first report of a complete redox neutral method to synthesize isocoumarins using C−H functionalization strategy. In the catalytic cycle of this reaction, there are two possible pathways for the C−C coupling between ortho-positioned carbon atom of benzoic acid and the diazo carbon atom: (i) concerted 1,2-aryl shift and (ii) stepwise metal−carbene formation followed by migratory insertion. DFT study has predicted that the concerted pathway has lower activation energy as compared to the stepwise pathway by 1.5 kcal/mol.

INTRODUCTION

Isocoumarins are considered as one of the most significant classes of lactones for their existence in numerous biologically active molecules including natural products.[1] Isocoumarins with substitution at only the 3-position are more abundant in biologically active molecules as compared to both of the 4-substituted isocoumarins and 3,4-disubstituted isocoumarins.[1] These 3-substituted isocoumarins without any substituent at the 4-position show a wide range biological activities such as antimicrobial,[2] anti-inflammatory,[3] antidiabetic,[4] antitumor,[5,6] and HIV-1-specific reverse transcriptase inhibitor[7] properties, etc. (Figure 1).

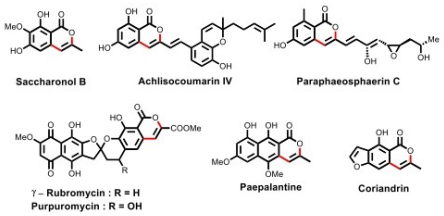

Figure 1. Some naturally occurring bioactive isocoumarins

Currently, there are several reports regarding the synthesis of 3-substituted isocoumarins such as transition-metal-catalyzed cyclization of *o*-halo aryl esters or acids with π-components, carbonylative cyclization of *o*-halo phenols with π- components, and electrophilic cyclization of substituted alkynes.[8−15] However, in all of these reaction protocols, a preactivated coupling partner C−X or C−M reacting species is used as a starting material to deliver isocoumarins.

Recently, a few methods have been developed to access these lactones without using *o*-halo aryl esters/acids/phenols. These methods are basically metal-catalyzed chelation-assisted oxidative cyclization of the *o*-aryl or alkenyl C−H bond with carbon−carbon π-components.[16−26] These methods also require stoichiometric amount of oxidizing agents. Stoichiometric use of metal species or oxidizing agents restrict any reaction protocol to be environmentally benign, and the

Received: February 8, 2021
Published: May 12, 2021

https://doi.org/10.1021/acs.joc.1c00311
J. Org. Chem. 2021, 86, 7069−7077

Check for updates

ChemPubSoc Europe

DOI: 10.1002/ejoc.201900242

EurJOC European Journal of Organic Chemistry

Communication

Decarboxylative Acylation

Rh^{III}-Catalyzed Decarboxylative *o*-Acylation of Arenes Bearing an Oxidizing Directing Group

Suvankar Bera,[a] K. Chandrasekhar,[a,b] Satadru Chatterjee,[a] Sunil Kumar Killi,[a] Debabrata Sarkar,[a] and Biswadip Banerji*[a,b]

Abstract: Here in we report, rhodium(III)-catalyzed decarboxylative acylation of arenes using α-oxocarboxylic acids as acyl surrogate. In this strategy, O–NHAc group act as an autocleavable oxidizing directing group (ODG^{auto}), thus giving rise to *ortho*-acylated phenols in moderate to good yields. Mechanistic studies provided strong support for a kinetically relevant C–H bond activation. According to the best of our knowledge, this is the first report of Rhodium catalyzed decarboxylative acylation.

Introduction

Transition-metal-catalyzed chemical transformation of C–H bond has emerged as a highly focused area of research to the synthetic community since last few decades. Diverse types of C–H bond functionalization have been explored intensely. Acyl functionalization to C–H bond always draw considerable attention due to the large abundance of acyl group in the family of organic molecular systems. In the recent years, α-oxocarboxylic acids have been explored as efficient acyl surrogates for acylation to C–H bond of aryl systems containing diverse types of directing groups such as pyridines,[1] acetanilides,[2] azoarene,[3] *O*-methyl ketoximes,[4] amides,[5] *N*-nitrosoanilines[6] etc. These methods produce CO_2 as the waste instead of often toxic species. Goossen was the pioneer person to develop a synthetic route to achieve aryl ketones via Pd-catalyzed decarboxylative cross coupling using aryl halides with potassium α-oxocarboxylates in the presence of a Cu^{I} source.[7] After this pioneering work, several groups have reported C–H acylation through Pd-catalyzed decarboxylation of α-oxocarboxylic acids. But there is no report of Rhodium catalyzed decarboxylative acylation. Now, the catalytic activity changes altering the transition metal. Specific transition metal is required for a particular type of C–H bond transformation. Thus any kind of new catalytic activity of any transition metal always draw considerable attention. In past few years, Rhodium or Iridium-catalyzed various kinds of aryl C–H functionalization have been reported using auto cleavable oxidizing directing group (ODG^{auto}) such as CONH-OMe,[8] N–NHR,[9] O–NHAc.[10] These types of directing groups, become traceless in the products to generate valuable functional groups. In case of traditional directing groups(DG) mediated C–H functionalization, generally very harsh conditions are required for removal of the DG after C–H functionalization to achieve the target molecule, whereas use of auto cleavable DG's circumvent the harsh conditions.

In accordance with the above information and inspired by the recent advances in transition-metal-catalyzed C–H functionalization to access phenol,[10e,10g,11] we aimed to synthesize *ortho*-acylated phenols via Rh^{III}-catalyzed direct C–H acylation of arenes bearing O–NHAc group as ODG^{auto}. Phenols containing acyl group are considered as significant structural motifs for their great abundance in diverse type of bio-active molecules including natural products[12] (Figure 1). Among the family of acyl group assisted phenols, *o*-acyl phenols are most important for their wide range of application. They serve as the prime building blocks for the synthesis of various drugs such as celiprolol, acebutolol, warfarin, propafenone etc.[13] In addition to this, *o*-acylated phenols are effecttive synthetic intermediates to access various types of oxygen-containing heterocyclic scaffolds such as benzoxazole, benzofuranone, dibenzoxazepine and chromanone etc. Therefore, development of a method for the preparation of *ortho*-acyl phenols is always appreciated.

The traditional methods involved in synthesis of *o*-acylated phenols (like Friedel–Craft acylation, Fries Rearrangement)[14,15] suffer from various kinds of drawbacks such as lack of regioselectivity or harsh reaction condition etc. Since, last few decades direct C–H functionalization technique has become complementary to the classical protocols. So, accessing *o*-acyl phenol through C–H functionalization is in focus now a days to overcome the problems of classical methods. Recently transition metal catalyzed direct *ortho*-hydroxylation of aromatic ketone has been explored for the preparation of *o*-acyl phenols but this approach also suffers from site selectivity in few cases of bi-aryl ketones.[16] Therefore synthesis of *o*-acyl phenols via

[a] Organic & Medicinal Chemistry Division, Indian Institute of ChemicalBiology, (CSIR-IICB), 4 Raja S. C. Mullick Road, Kolkata 700032, India
[b] Academy of Scientific and Innovative Research (AcSIR), 4 Raja S. C. Mullick Road, Kolkata 700032, India
E-mail: biswadip.banerji@gmail.com
http://iicb.res.in/divisionwiselistofscientists/chemistry/biswadipb.html
Supporting information and ORCID(s) from the author(s) for this article are available on the WWW under https://doi.org/10.1002/ejoc.201900242.

Bioresource Technology 225 (2017) 367–376

Contents lists available at ScienceDirect

Bioresource Technology

journal homepage: www.elsevier.com/locate/biortech

Anionically functionalized guar gum embedded with silica nanoparticles: An efficient nanocomposite adsorbent for rapid adsorptive removal of toxic cationic dyes and metal ions

Abhay Shankar Patra [a,b,1], Soumitra Ghorai [a,b,1], Debabrata Sarkar [a], Raghunath Das [a,c], Supriya Sarkar [b], Sagar Pal [a,*]

[a] Polymer Chemistry Laboratory, Department of Applied Chemistry, Indian Institute of Technology (ISM), Dhanbad 826004, India
[b] Tata Steel R&D, Jamshedpur 831007, India
[c] Department of Civil and Chemical Engineering, University of South Africa (UNISA), South Africa

HIGHLIGHTS

- h-GG/SiO_2 nanocomposite has been synthesized through sol-gel technique.
- The nanocomposite is an efficient adsorbent for removal of toxic dyes/metal ions.
- The nanocomposite based adsorbent showed good recyclability.

GRAPHICAL ABSTRACT

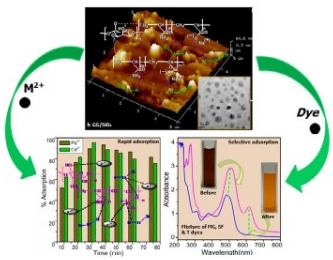

ARTICLE INFO

Article history:
Received 15 July 2016
Received in revised form 21 November 2016
Accepted 23 November 2016
Available online 25 November 2016

Keywords:
Adsorption
Guar gum
Nanocomposite
Sol-gel

ABSTRACT

In the present work, a novel biodegradable nanocomposite has been developed (h-GG/SiO_2) based on anionically modified guar gum and *in-situ* deposited SiO_2 NPs through sol-gel technique. Here the anionically modified guar gum stimulates the silica polymerization process and hence acts as a unique template for the development of spherical SiO_2 NPs. Batch adsorption studies indicate that h-GG/SiO_2 nanocomposite shows remarkable adsorption capacity for cationic dyes/metal ions (Q_{max}: 781.25 mg g^{-1}- for malachite green (MG), 281.69 mg g^{-1} for safranin (SF); 645.16 mg g^{-1} for Pb^{2+}, 709.21 mg g^{-1} for Cd^{2+}) as well as it efficiently and selectively removes cationic MG from mixture of dye solutions. Finally the worthy regenerative efficacy of h-GG/SiO_2 facilitates the adsorbent to be economically promising for practical application in the field of wastewater management.

1. Introduction

In the field of wastewater technology, the simultaneous coexistence of toxic organic and inorganic contaminants is a major environmental concern in worldwide (Kyung et al., 2005). Both dyes and heavy metals have significant ecological effect on ecosystem because of their durable toxicity, environmental persistence, mutagen and bioaccumulation (Sun et al., 2011; Zhao et al., 2011). Hence, dyes and heavy metals must be efficiently separated from the discharged wastewater to defend ecological, biological and industrial environment on a global scale (Visa et al., 2010; Hernández-Montoya et al., 2013).

* Corresponding author.
E-mail address: sagarpal1@hotmail.com (S. Pal).
[1] ASP and SG equally contributed to this manuscript.

http://dx.doi.org/10.1016/j.biortech.2016.11.093
0960-8524/